Twentieth NASTRAN® Users' Colloquium

Computer Software Management and Information Center
University of Georgia
Athens, Georgia

Proceedings of a colloquium held in
Colorado Springs, Colorado
April 27–May 1, 1992

FOREWORD

NASTRAN® (NASA STRUCTURAL ANALYSIS) is a large, comprehensive, nonproprietary, general purpose finite element computer code for structural analysis which was developed under NASA sponsorship and became available to the public in late 1970. It can be obtained through COSMIC® (Computer Software Management and Information Center), Athens, Georgia, and is widely used by NASA, other government agencies, and industry.

NASA currently provides continuing maintenance of NASTRAN through COSMIC. Because of the widespread interest in NASTRAN, and finite element methods in general, the Twentieth NASTRAN Users' Colloquium was organized and held at the Sheraton Colorado Springs, Colorado Springs, Colorado on April 27 - May 1, 1992. (Papers from previous colloquia held in 1971, 1972, 1973, 1975, 1976, 1977, 1978, 1979, 1980, 1982, 1983, 1984, 1985, 1986, 1987, 1988, 1989, 1990 and 1991 are published in NASA Technical Memorandums X-2378, X-2637, X-2893, X-3278, X-3428, and NASA Conference Publications 2018, 2062, 2131, 2151, 2249, 2284, 2328, 2373, 2419, 2481, 2505, 3029, 3069 and 3111.) The Twentieth Colloquium provides some comprehensive general papers on the application of finite element methods in engineering, comparisons with other approaches, unique applications, pre- and post-processing or auxiliary programs, and new methods of analysis with NASTRAN.

Individuals actively engaged in the use of finite elements or NASTRAN were invited to prepare papers for presentation at the Colloquium. These papers are included in this volume. No editorial review was provided by NASA or COSMIC; however, detailed instructions were provided each author to achieve reasonably consistent paper format and content. The opinions and data presented are the sole responsibility of the authors and their respective organizations.

NASTRAN® and COSMIC® are registered trademarks of the National Aeronautics and Space Administration.

PRECEDING PAGE BLANK NOT FILMED

CONTENTS

Page

NASTRAN INTERNAL IMPROVEMENTS FOR 92 RELEASE

by

Gordon C. Chan
NASTRAN Maintenance Group
UNISYS Corporation
Huntsville, Alabama

SUMMARY

The 1992 NASTRAN release incorporates a number of improvements transparent to users. The NASTRAN executable has been made smaller by 70 percent for the RISC base Unix machines by linking NASTRAN into a single program, freeing some 33 megabytes of system disc space that can be used by NASTRAN for solving larger problems. Some basic matrix operations, such as forward-backward substitution (FBS), multiply-add (MPYAD), matrix transpose, and fast eigensolution extraction routine (FEER), have been made more efficient by including new methods, new logic, new I/O techniques, and, in some cases, new subroutines. Some of the improvements provide ground work ready for system vectorization. These are finite element basic operations, and are used repeatedly in a finite element program such as NASTRAN. Any improvements on these basic operations can be translated into substantial cost and cpu time savings. This paper also discusses NASTRAN in various computer platforms.

NASTRAN SINGLE LINK

The 91 NASTRAN RSIC base Unix version was released as a single link program. (The multi-link version can also be built.) The shell program that controls NASTRAN's execution was modified so that it can run NASTRAN under single- or multi-link environments automatically. The success of the single link Unix version (previously referred to as NASTRAN superlink) prompts the conversion of the 92 VAX/VMS NASTRAN into a single link program. The VAX single link program is extremely useful in debugging the Unix RISC version since the latter has extremely poor system diagnostics and provides no error trace-back. The biggest advantage of the single link version, and particularly in a small workstation environment, is that it needs only 25 percent of the disc space to hold the executable program as compared to the multi-link version, and 33 megabytes of disc space is returned to the system that can be used by NASTRAN for solving larger structures. It is also faster by almost 70 percent to build the single link NASTRAN as compared to the complete multi-link version. In program execution, the single link has no overhead for link-switching, and data saving and recovering between links are not needed. The single link versions, both in RISC base machines and VAX/VMS, appear to be running faster

1

since the program could be executing several "links" ahead of the screen printout if NASTRAN is executed interactively. For purposes of consistency, the single link program issues the link numbers as if the program were generated in multiple links. Presently, there are no single link versions for IBM, CDC, and UNIVAC machines.

NASTRAN IN VARIOUS MACHINE PLATFORMS

COSMIC/NASTRAN is supported in five computer platforms: IBM, CDC, UNIVAC, VAX/VMS, and DEC/ULTRIX (a RISC base Unix machine). However, the COSMIC/NASTRAN is continuously improved aiming towards a unified environment. ANSII standard FORTRAN 77 is used; and most of the machine dependent items are removed if possible. Some source codes are modified or re-written with system vectorization in mind. A far-reaching plan is initialized in the boot-strap (BTSTRP) subroutine that is used to set up machine-dependent constants for the five machines that COSMIC supports. The 92 COSMIC/NASTRAN has expanded the machine-dependent constant table in BTSTRP for 18 major computers and two dummies. A user, or a third-party organization, can install NASTRAN to a new platform currently not supported by COSMIC. Also, the users or third parties using the new computer platform can talk to one another since the machine type has been pre-arranged. The machine-constant table in BTSTRP is arranged for the following computers:

DUMMY, IBM, UNIVAC, CDC, VAX, DEC/ULTRIX (RISC base Unix), SUN, IBM/AIX, HP, SILIC.GRAPHICS, MAC, CRAY, CONVEX, NEC, FUJITSU, DATA GENERAL, AMDAHL, PRIME, 486, DUMMY

BTSTRP sets up the machine constants correctly only for the first six machines. The first DUMMY is set up for IBM 7094, which has long been obsolete, and therefore can be reused for any machine not on the list. The last DUMMY is intended for the same purpose. The constants for the remaining 14 machines are dummies or guess-values. Therefore before moving COSMIC/NASTRAN to any computer platform, one must first re-supply the correct machine dependent constants in BTSTRP for that machine. The machine constants are well defined in the BTSTRP subroutine, such as NBPW, number of bits per word; NBPC, number of bits per character; NLPP, number of lines per printout page, etc.

There are also a few machine-dependent constants outside BTSTRP that need to be set locally. These few constants are scattered in about eight or nine NASTRAN subroutines. For example, some of these constants involve convergent criteria used only locally, and therefore not at the same level of importance as those in BTSTRP. To locate these few machine-dependent constants has been made easy in the 92 NASTRAN release. If the first word of labeled common /MACHIN/ in a subroutine is MACHX, not just MACH, there are machine dependent constants that require fixing.

The main NASTRAN program in the single link environment is called NASTRN. In the

multi-link environment, each of the 15 links is a complete program by itself, and the main programs are NAST01, NAST02, NAST03,..., NAST15. There is something very special in NASTRN and in NAST01 in the 92 NASTRAN release. If the DEBUG flag in NASTRN or NAST01 is changed to 1, the so-called <LINK 1> portion of the single link NASTRAN, or the regular LINK 1 in the multi-link program, will go through a series of machine compatibility checks. The results will echo back to the user. If some things, or some parameters, are set incorrectly, NASTRAN will stop. For example, if the FORTRAN OPEN statement of a new computer platform is in byte count for the record length, RECL, and the user sets the corresponding constant in BTSTRP to word count, an error diagnostic will appear.

Due to COSMIC policy, the NASTRAN Maintenance Group has never tried to move NASTRAN outside the five designated computer domains. However, it was demonstrated by a user in 1991 that the DEC/ULTRIX version required only two minor changes to move NASTRAN to a SiliconGraphics machine; and those two changes have been incorporated back into the 1992 COSMIC/NASTRAN release. The NASTRAN Maintenance Group in UNISYS welcomes any contribution from the users or third parties, concerning the migration of NASTRAN to different computer platforms.

INTERNAL IMPROVEMENTS

The PROFILER, a performance analyzer of the VAX/VMS machine, was used to identify the major time consuming elements in several typical NASTRAN runs. This was followed by a major effort to look into the logic, computing mechanism, methods of calculation, order of execution, paging, vectorization etc. of the time consuming areas, and to search for improvements. Most of the time consuming elements are basically standard matrix operations, and they are the essential elements of a finite element program. Their treatments are either "textbook standard", or "company proprietary". Generally speaking, the original NASTRAN developer did a very fine job in these areas. Further improvements are not easy, and cannot be treated lightly or as short projects. Indeed, several of the 1992 internal improvements were made in periods of several weeks, not days. Some improvements were made on top of previous improvements or newly written subroutines. Sometimes a simple line of improvement may require days of careful study, thorough understanding of the program algorithms, and the theoretical treatment of the subject. The final improvements in the 92 NASTRAN release are quite satisfactory. Several slow moving areas are speeded up 25 to 30 percent, and in some areas, three to five times faster. Appendix A tabulates some of the test results. Most of the new internal improvements of the 92 NASTRAN release can be removed by DIAG 41.

The following sections of internal improvements apply only to large matrix operations. Usually the matrices are many times larger than the available computer core memory can hold at one time. Many of the matrix operations must be done by parts, or in a number of passes.

IMPROVED FORWARD-BACKWARD SUBSTITUTION

The forward-backward substitution (FBS) is used for matrix inversion, load-solution, eigenvalue iteration, and many other applications that follow matrix decomposition. If the number of columns on the solution side of the equation is large, FBS can be very time consuming. It could easily take 10 to 20 times longer to go through FBS than to do the matrix decomposition.

In NASTRAN, the driver for FBS is the subroutine FBS. The actual FBS computation takes place in FBS1, FBS2, FBS3, or FBS4 for real single precision, real double precision, complex single precision, and complex double precision calculation respectively. If FBS requires more than seven passes, the new improvements will automatically kick in. The improvements are in four new subroutines, FBSI, FBSII, FBSIII, and FBSIV, similarly arranged as the subroutines FBS1/2/3/4. The new improvements include reduced I/O operations, large data blocks, and new row-and-column matrix multiplication. The new FBSI/II/III/IV are about 30 to 50 percent faster than the original FBS1/2/3/4, as tested in COSMIC's VAX/VMS machine.

THE FEER METHOD

Seventy to seventy-five percent of the cpu time used by the FEER method (the fast eigenvalue extraction method, with real tridiagonal reduction) is actually spent in the subroutine FNXTVC (double precision version) or FNXTV (single precision version). The main time consumer in FNXTVC/FNXTV is the forward-backward substitution operation. Unlike the FBS module, the open core in FEER method is not fully used, and particularly not in FNXTVC/ FNXTV subroutines. The improvements in FNXTVC/FNXTV include reduced I/O operations, full utilization of the core space, and new row-and-column matrix multiplication. The new improvements in FNXTVC/FNXTV alone produce impressive results – reducing the FEER method cpu timing by 30 to 200 percent, as tested on the VAX/VMS machine, and on a CRAY (tested on RPK/NASTRAN).

COSMIC/NASTRAN sometimes gives negative values for the rigid body eigenvalues. (They should be zeros.) Sometimes the negative values could be quite large (-1.E+5 range) particularly on the IBM machine. The explanation for this strange behavior, and the solution to the problem, may or may not match. On the solution side, since the rigid body frequencies are zeros, the 92 COSMIC/NASTRAN FEER method, by default, will set them to zeros. The second solution option is to reinforce certain key areas of computation in FNXTVC/FNXTV by quad-precision (real*16) for the 32-bit word machines, and by double-precision for the 60- or 64-bit word machines. This second option gives good results and moves the rigid body frequencies down to 1.E-6 to 1.E-12 range. However, it takes 2 to 3 times longer to compute.

To activate quad-precision calculation in a 32-bit word machine or double-precision in a 60- or 64-bit word machine in FEER method, one only needs to replace the BCD word "FEER" on the third field of the EIGR bulk data card by "FEER-Q". Replacing "FEER" by "FEER-X"

will prohibit the substitution of zeros for the rigid body frequencies.

Now to explain what happens to produce the negative eigenvalues. The criterion for orthogonality convergence EPSILON is 1.E-28 for the 32-bit word machines using double precision computation, and 1.E-24 for the 60- and 64-bit word machines using single precision computation. In FNXTVC/FNXTV, the accumulated sum of a mode shape is compared to EPSILON. The accumulated sum at the end of a do loop is the difference of two very close numbers. Therefore this very small numeric difference is a function of the number of digits a computer word can hold. Most 32-bit word machines with double precision calculation, and most 60- or 64-bit word machines with single precision, are limited to 14 to 16 digits per word, and therefore down to only 1.E-14 to 1.E-16 numeric accuracies. Here, the mantissa as well as the exponent of a data word is important! Since all five computers supported by COSMIC exhibit this accuracy problem, it becomes meaningless to do an orthogonality check by comparing the result to EPSILON, which is another 10 to 14 decades smaller. To home in to the size of EPSILON could end up producing big numeric errors. (Just a guess here.) Since the mantissa of an IBM machine word, in double precision, is smaller than a VAX, IBM seems to produce big negative rigid body eigenvalues more often than the VAX. Similarly the 60-and 64-bit machine using single precision computation could be worse than IBM.

In the 92 NASTRAN release, an attempt is made to avoid the above dilemma. The orthogonality convergence criterion is based on a ratio instead of the finite difference of two very close numbers. However, presently there is not enough test data to verify that is a good fix.

NEW LOGIC FOR MATRIX TRANSPOSE

Matrix transpose of a matrix which is too big to reside completely in the computer core memory is not an easy task. It can be done, but it may use up lots of cpu time. Lots of I/O may be involved here, and perhaps a high percentage of system paging if a virtual machine is used. The problem here is how to do the matrix transpose in seconds instead of minutes, or in minutes instead of hours. A good algorithm here is a treasure, and quite often, it becomes a "company proprietary" product.

The out-of-core matrix transpose in NASTRAN is handled by the subroutine TRNSP. The algorithm there is amazingly powerful. The only drawback is that it uses up to nine scratch files. The scratch files are supplied by the calling routines. The more scratch files passing over to TRNSP, the bigger matrix transpose TRNSP can do. There is no check in TRNSP of the actual scratch files requirement. Again, there are lots of I/O, data packing, and unpacking involved.

If only 1/50th of the matrix can be loaded into the computer core memory space at one time, TRNSP will complete the transpose task in 50 passes. A new matrix transpose subroutine TRNSPS has been written for 92 COSMIC/NASTRAN. If the passes exceed seven, TRNSP will switch over to TRNSPS automatically, if and only if DIAG 41 is not turned on by the user.

5

TRNSPS uses only one scratch file. The I/O department and the data packing and unpacking are greatly reduced. The new TRNSPS is two to four times faster than the original TRNSP.

MPYAD, MPY4T, AND MPYDRI

Matrix multiplication and addition are basically the most important and most widely used tools for a finite element program. If the matrices are small and can reside completely in core, multiply-add has no problem; and three simple do-loops will complete the job. Again, if the matrices are bigger than the computer core can hold, matrix multiplication and addition have to be done by parts, and there will be many passes, many I/O operations, and many row- and column-packings and unpackings. The problem can become I/O bound, and lots of cpu time will be spent on getting and saving the intermediate results. The situation is further complicated in NASTRAN in that the matrices can be of different types (single precision or double precision; real or complex), or of different forms (rectangular, square, diagonal, identity that may or may not exit, lower or upper triangular, row vector, or symmetric), or transpose and non-transpose matrices.

There are five multiply-add (MPYAD) methods in NASTRAN, two methods for the non-transpose case (MPY1NT and MPY2NT) and three for MPYAD with transpose (MPY1T, MPY2T and MPY3T). NASTRAN selects internally the best method to use based on the cpu time requirement of each method that fits best for a given matrices-and-core environment. The cpu time requirement is a function of size and shape (rows and columns), form and density of the matrices, and core space. The cpu time requirement is also a function of the relative sizes and shapes of the matrices. That is, matrix A may be very big and cannot reside in core, while matrix B is small, and matrix B may or may not be loaded entirely into the available core space. Or vice versa. All five MPYAD methods are written in assembly languages for four out of five COSMIC supported machines, except VAX.

Matrix transpose is supposedly very slow. The programmer manual recommends matrix transpose be done via MPYAD with transpose, and an identity matrix. This turns out not to be very efficient. Two test matrices A and B, 5166x5166 each, using the best of MPY1NT or MPY2NT, can be multiplied together in 470 cpu seconds (on the VAX machine), while A-transpose times B, using the best of MPY1T, MPY2T, and MPY3T requires 6680 cpu seconds. That is 12 times longer! If matrix A is transposed first by TRNSP routine (TRNSPS is not used), then followed by MPYAD without transposing, the total cpu time can be cut to half. The only problem here is that at least one extra scratch file is needed to save the transpose file, and in many instances, there is no extra scratch file available.

MPY1NT and MPY1T share much common logic, and operate quite similarly. The same holds true for the MPY2NT and MPY2T pair. MPY3T is a third method for the transpose case. The best method for the test matrices A and B above, with transpose, is MPY2T. One would think that since NASTRAN stores a matrix by column, and that a column of matrix A transpose

6

is a row of A, the row-and-column multiplication (matrix A in row and matrix B in column) should be very fast, very smooth, and very convenient. One could almost feel and touch the natural flow of the multiplication algorithm. But what one can feel or imagine, is not what a computer sees. The row-and-column multiplication produces only one element in the resulting matrix. There are more than 26 million (5166^2) double precision elements to go. Anyway, the fact is that MPY2T takes 12 times longer than MPY2NT.

Several methods, several logics, and several new algorithms were developed and tested to beat the clock set by MPY2T. The ultimate goal is to match the MPY2NT performance if possible. Finally, after many trials, a fourth method, MPY4T, was developed based on the scheme similar to MPY2T, except that matrix B (and matrix C, to be added if it is present), and the resulting matrix D are processed by column instead of by element. Of course, the logic in MPY4T becomes much more complicated and the open core must be rearranged. But MPY4T is three to five times faster than MPY2T. In the 92 NASTRAN release, MPY4T will be automatically substituted for MPY2T, unless DIAG 41 is turned on by the user. MPY4T is written in FORTRAN, and it is machine independent.

The original MPYAD does not take advantage of certain types of matrices. For example, the transpose of matrix A which is symmetric, need not go through the transpose route. (This is already checked in the 91 release.) A new subroutine, MPYDRI, is added to the 92 release to handle special cases involving diagonal matrix, row vector, and identity matrix.

The correct handling of these special matrices expedites the MPYAD process by manyfold.

NEXT IMPROVEMENTS UNDER CONSIDERATION

The internal improvements in the 1992 NASTRAN release tackle a few important, and often-used, basic finite element tools with satisfactory results. However, there are many more areas in NASTRAN that can be explored. There are still several areas involving FBS that have not been touched. The matrix decomposition process could be improved. All the complex computations involving complex FBS, complex decomposition, complex FEER method, and more, are targets for the next improvements. Nevertheless, the internal improvements in 1992 NASTRAN release represent the beginning of an extraordinary effort to bring NASTRAN up to par.

APPENDIX A

Demo problem D03012A was used in most of the following tests. The D03012A demo produced a double precision KGGX matrix of size (5166 x 5166) and a KAA (2380 x 2380), double precision. The trailer of the KGGX matrix in some cases had to changed from "symmetric" to "square" so that NASTRAN did not take the symmetric route processing the modules under investigation. Tests were done on a VAX/VMS machine, unless stated otherwise. In most cases, HICORE is 350,000 words.

FBS test: KAA

1991 Version	1992 First Version	1992 Second Version
5644 cpu seconds	3508 cpu seconds	3120 cpu seconds

FEER method

1991 VAX Version	1992 VAX Version		
	GINO Improvement	Open Core Not Used	Open Core Used
1043 cpu seconds	978 cpu seconds	907 cpu seconds	763 cpu seconds
1991 CRAY Version	1991 CRAY Version Plus Changes – Open Core Used		
45.7 cpu seconds	21.8 cpu seconds		

MPYAD, KGGX(transpose) * KGGX + KGGX

DIAG 41 On	With MYADT (Obsolete)	MPYAD With New TRNSPS	MPYAD With New MPY4T	If Symmetric Matrix Allowed
6681 cpu secs.	3871 cpu secs.	2114 cpu secs.	1358 cpu secs.	469 cpu secs.

EVOLUTION OF A NASTRAN TRAINER

H.R. Grooms, P.J. Hinz, and M.A. Collier

Rockwell International
Downey, California

INTRODUCTION

This paper traces the development of a NASTRAN training system. It encompasses the design and organization of the program, including the static and dynamic modules. A discussion of how user feedback, in the form of questionnaire responses, was used to evaluate and improve the trainer is included.

BACKGROUND

The user-friendly NASTRAN trainer was originally designed as a segment of a larger system (ref. 1). After the static module was developed, used, and evaluated (ref. 2), it became clear that the trainer concept readily lent itself to a wide range of applications.

The NASTRAN trainer (figure 1) was initially conceived as a low-cost, convenient tool for giving engineers who were novices in finite element analysis a few practical applications of the method. Although several very good short courses and classes on NASTRAN are available, most are offered periodically and cost $200 to $800 per person. These classes usually require the engineer to set aside his current work assignment and devote his full time to the class for anywhere from a couple of days to a couple of weeks. When funds are low or schedules are tight, the money or time required for these classes can be insurmountable barriers.

Various researchers have developed computer programs for structural analysis and design applications. Ginsburg (ref. 3) addresses computer literacy, and Woodward and Morris discuss improved productivity through interactive processing (ref. 4). Wilson and Holt (ref. 5) developed a system of computer-assisted learning in structural engineering. Sadd and Rolph (ref. 6) describe the various ways in which design engineers could be trained to use the finite element method. Self-adapting menus for computer-aided design (CAD) software are covered by Ginsburg (ref. 7).

Bykat (ref. 8) is developing a system that will have features for training, analysis control, and interrogation.

STATIC MODULE

The static module was developed to provide the user a variety of different types of problems. The ten problems generally increase in difficulty as their numbers increase. Table I describes each problem, and figures 2 and 3 show the problems. Figure 4 gives the classical solution for static example 6.

The user may work the problems in any order.

DYNAMIC MODULE

The dynamic module contains eight problems (table II) of increasing complexity. The problems are shown in figures 5 and 6. A classical solution for dynamic problem 4 is presented in figure 7. The examples were selected to allow the user to decide on:

1. Grid fineness

2. Mass representation

3. Number of degrees of freedom retained

4. Particular degrees of freedom retained

Each of these decisions can have a significant bearing on the accuracy of the eigensolution.

A complete description of this module is given in ref. 9.

TRAINER ORGANIZATION

The NASTRAN Environment (NE) is written for the IBM computer system running MVS/ESA SP 4.1.0 using TSO/E 2.1.0. It uses the features provided by the dialogue management services under ISPF/PDF to the fullest extent. This includes panels, skeletons, CLISTs, and tutorial services. In addition, the trainer requires VS/FORTRAN and VS/Pascal compilers if the executable code is not directly portable. Newer versions of any of these services should not invalidate the NE if the improvements are upwardly compatible.

The NE has job setups to execute MSC/NASTRAN and COSMIC/NASTRAN on IBM and/or MSC/NASTRAN on the Cray running Unicos 6.1. At least one of these programs must be available for the NE to be used as intended. These codes are not delivered with the NE.

The NE comprises 15 datasets; 14 are partitioned and 1 is sequential. These datasets are listed below with a brief explanation of their contents. Figure 8 illustrates the organization of the NE datasets.

- ALTER—Rigid format alter library for NASTRAN. Must be updated with each release of a new version of NASTRAN. Not a requirement for the trainer and most NASTRAN users.

- CLIST—Procedural commands to invoke the NE, allocate and manage datasets, create and submit batch jobs, invoke the SPF editor and initialize profile variables.

- MSGS—Messages that appear on panels for information, caution, and warning.

- PNLZ (Environment)—Panels that serve as the user interface. All information that the user inputs and the system outputs is through panels. This includes data entry screens, system news, help sections, user manuals, problem descriptions, and classical solutions.

- DOC—Documentation on efforts to develop NASTRAN expert systems.

- FORT—FORTRAN programs and subroutines that compute the classical solutions and extract system jobcard information.

- INP—Input decks that are example solutions to the NASTRAN trainer problems.

- LOAD—Load modules of the compiled and linked FORTRAN and Pascal programs.

- LOG—Log of NASTRAN trainer usage for each NASTRAN trainer job submitted.

- OBJ—Object modules of the compiled FORTRAN and Pascal programs.

- OUT—Output decks that are example solutions to the NASTRAN trainer problems.

- PVS—Pascal program that produces a report of the usage of the NASTRAN trainer.

FUTURE ENHANCEMENTS AND USER FEEDBACK

Modules for elastic stability (buckling) and substructuring are in the planning stage. These additions are planned as self-contained units that can be used by anyone who has completed the static module.

Users of the static module were asked to fill out a questionnaire. The questions and responses are shown in figure 9. Another questionnaire is currently being used to solicit opinions about the dynamic module.

CONCLUSIONS

The NASTRAN trainer has been used by a number of engineers, who found it to be a versatile low-cost tool. It is particularly helpful in bridging the gap from theory to practical application of the finite element method for structural analysis. The program, along with documentation, is available through COSMIC.

REFERENCES

1. Grooms, H.R., W.J. Merriman, and P.J. Hinz: An Expert/Training System for Structural Analysis. Prepared for presentation at the ASME Conference on Pressure Vessels and Piping, New Orleans, Louisiana, June 1985.

2. Grooms, H.R., P.J. Hinz, and K. Cox: Experiences With a NASTRAN Trainer. Prepared for presentation at the 16th NASTRAN Users' Colloquium, Arlington, Virginia, April 1988.

3. Ginsburg, S.: Computer Literacy: Mainframe Monsters and Pacman. Prepared for presentation at the Symposium on Advances and Trends in Structures and Dynamics, Washington, D.C., October 1984.

4. Woodward, W.S., and J.W. Morris: Improving Productivity in Finite Element Analysis Through Interactive Processing. Finite Elements in Analysis and Design, vol. 1, no. 1, 1985.

5. Wilson, E.L., and M. Holt: CAL-80-Computer Assisted Learning of Structural Engineering. Prepared for presentation at the Symposium on Advances and Trends in Structures and Dynamics, Washington, D.C., October 1984.

6. Sadd, M.H., and W.D. Rolph III: On Training Programs for Design Engineers in the Use of Finite Element Analysis. Computers and Structures, vol. 26, no. 12, 1987.

7. Ginsburg, S.: Self-Adapting Menus for CAD Software. Computers and Structures, vol. 23, no. 4, 1986.

8. Bykat, A.: Design of FEATS, a Finite Element Applications Training System. Prepared for presentation at the 16th NASTRAN Users' Colloquium, Arlington, Virginia, April 1988.

9. Grooms, H.R., P.J. Hinz, and G.L. Commerford: A NASTRAN Trainer for Dynamics. Prepared for presentation at the 18th NASTRAN Users' Colloquium, Portland, Oregon, April 1990.

TABLE I.-STATIC EXAMPLE PROBLEMS

Example	Description	Significant Features
1	Statically determinate plane truss subjected to point load	Bar elements, stability constraints
2	Beam simply supported on one end and fixed at the other subjected to point load	Beam elements
3	Beam fixed at both ends subjected to through-the-depth temperature difference	Temperature input
4	Plane frame subjected to point load	Half-model, symmetric, and antisymmetric loads
5	Simply supported beam subjected to temperature pattern	Half-model, temperature distribution decomposed into symmetric and antisymmetric parts
6	Plate with hole in center subjected to in-plane load	Plane stress, quarter-model, fine grid around hole
7	Simply supported square plate subjected to out-of-plane point load at center	Plate-bending elements, quarter-model
8	Three-dimensional frame subjected to point load	Tapered beams, three-dimensional
9	Cylindrical shell subjected to hydrostatic loading	Three-dimensional simulation of curved surface using flat elements
10	Cylindrical shell with ring frames closed at both ends subjected to internal pressure	Self-equilibrating loading, three-dimensional

TABLE II.-DYNAMIC EXAMPLE PROBLEMS

Example	Description	Significant Features
1	Beam simply supported on both ends with lumped mass in middle	Motion in one plane only, lumped mass only
2	Beam simply supported on both ends with uniformly distributed mass	Motion in one plane only, distributed mass
3	Beam fixed on one end with a lumped mass at the free end	Motion in any direction, lumped mass only
4	Beam fixed on one end with a uniformly distributed mass	Motion in any direction with uniformly distributed mass
5	Rectangular plate clamped on one edge, all other edges free, with a uniformly distributed mass	Plate bending with distributed mass
6	Rectangular plate, free-free with uniformly distributed mass	Free-free (implies six modes with zero frequency)
7	Two beams connected by springs, each with distributed and lumped mass	Multibody problem, free-free
8	Problem 7 with a forcing function added	Forcing function

Primary Menu
- Overview
  - System Supplement
  - System Overview
  - System Commands
- User's Guide
  - What is NASTRAN?
  - A NASTRAN Data Deck
  - Modeling Guidelines
  - Getting Started
  - MSC Vs. COSMIC
- Problem Set and Main Menu
  - Statics
    - Problem Discussion
    - NASTRAN Environment
    - Classical Solution
  - Dynamics
    - Problem Discussion
    - NASTRAN Environment
    - Classical Solution

NASTRAN Environment
- Edit
- MSC
- COSMIC
- Status
  - Browse
  - Print
  - Help
    - Model Bombed During Execution
    - Model Gives Incorrect Results
    - Example Input Deck
    - Example Output Deck
    - MSC/NASTRAN Alter Library
    - Bulk Data Cards
    - Plotting Information
    - Coordinate Systems
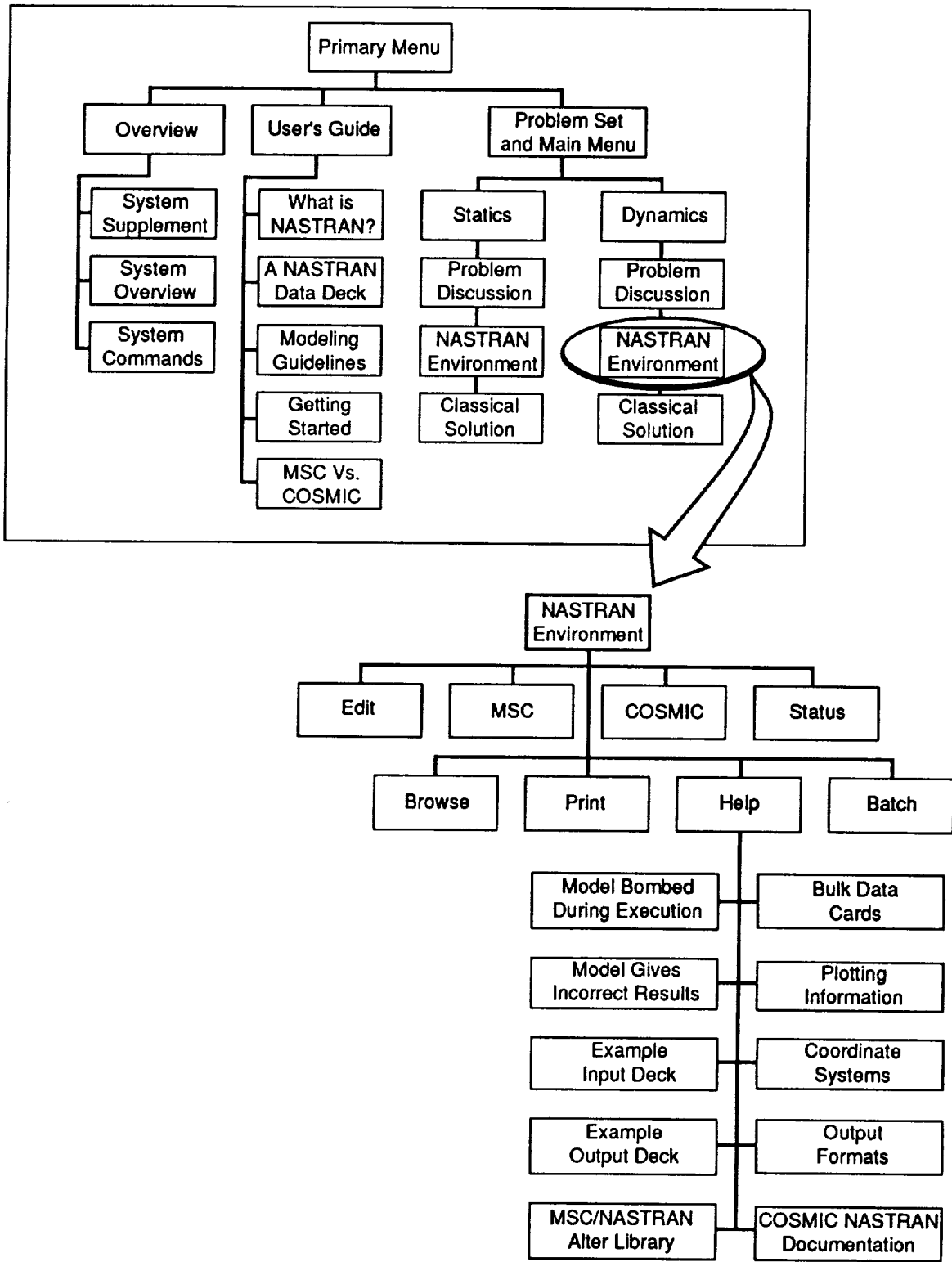   - Output Formats
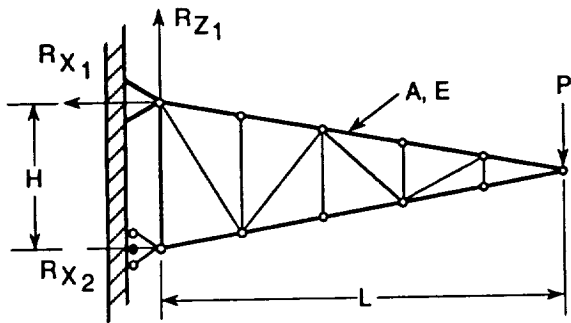   - COSMIC NASTRAN Documentation
  - Batch

MTD 920210-3132

FIGURE 1.–THE STRUCTURE OF THE TRAINER

14

Static Problem 1 – Two-Dimensional Truss
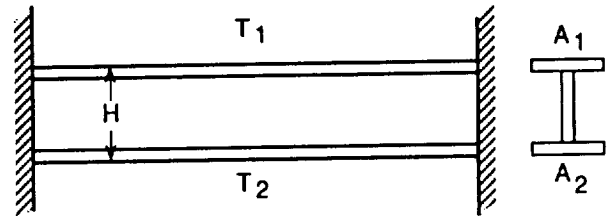
Static Problem 3 – Beam Fixed at Both Ends
With Temperature Loading
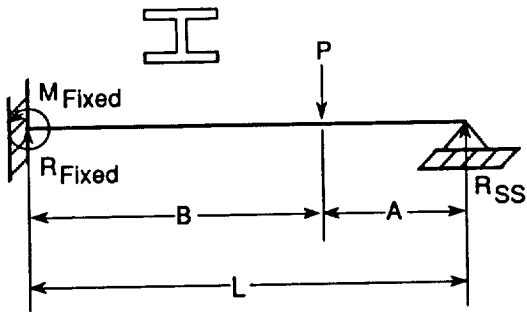
Static Problem 2 – Beam With Point Load
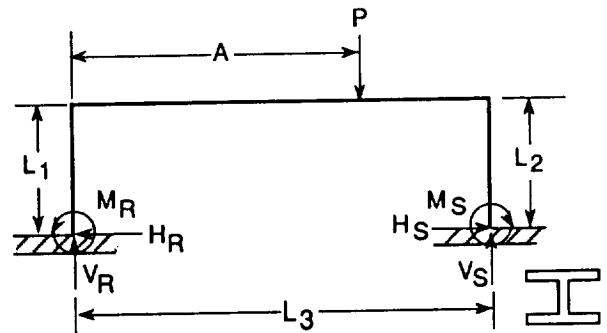
Static Problem 4 – Plane Frame Subjected
to Point Load

MTD 920210-3133

FIGURE 2.–STATIC PROBLEMS 1 TO 4
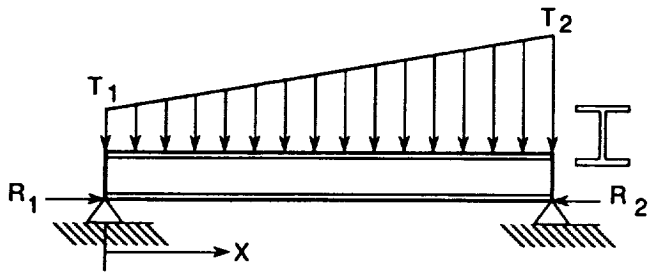
Static Problem 5 – Simply Supported Beam Subjected to Temperature Pattern
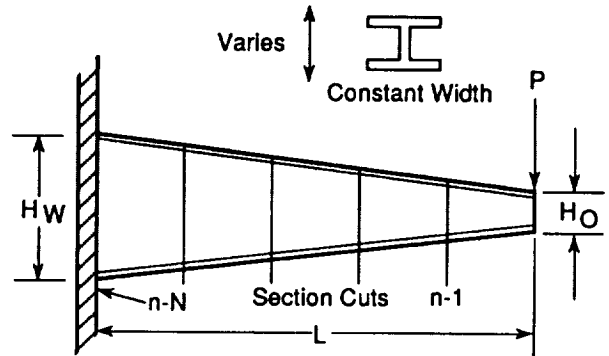
Static Problem 8 – Tapered Beam Subjected to Point Load
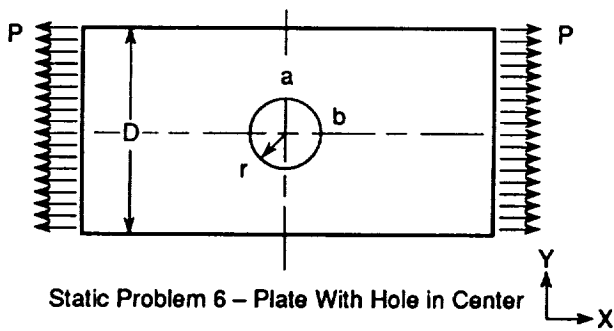
Static Problem 6 – Plate With Hole in Center
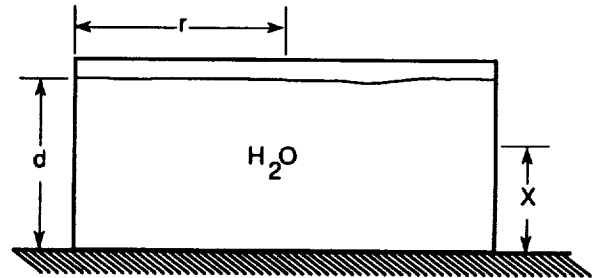
Static Problem 9 – Cylindrical Shell Subjected to Hydrostatic Loading
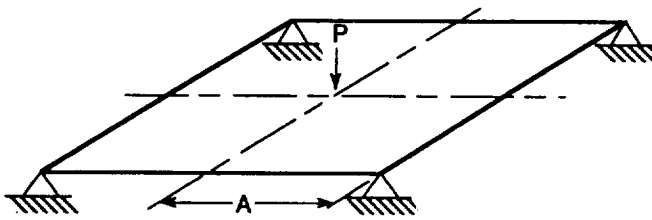
Static Problem 7 – Simply Supported Square Plate
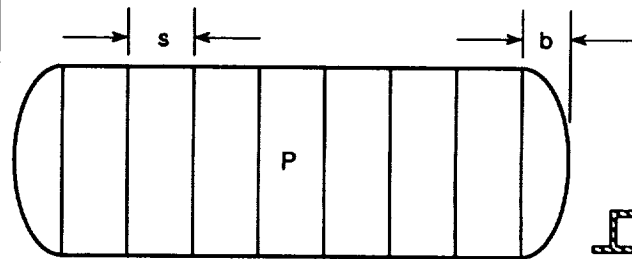
Static Problem 10 – Cylindrical Shell With Ring Frames Subjected to Internal Pressure

MTD 920211-3134

FIGURE 3.–STATIC PROBLEMS 5 TO 10

16

Static Problem 6 – Plate With Hole in Center
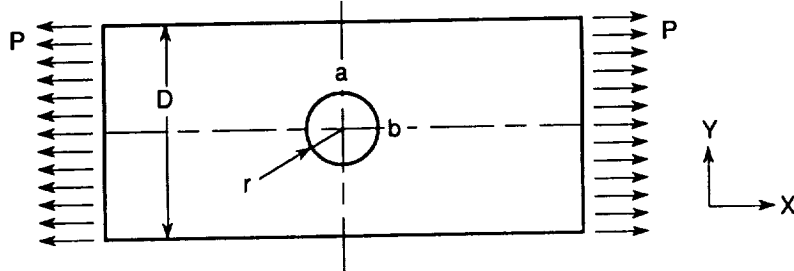
P = Running Load (lb/in.)
D = Width of Plate (in.)
t = Thickness of Plate (in.)
r = Radius of Hole (in.)
σ_T = Stress at Distance From Hole (psi)
σ_X = Stress (X) at Hole (psi)
σ_Y = Stress (Y) at Hole (psi)

Classical Solution:

Calculate σ_X at Point a:

$$\sigma_X = \sigma_{max} = \sigma_a = k\sigma_{nom}$$

Where $\sigma_{nom} = \dfrac{PD}{t(D - 2r)}$

$$k = 3.00 - 3.13(\frac{2r}{D}) + 3.66(\frac{2r}{D})^2 - 1.53(\frac{2r}{D})^3$$

Calculate σ_Y at Point b:

$$\sigma_T = \text{Stress at Distance From Hole} = \frac{P}{t}$$

$$\sigma_Y = \sigma_b = -\sigma_T$$

Reference: Roark and Young. Formulas for Stress and Strain, 5th Edition, p. 594.

MTD 920210-3135

FIGURE 4.–CLASSICAL SOLUTION FOR STATIC PROBLEM 6

Dynamic Problem 1 – Simply Supported Beam With Concentrated Mass

Dynamic Problem 3 – Cantilever Beam With Concentrated Mass

Dynamic Problem 2 – Simply Supported Beam With Uniformly Distributed Mass

Dynamic Problem 4 – Cantilever Beam With Uniformly Distributed Mass
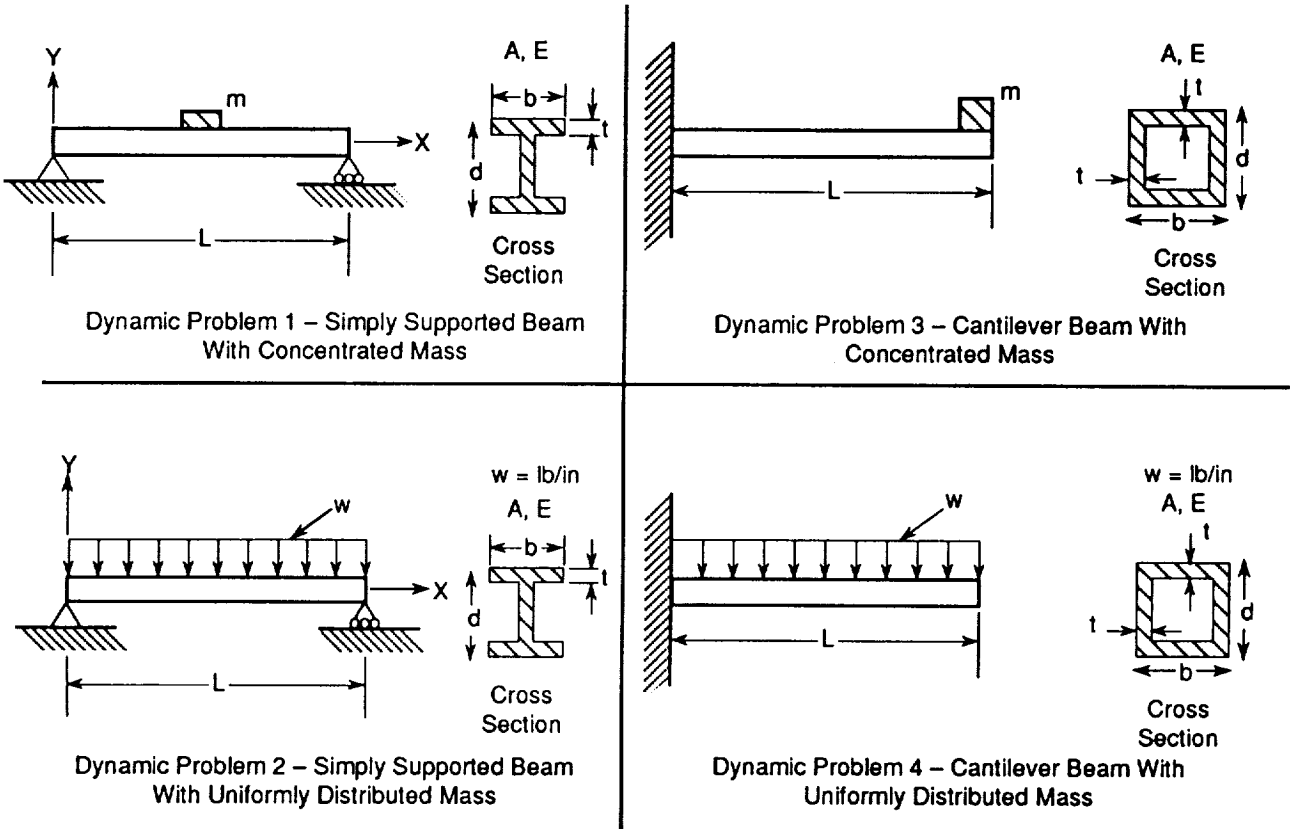
MTD 920210-3136

FIGURE 5.–DYNAMIC PROBLEMS 1 TO 4

18
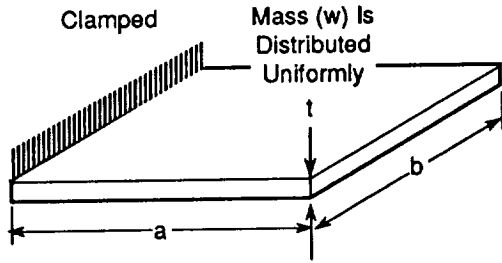
Dynamic Problem 5 – Rectangular Plate
Clamped at One Edge

Dynamic Problem 6 – Rectangular Plate
Free on All Sides

Dynamic Problem 7 – Two Beams Connected
by Two Springs
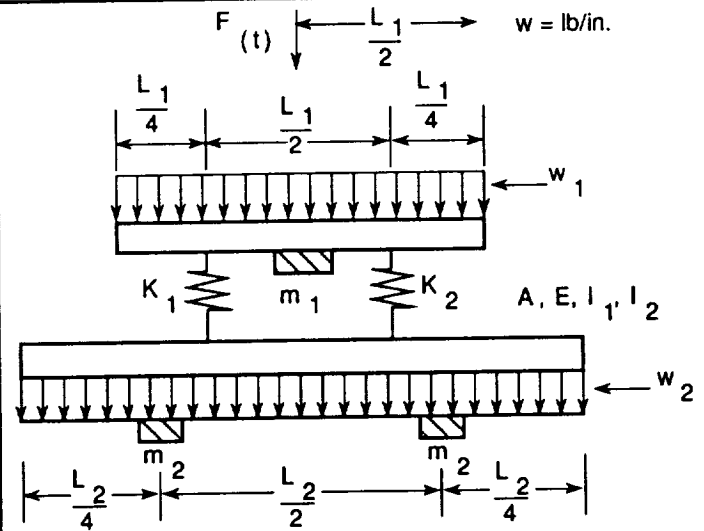
Dynamic Problem 8 – Two Beams Connected by
Two Springs Driven by a Forcing Function

MTD 920211-3137

FIGURE 6.–DYNAMIC PROBLEMS 5 TO 8

19

Dynamic Problem 4 – Cantilever Beam With Uniformly Distributed Mass
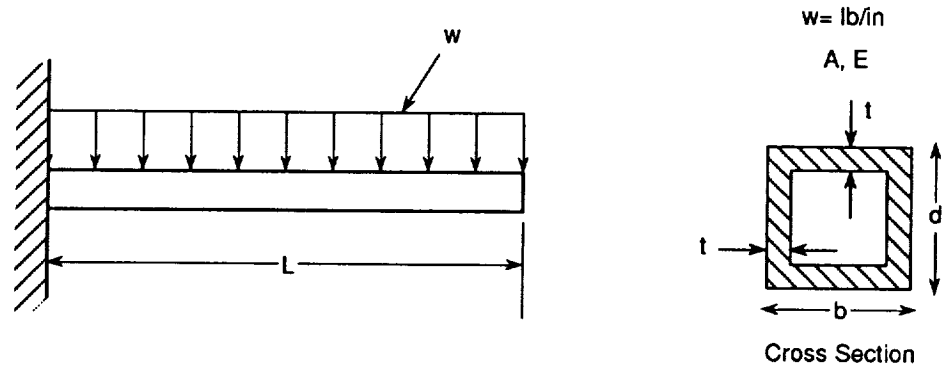
E = Modulus of Elasticity (psi)

I = Moment of Inertia (in.^{4})

μ = Distributed Mass (lb-sec^2/in.^{2})

L = Length of Beam (in.)

ω_n = Natural Frequency - Angular (rad/sec)

f$_n$ = Natural Frequency (cycles/sec or hertz)

Reference: Flügge, W.: Handbook of Engineering
Mechanics. McGraw-Hill
1962, pp. 61-8.

Classical Solution:

Calculate Natural Frequencies:

$$\omega_i = \frac{(0.597\,\pi)^2}{L^2}\sqrt{\frac{EI}{\mu}} \quad \text{(Fundamental Mode)}$$

$$\omega_n = \frac{(n - 1/2)^2\,\pi^2}{L^2}\sqrt{\frac{EI}{\mu}} \quad \text{(Higher Order Modes)} \atop (n > 1)$$

$$f_n = \frac{\omega_n}{2\pi}$$

Where n = 1, 2, ... (the Mode Number)

MTD 920212-3138

FIGURE 7.–CLASSICAL SOLUTION FOR DYNAMIC PROBLEM 4

20
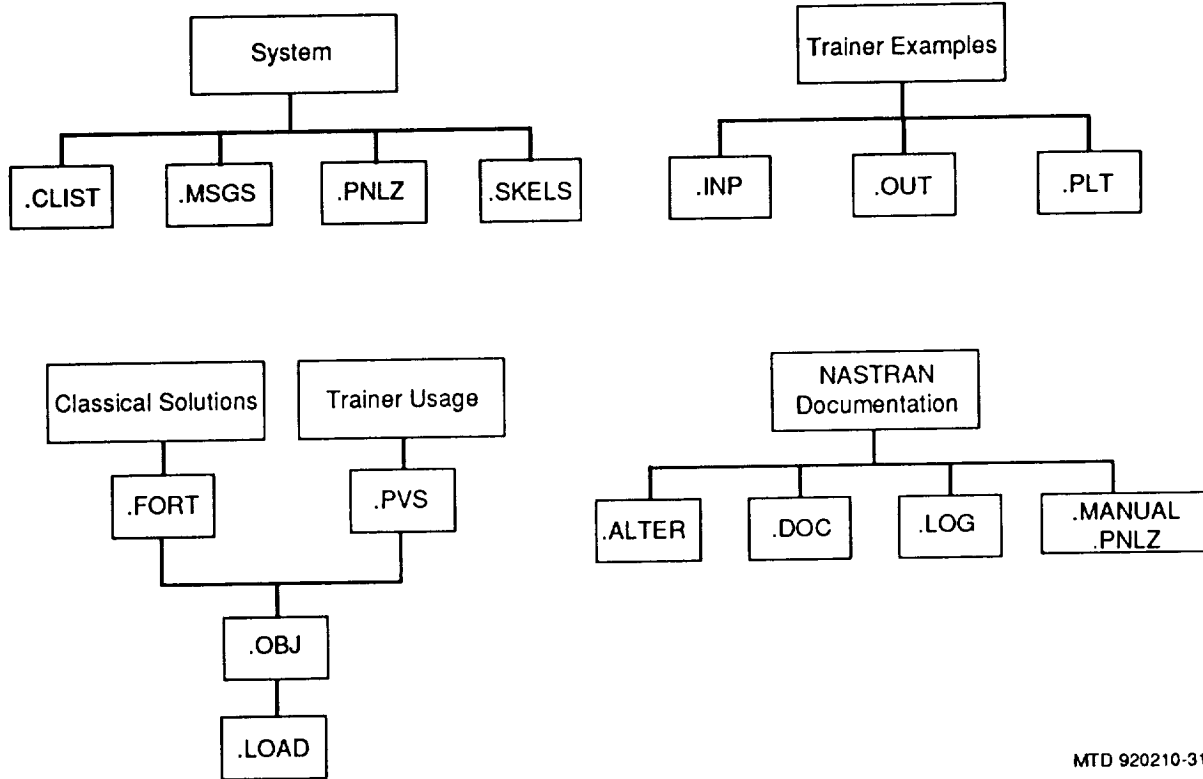
FIGURE 8.–NASTRAN ENVIRONMENT DATASET ORGANIZATION

Critique of NASTRAN Trainer

1   Was using this system a worthwhile expenditure of your time?
    a. Yes   (89%)
    b. No   (0%)
    c. Undecided   (11%)

2   How much total time would you estimate that you spent using the trainer?
    60 hours

3   How much total time would you have spent (estimate) to gain this knowledge if the trainer had not been available 135 hours

4   The number of examples was
    a. Too few   (17%)
    b. Too many   (6%)
    c. About right   (77%)

5   The system was
    a. Too simple   (17%)
    b. Too complicated   (6%)
    c. About right   (77%)

6   Could the trainer be improved by adding other topics?
    a. Yes   (67%)
    b. No   (22%)
    c. Maybe   (11%)

7   Which section, if any, should be expanded upon?
    (Wide variety of responses.)

8   How often (average) did you invoke the NASTRAN documentation manual section?
    a. Never   (44%)
    b. 0-2 times/example   (22%)
    c. More than 2 times/example   (34%)

9   Was the NASTRAN documentation section useful?
    a. Yes   (38%)
    b. No   (33%)
    c. Never used it   (29%)

10 How often did you use (average) the printed COSMIC or MSC NASTRAN manuals?
    a. Never   (6%)
    b. 0-2 times/example   (17%)
    c. More than 2 times/example   (77%)

11 Please add any additional comments you desire.
    (Responses vary from "great" to "give us more advanced problems.")

MTD 920211-3140

FIGURE 9.–QUESTIONNAIRE FOR USER FEEDBACK (STATIC)

ANIMATION OF FINITE ELEMENT MODELS AND RESULTS

Robert R. Lipman

David Taylor Research Center
Computational Signatures and Structures Branch (Code 1282)
Bethesda, Maryland 20084-5000

SUMMARY

Several years ago, the phrase 'visualization in scientific computing' (ref. 1) was coined for what we used to call computer graphics. Although computer graphics is part of visualization, visualization encompasses computer graphics hardware and software, network communications, user interfaces, computer-aided-design, and more. The purpose of visualization is to provide insight into the engineer's models and calculations. Animation of finite element models and results is a visualization process that can provide the insight.

The paper is not intended to be a complete review of computer hardware and software that can be used for animation of finite element model and results, but is instead a demonstration of the benefits of visualization using selected hardware and software. Opinions expressed are solely those of the author and are not those of the David Taylor Research Center, the Navy, or the Department of Defense. Good reviews of visualization hardware and software can be found in the following journals: Computer Graphics World, Supercomputing Review, IEEE Computer Graphics and Applications, and CAE Computer-Aided Engineering. A videotape showing visualization and animation of finite element models and results is an integral part of this paper although it is not included in the proceedings.

INTRODUCTION

Visualization and animation give an engineer insight into his finite element model and results. Wire-frame plots of a finite element mesh do not convey the sense that a 'real' structure has been modeled. We do not live in a wire-frame world. We live in a world of color, light, shading, and perspective. A beam is not a line between two points. A beam has a web and a flange of substantial size and cross-section. The transient motion of a structure cannot be determined from static plots at selected time steps or plots of the response of a node versus time. Visualization and animation can be used to show an engineer the realistic configuration and response of a structure.

The earliest animations of finite element analysis results were made by painstakingly recording a sequence of static plots on film. Some of the first computer animations of finite element analysis results were made on Evans & Sutherland graphics hardware (ref. 2). Today, with the price/performance of computer graphics hardware so low and visualization software packages becoming more mature, finite element model visualization and animation is now a desktop tool.

HARDWARE

It seems that computer workstation vendors are announcing faster and less expensive hardware almost every day. Current Cray X-MP supercomputer computational speeds should be available in desktop computer workstations in 1-2 years. By the time this paper is presented, the 1-2 year time frame may have been reduced from years to months. The cost of memory and hard disk storage is also falling.

As important as raw computational power is to animation and visualization, graphics speed is equally important. Graphics speed, usually quoted in polygons per second, is not increasing as fast as computational speed. Rather, the cost of current graphics power is getting less expensive. Current peak graphics speeds of 200,000 polygons per second can be found on the top-of-the-line graphics workstations. The user must beware of the type of polygon that the vendor uses when quoting graphics speed. Quotes of one million polygons per second are usually for highly optimized meshes of triangles without light-source shading. For animation of finite element models, the graphics speed for independent quadrilateral polygons is more relevant.

When computation and visualization take place in a distributed environment, communications speed between the client and server is another important issue. Today, animations of finite element analysis results are typically done in a batch mode. The analysis is done on a large mainframe or supercomputer and the results are sent to a workstation to be used with visualization software. In the future, the two processes of analysis and visualization will be more tightly coupled where the analysis and visualization are being computed concurrently. For this scenario to take place, much higher network communications speed between the computational server and visualization server will be necessary than current local- and wide-area networks provide.

Finally, animation sequences have to be recorded to videotape. There are two methods for recording computer graphics animations on videotape: real-time and frame-by-frame. For real-time recording, the computer graphics display is converted, in real-time, to a television signal suitable for recording on videotape and being displayed on a regular television monitor. Therefore, whatever is being displayed on the computer graphics display can be recorded to videotape. If the graphics speed is fast enough to animate a finite element model in real-time, then this process is sufficient.

With graphics hardware that is not fast enough and with visualization software that has a rendering capability, then frame-by-frame recording can be used. The visualization software renders individual images that are recorded one-by-one on videotape. The result is a continuous animation sequence. Frame-by-frame recording also produces higher quality animations and renderings than real-time animation.

SOFTWARE

Visualization software packages can be separated into three categories: general-purpose, modular, and application specific. The types of data that the packages can visualize are usually either structured or unstructured grids. A structured grid is typical for finite-difference applications such as computational fluid dynamics. A finite element mesh is an example of an unstructured grid. Many of the general-purpose visualization packages (PV-Wave, Spyglass, Data Visualizer) are very good with structured grids and less useful for finite element applications. There are also several application specific visualization packages (Fieldview, Fast, Plot3D) that

can be used with only structured grids. The modular visualization packages (AVS, Iris Explorer, apE) allow users to write their own applications specific software modules to be integrated with the visualization software.

There are few choices for application-specific visualization packages for finite element analysis animation. The popular finite element pre and postprocessors (Patran, I-DEAS) have animation capabilities, but are not oriented to the visualization process and to recording video-tapes. FOTO (ref. 3) is a data visualization software package geared towards finite element models and animation. FOTO was used to make the videotape that is part of this paper. FOTO is easy to interface with analysis codes; is user-definable menu driven; has many visualization types including: color, displacement, contour lines, vectors, transparency, and culling operators; and has a tightly coupled videotape system.

There are also free visualization software packages available from the national supercomputer centers. Because they are free, the source code is provided allowing the user to tailor the code to his application. However, because they are free, the user will not get the same type of support or updates to the software that a commercially available package would provide.

THE FUTURE

What is currently possible for finite element animation and visualization is not the final product, but only a step towards a more interactive, dynamic environment for doing analysis and visualization. In the future, analysis and visualization will occur concurrently in near real-time and the engineer will have the capability to interact with the analysis by changing the finite element model as the computations are taking place to explore new configurations of the model.

REFERENCES

1. McCormick, B.H., T.A. DeFanti, and M.D. Brown; Editors, "Visualization in Scientific Computing," ACM SIGGRAPH, November 1987.

2. Lipman, R.R., "Computer Animation of Modal and Transient Vibrations," in: *Proceedings of 15th NASTRAN Users' Colloquium,* 4-8 May 1987, Kansas City, Mo., National Aeronautics and Space Administration, NASA CP-2481, pp. 111-117, Washington, D.C. (1987).

3. "FOTO User Manual," Cognivision, Inc., Westford, MA, 1992.

ACCURACY OF THE TRIA3 THICK SHELL ELEMENT

William. R. Case, Marco Concha and Mark McGinnis
NASA/Goddard Space Flight Center

SUMMARY

The accuracy of the new TRIA3 thick shell element is assessed via comparison with a theoretical solution for thick homogeneous and honeycomb flat simply supported plates under the action of a uniform pressure load. The theoretical thick plate solution is based on the theory developed by Reissner and includes the effects of transverse shear flexibility which are not included in the thin plate solutions based on Kirchoff plate theory. In addition, the TRIA3 is assessed using a set of finite element test problems developed by the MacNeal-Schwendler Corp. (MSC). Comparison of the COSMIC TRIA3 element as well as those from MSC and Universal Analytics Inc. (UAI), for these test problems is presented. The current COSMIC TRIA3 element is shown to have excellent comparison with both the theoretical solutions and also those from the two commercial versions of NASTRAN with which it was compared.

INTRODUCTION

The TRIA3 thick shell element was added to the 1990 release of COSMIC NASTRAN. Along with the QUAD4, the two new shell elements represent a significant increase in the capability of COSMIC NASTRAN to model complicated shell structures. The deficiencies of the original TRIA1,2 and QUAD1,2 shell elements have been recognized for years and have been reported in the literature. At the Goddard Space Flight Center (GSFC), the triangular and quadrilateral shell elements are used in virtually all structural analyses of our spacecraft and related hardware. Typical applications are for the modeling of cylindrical shells and flat plates made of honeycomb or machined, lightweighted, metal that make up the structure of spacecraft and scientific instruments. In some cases these models require that the effects of transverse shear flexibility be included due to their thickness. The TRIA3 and QUAD4 elements include these effects. The QUAD4 element has, in addition, an improved membrane capability for in-plane loading. The TRIA3 element, due to it's limited number of degrees of freedom retains the constant strain membrane capability of the older TRIA1 and TRIA2 elements. This necessitates finer meshes for in plane loading cases than would be required when using the QUAD4 element.

The purpose of the study reported herein is to assess the accuracy of the TRIA3 element in modeling a variety of situations involving both solid cross-section plates as well as those constructed of honeycomb. An identical study for the QUAD4 element was reported in the 18th NASTRAN User's Colloquium and is documented in reference 1. As with the QUAD4 study, the three goals of the TRIA3 study were to determine:

a) what is the rate of convergence to the theoretical solution as the mesh is refined

b) whether the element exhibits sensitivity to aspect ratios significantly different than 1.0

c) how the element behaves in a wide variety of modeling situations, such as those included in the MSC element test library (discussed below).

The first two questions were addressed in the same manner as several other studies reported by one of the authors in prior NASTRAN colloquia (references 1 - 3). The procedure used in those studies, and followed here also, is to isolate the effects of mesh refinement and aspect ratio. That is, the mesh refinement study is done using elements with an aspect ratio of 1.0. Then, once a fine enough mesh has been reached such that the errors are small, the effects of aspect ratio can be investigated by keeping the mesh the same (i.e. same number of elements) and varying the overall dimensions of the problem, thus resulting in each element aspect ratio changing. Obviously, in order to accomplish this latter step there must be a theoretical solution (or some other equally acceptable comparison solution) to the problem with which to compare the finite element model results. This is needed since, at each step, a problem of different dimensions (and therefore different theoretical solution) is being modeled.

The above tests are important in that they show the rate of convergence toward the theoretical solution as the mesh is refined. Those tests, however, are not sufficient to completely test the accuracy of a finite element since they do not test irregular geometries, or a variety of loadings or material properties. The MSC has developed a comprehensive set of problems for testing finite elements in a variety of situations (reference 4). The library of problems consists of 15 test problems for shell elements that cover all of the parameters mentioned above. This element test library was used to test the TRIA3 element as was done for the QUAD4 element reported in reference 1.

RESULTS OF MESH AND ASPECT RATIO STUDY

For the mesh and aspect ratio study a theoretical comparison solution is highly desirable. Since the effects of transverse shear flexibility are included in the TRIA3 element formulation, a theoretical solution for moderately thick plates, based on Reissner (or Mindlin) thick plate theory is also desirable. Such a solution is given in references 5 and 6 for rectangular simply supported thick plates under the action of a pressure load. Thus, this problem was used for the mesh and aspect ratio portions of the study.

Figure 1 defines the geometry, coordinate system, boundary conditions and loading for the rectangular plate. The thickness indicates a moderately thick plate of length to thickness ratio of 20. The effect of transverse shear flexibility is only approximately 1% on the maximum displacement but is important in discerning the quality of the convergence of the finite element results to the exact theoretical solution. By exact is meant the theoretical basis for the TRIA3 element, which is expressed in the Reissner thick plate theory. Figure 2 shows the finite element mesh geometry used in the mesh and aspect ratio studies. Due to symmetry only

one quarter of the plate was modeled. The 4 x 4 mesh shown in figure 2 is an example only; the mesh was varied during the mesh study. However, as was done for all problems, the quad areas were subdivided into triangles in the alternating orientation shown in figure 2.

Figures 3a - 3c show characteristics of the theoretical solution. As indicated in figure 3a the central displacement solution is represented as an infinite series of hyperbolic functions. A FORTRAN computer program was written to compute the theoretical solutions for displacements (using the series shown) as well as stresses (solution not shown). Figures 3b and 3c show the stiffness parameters needed in the theoretical solution for the homogeneous and honeycomb plates. For the honeycomb plate, two different core stiffnesses were investigated. The stiffer one is representative of aluminum honeycomb construction that has been used at the GSFC. The more flexible one was chosen because it represents a core flexibility that is quite low and was expected to be a more critical test of the TRIA3's shear flexibility formulation.

The results of the mesh study, showing the convergence of the TRIA3 solutions to the theoretical, are presented in tabular form in tables 1 - 2 and in graphical form in figures 4 - 7. Both formats show percent error in displacement at the center of the plate as a function of mesh refinement. Results are included for COSMIC 9.0, UAI 11.1 and MSC 66A NASTRAN. The tables merely give exact numbers (along with the theoretical displacements) and the figures contain the same error information, but in graphic form. Figures 4 and 5 and table 1 are the results for the homogeneous plate. The difference between the results in figures 4 and 5 (and that in the two parts of table 1) is that figure 4 (and the top half of table 1) is for a solution in which shear flexibility is included and figure 5 (and the bottom half of table 1) neglects shear flexibility. These two situations were investigated to test the MID3 option on the PSHELL NASTRAN bulk data deck card which allows the effects of shear flexibility to be ignored if MID3 is left blank. As seen in figures 4 and 5 the NASTRAN results converge very rapidly with mesh refinement for COSMIC 9.0, MSC 66A and UAI 11.1. As seen, all versions converge to less than 1% error for a mesh size of 8 x 8.

Figures 6 and 7 and table 2 are the results for the honeycomb plate. Figure 6 (and the top half of table 2) are for the honeycomb plate with the stiffer core and figure 7 (and the bottom half of table 2) are for the more flexible core. As seen in figures 6 and 7 the NASTRAN results for COSMIC 9.0 and the two commercial NASTRAN versions converge very rapidly for the two honeycomb plates as they did for the homogeneous plate.

In order to test the TRIA3's sensitivity to aspect ratio, the model with a 12 x 12 mesh was run in which the plate side dimension in the x direction was varied. This causes the element aspect ratio to vary while maintaining a constant mesh in an attempt to prevent mesh refinement errors from significantly affecting the results. As seen in tables 1 and 2, the TRIA3 results with a 12 x 12 mesh (and aspect ratio of 1.0) have very little error. The results of the aspect ratio study are presented in figures 8 - 10 and tables 3 - 5. Tables 3 - 5 give percent error in the displacement at the center of the plate versus aspect ratio for a model with a mesh of 12 x 12 TRIA3 elements (over one quarter of the plate). As mentioned above, the aspect ratio was varied by changing the dimension of the plate along the x axis. For example, the results for the aspect ratio of 10 are for a plate (and all TRIA3 elements) that is 10 times as long in the x direction as in the y direction. Therefore, the theoretical solution changes with aspect ratio. Figure 8 and table 3 are for the homogeneous

28

plate (with transverse shear flexibility) while figure 9 and table 4 are for the stiff core honeycomb plate and figure 10 and table 5 are for the more flexible core honeycomb plate. Investigation of the percent error in the tables, as well as in figures 8 - 10 show that the TRIA3 has essentially no aspect ratio sensitivity over the range investigated.

Based on the above results, the COSMIC TRIA3 element is seen to give very accurate results for the displacements in the problem investigated, both in comparison to the exact theory and in comparison to the two commercial versions of NASTRAN that we have at the GSFC. Although the results are not presented herein, similarly accurate results were obtained for the shear and moment stress resultants as well. In addition, the rates of convergence for the TRIA3 compare quite favorably with that found for the QUAD4 in reference 1 for this plate bending problem.

RESULTS OF TESTING USING THE MSC ELEMENT TEST LIBRARY

As mentioned earlier, the mesh and aspect ratio studies, while a very useful tool in the evaluation of an element, do not test all of the important variables that affect accuracy in a finite element solution. The MSC element test library mentioned above represents a rather exhaustive series of tests that include many of the element related parameters which affect the accuracy of a finite element solution. Reference 4 gives a detailed description of the test problems along with theoretical answers and the results of the testing on several MSC elements. The reader should consult reference 4 for a complete description of the various problems in the test series. The portion of this series of element tests that relate to shell elements was run by the authors on the TRIA3 elements contained in COSMIC 9.0, UAI 11.1 and MSC 66A. As the MSC does in their report, the results are presented in detail and also in a summary form in which the element is given a letter grade of A through F based on the magnitude of the error. Table 6 shows the summary results for the 15 tests in the series ranging from a simple patch test to modeling of beams (using the TRIA3 element through the depth) and various plates and shells. The meaning of the letter grades is given at the bottom of the table. As pointed out in reference 4, a failing grade for an element in one test is not a reason to dismiss the element. For one thing, the test scores would improve with mesh refinement; the mesh used in most of the problems was quite coarse. Of importance in this discussion is not the actual grades listed in table 6 but the comparison of the COSMIC grades with those from the other two programs. As seen in table 6, the COSMIC TRIA3 element is as good as, or better than, those of the commercial programs. All of the low marks (D or F) are apparently due to the constant strain membrane portion of the TRIA3 element and the low order mesh used in those problems. For example, the straight beam bending, with in-plane loading, had only one TRIA3 through the thickness. This was done to keep the same mesh as MSC used for the QUAD4 element tests, and was also done in reference 1. Refining the mesh would have improved the answers to any degree of accuracy desired; the low grades are not indicative of any failure of the element to converge. Although not shown in table 6, the old TRIA2 element (included in reference 4) has a D or F grade in 9 of the 15 problems. The twisted beam test (number 11 in table 6) is really used to test the effect of warp on quadrilateral elements, which is not applicable for the TRIA3 element.

CONCLUSIONS

The COSMIC TRIA3 general purpose flat shell element has been shown to be an excellent element and, together with the QUAD4 quadrilateral flat shell element, significantly enhances the usefulness of COSMIC NASTRAN. The element has been shown to compare excellently with those available in two commercial versions of NASTRAN that are currently being used at the GSFC.

REFERENCES

1. Case, W. R., et al, "Accuracy of the QUAD4 Thick Shell Element", Eighteenth NASTRAN User's Colloquium, pg 30, Portland, OR, April, 1990.

2. Case, W. R. and Mason, J. B., "NASTRAN Finite Element Idealization Study", Sixth NASTRAN User's Colloquium, pg 383, Cleveland, OH, October, 1977.

3. Case, W. R. and Vandegrift, R. E., "Accuracy of Three Dimensional Solid Finite Elements", Twelfth NASTRAN Users Colloquium, pg 26, Orlando, FL, May, 1984

4. MacNeal, R. H. and Harder, R. L. "A Proposed Standard Set of Problems to Test Finite Element Accuracy", MSC/NASTRAN Application Note, MSC/NASTRAN Application Manual, Section 5, March 1984

5. Reissner, E., "On Bending of Elastic Plates", Quarterly of Applied Math, Vol V, No. 5, pg 55, 1947

6. Salerno, V. L. and Goldberg, M. A., "Effect of Shear Deformations on the Bending of Rectangular Plates", Journal of Applied Mechanics, pg 54, March 1960

List of Symbols

w = plate displacement in the z direction

x,y,z = coordinate directions

p = pressure load on the plate in the z direction

a, b = plate dimensions (length, width)

t = overall plate thickness

D = plate bending rigidity (see Figures 3b, 3c)

Cs, C_n = plate shear stiffness (see Figures 3b, 3c)

t_f = thickness of face sheets for honeycomb plate

t_c = thickness of the core for honeycomb plate

N_x = number of elements in x direction in one quarter of plate

N_y = number of elements in y direction in one quarter of plate

AR_e = element aspect ratio (see Figure 2)

E = Young's modulus

G = shear modulus

v = Poisson's Ratio

TABLE 1: TRIA3 Error in Displacement at Center of Plate
Mesh Size Study (Element Aspect Ratio 1.0)
Simply-Supported, Homogeneous Plate Under Uniform Pressure Load

Theoretical Displacements

With Transverse Shear Flexibility: 3.571×10^{-5} m

$(1.406 \times 10^{-3}$ in.$)$

Without Transverse Shear Flexibility: 3.529×10^{-5} m

$(1.390 \times 10^{-3}$ in.$)$

Mesh	Cosmic 90	% Error UAI Ver. 11.1	MSC Ver. 66A
With Transverse Shear Flexibility			
1x1	39.33	27.64	16.62
2x2	13.63	11.36	9.01
4x4	3.29	2.77	2.06
8x8	0.01	0.55	0.34
12x12	0.00	0.13	0.04
Without Transverse Shear Flexibility			
1x1	40.56	28.37	17.45
2x2	14.31	11.72	9.52
4x4	3.74	3.01	2.43
8x8	0.95	0.76	0.62
12x12	0.42	0.34	0.27

TABLE 2: TRIA3 Error in Displacement at Center of Plate
Mesh Size Study (Element Aspect Ratio 1.0)
Simply-Supported, Honeycomb Plate
Under Uniform Pressure Load with Transverse Shear Flexibility

Theoretical Displacements

$G_z = 1.517 \times 10^8$ N/m^2 : 2.422×10^{-3} m

$(9.535 \times 10^{-2}$ in.)

$G_z = 1.379 \times 10^7$ N/m^2 : 3.102×10^{-3} m

$(1.221 \times 10^{-1}$ in.)

| | | % Error | |
Mesh	Cosmic 90	UAI Ver. 11.1	MSC Ver. 66A
$G_z = 1.517 \times 10^8$ N/m^2 (22000 psi)			
1x1	38.28	27.13	16.08
2x2	13.36	11.36	8.88
4x4	3.35	2.92	2.16
8x8	0.81	0.73	0.52
12x12	0.37	0.33	0.24
$G_z = 1.379 \times 10^7$ N/m^2 (2000 psi)			
1x1	24.07	17.82	7.37
2x2	9.71	8.83	6.35
4x4	2.48	2.26	1.60
8x8	0.60	0.55	0.38
12x12	0.30	0.28	0.02

TABLE 3: TRIA3 Error in Displacement at Center of Plate
Aspect Ratio Study (12 x 12 Mesh)
Homogeneous, Simply-Supported Plate
Under Uniform Pressure Load with Transverse Shear Flexibility

AR	theoretical w, m (in.)	Cosmic 88	% Error UAI Ver. 10.0	MSC Ver. 65C
1	3.571×10^{-5} (1.406×10^{-3})	0.17	0.13	0.04
2	8.865×10^{-5} (3.490×10^{-3})	0.14	0.10	0.03
5	11.34×10^{-5} (4.465×10^{-3})	0.11	0.11	0.07
10	11.38×10^{-5} (4.482×10^{-3})	0.08	0.08	0.05

TABLE 4: TRIA3 Error in Displacement at Center of Plate
Aspect Ratio Study (12 x 12 Mesh)
Stiff Core, Simply-Supported, Honeycomb Plate
Under Uniform Pressure Load with Transverse Shear Flexibility

AR	theoretical w, m (in.)	Cosmic 88	% Error UAI Ver. 10.0	MSC Ver. 65C
1	2.422×10^{-3} (9.535×10^{-1})	0.37	0.33	0.24
2	5.974×10^{-3} (2.352×10^{-1})	0.28	0.24	0.17
5	7.631×10^{-3} (3.004×10^{-1})	0.21	0.21	0.17
10	7.660×10^{-3} (3.016×10^{-1})	0.21	0.21	0.17

TABLE 5: TRIA3 Error in Displacement at Center of Plate
Aspect Ratio Study (12 x 12 Mesh)
Flexible Core, Simply-Supported, Honeycomb Plate
Under Uniform Pressure Load with Transverse Shear Flexibility

AR	theoretical w, m (in.)	Cosmic 90	% Error UAI Ver. 11.1A	MSC Ver. 66A
1	3.102×10^{-3} (1.221×10^{-1})	0.30	0.28	0.20
2	7.026×10^{-3} (2.766×10^{-1})	-0.67	0.24	0.18
5	8.785×10^{-3} (3.459×10^{-1})	0.22	0.22	0.17
10	8.815×10^{-3} (3.470×10^{-1})	0.17	0.17	0.13

TABLE 6

SUMMARY OF TEST RESULTS FOR TRIA3 SHELL ELEMENTS

Test	Elem. Loading		Element Shape	COSMIC 90	UAI 11.1A	MSC 66A
	In Plane	Out of Plane				
1. Patch Test	X		Irregular	A	A	A
2. Patch Test		X	Irregular	A	A	A
3. Straight Beam, Extension	X		All	A	A	A
4. Straight Beam, Bending	X		Regular	F	F	F
5. Straight Beam, Bending	X		Irregular	F	F	F
6. Straight Beam, Bending		X	Regular	B	B	B
7..Straight Beam, Bending		X	Irregular	B	B	B
8. Straight Beam, Twist			All	F	F	F
9. Curved Beam	X		Regular	F	F	F
10. Curved Beam		X	Regular	F	F	F
11. Twisted Beam	X	X	Regular	C	C	D
12. Rectangular Plate (N=4)		X	Regular	B	B	B
13. Scordelis-Lo Roof (N=4)	X	X	Regular	D	D	D
14. Spherical Shell (N=8)	X	X	Regular	A	A	A
15. Thick-Walled Cylinder (nu=.4999)	X		Regular	A	A	A
Number of Failed Tests (D's and F's)				6	6	7

Grading for Shell Element Test Results

Grade	Requirement
A	$2\% \geq$ Error
B	$10\% \geq$ Error $> 2\%$
C	$20\% \geq$ Error $> 10\%$
D	$50\% \geq$ Error $> 20\%$
F	Error $\geq 50\%$

Fig. 1
Test Problem
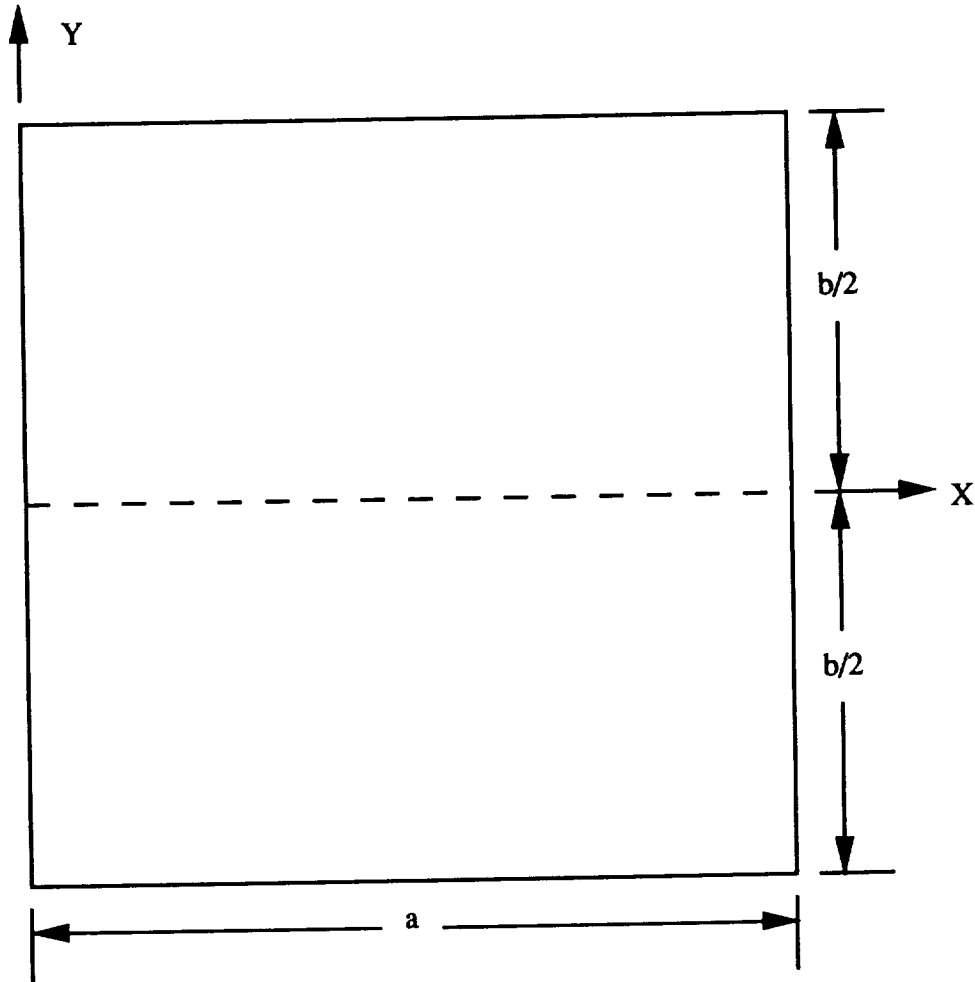
Plate Size: a=1.016 m (40. in.)* b=1.016m (40.in.)
Boundary Conditions: simply supported on all edges
Loading: pressure load, p=6895. N/m^2 (1.0 psi) +Z direction
Thickness: t=0.0508 m (2.0 in.)

*: Variable in aspect ratio studies

Fig. 2
Mesh Geometry
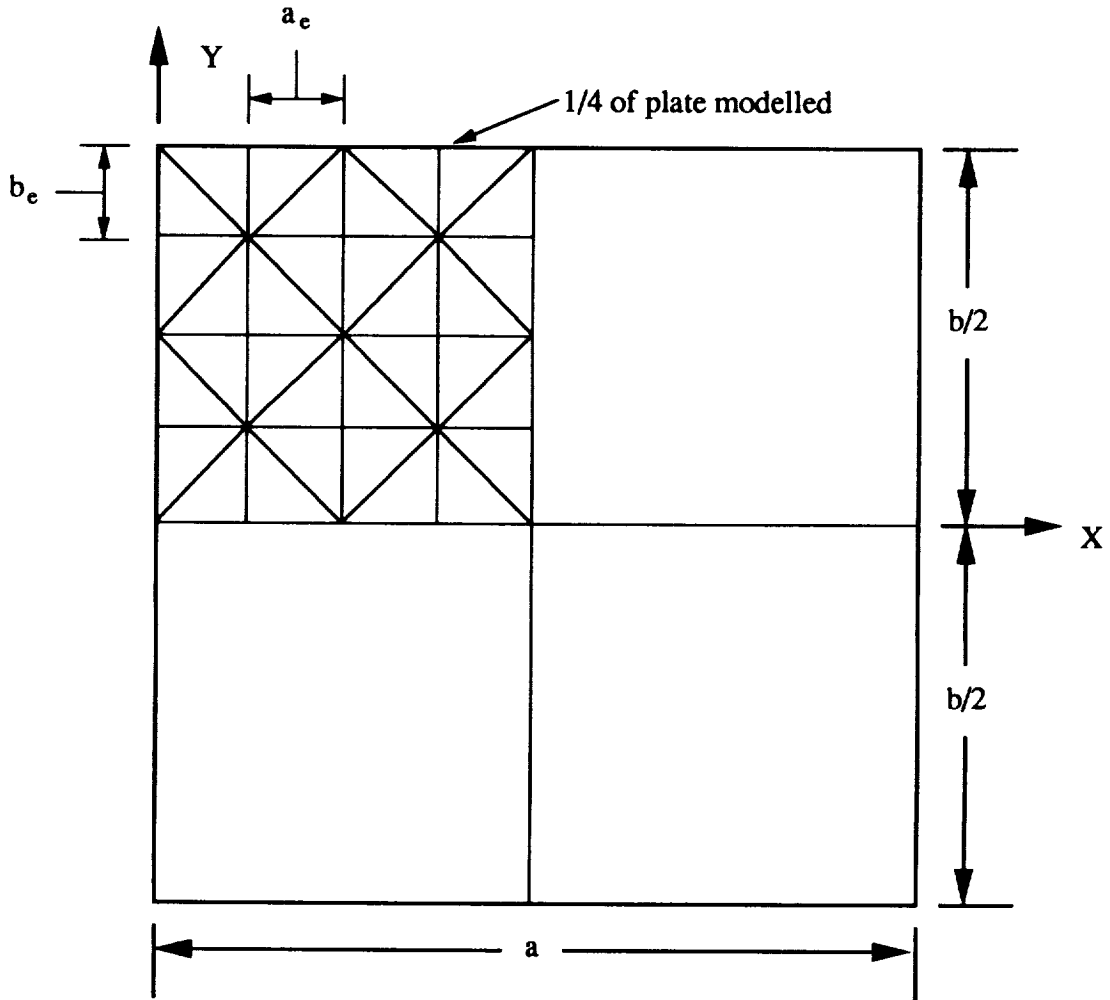
$AR_e = a_e/b_e$ = element aspect ratio
$N_x = a/2a_e$ = number of elements in X direction in 1/4 of plate
$N_y = b/2b_e$ = number of elements in Y direction in 1/4 of plate

Theoretical Solution - Central Displacement

Central Displacement

$$w(x=\frac{a}{2},y=0) = \frac{4p}{aD} \sum_{m=1,3,5,\ldots} \left[1 + C_5 \cosh(\mu y) + \mu y C_6 \sinh(\mu y) + \mu^2 D\left(\frac{1}{C_s} - \frac{1+v}{C_n}\right) \right] \frac{\sin \mu x}{\mu^5}$$

where,

$$C_5 = - \frac{1}{\cosh \alpha_m} \left[1 + \mu^2 D\left(\frac{1}{C_s} - \frac{1+v}{C_n}\right) + \frac{1}{2} \alpha_m \tanh(\alpha_m) \right]$$

$$C_6 = \frac{1}{2 \cosh \alpha_m}$$

$$\alpha_m = \frac{m\pi}{2}\frac{b}{a} , \quad \mu = \frac{m\pi}{a}$$

Fig. 3b

Theoretical Solution - Homogeneous Plate Parameters

Homogeneous Plate

$$D = \frac{Et^3}{12(1-v^2)}$$

$$C_n = \frac{5}{6}\frac{Et}{v}$$

$$C_s = \frac{5}{6}Gt, \quad G = \frac{E}{2(1+v)}$$

$$E = 6.89 \times 10^{10} \text{ N/m}^2 \quad (10.0 \times 10^6 \text{ lb/in}^2)$$

$$v = 0.33$$

$$t = .0508 \text{ m } (2.0 \text{ in.})$$

Theoretical Solution - Honeycomb Plate Parameters

Honeycomb Plate

$$D = \frac{E_f t_f (t_c + t_{f/2})^2}{4(1 - v^2)}$$

$$C_n = \infty$$

$$C_s = t_c G_c$$

$$E_f = 6.89 \times 10^{10} \ N/m^2$$
$$(10 \times 10^6 \ lb/in^2)$$

$$v = 0.33$$

Face Sheet

E_f, v

$1/2 t_f$

t_c

$1/2 t_f$

Honeycomb Core

G_c

Core Detail

$$G_c = 1.379 \times 10^7 \ N/m^2 \quad (2000. \ lb/in^2) \ \text{Flexible Honeycomb Plate}$$
$$\text{or}$$
$$1.517 \times 10^8 \ N/m^2 \quad (22000. \ lb/in^2) \ \text{Stiff Honeycomb Plate}$$

$$t_c = .0508 \ m \quad (2.0 \ in)$$

$$t_f = .254 \ mm \quad (.01 \ in.)$$

$$t = t_c + t_f$$
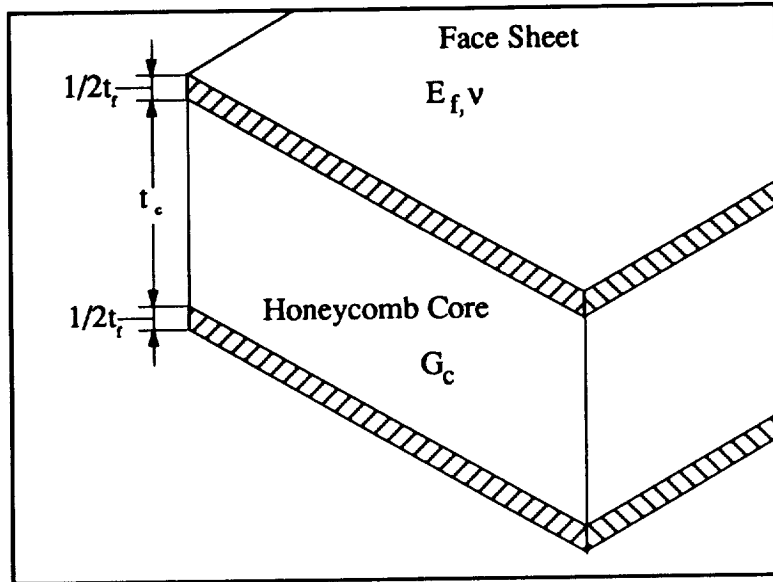
Fig. 4
TRIA3 Error in Displacement at Center of Plate

Mesh Size Study (Element Aspect Ratio 1.0)
Simply-Supported, Homogeneous Plate
Under Uniform Pressure Load with Transverse Shear Flexibility
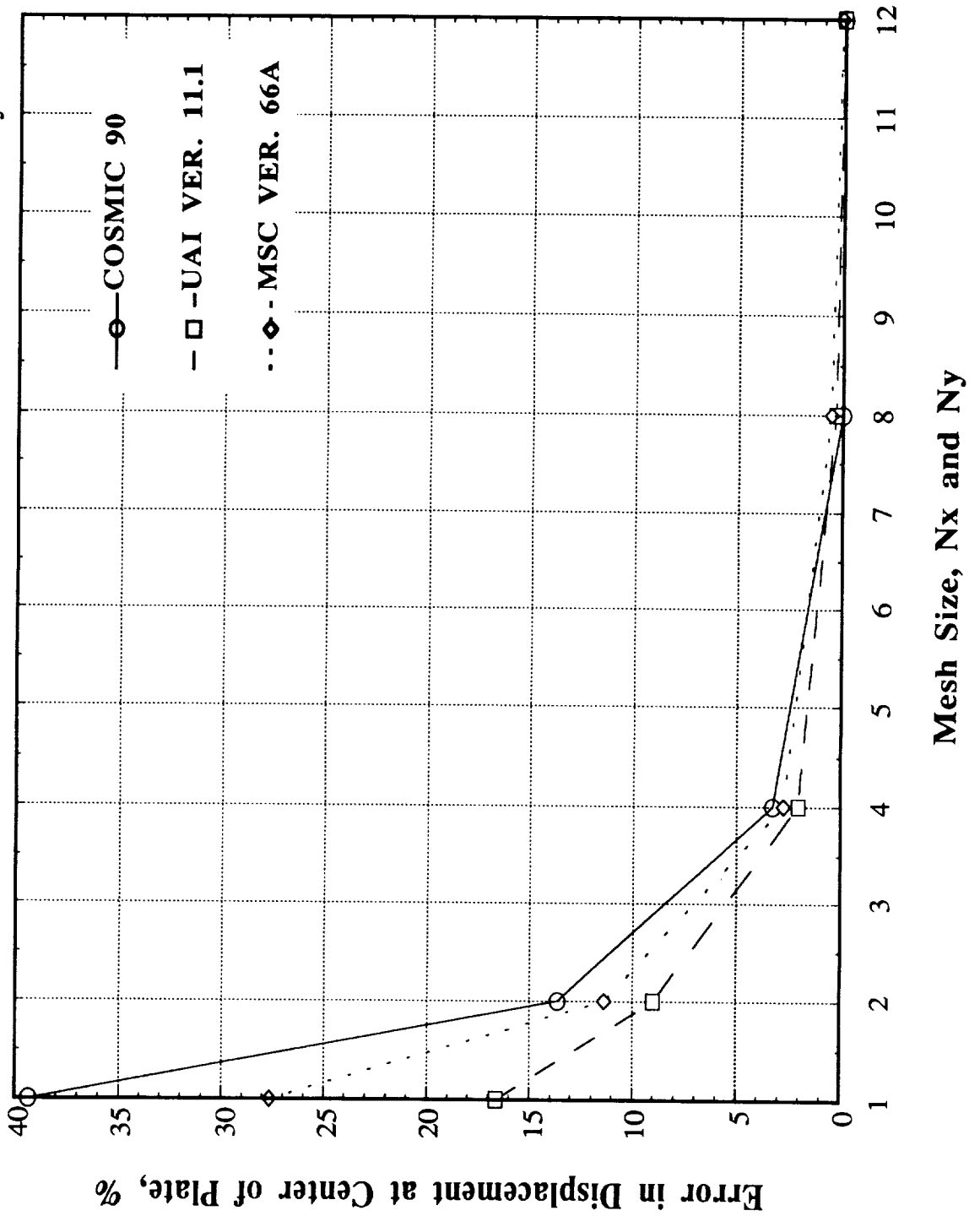
Fig. 5

TRIA3 Error in Displacement at Center of Plate

Mesh Size Study (Element Aspect Ratio 1.0)
Simply-Supported, Homogeneous Plate
Under Uniform Pressure Load without Transverse Shear Flexibility

COSMIC 90
UAI VER. 11.1A
MSC VER. 66A

Mesh Size, Nx and Ny

Error in Displacement at Center of Plate, %

45
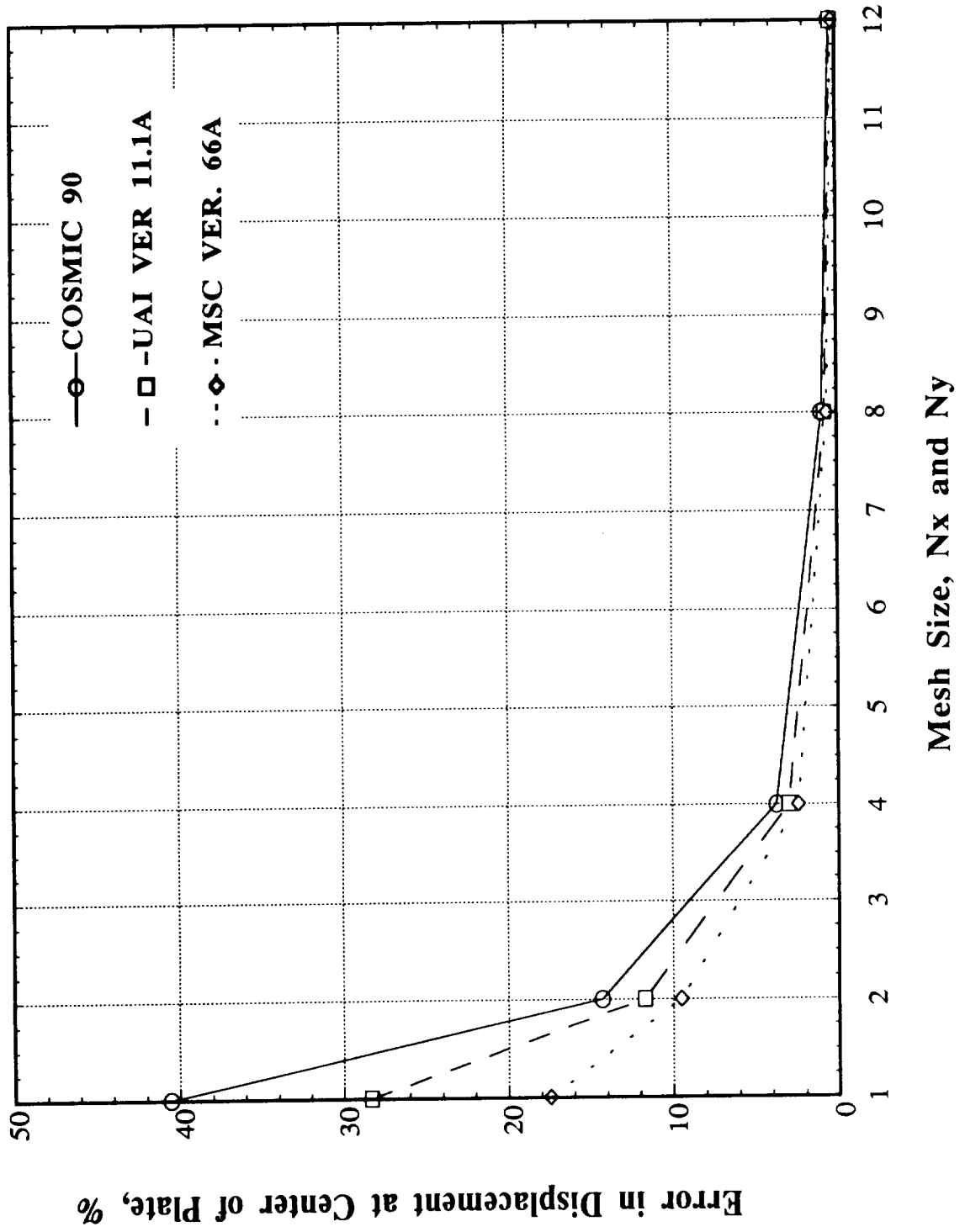
Fig. 6
TRIA3 Error in Displacement at Center of Plate
Mesh Size Study (Element Aspect Ratio 1.0)
Stiff Core, Simply-Supported, Honeycomb Plate
Under Uniform Pressure Load with Transverse Shear Flexibility

— COSMIC 90
— UAI VER. 11.1
— MSC VER. 66A

Error in Displacement at Center of Plate, %

Mesh Size, Nx and Ny

Fig. 7
TRIA3 Error in Displacement at Center of Plate
Mesh Size Study (Element Aspect Ratio 1.0)
Flexible Core, Simply-Supported, Honeycomb Plate
Under Uniform Pressure Load with Transverse Shear Flexibility

COSMIC 90

UAI VER. 11.1A

MSC VER. 66A

Mesh Size, Nx and Ny

Error in Displacement at Center of Plate, %

Fig. 8
TRIA3 Error in Displacement at Center of Plate

Aspect Ratio Study (12 x 12 Mesh)
Homogeneous, Simply-Supported Plate
Under Uniform Pressure Load with Transverse Shear Flexibility

—⊖—COSMIC 90

–□–UAI VER. 11.1A

··◆··MSC VER. 66A

Error at Maximum Displacement Location, %

Element Aspect Ratio

Fig. 9
TRIA3 Error in Displacement at Center of Plate
Aspect Ratio Study (12 x 12 Mesh)
Stiff Core, Simply-Supported, Honeycomb Plate
Under Uniform Pressure Load with Transverse Shear Flexibility
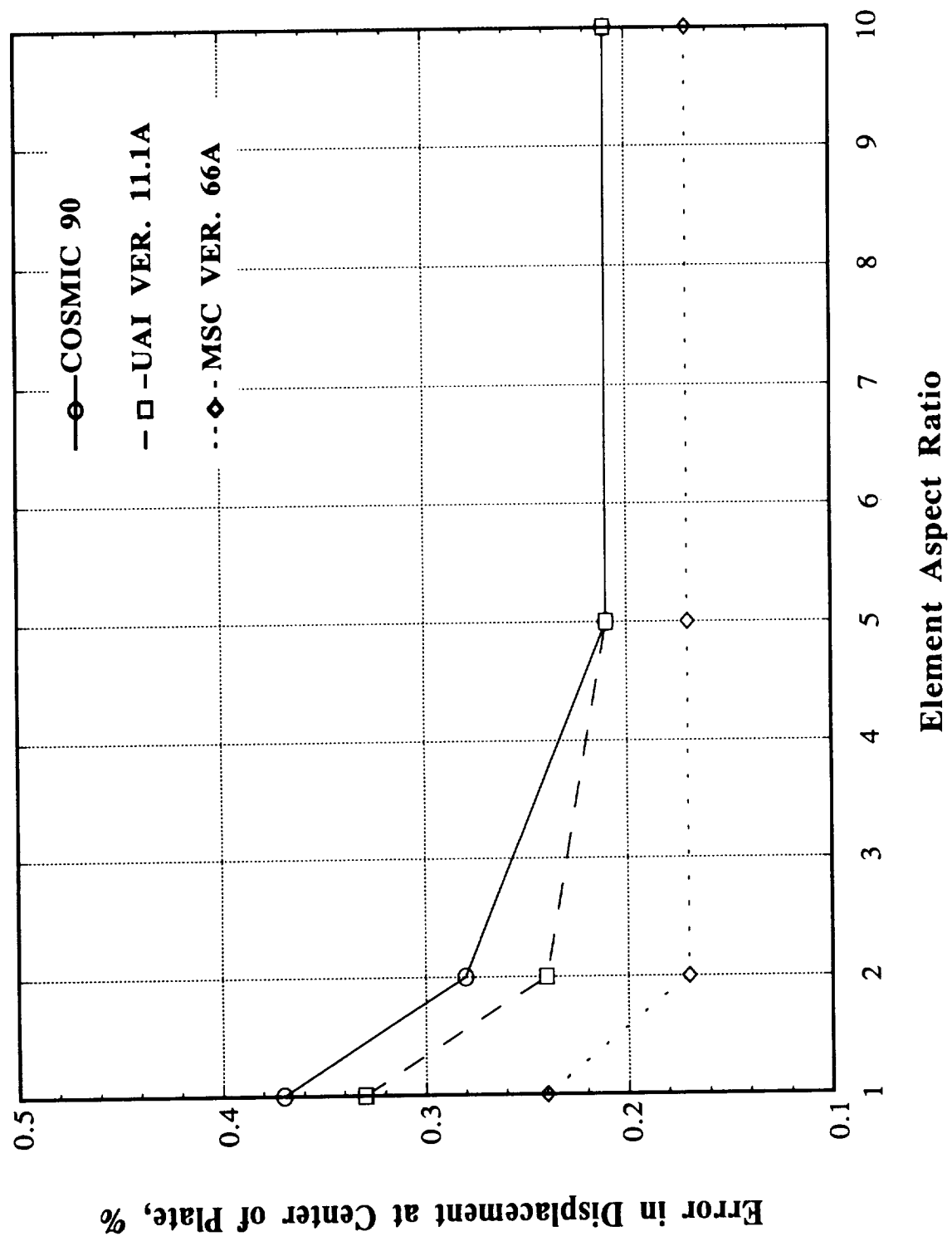
Fig. 10
TRIA3 Error in Displacement at Center of Plate

Aspect Ratio Study (12 x 12 Mesh)
Flexible Core, Simply-Supported, Honeycomb Plate
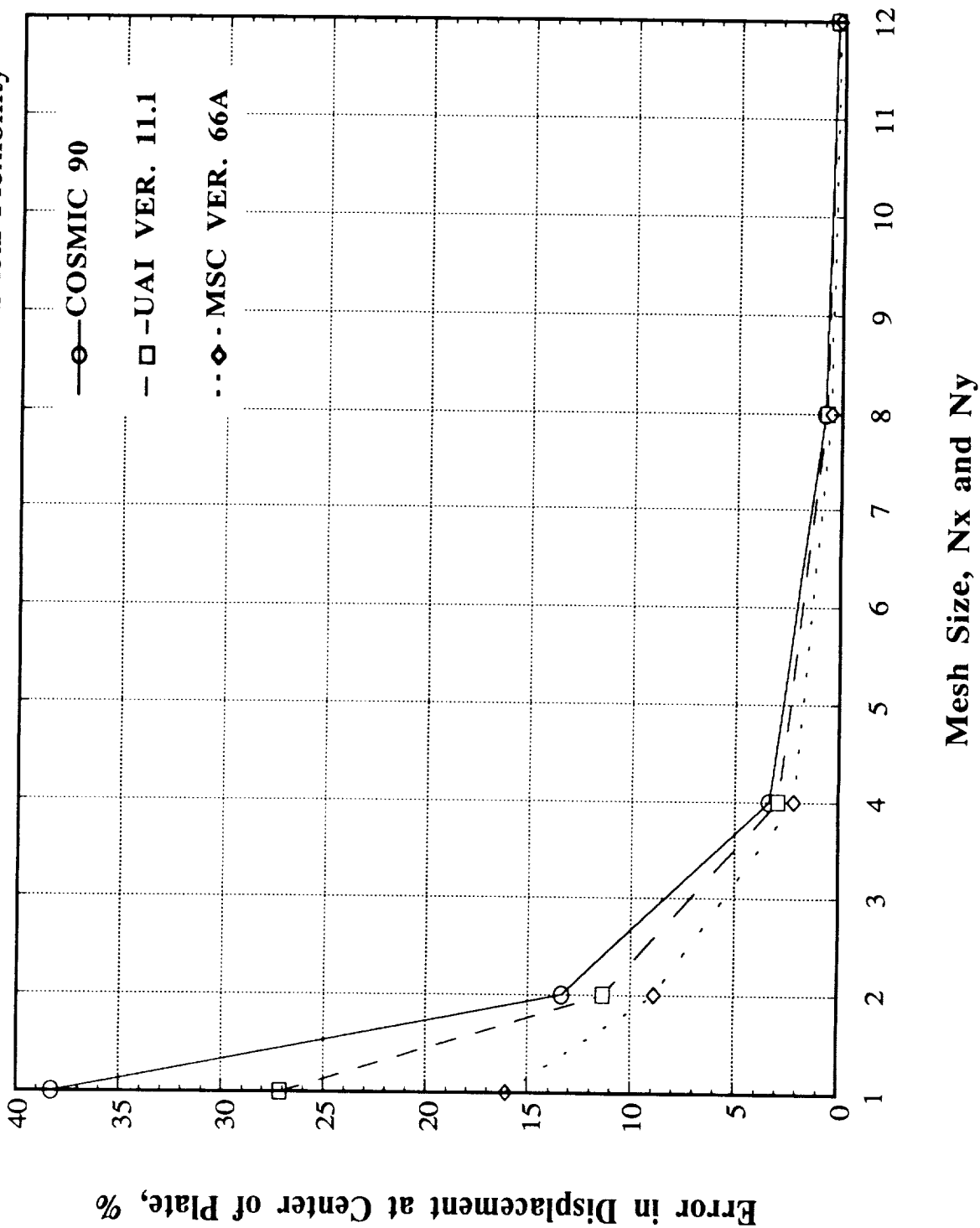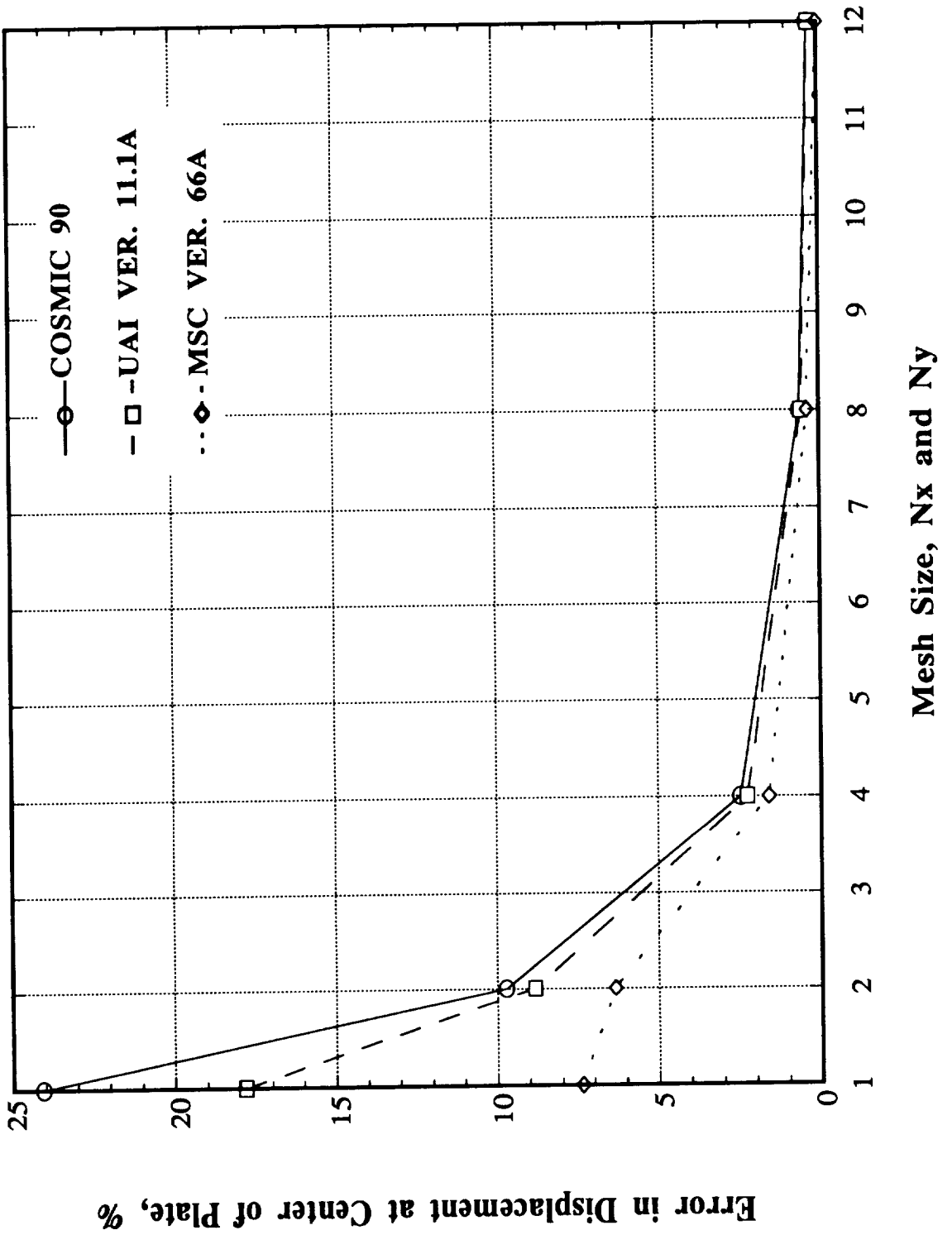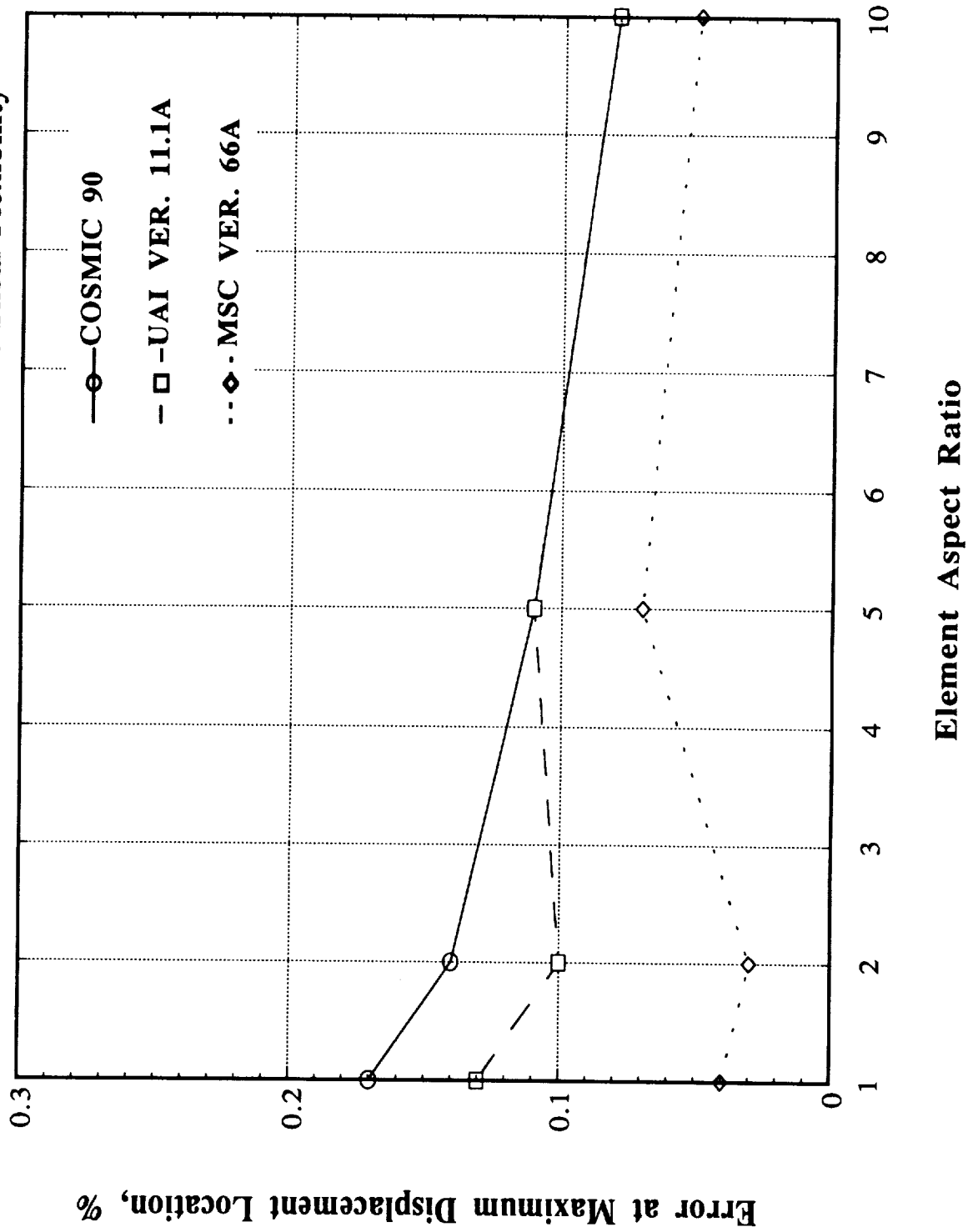Under Uniform Pressure Load with Transverse Shear Flexibility
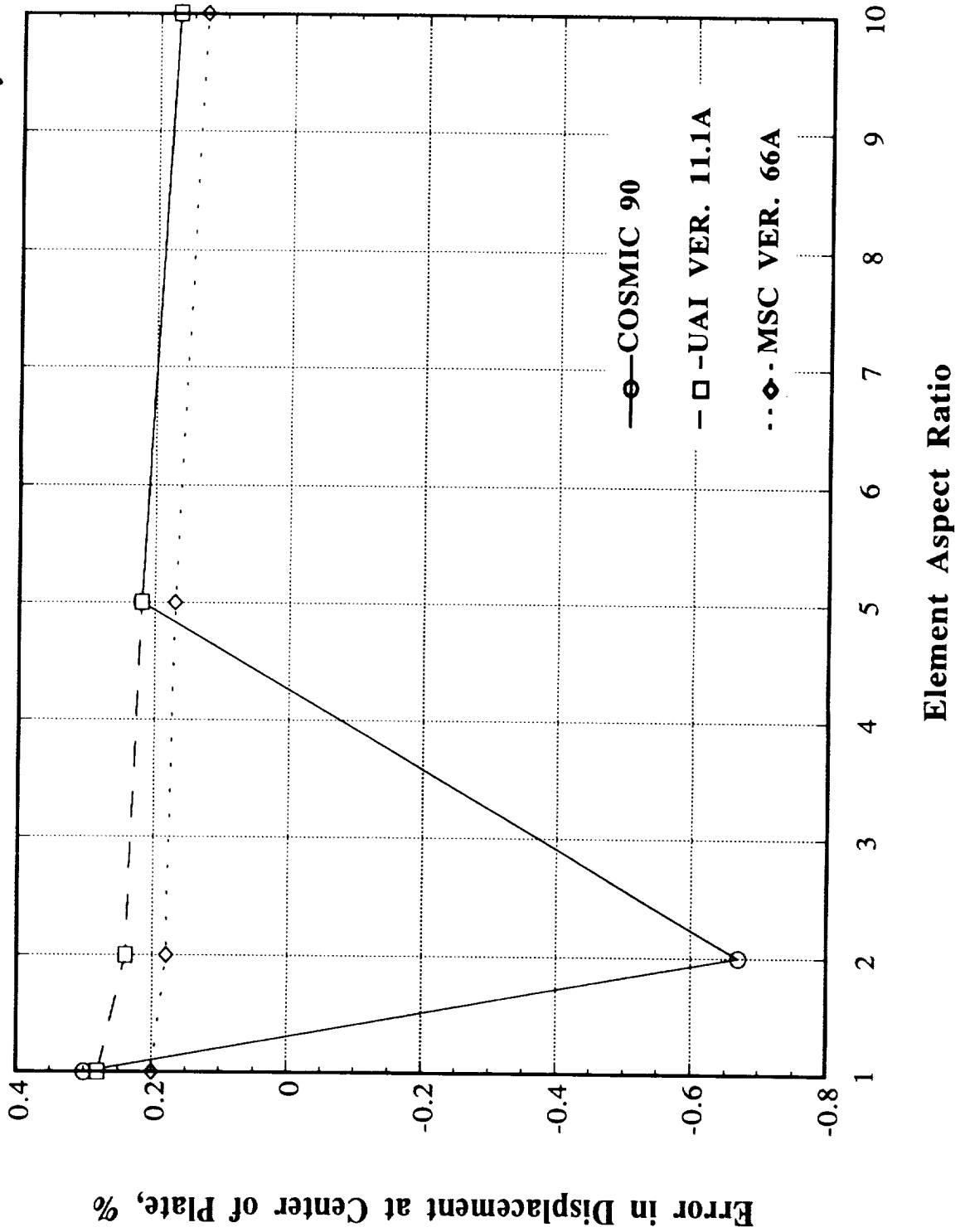
VALIDATION OF THE CQUAD4 ELEMENT FOR VIBRATION AND SHOCK ANALYSIS OF THIN LAMINATED COMPOSITE PLATE STRUCTURE

by

Douglas E. Lesar
Ship Structures and Protection Department
Carderock Division, Naval Surface Warfare Center
Bethesda, Maryland 20084-5000 U.S.A.

ABSTRACT

The CQUAD4 thin plate element implemented in COSMIC NASTRAN is capable of modeling thin layered plate and shell structures composed of orthotropic lamina. Fiber-reinforced composites are among the classes of inhomogeneous and non-isotropic materials which can be treated. Although the CQUAD4 has been extensively checked in static cases, little validation has been carried out for vibration response modeling. This paper documents validation of the CQUAD4 element's accuracy for vibration response analysis of thin laminated composite plates.

The lower-order natural frequencies and mode shapes of ten glass fiber-reinforced plastic (GFRP) and carbon fiber-reinforced plastic (CFRP) plates are computed and compared to published experimental and numerically-computed data. A range of ply geometries including unidirectional, cross-ply, and angle-ply are considered. The plates' length-to-thickness ratios all lie in the vicinity of 100 to 150. The CQUAD4 plate idealizations provide natural frequency predictions within ten percent of measured data for all six lowest modes of seven of ten plates. For two of the remaining three plates, only the fundamental frequency is predicted with an error greater than ten percent. Results for the one remaining plate do not correlate with published data, possibly because of erroneous reporting of its geometry or material properties in the literature. To obtain accurate frequency predictions, lamina in-plane elastic moduli had to be tuned to reflect each plate's fiber volume fraction.

These results show that the NASTRAN CQUAD4 plate element is useful and reasonably accurate for vibration and shock analysis of structures composed of thin fiber-reinforced plastic plates.

INTRODUCTION

There is strong current Navy interest in exploitation of fiber-reinforced plastics as lightweight materials for a wide variety of ship structures. These structures must be designed to withstand in-service loads of quasi-static, transient dynamic, and steady-state dynamic nature. For many ship structures, transient shock is a primary load. For these and others, steady-state vibration response

impacts the ship's acoustic signature. In both cases, the structure's modal properties (natural frequencies, mode shapes, and modal loss factors) are key parameters governing its transient and steady-state response. In most cases, the ship structures being designed are complex enough so that numerical (finite element) methods must be employed to obtain realistic modal property estimations.

The NASTRAN finite element code is one of the Navy's premier tools for steady-state vibration response analysis of ship and submarine structures. Undamped natural mode analysis and forced vibration response analysis with hysteretic damping can be performed by NASTRAN, as well as modal frequency and loss factor analysis for structures with viscoelastic damping materials (Ref. 1). NASTRAN is also a key component of the NASHUA suite of codes for performing radiated noise and acoustic scattering analysis of vibrating submerged structures (Ref. 2,3).

The COSMIC NASTRAN CQUAD4 element is designed to model anisotropic layered plates as well as homogeneous and isotropic plates. The theory and assumptions behind the CQUAD4 have been informally documented (Ref. 4). The CQUAD4 has been found to be more accurate for a given finite element grid than its predecessor, the CQUAD2 element, for prediction of low frequency eigenmodes of thin-walled cylindrical shells composed of isotropic materials (Ref. 5). To the author's knowledge, no comparable study of the accuracy of the CQUAD4 formulation for anisotropic plate or shell vibration yet exists, particularly for plates and shells composed of layers of fiber-reinforced plastic lamina.

This paper summarizes an investigation of the accuracy of the NASTRAN CQUAD4 membrane and plate bending element for vibration analysis of structures composed of thin fiber-reinforced composite plates. This is accomplished by comparisons of NASTRAN-computed undamped natural frequencies of ten GFRP and CFRP plates with published experimental data and other numerical predictions.

NOTATION

E_{11}	Lamina extensional modulus in direction parallel with fibers
E_{22}	Lamina extensional modulus in direction transverse to fibers
E_{33}	Through-thickness extensional modulus
G_{12}	In-plane lamina shear modulus
G_{13}	Transverse lamina shear modulus for out-of-plane shearing of a fiber cross section

G_{23}	Transverse lamina shear modulus for in-plane shearing of a fiber cross section
L	Plate side length
t	Plate thickness
V_f	Fiber volume fraction
γ_{12}	In-plane shear strain
γ_{13}, γ_{23}	Out-of-plane shear strains
ϵ_1, ϵ_2	In-plane extensional strains
θ	Fiber orientation angle with respect to one plate side
ν_{12}, ν_{21}	In-plane lamina Poisson's ratios
ν_{23}	Transverse lamina Poisson's ratio
ρ	Average mass density
σ_1, σ_2	In-plane extensional stresses
τ_{12}	In-plane shear stress
τ_{13}, τ_{23}	Out-of-plane shear stresses

ABBREVIATIONS

avg.	Average
CFRP	Carbon fiber-reinforced plastic
CLT	Classical lamination theory
consis.	Consistent
CPT	Classical plate theory
DOF	Degree(s)-of-freedom
FEA	Finite Element Analysis
GPa	Gigapascals
GFRP	Glass fiber-reinforced plastic
Hz	Hertz
kg	Kilograms

m	Meters
mm	Millimeters
params.	Parameters
psi	Pounds (force) per square inch
ref.	Reference(s)
RMS	Root-mean-square
sym	Midplane-symmetric

BACKGROUND

Anisotropic plate analysis is more difficult and involves more variables and parameters than isotropic plate analysis. The importance of accounting for transverse shear flexibility in relatively thin composite laminates is discussed in the next section. The ways by which the CQUAD4 addresses these difficulties are also briefly described.

TRANSVERSE SHEAR DEFORMATION ISSUES

In composite plate mechanics, the counterpart of the well-known Kirchhoff (Classical plate) theory (CPT) for isotropic plates is the so-called "Classical Lamination Theory" (CLT). The two theories invoke the same kinematic assumptions regarding the deformation of the plate with respect to its middle surface; that is, sections originally planar and perpendicular to the middle surface remain planar and perpendicular in the deformed state. The mathematical development of CLT occupies much of the text by Jones (Ref. 6). The reader should consult this (or some other) text for detailed exposition of CLT assumptions and derivation of the CLT equations.

The accuracy of the Kirchhoff kinematic assumption in isotropic plate mechanics degrades when the plate thickness becomes significant compared to its span length. For isotropic metallic plates, transverse shear-stiffness-governed transverse deflection becomes significant relative to flexural deflection when the span length-to-thickness ratio (L/t) is sufficiently small. An idea of required smallness can be gained from the discussion of "corrected" plate flexural waves in Chapter II, Section 3b of Cremer, Heckl, and Ungar (Ref. 7). They show, for a uniformly thick plate composed of an _isotropic_ material, that transverse shear effects decrease flexural wavespeed by ten percent when the flexural wavelength is about six times the plate thickness. For one-half wavelength over a plate span length, this limitation translates to an L/t ratio of 3.

In the case of high modulus composite plates, an analogous limitation of the adequacy of CLT is encountered at _larger_ L/t. This more stringent limit arises because the ratio of effective laminate extensional elastic modulus to shear modulus is a key fac-

tor (other than section geometry) governing the magnitude of shear deformation relative to flexure. A rough idea of limiting L/t ratios for the adequacy of CLT for composite plates follows from insertion of some "ballpark" ratios of effective laminate extensional and transverse shear moduli for GFRP and CFRP into the approximate expression for shear-corrected plate flexural wavespeed found on page 115 of Reference 7. Using $E_{11} / G_{23} = 13$ for GFRP and 125 for CFRP, ten percent differences in wavespeed arise for L/t of 6.75 and 20.9, respectively. (A comparable modulus ratio for isotropic materials is 2.6). These ad hoc assessments are qualitatively corroborated by static examples found in section 6.5 of Reference 6. In the problem of cylindrical bending of a CFRP strip with $E_{11} / G_{23} =$ 125, maximum static deflection predicted by CLT is twenty percent smaller than the true shear-corrected solution at L/t = 20.

The low frequency composite plate vibration literature is dominated by evaluation of methods for account of transverse (interlaminar) shear in prediction of natural vibration frequencies and modal deflections. The inadequacies of CLT even for fundamental plate frequencies are repeatedly demonstrated in the literature for L/t's of 5 or 10. Many approaches have been developed to provide finite element-based plate formulations to handle through-thickness stress fields for arbitrary L/t. In these complex formulations, transverse normal stresses are no longer assumed to be zero, transverse shear stresses are constrained to be zero on upper and lower laminate surfaces, and shear stress continuity between laminae is maintained. As a result, sections perpendicular to the plate midplane rotate with respect to the midplane and warp out of a planar configuration.

The plate finite elements simulating through-thickness stress fields in laminates are, obviously, quite sophisticated. Tables III and VI of Mallikarjuna and Kant (Ref. 8) provide a good flavor for the performance of some higher-order approaches for reckoning with the effect of transverse shear and normal strains in plate vibration frequency prediction. Table III shows that CLT provides reasonable fundamental frequency predictions for a simply-supported CFRP angle-ply plate for L/t at and above 20. Even for such highly anisotropic plates, the complications of very complex high-order transverse shear theories, necessary for laminate strength and structural integrity problems, are not justified in vibration problems unless L/t is less than about 20, or if short-wavelength (high frequency) vibration modes are of interest.

The NASTRAN CQUAD4 membrane and bending element embodies the assumptions of CLT, but contains first-order corrections for transverse shear flexibility. When the CQUAD4 is used to model homogeneous plates, transverse shear strains vary linearly with the thickness coordinate, and zero shear stress and strain boundary conditions on upper and lower plate surfaces are not satisfied. The shear energy implied by the linear distribution is corrected by a multiplicative constant to produce the energy implied by the true quadratic distribution. As a result of these assumptions, sections perpendicular to the plate midplane are allowed to rotate with

respect to the midplane, but remain straight when the plate is in the deflected state. This ad hoc transverse shear correction extends the element's range of validity to thicker homogeneous plates, but is not acceptable for inhomogeneous layered plates.

When modeling inhomogeneous plates composed of orthotropic layers, a quadratic transverse shear strain distribution is assumed in each layer of the CQUAD4 element. Interlaminar shear strains are matched at lamina interfaces, and zero shear stress boundary conditions are enforced on the upper- and lower-most lamina surfaces. However, the through-thickness normal stress is assumed to be zero, and complete consistency between the strain-displacement equations for in-plane direct strain and transverse shear strain is not maintained. The CQUAD4 is thus seen to overcome the limitations of CLT for laminated plates, but does not represent all aspects of the kinematics of three-dimensional continua taking place in relatively thick laminates.

The CQUAD4 element is discussed in more depth in the following section.

THE CQUAD4 ELEMENT

The CQUAD4 is a four-noded planar element possessing membrane, flexural, and transverse shear stiffness. In the case of layered plates, individual laminae are not modeled explicitly; rather, equivalent stiffness matrices for the plate as a whole are defined. Each lamina is assumed to be in a state of plane stress, and the laminae are presumed to be perfectly bonded by infinitesimally thin non-shear-deformable layers. Each lamina is assumed to be specially orthotropic, with six independent elastic moduli when through-thickness direct stresses and strains are ignored. Any alignment of lamina fiber axis with respect to the local element coordinate system can be accomodated. Hence, any layup or stacking sequence can be handled (unidirectional, cross-ply, regular or irregular angle-ply). Layups unsymmetric with respect to plate midplane can also be modeled, as membrane-bending coupling is accounted for when it occurs. Each lamina may also be composed of a different orthotropic material, if desired.

The element's stiffness matrix terms for determining in-plane displacements and flexural rotations as a function of imposed forces and moments arise from CLT assumptions. The CQUAD4's force-versus strain equations for membrane, flexural, and membrane-flexure coupling (Ref. 4) are identical to those developed in sections 2.1 through 2.6 of Reference 6. The kinematic assumptions regarding in-plane and flexural strains and displacements follow classical assumptions and require no explanatory remarks here. Reference 4 documents the force-versus strain matrix terms for transverse shear strains. These are based on overall element equilibrium, continuity of transverse shear between adjacent laminae, and satisfaction of zero shear strain and stress boundary conditions on the upper- and lower-most laminate facings. As mentioned earlier, the strain-versus displacement matrix is based on the assumption that through-

thickness planar sections rotate with respect to the plate midsurface and also distort out of planes originally perpendicular to the midsurface.

The CQUAD4 is an isoparametric element, whose displacement fields are interpolated through space by linear variations of in-plane and transverse displacements (and rotations about midsurface) between grid points. The associated in-plane strains are constant between grid points but vary linearly with the thickness coordinate. However, transverse shear strain varies quadratically through each lamina thickness.

Those who use the CQUAD4 to model fiber-reinforced composite plates must realize that the input elastic moduli are _effective moduli for a <u>particular fiber-matrix combination</u>. There are many different fibers in use (glass, carbon, kevlar, and boron are examples) and many resins or matrix materials, each of which has their own unique elastic moduli. Although matrix resins are usually considered to be isotropic, fibers have distinct extensional, transverse, and shear moduli. The effective in-plane moduli of an orthotropic continuum defined to be equivalent to the actual inhomogeneous fiber and resin system are (sometimes nonlinear) functions of the extensional, transverse, and shear moduli of the fiber, the extensional and shear moduli of the resin, and the Poisson's ratios of the fiber and resin. The fraction of the lamina volume occupied by fiber material is an important variable defining the magnitude of effective in-plane lamina moduli. Some strength-of-materials relationships defining effective lamina in-plane moduli as a function of constituent matrix and fiber moduli and fiber volume fraction are developed in sections 3.1 and 3.2 of reference 6. Reference 9 provides a handy tabulation of effective lamina elastic moduli under the assumption of a transversely isotropic lamina. Chamis provides formulas for effective out-of-plane shear moduli as well as the more commonly reported in-plane extension and shear moduli.

APPROACH

Specifics of the present vibration modeling study are now described.

PLATE VIBRATION SPECIMENS

It was desired that the validity of the CQUAD4 be proven by comparison to numerical results obtained independently by other researchers, and to experimental data, if possible. Lin, Ni, and Adams (Ref. 10,11) and Xiao, Lin, and Ju (Ref. 12) have published experimental data and finite element computations for the lowest six vibration modes of square CFRP and GFRP plates for free, unconstrained boundary conditions. They measured and computed both natural frequencies and damping loss factors, which makes their work almost uniquely complete and thorough. Reference 11 contains data for nine plates repeating that for four plates treated in reference 10. Reference 12 revisits three previously examined plates with a

more refined finite element formulation allowing plane sections to rotate and warp, with consistent correction of all strain-displacement relations for these kinematic conditions. This paper contains data for one additional new plate, making a total of ten unique plates in all (four CFRP and six GFRP). Refinement of their finite element method (Ref. 12) improved correlation of their predictions with measurements.

The geometric and material parameters of the ten plates studied by Lin et. al. and Xiao et. al. are listed (in SI units) in Table 1. The parameters given in reference 12 for plates 770 and 772 are inconsistent with those reported in reference 11. The NASTRAN study confirmed that the side lengths, thicknesses, average mass densities, and fiber volume fractions given for plates 770 and 772 in reference 11 are the correct values. Further correlation of plate parameters, frequencies, and mode shapes between references 10-12 revealed accidental reversal of mode shape plot labels in reference 11. In addition, two unidirectional GFRP plates of different size are reported in references 11 and 12 with the identification number 761. (They are herein distinguished from the other as 761L and 761X). These discrepancies initially caused much confusion, but the author is confident that the data in Table 1 is correct.

Some features of these plate specimens are notable. All of them are square, and have L/t ratios in the vicinity of 100 to 150. Even though such L/t would seem to be in the range of applicability of CLT, Xiao et. al. show that CLT, which totally ignores transverse shear deformations, overestimates natural frequencies by factors as high as sixteen percent over a theory with first-order shear correction. All of the laminates listed in Table 1 are symmetric about the plate midplane, eliminating flexure/extension coupling effects. Five plates (GFRP specimens 734, 761(L), 761(X) and CFRP specimens 762 and 764) have "specially orthotropic" lamina (all fibers aligned with the plate sides). For these plates, there is no coupling between in-plane extension and in-plane shearing, so their vibration mode shapes have nodal lines more or less parallel with the plate edges. The other five plates (765, 769, 771, 770, 772) have at least some plies with fibers angled relative to plate edges, providing more complex mode shapes.

All plates were tested with "free" edges (supported by soft foam rubber strips) and numerically analyzed with zero-constraint boundary conditions. (Although many practical design problems of interest would involve plate structures with boundary constraints, this feature eliminates uncertainties about which boundary degrees-of-freedom (DOF) to constrain to obtain "simply supported" edges). An iterative technique was used to obtain natural frequencies and modal damping loss factors. First, the specimens were excited into steady-state vibration by an electrodynamic shaker, and approximate resonance frequencies were determined. Nodal lines for each excited natural mode were located by the classical Chladni sand pattern technique. Then, for each mode of interest, locations of the support strips were then adjusted to align with nodal lines. A transient excitation technique was then used to obtain more precise

estimates of resonance frequencies and modal damping loss factors.

LAMINA MATERIAL PROPERTIES

Effective in-plane lamina elastic moduli are reported in Lin et. al. and Xiao et. al. These are listed in Table 2, in both SI and English units. These moduli pertain to a lamina microstructure where half of the total ply volume is occupied by fibers and half by the matrix. For each plate analyzed here, the moduli input to NASTRAN must be adjusted up or down from these nominal values, according to the measured fiber volume fraction (V_f) for each plate. In general, the moduli vary nonlinearly with V_f, but experimentally-verified semi-empirical equations are available for determining V_f-adjusted moduli. References 10-12 reported only the nominal moduli in Table 2, but provided a literature source (Ref. 13) for accomplishing the adjustments.

For orthotropic laminae in a state of plane stress (in the 1-2 plane), the only independent engineering moduli are E_{11}, E_{22}, G_{12}, and ν_{12}. The additional Poisson's ratio ν_{21} must satisfy the relationship:

$$\nu_{12} / E_{11} = \nu_{21} / E_{22}$$

The NASTRAN CQUAD4 element enforces this constraint on ν_{21} (Ref. 4). With these moduli, all in-plane strain and stress components are defined by the CLT. However, the NASTRAN CQUAD4 element also requires, as input, nonzero transverse shear moduli G_{13} and G_{23}, associated with out-of-plane shearing, which are not specified or required in CLT. Fortunately, fiber-reinforced lamina may often be assumed to be "transversely isotropic" in analysis of composite structures, as implied by reference 9. This means that if the lamina lies in the 1-2 plane, and the fibers are aligned in the 1-direction, then the transverse shear modulus G_{13} is equal to the in-plane shear modulus G_{12}. The transverse shear modulus associated with shearing of the matrix "around" the fibers and distortion of the fiber in a plane perpendicular to its axis (G_{23}) remains to be determined. To clarify these matters, the stress and strain components for a transversely isotropic lamina with zero direct stress normal to the lamina are illustrated in Figure 1.

Lin et. al. and Xiao et. al. did not report either of the transverse shear moduli used in their analyses. Educated guesses had to be made for both the CFRP and GFRP G_{23}. Reference 8 provides nondimensional elastic moduli for a CFRP-like material which are closely satisfied by the in-plane parameters for the CFRP in Table 2. According to reference 8, G_{23} should equal $0.2E_{22}$. This implied value of G_{23} was used in the present CFRP plate analyses, based on fiber volume fraction-adjusted E_{22}. For the glass fiber lamina, $G_{23} = 0.6G_{12}$ was assumed, based on in-house experience with such materials. The assumed out-of-plane moduli are indicated in the "notes" section of Table 2. G_{23} could also be estimated by methods reported in reference 9.

Table 3 contains lamina elastic moduli for each of the ten plates, after adjustment of the nominal moduli in Table 2 for fiber volume fraction. Lin et. al. did not correct the in-plane Poisson's ratio for fiber volume fraction, even though Ni and Adams show that it decreases appreciably for increasing V_f. Lin et. al. claim that accounting for this decrease had no significant effect on their calculated natural vibration frequencies. We match their assumption by keeping ν_{12} constant at 0.3 for all ten plates. In general, ν_{12} should be adjusted for V_f.

ASSUMPTIONS REGARDING LAMINATE BEHAVIOR

The kinematic assumptions of the CQUAD4 element have been discussed previously; namely, that planar sections perpendicular to the plate midplane can rotate and warp relative to the midplane. NASTRAN-computed natural frequencies for CQUAD4 plate idealizations will, subsequently, be compared to some CLT predictions (Ref. 12) and to the FEA predictions of Lin et. al. (Ref. 11) and Xiao et. al. (Ref. 12) These three approaches differ in accuracy, and it is important to understand how the NASTRAN predictions should compare with them. Kinematic assumptions are discussed first.

As discussed previously, CLT totally ignores any transverse shear deformation effect, and will always predict lower-order vibration frequencies which are too high for laminates with low L/t and high extensional-to-shear modulus ratios. In terms of through-thickness lamina kinematics, CLT prescribes linear variations of direct and in-plane shear strains, and zero transverse shear strains. The kinematic assumptions of Lin et. al. (Ref. 11) and within the CQUAD4 (Ref. 4) are identical, and imply linear through-thickness variations of direct and in-plane shear strains and quadratic through-thickness variations of transverse shear strains, with zero shear stress boundary conditions on the upper- and lowermost lamina facings satisfied. However, this thick plate-type theory is only an approximation; consistent correction of all strain-displacement relationships when cross-section warping is allowed requires cubic through-thickness variations of direct and in-plane shear strains. Xiao et. al. (Ref. 12) include this considerable complication in their plate-type FEA formulation, which can be understood as a special case of three-dimensional elasticity.

From an understanding of kinematic assumptions alone, CQUAD4 composite plate idealizations should provide natural frequency estimates that are (1), more accurate than CLT, (2) as accurate as the Lin et. al. predictions, and (3) less accurate than the Xiao et. al. predictions. However, other factors will influence the comparisons between FEA-predicted frequencies; particularly, the polynomial form of the interpolation functions expressing element displacement fields in terms of grid point displacements, and the mass matrix formulation (consistent or lumped). The CQUAD4 utilizes linear interpolation functions with respect to the element's four grid points. Lin et. al. do not specify the interpolation func-

tions used in their "8-node 40-degree-of-freedom" elements, although they can be guessed to be of at least quadratic order.

NASTRAN ANALYSES

The results of the NASTRAN computations are now compared to the calculations and experimental data in references 10-12.

FEATURES OF THE NASTRAN PLATE IDEALIZATIONS

Lin et. al. and Xiao et. al. employed a 6-by-6 mesh of 8-noded isoparametric rectangular elements in all of their plate FEA idealizations. Each element possessed 40 DOF, (5 per grid point), implying that all rotations about axes normal to the plate surface were constrained. As in the CQUAD4, they applied a numerical conditioning factor to transverse shear stiffness terms to eliminate excessive shear stiffness ("shear locking"); a consequence of numerical integration of element stiffness. The NASTRAN CQUAD4 elements also have five DOF per node, with normal axis rotation constraints applied, and are also conditioned to avoid shear locking.

The CQUAD4 differs from the Lin and Xiao et. al. elements in one important way; they are 4-noded isoparametric quadrilaterals and thus have _linear_ interpolation of in-plane displacements between grid points instead of _quadratic_ interpolation. Thus, although the Lin et. al. element is kinematically similar to the CQUAD4 as far as through-thickness shear effects are concerned, the elements' assumed in-plane displacement fields differ as a function of the plate's in-plane dimensions. The Xiao et. al. element provides for a more complex through-thickness displacement and strain distribution than the Lin et. al. element and the CQUAD4, as discussed earlier.

The NASTRAN CQUAD4 meshes used here consist of a 12-by-12 grid of elements, with 169 grid points and 845 unconstrained DOF. These idealizations are roughly comparable to the Lin and Xiao models in modal displacement field interpolation quality. Three of the plates were initially modeled with 6-by-6 meshes with 49 grid points and 245 DOF, but these idealizations did not provide sufficient mode shape resolution to be acceptable. The Lin and Xiao et. al. mesh is compared to the NASTRAN mesh in Figure 2.

The edges of the NASTRAN plate idealizations were unconstrained, and all rotations about axes normal to the plate surface were suppressed. A SUPORT input record imposing fictitious constraints on all five remaining DOF on one grid point was used to provide zero-frequency rigid body modes. The FEER eigenmode extraction method was used in NASTRAN Rigid Format 3 (normal modes analysis), with the lowest twenty modes requested. The Inverse Power method was employed in some trial runs; it provided about half as many frequencies as FEER but at more than two times greater run time and cost. All computations were performed by RPK COSMIC NASTRAN, 1990 release, installed on the DTRC CRAY X-MP supercomputer in a COS operating system environment. Typically, 22 to 24 modes were extracted by FEER in 23 to 24 CP seconds.

Lin and Xiao do not mention whether they used lumped or consistent mass matrix formulations. Both options were considered in the NASTRAN study.

NASTRAN MODAL ANALYSIS RESULTS

Initial NASTRAN analyses utilized nominal elastic moduli based on fifty percent fiber volume fraction. Although predicted frequencies were in the general vicinity of measured values, they did not compare with CLT results, the Lin et. al. results, or the Xiao et. al. results in the expected way. That is, the CQUAD4 did not necessarily appear more accurate than CLT and less accurate than the Xiao et. al. approach. It suffices to say that fiber volume fraction strongly influences effective moduli and must be accounted for to obtain credible composite plate modal predictions.

Relative NASTRAN frequency predictions are compared with CLT, Lin's, and Xiao's results in Table 4. There is, in general, good correlation with measurements, and NASTRAN's frequency error trends are comparable to those in the Lin et. al. analyses (especially those for a consistent mass matrix). The fact that effective lamina elastic moduli must be corrected for fiber volume fraction to obtain credible natural frequency predictions for laminated composite plates is emphasized in Table 5, where root-mean-square (RMS) values of frequency prediction percentage error are tabulated for the six modes of each plate. RMS error is seen to be significantly reduced in most cases when fiber volume fraction-corrected lamina moduli are employed. The major exception is plate 765, which still suffers from some large unknown systematic error making predicted frequencies far too low. Results for plate 770 were not much changed since actual V_f was already close to one-half. RMS errors for plates 764 and 771 remain at ten percent and above. However, the major part of these high errors involves their fundamental modes, which can be easily impacted by test article boundary constraint. (The Lin et. al. analysis also predicted overly high frequencies for these modes).

Absolute measured and predicted natural frequencies are summarized in Table 6, which lists Lin et. al. measurements and computations and the NASTRAN CQUAD4 idealization results for lumped and consistent mass. Mode-by-mode and average percentage frequency prediction errors are listed in Table 7 along with mode shape descriptions. The NASTRAN lumped mass model gives the lowest average error in seven of ten cases, and the NASTRAN consistent mass model is best in two of the three remaining cases. (Interestingly, the consistent mass model errors roughly parallel those of the Lin model). Lin et. al. calculations are "best" only for plate 765, for which the author believes a parameter was misdocumented in reference 11. In six of the nine plates other than 765, NASTRAN predicts frequencies that are all at or within ten percent of measured. In the other three, errors are greater than ten percent only for the first and/or second modes, and these roughly parallel the errors in the Lin et. al. analyses.

Plots of chosen NASTRAN-computed eigenmodes are presented in Figures 3-8. Plate 761X does not appear since its mode shapes are identical to plate 761L, and plates 764, 770, and 772 are omitted since their mode shapes are very similar to those of plates 734, 769, and 771. The nodal patterns can be confirmed as being identical to those measured. (Figures 3-8 should be compared to Tables 8, 7, 10, 9, 11, and 3, respectively, of reference 11). Finer details of some NASTRAN modes, particularly the veering of nodal lines away from each other in plates with angled plies, are more easily seen in colored graphics terminal displays. Only the plates with specially orthotropic ply layups (734, 761L, 761X, 762, 764) exhibit eigenmodes with nodal lines more or less parallel to the plate sides. Most of these modes are essentially beam-like flexural modes with or without phase changes at one symmetry plane. In contrast, plates with angled plies possess a larger number of more complex plate flexural modes.

The natural frequency results obtained via NASTRAN CQUAD4 plate element idealizations in these simple composite plate vibration problems are judged to be acceptably accurate for engineering purposes. The element performs as well as alternative formulations of similar accuracy (the Lin et. al. element) for both GFRP and highly anisotropic CFRP plates for a variety of ply geometries. Potential users of the element must be cautioned that this validation effort concerned plates with L/t ratios in the vicinity of 100 to 150. For such L/t, modeling of laminate transverse shear stiffness helps to eke out a few percent in low-order natural frequency accuracy, but is not absolutely essential to obtain rough-cut results. A more critical test of the CQUAD4 for modeling highly anisotropic laminates would have to concern plates with L/t lower than, say, about 50.

It should be mentioned that Lin et. al. and Xiao et. al. also measured and computed the specific damping capacities (2π times the modal loss factor) of each mode. Their FEA program was capable of modeling orthotropic lamina damping properties. No attempt was made to predict modal damping factors in this effort, as NASTRAN is currently restricted to the modeling of isotropic material damping.

SUMMARY

The performance of the NASTRAN CQUAD4 membrane and plate element in analysis of undamped natural vibration modes of thin fiber-reinforced composite plates has been evaluated. The element provides natural frequency estimates that are comparable in accuracy to alternative formulations, and, in most cases, deviate by less than ten percent from experimentally measured frequencies. The predictions lie within roughly equal accuracy bounds for the two material types treated (GFRP and CFRP), and for the ply layups considered (unidirectional, cross-ply, angle-ply). Effective elastic lamina moduli had to be adjusted for measured fiber volume fraction to attain this level of accuracy; nominal moduli at fifty percent volume fraction gave significantly inferior frequency estimates. The lumped mass option provided more accurate frequen-

cies than the consistent mass option.

This evaluation concerned only plates with L/t ratios on the order of 100 to 150. Since the CQUAD4 utilizes first-order corrections for transverse laminate shear stiffness, the element should provide useful frequency estimates for plate-like structures with lower L/t. For plates with L/t below 20, consideration should be given to idealizing with 3-D solid elements.

Based on the observation that natural frequencies and mode shapes are predicted with acceptable engineering accuracy, it is concluded that the CQUAD4 should be a useful and accurate element for transient shock and steady-state vibration analysis of Naval ship structures.

REFERENCES

1. Everstine, G. C. and M. S. Marcus, "Finite Element Prediction of Loss Factors for Structures with Frequency-Dependent Damping Treatments", 13th NASTRAN User's Colloquium, NASA CP-2373, National Aeronautics and Space Administration, Washington, D. C., pp. 419-430 (May 1985).

2. Everstine, G. C., F. M. Henderson, E. A. Schroeder, R. R. Lipman, "A General Low Frequency Acoustic Radiation Capability for NASTRAN", 14th NASTRAN User's Colloquium, NASA CP-2419, National Aeronautics and Space Administration, Washington, D. C., pp. 293-310 (May 1986).

3. Everstine, G. C. and A. J. Quezon, "User's Guide to the Coupled NASTRAN/ Helmholtz Equation Capability (NASHUA) for Acoustic Radiation and Scattering", Third Edition, DTRC CMLD-88/03 (Feb 1988).

4. Venkayya, V. B., "CQUAD4 Seminar," Presentation given at 16th NASTRAN User's Colloquium (Apr 1988).

5. Marcus, M. S., G. C. Everstine, M. M. Hurwitz, "Experiences with the QUAD4 Element for Shell Vibrations", 16th NASTRAN User's Colloquium, NASA CP-2505, pp. 39-43 (Apr 1988).

6. Jones, R. M. Mechanics of Composite Materials, Hemisphere Publishing Corporation, New York, New York, 1975.

7. Cremer, L., M. Heckl, E. Ungar, Structure-Borne Sound, Springer-Verlag, New York, New York, 1973.

8. Mallikarjuna and T. Kant, "Free Vibration of Symmetrically Laminated Plates using a Higher-Order Theory with Finite Element Technique", Int. J. Num. Meth. Eng., Vol. 28, pp. 1875-1889 (1989).

9. Chamis, C. C., "Simplified Composite Micromechanics Equations for Hygral, Thermal, and Mechanical Properties", SAMPE Quarterly, Vol. 15, No. 3, pp. 14-23 (Apr 1984).

10. Adams, R. D., D. X. Lin, R. G. Ni, "Prediction and Measurement of the Natural Frequencies and Damping Capacity of Carbon Fiber-Reinforced Plastic Plates", Journal de Physique, Colloque No. 9, pp. C9-525 - C9-530 (1983).

11. Lin, D. X., R. G. Ni, R. D. Adams, "Prediction and Measurement of the Vibrational Damping Parameters of Carbon and Glass Fibre-Reinforced Plastic Plates", J. Composite Materials, Vol. 18, pp. 132-152 (Mar 1984).

12. Xiao, C. Z., D. X. Lin, F. Ju, "Finite Element Analysis on Modal Parameters of Anisotropic Laminated Plates", ASME J. Vib. Acous. Stress and Reliability in Design, Vol. 110, pp. 473-477 (Oct 1988).

13. Ni, R. G. and R. D. Adams, "A Rational Method for Obtaining the Dynamic Mechanical Properties of Laminae for Predicting the Stiffness and Damping of Laminated Plates and Beams", Composites, Vol. 15, No. 3, pp. 193-199 (Jul 1984).

Table 1. Geometric and material parameters
of ten fiber-reinforced plastic
plates tested and analyzed by
Lin et. al. and Xiao et. al.

Plate Ident. Number	Plate Material	Plate Length L (mm)	Plate Thickness t (mm)	Fiber Volume Fraction V_f	Mass Density ρ_3 (kg/m^3)	Number of Plies	Ply Layup (degrees; see Figure 2)	Source of Data (ref. no.)
734	GFRP	227.0	2.05	0.451	1813.9	8	[0/90/0/90]	10,11,12
761L	GFRP	182.75	1.64	0.568	1971.0	8	[0]	11
761X	GFRP	249.0	2.28	0.530	1924.7	8	[0]	12
765	GFRP	230.5	1.45	0.607	2023.6	8	[45/-45/45/-45]	11
769	GFRP	224.2	1.37	0.621	2041.7	8	[0/90/45/-45]	11
771	GFRP	204.6	2.11	0.592	2003.5	12	[(0/-60/60)$_2$]	10,11
762	CFRP	178.0	1.58	0.516	1566.0	8	[0]	11
764	CFRP	234.5	2.12	0.342	1446.2	8	[0/90/0/90]	10,11
770	CFRP	215.0	1.62	0.494	1551.4	8	[0/90/45/-45]	11,12
772	CFRP	215.6	2.02	0.618	1636.4	12	[(0/-60/60)$_2$]	10,11,12

NOTE: All laminates are symmetric about plate midplane.

Table 2. Nominal in-plane effective elastic
moduli of GFRP and CFRP laminae at
fifty percent fiber volume fraction

Material	Fiber type	Resin type	E_{11} (Gpa)	E_{11} (psi /10^6)	E_{22} (GPa)	E_{22} (psi /10^6)	G_{12} (GPa)	G_{12} (psi /10^6)	ν_{12}
GFRP	"Glass"	DX210 epoxy	37.78	5.48	10.90	1.58	4.91	0.71	0.3
CFRP	HM-S	DX210 epoxy	172.7	25.0	7.20	1.04	3.76	0.55	0.3
DX210 epoxy	-----	-----	3.21	0.47	3.21	0.47	1.20	0.17	0.34

NOTE: $G_{23} = 0.6(G_{12}) = 2.94$ GPa is assumed for GFRP,
$G_{23} = 0.2(E_{22}) = 1.44$ GPa is assumed for CFRP.

Table 3. In-plane and out-of-plane effective elastic
moduli for GFRP and CFRP laminae, adjusted
for fiber volume fraction of each plate

Plate Ident. Number	Plate Material	Fiber Volume Fraction V_f	E_{11} (GPa)	E_{22}, E_{33} (GPa)	G_{12}, G_{13} (GPa)	G_{23} (GPa)
734	GFRP	0.451	34.4	9.7	4.3	2.6
761L	GFRP	0.568	42.5	13.0	5.7	3.4
761X	GFRP	0.530	39.9	12.0	5.2	3.1
765	GFRP	0.607	45.2	14.2	6.5	3.9
769	GFRP	0.621	46.2	14.4	6.7	4.0
771	GFRP	0.592	44.1	14.0	6.2	3.7
762	CFRP	0.516	178.0	7.4	3.9	1.5
764	CFRP	0.342	119.0	5.6	2.6	1.1
770	CFRP	0.494	171.0	7.1	3.7	1.4
772	CFRP	0.618	213.0	8.7	5.0	1.7

NOTE: ν_{12} = 0.30 is assumed for all laminates, with no V_f adjustment.

Table 4. Comparison of natural frequencies from final
NASTRAN CQUAD4 idealizations and predictions of
Lin and Xiao et. al. to measured data

Plate Number and params.	Mode Number	Natural Frequency Ratios, (computed / measured)				
		CLT ref. 12	Lin et. al. ref. 11,12	Xiao et. al. ref. 12	NASTRAN 12-by-12 lumped	NASTRAN 12-by-12 consis.
734 GFRP	1	1.20	1.07	0.98	1.03	1.05
8 plies	2	1.09	1.00	1.00	0.94	0.97
[0/90/0/ 90]sym	3	1.20	1.03	1.00	0.98	1.01
L/t =	4	1.11	1.05	1.03	0.99	1.03
110.7	5	1.12	1.04	1.01	1.00	1.03
	6	1.11	1.06	1.01	0.98	1.04

68

Table 4. (Continued)

Plate Number and params.	Mode Number	Natural Frequency Ratios, (computed / measured)				
		CLT ref. 12	Lin et. al. ref. 11	Xiao et. al. ref. 12	NASTRAN 12-by-12 lumped	NASTRAN 12-by-12 consis.
761L GFRP 8 plies [0] sym L/t = 111.4	1	----	1.13	----	1.11	1.13
	2	----	1.00	----	0.97	1.00
	3	----	1.05	----	1.02	1.05
	4	----	1.00	----	0.94	0.97
	5	----	1.04	----	0.99	1.02
	6	----	1.03	----	0.97	1.03
761X GFRP 8 plies [0] sym L/t = 109.2	1	1.18	1.09	0.98	1.10	1.11
	2	1.20	1.08	1.00	1.02	1.05
	3	1.20	1.08	0.98	1.05	1.08
	4	1.08	0.99	0.99	0.94	0.96
	5	1.10	1.02	0.99	0.98	1.02
	6	1.14	1.03	0.99	0.95	1.01
765 GFRP 8 plies [45/-45/ 45/-45] sym L/t = 159.0	1	----	1.09	----	0.82	0.83
	2	----	0.88	----	0.65	0.67
	3	----	0.95	----	0.68	0.70
	4	----	1.07	----	0.78	0.81
	5	----	1.06	----	0.78	0.81
	6	----	1.02	----	0.72	0.77

Table 4. (Continued)

Plate Number and params.	Mode Number	Natural Frequency Ratios, (computed / measured)				
		CLT ref. 12	Lin et. al. ref.11	Xiao et. al. ref. 12	NASTRAN 12-by-12 lumped	NASTRAN 12-by-12 consis.
769 GFRP 8 plies [0/90/45/ -45]sym L/t = 163.6	1	----	0.95	----	0.93	0.95
	2	----	1.08	----	1.03	1.06
	3	----	0.98	----	0.92	0.94
	4	----	1.01	----	0.96	0.99
	5	----	1.04	----	0.99	1.03
	6	----	1.01	----	0.94	0.99
771 GFRP 12 plies [0/-60/60 /0/-60/60] sym L/t = 97.0	1	----	1.20	----	1.19	1.20
	2	----	1.17	----	1.13	1.16
	3	----	0.98	----	0.93	0.96
	4	----	1.06	----	1.02	1.06
	5	----	1.07	----	1.03	1.07
	6	----	1.03	----	0.95	1.01
762 CFRP 8 plies [0] sym L/t = 112.7	1	----	1.03	----	1.01	1.02
	2	----	1.10	----	1.02	1.05
	3	----	1.06	----	0.99	1.04
	4	----	1.11	----	1.01	1.08
	5	----	1.10	----	1.00	1.07
	6	----	1.03	----	1.00	1.03

Table 4. (Continued)

Plate Number and params.	Mode Number	Natural Frequency Ratios, (computed / measured)				
		CLT ref. 12	Lin et. al. ref. 11	Xiao et. al. ref. 12	NASTRAN 12-by-12 lumped	NASTRAN 12-by-12 consis.
764 CFRP 8 plies [0/90/0/ 90] sym L/t = 110.6	1	----	0.84	----	0.81	0.82
	2	----	0.97	----	0.95	0.97
	3	----	0.97	----	0.93	0.96
	4	----	0.99	----	0.97	0.99
	5	----	1.00	----	0.97	1.00
	6	----	0.98	----	0.92	0.97
770 CFRP 8 plies [0/90/45 /-45]sym L/t = 132.7	1	1.14	1.11	1.08	1.10	1.12
	2	1.16	1.11	1.06	1.09	1.12
	3	1.15	1.09	1.00	1.06	1.10
	4	1.07	1.00	1.00	0.98	1.01
	5	1.15	1.08	0.99	1.06	1.09
	6	1.11	1.03	1.00	0.99	1.04
772 CFRP 12 plies [0/-60/60 /0/-60/60] sym L/t = 106.7	1	1.07	1.05	1.00	1.04	1.05
	2	1.05	1.03	1.00	0.99	1.02
	3	1.07	1.04	1.01	1.01	1.04
	4	1.10	1.06	1.00	1.02	1.06
	5	1.09	1.05	1.00	1.02	1.05
	6	1.09	1.03	0.99	0.97	1.03

Table 5. Root-mean-square errors in NASTRAN-computed natural
frequencies for ten composite plates for uncorrected
and corrected effective lamina elastic moduli

Plate Number	RMS error in NASTRAN-predicted frequency	
	With uncorrected moduli (percent)	With corrected moduli (percent)
734	5.3	2.9
761L	8.8	5.5
761X	10.7	5.7
765	34.4	26.7
769	15.6	5.4
771	9.7	10.1
762	2.1	0.8
764	11.9	9.6
770	7.1	6.6
772	9.6	2.5

Table 6. Comparison of absolute measured and predicted
composite plate natural frequencies of Lin et. al.
with NASTRAN CQUAD4 computations

Plate Number and params.	Mode Number	Natural Frequencies (Hz)			
		Lin et. al., ref. 10-12		NASTRAN 12-by-12 lumped	NASTRAN 12-by-12 consis.
		measured	computed		
734 GFRP	1	62.2	66.4	64.2	65.0
8 plies	2	131.4	131.6	123.8	127.4
[0/90/0/ 90]sym	3	159.2	164.5	156.4	160.9
	4	180.5	189.8	177.9	184.0
L/t = 110.7	5	200.1	208.9	199.2	206.0
	6	326.7	347.2	321.2	338.4

Table 6. (Continued)

Plate Number and params.	Mode Number	Natural Frequencies (Hz)			
		Lin et. al., ref. 10-12		NASTRAN 12-by-12 lumped	NASTRAN 12-by-12 consis.
		measured	computed		
761L GFRP 8 plies	1	78.1	88.1	86.9	88.0
	2	131.2	130.7	127.1	130.7
[0] sym	3	211.5	222.2	215.0	222.2
L/t = 111.4	4	246.0	246.1	232.1	238.7
	5	287.1	297.8	284.1	294.2
	6	362.6	374.4	352.9	375.0
761X GFRP 8 plies	1	57.2	62.5	62.9	63.7
	2	90.3	97.4	92.5	95.2
[0] sym	3	148.7	160.5	155.9	161.2
L/t = 109.2	4	181.6	180.2	170.4	175.2
	5	211.2	215.9	207.5	214.9
	6	270.5	278.8	256.9	272.9
765 GFRP 8 plies	1	84.0	91.3	68.7	69.6
	2	114.0	99.9	74.4	76.6
[45/-45/ 45/-45]	3	157.0	149.5	107.1	110.0
sym	4	199.3	212.6	156.3	161.6
L/t = 159.0	5	213.4	226.7	167.2	173.4
	6	346.6	353.5	249.6	265.5

Table 6. (Continued)

Plate Number and params.	Mode Number	Natural Frequencies (Hz)			
		Lin et. al., ref. 10-12		NASTRAN 12-by-12	NASTRAN 12-by-12
		measured	computed	lumped	consis.
769 GFRP 8 plies [0/90/45/ -45]sym L/t = 163.6	1	58.2	55.5	54.4	55.1
	2	91.6	99.0	94.5	97.2
	3	125.5	123.0	115.2	118.4
	4	150.4	151.3	143.8	148.7
	5	156.8	163.0	155.7	161.1
	6	277.3	279.4	260.5	274.4
771 GFRP 12 plies [0/-60/60 /0/-60/60] sym L/t = 97.0	1	90.4	108.2	107.4	108.8
	2	144.7	168.6	163.6	168.4
	3	222.3	218.6	206.6	212.4
	4	264.1	280.2	270.6	279.8
	5	281.1	301.0	290.9	300.9
	6	492.6	505.2	469.7	499.3
762 CFRP 8 plies [0] sym L/t = 112.7	1	81.5	83.6	82.2	83.3
	2	107.4	118.4	109.4	112.5
	3	196.6	207.8	198.4	205.1
	4	295.5	329.4	299.2	318.2
	5	382.5	419.8	383.6	410.2
	6	531.0	546.9	530.6	545.9

Table 6. (Continued)

Plate Number and params.	Mode Number	Natural Frequencies (Hz)			
		Lin et. al., ref. 10-12		NASTRAN 12-by-12 lumped	NASTRAN 12-by-12 consis.
		measured	computed		
764 CFRP 8 plies [0/90/0/ 90] sym L/t = 110.6	1	68.9	58.1	55.5	56.2
	2	218.9	213.3	206.9	212.8
	3	251.2	243.5	233.3	241.5
	4	305.4	302.5	294.9	303.4
	5	323.5	324.2	312.7	323.7
	6	452.5	441.6	414.5	437.8
770 CFRP 8 plies [0/90/45 /-45]sym L/t = 132.7	1	77.8	86.3	85.9	87.0
	2	202.7	224.5	220.6	226.9
	3	258.0	280.4	273.9	283.4
	4	298.7	298.8	293.6	302.0
	5	322.0	348.4	340.6	352.4
	6	496.7	512.2	490.0	517.3
772 CFRP 12 plies [0/-60/60 /0/-60/60] sym L/t = 106.7	1	156.6	165.2	162.7	165.0
	2	272.0	279.1	269.9	277.6
	3	372.3	387.8	376.9	387.6
	4	407.8	432.6	416.7	431.1
	5	486.1	511.4	494.7	512.0
	6	779.0	800.4	752.6	799.4

Table 7. Mode-by-mode tabulation of NASTRAN CQUAD4 idealization frequency prediction errors, with averaged percentage errors and eigenmode descriptions

Plate Number and params.	Mode Number	Percentage errors			Eigenmode description
		Lin et. al.	NASTRAN 12-by-12 lumped	NASTRAN 12-by-12 consis.	
734 GFRP	1	+ 7	+ 3	+ 5	shear and flexure
8 plies	2	0	- 6	- 3	2-noded beam abt. weak axis
[0/90/0/ 90]sym	3	+ 3	- 2	+ 1	2-noded beam abt. strong axis
	4	+ 5	- 1	+ 3	2-noded beam abt. weak axis + shear
L/t = 110.7	5	+ 4	0	+ 3	2-noded beam abt. strong axis + shear
	6	+ 6	- 2	+ 4	fundamental plate flexure
	avg.	+ 4.2	- 1.3	+ 2.2	
761L GFRP	1	+ 13	+ 11	+ 13	shear and flexure
8 plies	2	0	- 3	0	2-noded beam abt. weak axis
[0] sym	3	+ 5	+ 2	+ 5	2-noded beam abt. weak axis + shear
L/t = 111.4	4	0	- 6	- 3	2-noded beam abt. strong axis
	5	+ 4	- 1	+ 2	2-noded beam abt. strong axis + shear
	6	+ 3	- 3	+ 3	3-noded beam abt. weak axis
	avg.	+ 4.2	0	+ 3.3	
761X GFRP	1	+ 9	+ 10	+ 11	shear and flexure
8 plies	2	+ 8	+ 2	+ 5	2-noded beam abt. weak axis
[0] sym	3	+ 8	+ 5	+ 8	2-noded beam abt. weak axis + shear
L/t = 109.2	4	- 1	- 6	- 4	2-noded beam abt. strong axis
	5	+ 2	- 2	+ 2	2-noded beam abt. strong axis + shear
	6	+ 3	- 5	+ 1	3-noded beam abt. weak axis
	avg.	+ 4.8	+ 0.7	+ 3.8	

Table 7. (Continued)

Plate Number and params.	Mode Number	Percentage errors			Eigenmode description
		Lin et. al.	NASTRAN 12-by-12 lumped	NASTRAN 12-by-12 consis.	
765 GFRP	1	+ 9	- 18	- 17	plate flexural
8 plies	2	- 12	- 35	- 33	plate flexural
[45/-45/ 45/-45]	3	- 5	- 32	- 30	plate flexural
sym	4	+ 7	- 22	- 19	plate flexural
L/t = 159.0	5	+ 6	- 22	- 19	plate flexural
	6	+ 2	- 28	- 23	plate flexural
	avg.	+ 1.2	- 26.2	- 23.5	
769 GFRP	1	- 5	- 7	- 5	shear and flexure
8 plies	2	+ 8	+ 3	+ 6	2-noded beam abt. weak axis
[0/90/45/ -45]sym	3	- 2	- 8	- 6	2-noded beam abt. strong axis
	4	+ 1	- 4	- 1	plate flexural
L/t = 163.6	5	+ 4	- 1	+ 3	plate flexural
	6	+ 1	- 6	- 1	plate flexural
	avg.	+ 1.2	- 3.8	- 0.7	
771 GFRP	1	+ 20	+ 19	+ 20	shear and flexure
12 plies	2	+ 17	+ 13	+ 16	2-noded beam abt. weak axis
[0/-60/60 /0/-60/60]	3	- 2	- 7	- 4	2-noded beam abt. strong axis
sym	4	+ 6	+ 2	+ 6	plate flexural
L/t = 97.0	5	+ 7	+ 3	+ 7	plate flexural
	6	+ 3	- 5	+ 1	3-noded beam abt. weak axis
	avg.	+ 8.5	+ 4.2	+ 7.7	

Table 7. (Continued)

Plate Number and params.	Mode Number	Percentage errors			Eigenmode description
		Lin et. al.	NASTRAN 12-by-12 lumped	NASTRAN 12-by-12 consis.	
762 CFRP	1	+ 3	+ 1	+ 2	shear and flexure
8 plies	2	+ 10	+ 2	+ 5	2-noded beam abt. weak axis
[0] sym	3	+ 6	- 1	+ 4	2-noded beam abt. weak axis + shear
L/t = 112.7	4	+ 11	+ 1	+ 8	3-noded beam abt. weak axis
	5	+ 10	0	+ 7	3-noded beam abt. weak axis + shear
	6	+ 3	0	+ 3	2-noded beam abt. strong axis
	avg.	+ 7.2	+ 0.5	+ 4.8	
764 CFRP	1	- 16	- 19	- 18	shear and flexure
8 plies	2	- 3	- 5	- 3	2-noded beam abt. weak axis
[0/90/0/ 90] sym	3	- 3	- 7	- 4	2-noded beam abt. weak axis + shear
	4	- 1	- 3	- 1	2-noded beam abt. strong axis
L/t = 110.6	5	0	- 3	0	2-noded beam abt. strong axis + shear
	6	- 2	- 8	- 3	fundamental plate flexure
	avg.	- 4.2	- 7.5	- 4.8	
770 CFRP	1	+ 11	+ 10	+ 12	shear and flexure
8 plies	2	+ 11	+ 9	+ 12	2-noded beam abt. weak axis
[0/90/45 /-45]sym	3	+ 9	+ 6	+ 10	plate flexural
	4	0	- 2	+ 1	2-noded beam abt. strong axis
L/t = 132.7	5	+ 8	+ 6	+ 9	plate flexural
	6	+ 3	- 1	+ 4	plate flexural
	avg.	+ 7.0	+ 4.7	+ 8.0	

Table 7. (Continued)

Plate Number and params.	Mode Number	Percentage errors			Eigenmode description
		Lin et. al.	NASTRAN 12-by-12 lumped	NASTRAN 12-by-12 consis.	
772 CFRP	1	+ 5	+ 4	+ 5	shear and flexure
12 plies	2	+ 3	- 1	+ 2	2-noded beam abt. weak axis
[0/-60/60 /0/-60/60]	3	+ 4	+ 1	+ 4	2-noded beam abt. strong axis
sym	4	+ 6	+ 2	+ 6	plate flexural
L/t = 106.7	5	+ 5	+ 2	+ 5	plate flexural
	6	+ 3	- 3	+ 3	3-noded beam abt. weak axis
	avg.	+ 4.3	+ 0.8	+ 4.2	
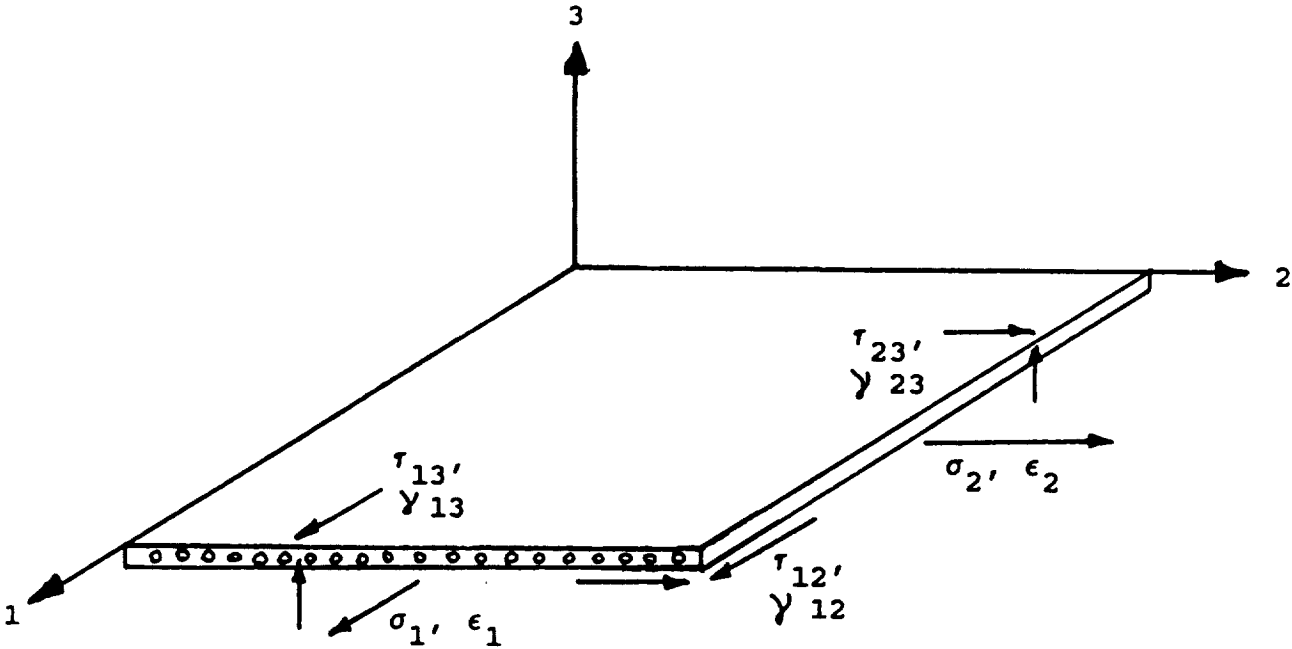
Notes: Positive X-axis: fiber orientation angle of 0 degrees
       Positive Y-axis: fiber orientation angle of 90 degrees

8-noded rectangles

4-noded CQUAD4's

6-by-6 mesh

12-by-12 mesh
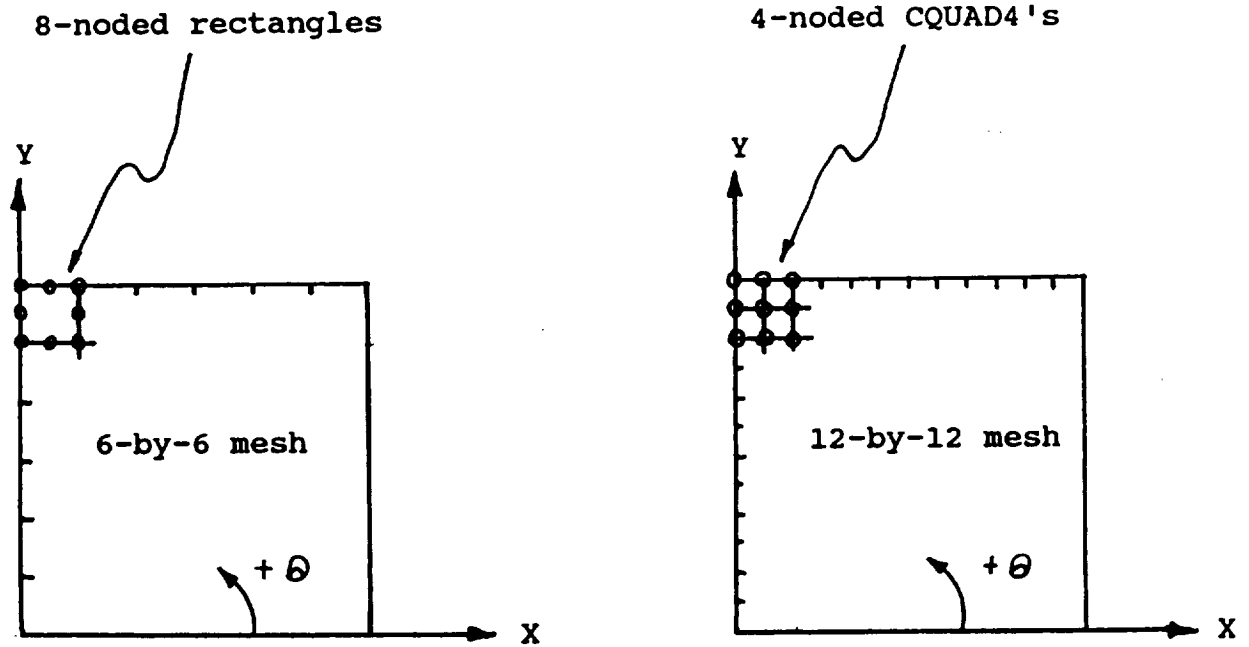
(i) Lin and Xiao et. al.
    idealization

(ii) NASTRAN CQUAD4
     idealization

Figure 2.   Plate element meshes used by Lin and
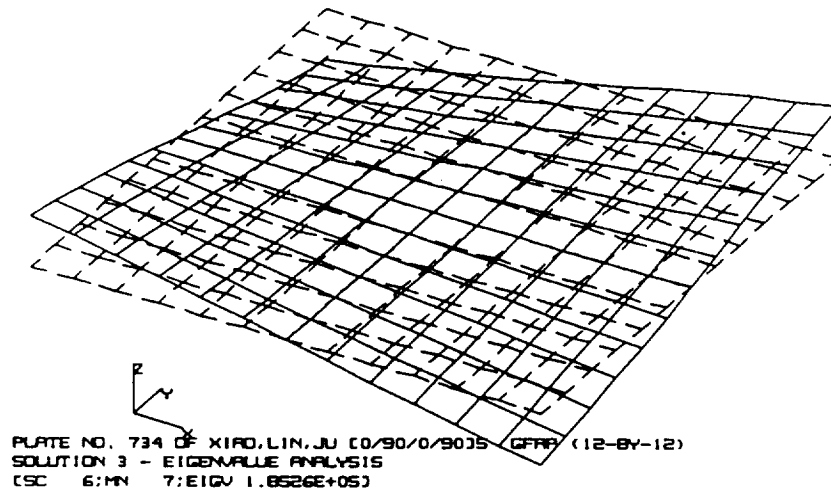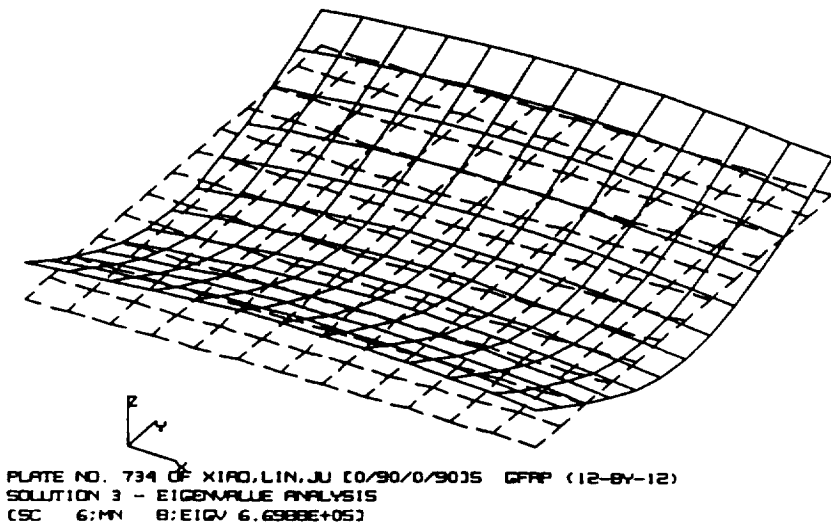   Xiao et. al. and in NASTRAN analyses

PLATE NO. 734 OF XIAO,LIN,JU [0/90/0/90]S GFRP (12-BY-12)
SOLUTION 3 - EIGENVALUE ANALYSIS
[SC   6;MN   7;EIGV 1.8526E+05]

Fig. 3a.   **Plate 734, Mode 1**

PLATE NO. 734 OF XIAO,LIN,JU [0/90/0/90]S GFRP (12-BY-12)
SOLUTION 3 - EIGENVALUE ANALYSIS
[SC   6;MN   8;EIGV 6.6988E+05]

Fig 3b.   **Plate 734, Mode 2**

Figure 3.   **NASTRAN-computed eigenmodes for plate 734**

82

PLATE NO. 734 OF XIAO,LIN,JU [0/90/0/90]S GFRP (12-BY-12)
SOLUTION 3 - EIGENVALUE ANALYSIS
[SC 6:MN 9:EIGV 1.0651E+06]

Fig. 3c.   Plate 734, Mode 3

PLATE NO. 734 OF XIAO,LIN,JU [0/90/0/90]S GFRP (12-BY-12)
SOLUTION 3 - EIGENVALUE ANALYSIS
[SC 6:MN 10:EIGV 1.4054E+06]
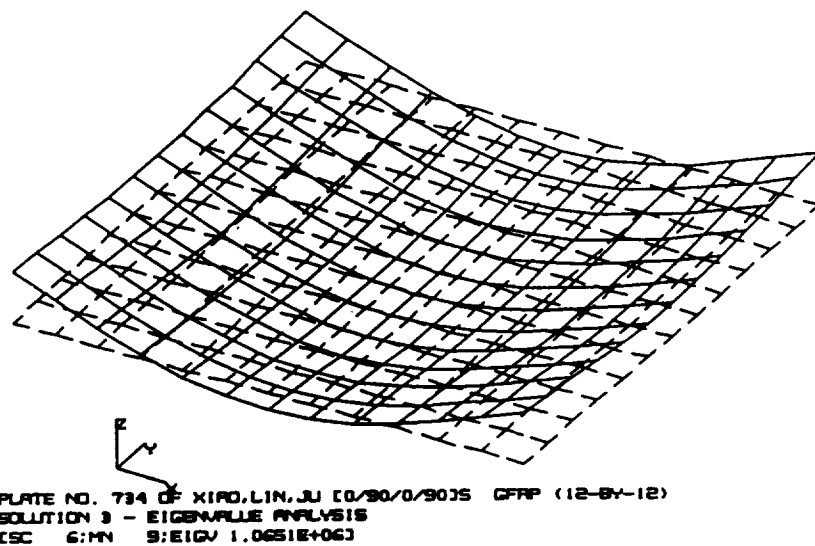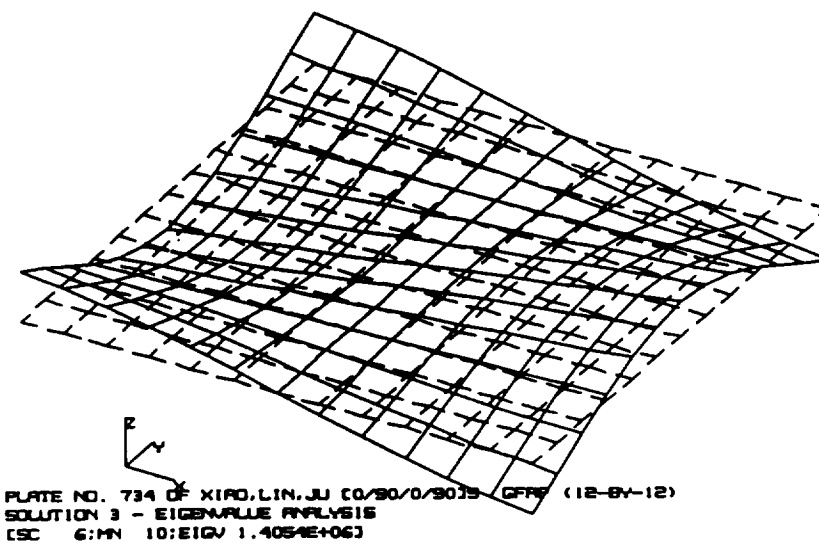
Fig. 3d.   Plate 734, Mode 4

Figure 3.   (Continued)

PLATE NO. 734 OF XIAO,LIN,JU [0/90/0/90]S GFRP (12-BY-12)
SOLUTION 3 - EIGENVALUE ANALYSIS
[SC   6;MN   11;EIGV 1.7489E+06]

Fig. 3e.   Plate 734, Mode 5

PLATE NO. 734 OF XIAO,LIN,JU [0/90/0/90]S GFRP (12-BY-12)
SOLUTION 3 - EIGENVALUE ANALYSIS
[SC   6;MN   12;EIGV 4.5868E+06]
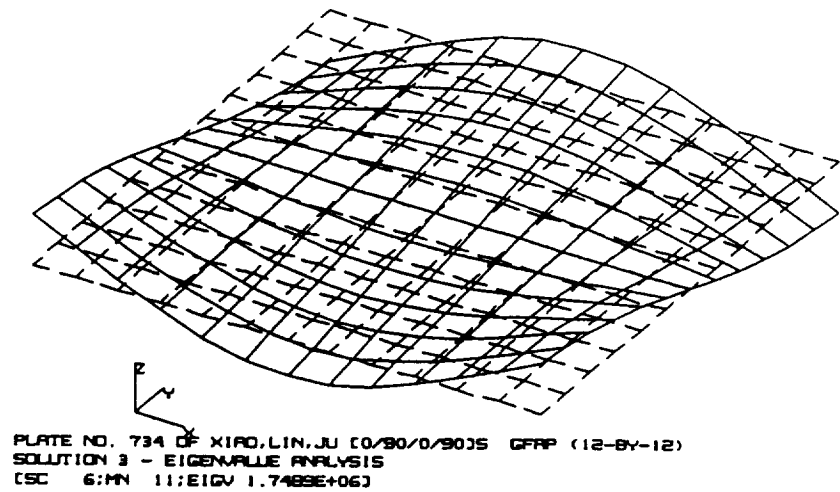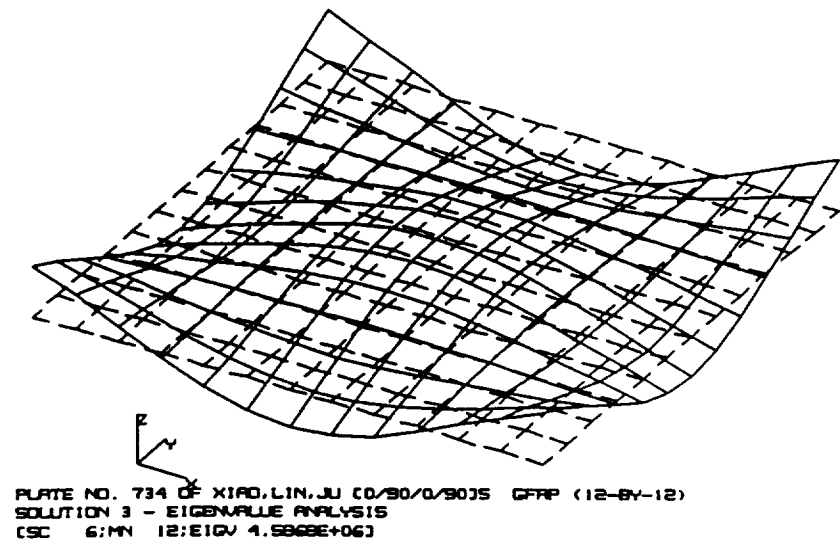
Fig. 3f.   Plate 734, Mode 6

Figure 3.   (Continued)

PLATE 761 OF LIN,NI,ADAMS (1984) [(0)8] GFRP (12-BY-12)
SOLUTION 3 - EIGENVALUE ANALYSIS
[SC   7:MN   7:EIGV 2.5643E+05]

Fig. 4a.   Plate 761L, Mode 1

PLATE 761 OF LIN,NI,ADAMS (1984) [(0)8] GFRP (12-BY-12)
SOLUTION 3 - EIGENVALUE ANALYSIS
[SC   8:MN   8:EIGV 5.3465E+05]
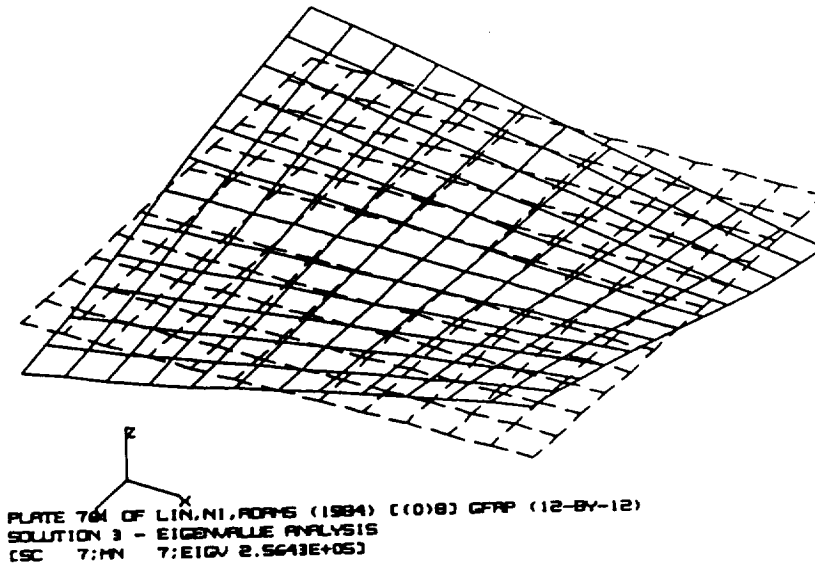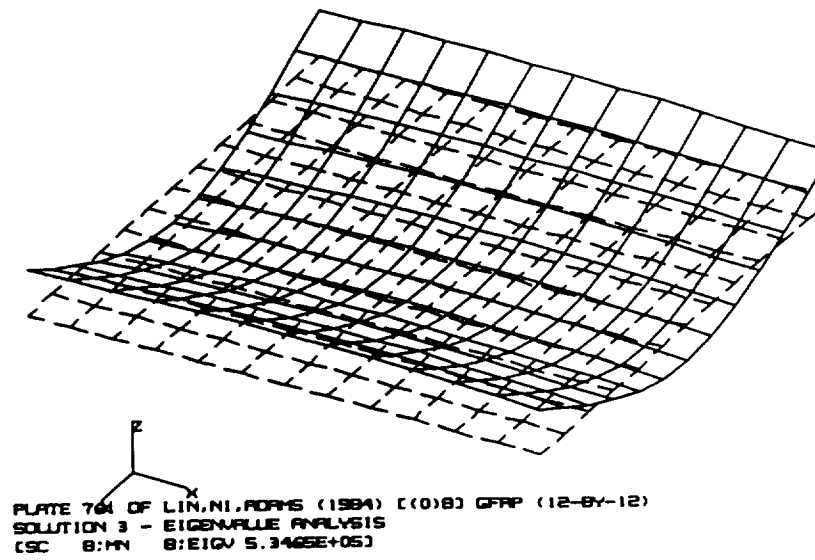
Fig 4b.   Plate 761L, Mode 2

Figure 4.   NASTRAN-computed eigenmodes for plate 761L

PLATE 761 OF LIN,NI,ADAMS (1984) [(0)8] GFRP (12-BY-12)
SOLUTION 3 - EIGENVALUE ANALYSIS
[SC   9:MN   9:EIGV 1.5564E+06]

Fig. 4c.   Plate 761L, Mode 3

PLATE 761 OF LIN,NI,ADAMS (1984) [(0)8] GFRP (12-BY-12)
SOLUTION 3 - EIGENVALUE ANALYSIS
[SC   10:MN   10:EIGV 1.8870E+06]
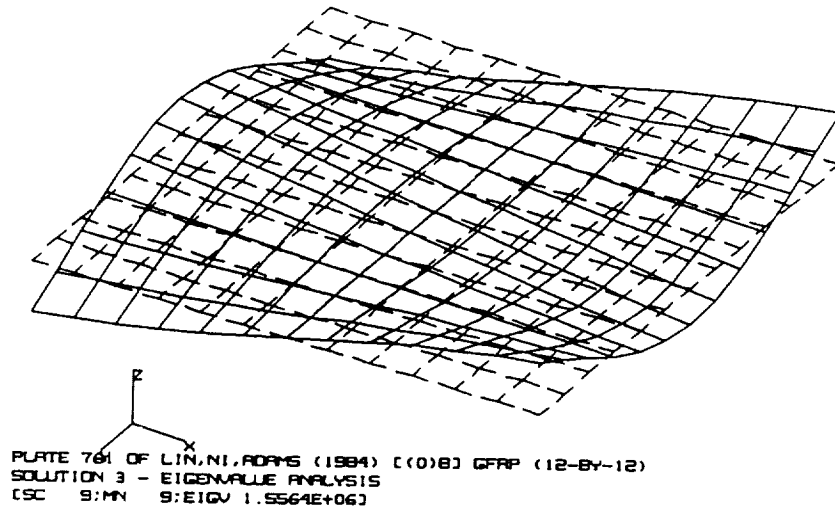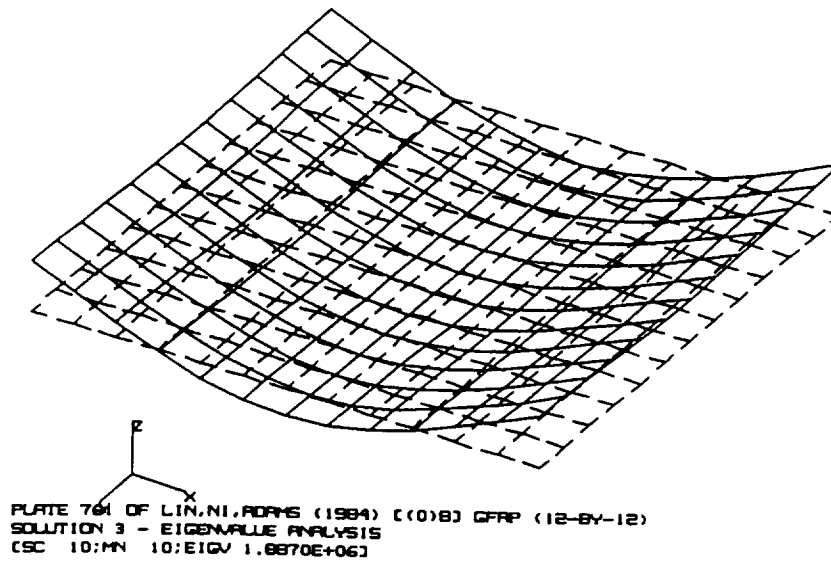
Fig. 4d.   Plate 761L, Mode 4

Figure 4.   (Continued)

86

PLATE 761 OF LIN,NI,ADAMS (1984) [(0)8] GFRP (12-BY-12)
SOLUTION 3 - EIGENVALUE ANALYSIS
[SC 11;MN 11;EIGV 2.7960E+06]

Fig. 4e.   Plate 761L, Mode 5

PLATE 761 OF LIN,NI,ADAMS (1984) [(0)8] GFRP (12-BY-12)
SOLUTION 3 - EIGENVALUE ANALYSIS
[SC 12;MN 12;EIGV 4.1244E+06]
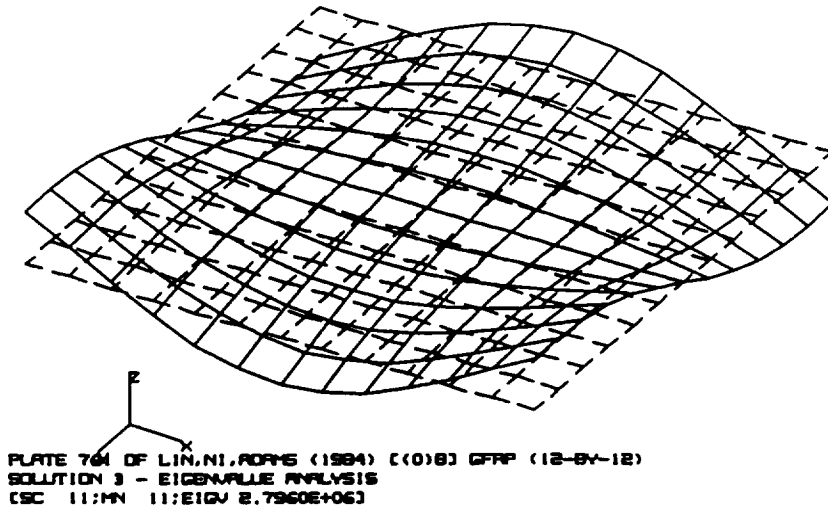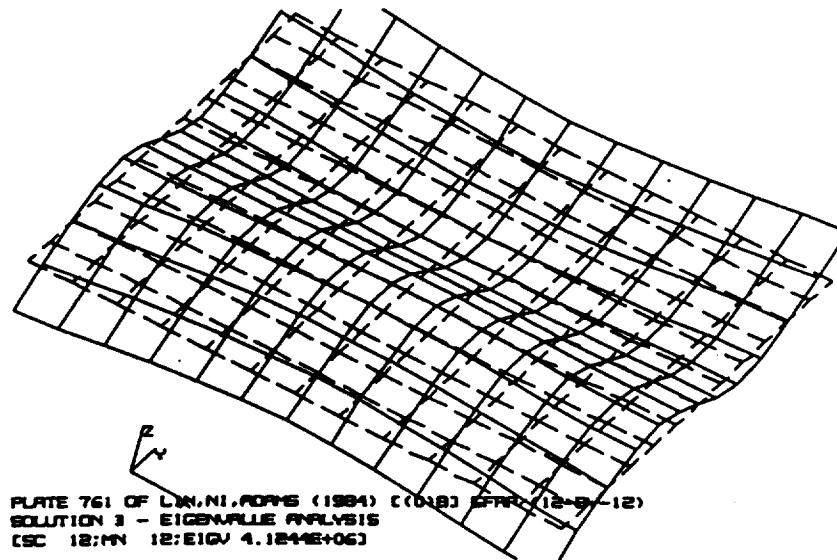
Fig. 4f.   Plate 761L, Mode 6

Figure 4.   (Continued)

87

PLATE 765 OF LIN,NI,ADAMS (1984) [45,-45,45,-45]S GFRP (12-BY-12)
SOLUTION 3 - EIGENVALUE ANALYSIS
[SC   7:MN   7:EIGV 1.5218E+05]

Fig. 5a.   Plate 765, Mode 1

PLATE 765 OF LIN,NI,ADAMS (1984) [45,-45,45,-45]S GFRP (12-BY-12)
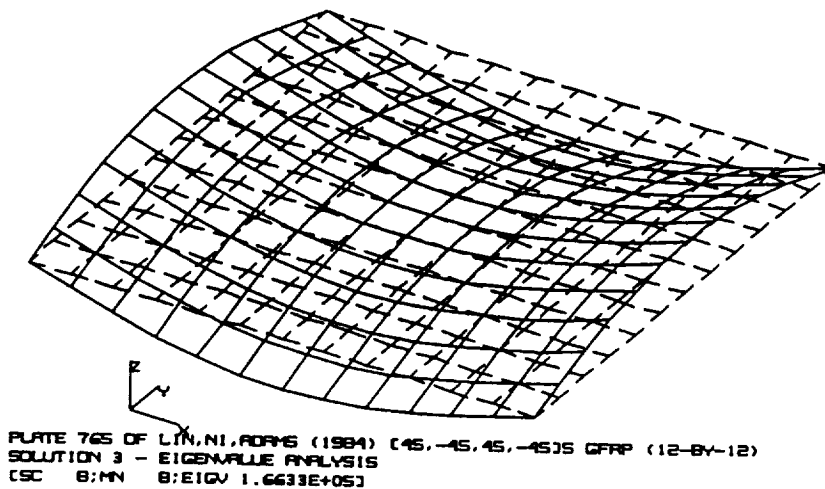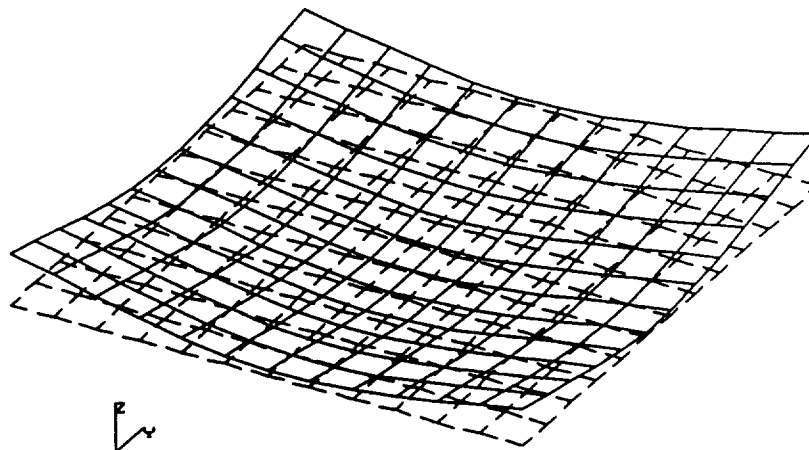SOLUTION 3 - EIGENVALUE ANALYSIS
[SC   8:MN   8:EIGV 1.6633E+05]
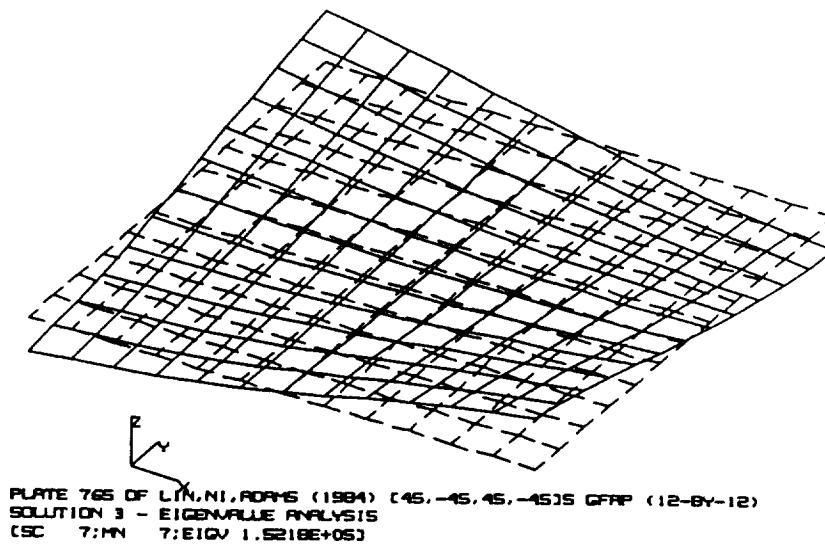
Fig 5b.   Plate 765, Mode 2

Figure 5.   NASTRAN-computed eigenmodes for plate 765

PLATE 765 OF LIN,NI,ADAMS (1984) [45,-45,45,-45]S GFRP (12-BY-12)
SOLUTION 3 - EIGENVALUE ANALYSIS
[SC   9:MN   9:EIGV 3.6477E+05]

Fig. 5c.   Plate 765, Mode 3
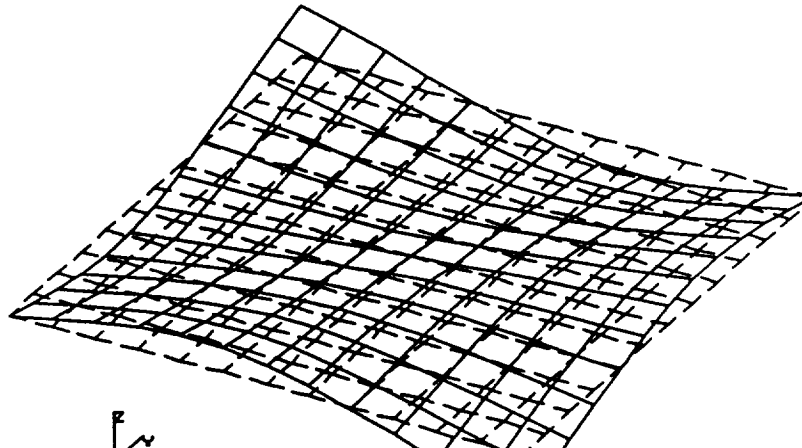

PLATE 765 OF LIN,NI,ADAMS (1984) [45,-45,45,-45]S GFRP (12-BY-12)
SOLUTION 3 - EIGENVALUE ANALYSIS
[SC   10:MN   10:EIGV 7.7870E+05]

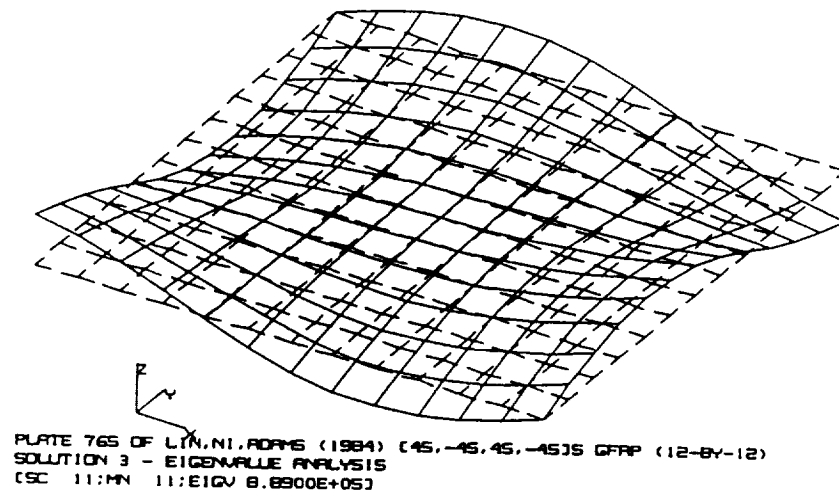Fig. 5d.   Plate 765, Mode 4
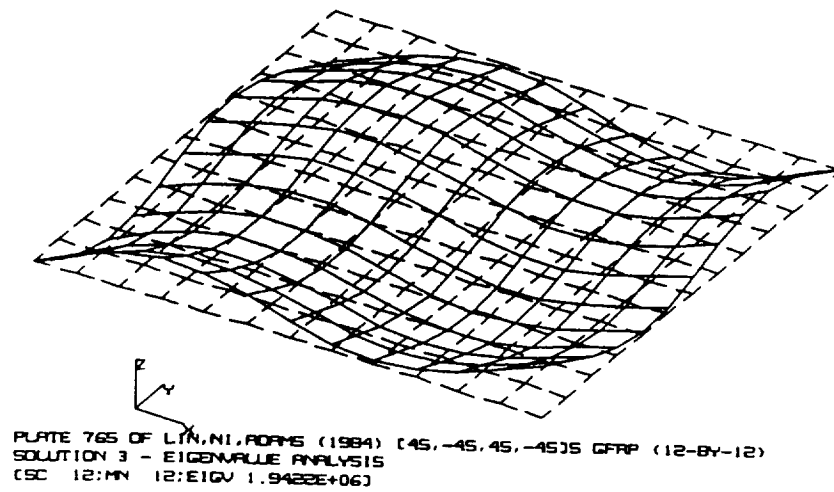
Figure 5.   (Continued)

89

PLATE 765 OF LIN,NI,ADAMS (1984) [45,-45,45,-45]S GFRP (12-BY-12)
SOLUTION 3 - EIGENVALUE ANALYSIS
[SC 11:MN 11:EIGV 8.8900E+05]

Fig. 5e.   Plate 765, Mode 5

PLATE 765 OF LIN,NI,ADAMS (1984) [45,-45,45,-45]S GFRP (12-BY-12)
SOLUTION 3 - EIGENVALUE ANALYSIS
[SC 12:MN 12:EIGV 1.9432E+06]

Fig. 5f.   Plate 765, Mode 6

Figure 5.   (Continued)

90

PLATE 769 OF LIN,NI,ADAMS (1984) [0,90,45,-45]S GFRP (12-BY-12)
SOLUTION 3 - EIGENVALUE ANALYSIS
[SC   7:MN   7:EIGV 8.7742E+04]

Fig. 6a.   Plate 769, Mode 1

PLATE 769 OF LIN,NI,ADAMS (1984) [0,90,45,-45]S GFRP (12-BY-12)
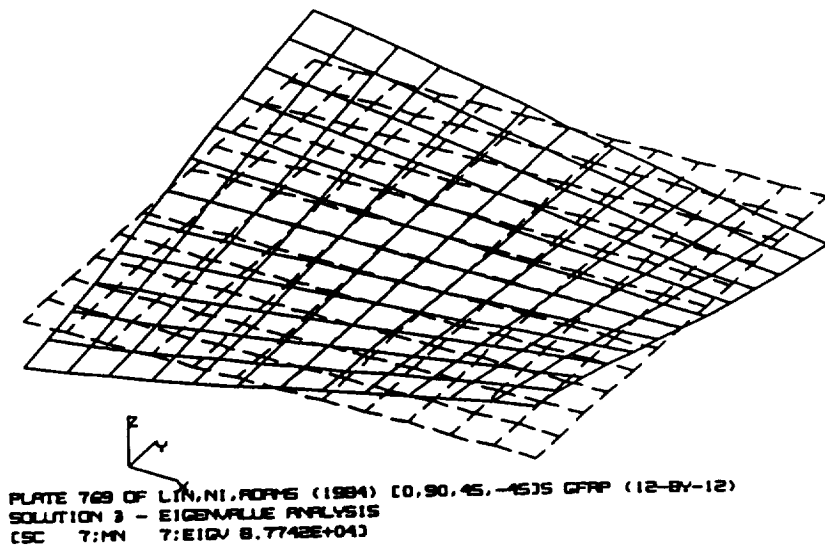SOLUTION 3 - EIGENVALUE ANALYSIS
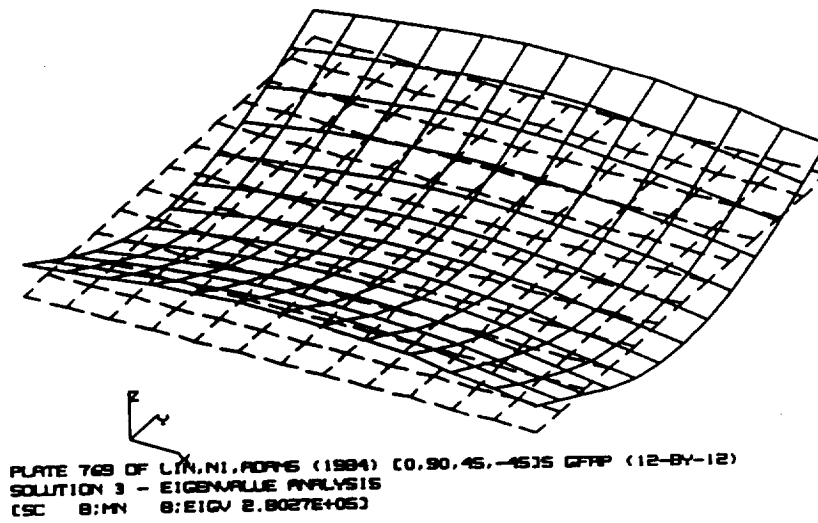[SC   8:MN   8:EIGV 2.8027E+05]

Fig 6b.   Plate 769, Mode 2

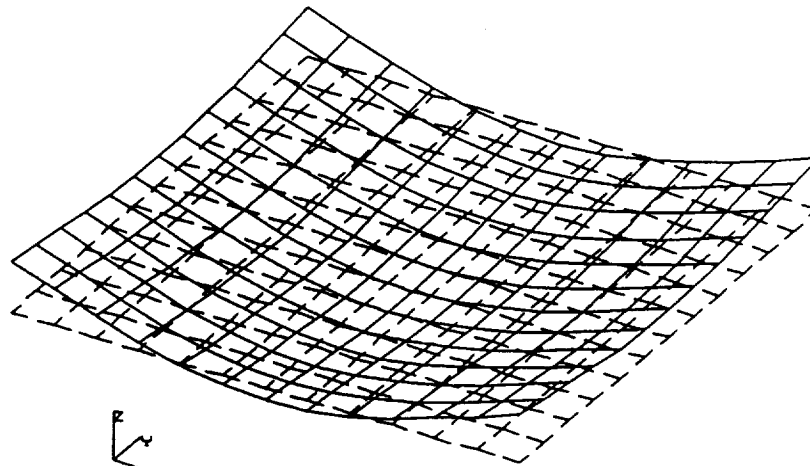Figure 6.   NASTRAN-computed eigenmodes for plate 769

91

PLATE 769 OF LIN,NI,ADAMS (1984) [0,90,45,-45]S GFRP (12-BY-12)
SOLUTION 3 - EIGENVALUE ANALYSIS
[SC   9;MN   9;EIGV 4.2015E+05]
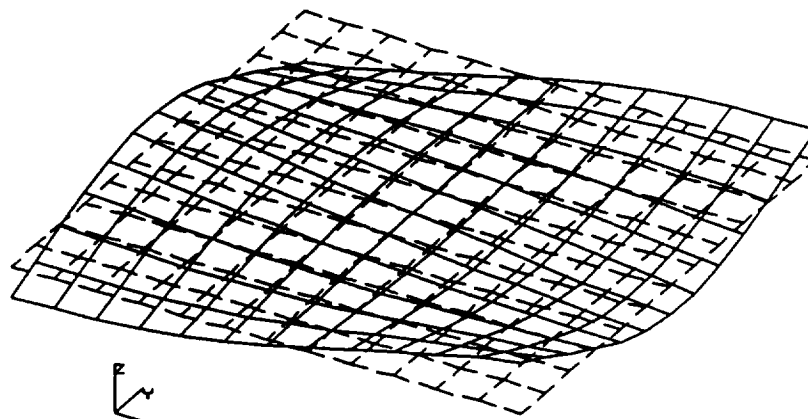
Fig. 6c.   Plate 769, Mode 3

PLATE 769 OF LIN,NI,ADAMS (1984) [0,90,45,-45]S GFRP (12-BY-12)
SOLUTION 3 - EIGENVALUE ANALYSIS
[SC   10;MN   10;EIGV 6.2768E+05]

Fig. 6d.   Plate 769, Mode 4

Figure 6.   (Continued)

PLATE 769 OF LIN,NI,ADAMS (1984) [0,90,45,-45]S GFRP (12-BY-12)
SOLUTION 3 - EIGENVALUE ANALYSIS
[SC 11:MN 11:EIGV 7.4704E+05]

Fig. 6e.   Plate 769, Mode 5

PLATE 769 OF LIN,NI,ADAMS (1984) [0,90,45,-45]S GFRP (12-BY-12)
SOLUTION 3 - EIGENVALUE ANALYSIS
[SC 12:MN 12:EIGV 2.0544E+06]

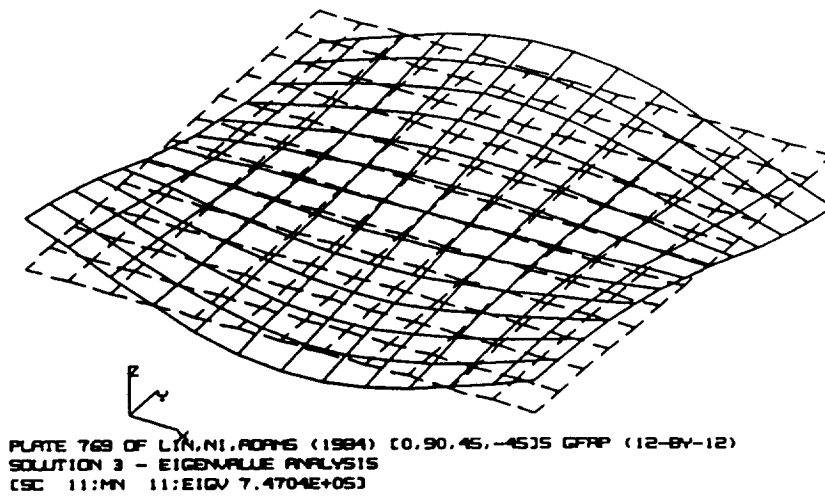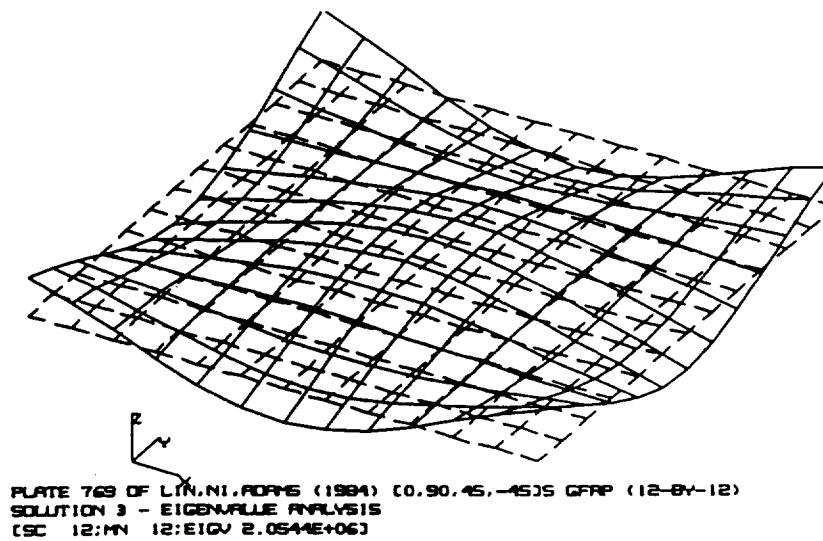Fig. 6f.   Plate 769, Mode 6

Figure 6.   (Continued)

93
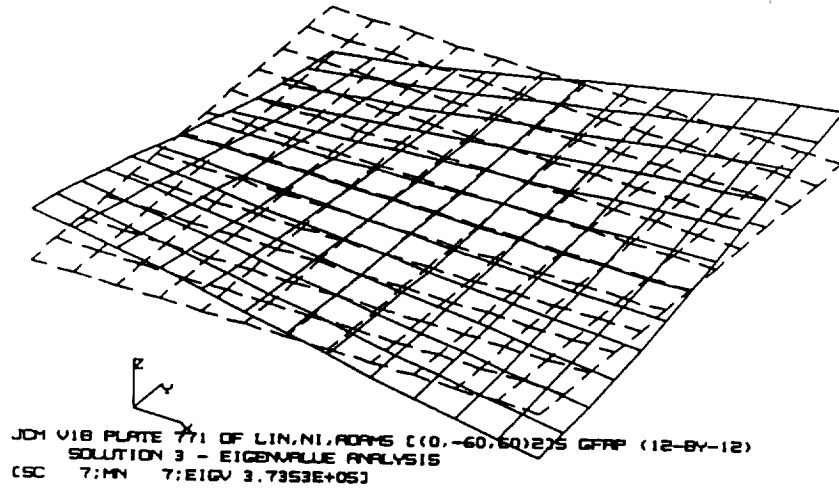
Fig. 7a.   Plate 771, Mode 1
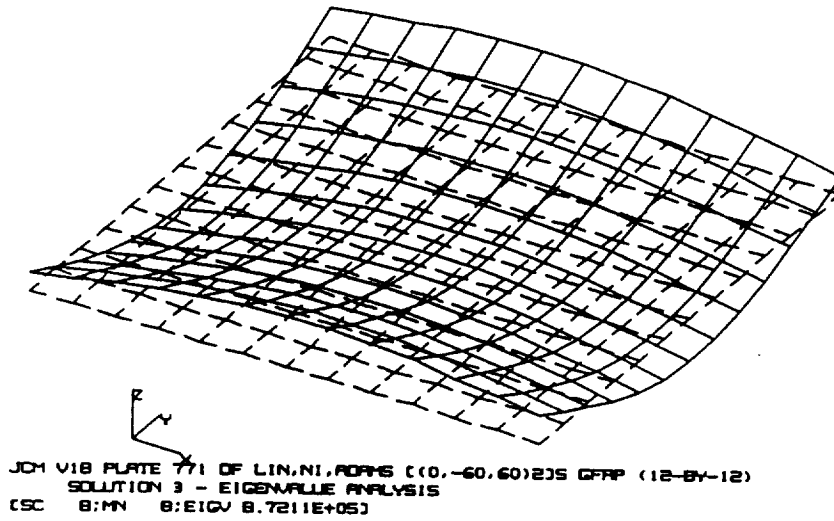
Fig 7b.   Plate 771, Mode 2

Figure 7.   NASTRAN-computed eigenmodes for plate 771

JCM VIB PLATE 771 OF LIN,NI,FORMS ((0,-60,60)2)S GFRP (12-BY-12)
SOLUTION 3 - EIGENVALUE ANALYSIS
(SC 9:MN 9:EIGV 1.4086E+06)

Fig. 7c.   Plate 771, Mode 3

JCM VIB PLATE 771 OF LIN,NI,FORMS ((0,-60,60)2)S GFRP (12-BY-12)
SOLUTION 3 - EIGENVALUE ANALYSIS
(SC 10:MN 10:EIGV 2.3678E+06)
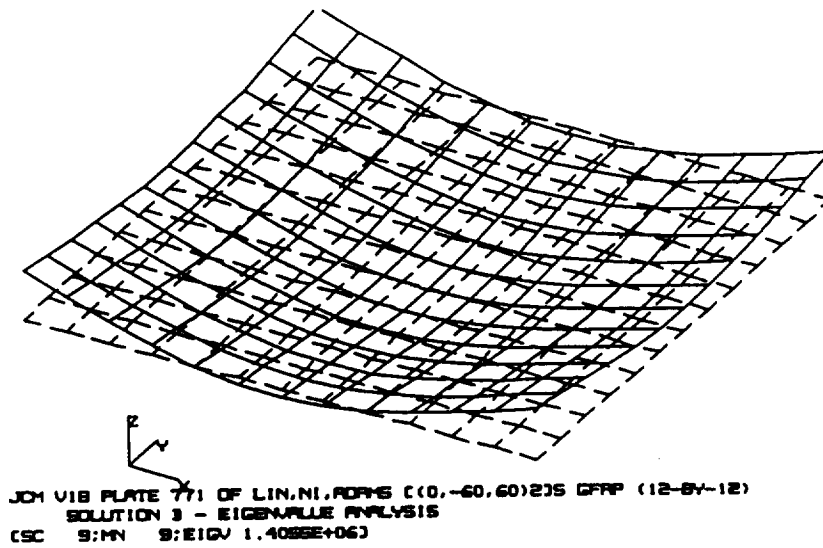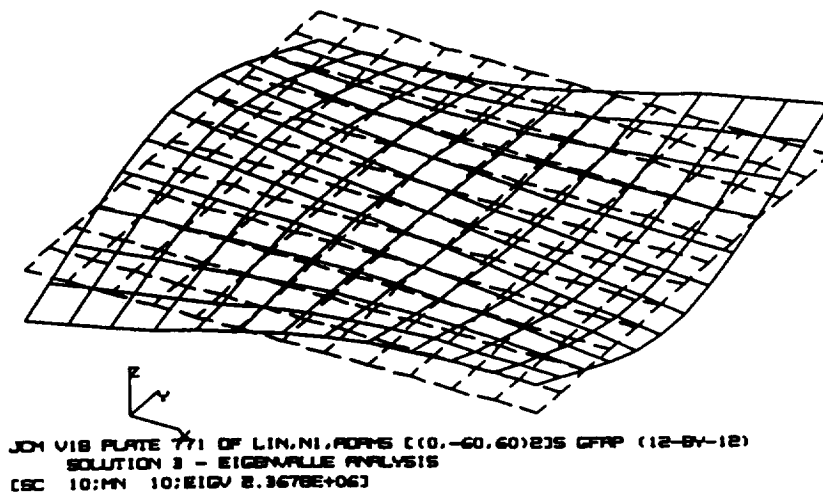
Fig. 7d.   Plate 771, Mode 4

Figure 7.   (Continued)

95

JCH VIB PLATE 771 OF LIN.NI.FORMS [(0.-60.60)2]5 GFRP (12-BY-12)
SOLUTION 3 - EIGENVALUE ANALYSIS
[SC 11;MN 11;EIGV 2.7710E+06]

Fig. 7e.   Plate 771, Mode 5

JCH VIB PLATE 771 OF LIN.NI.FORMS [(0.-60.60)2]5 GFRP (12-BY-12)
SOLUTION 3 - EIGENVALUE ANALYSIS
[SC 12;MN 12;EIGV 7.1441E+06]
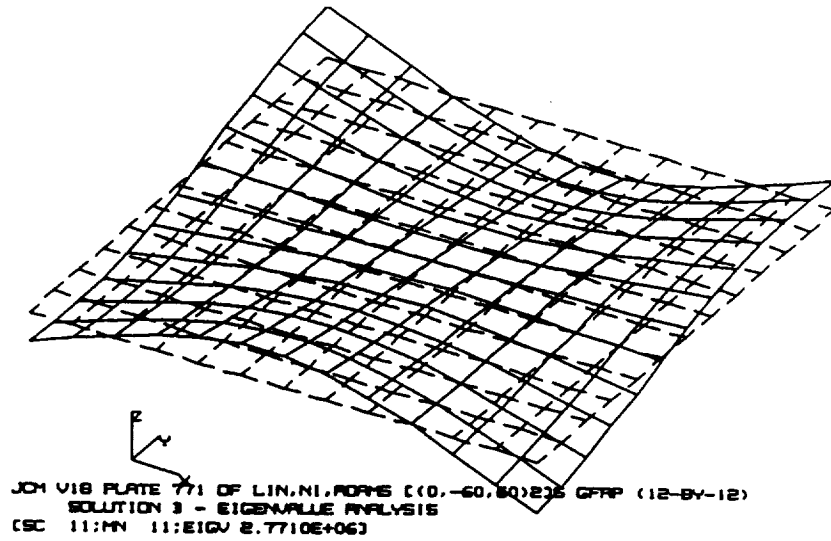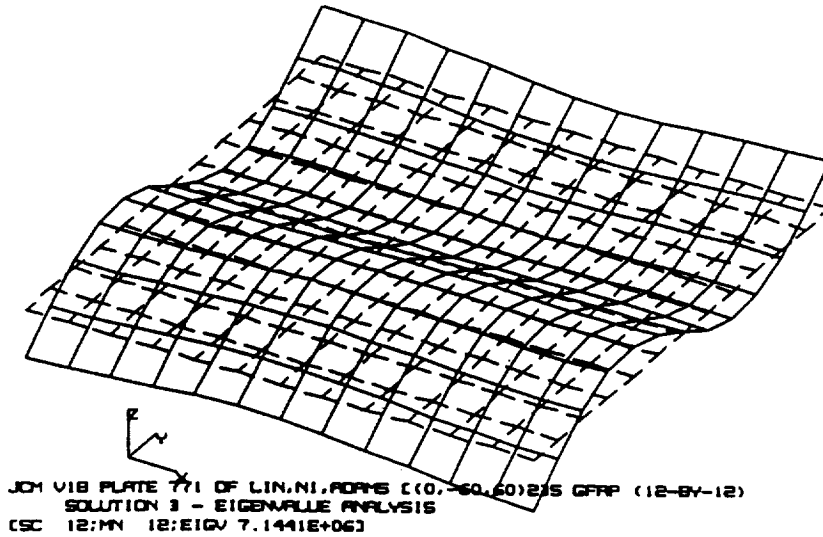
Fig. 7f.   Plate 771, Mode 6

Figure 7.   (Continued)

96

JCM VIB PLATE 762 OF LIN,NI,ADAMS [(0)8] CFRP (12-BY-12)
SOLUTION 3 - EIGENVALUE ANALYSIS

Fig. 8a.   Plate 762, Mode 1

JCM VIB PLATE 762 OF LIN,NI,ADAMS [(0)8] CFRP (12-BY-12)
SOLUTION 3 - EIGENVALUE ANALYSIS
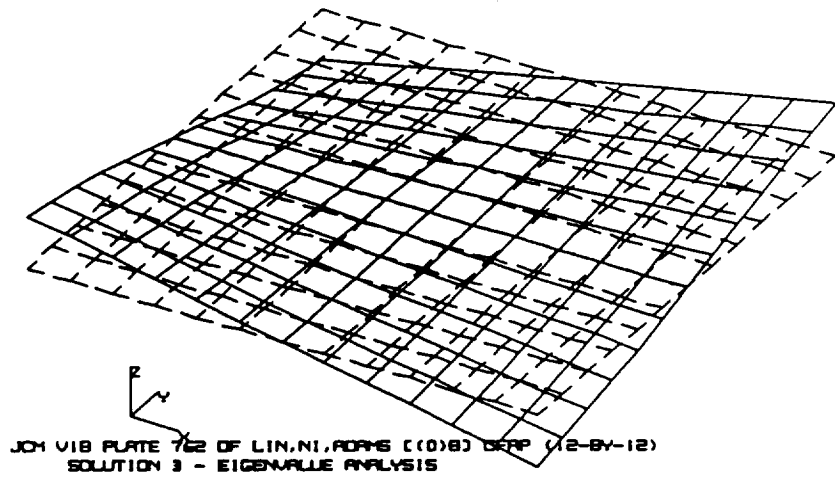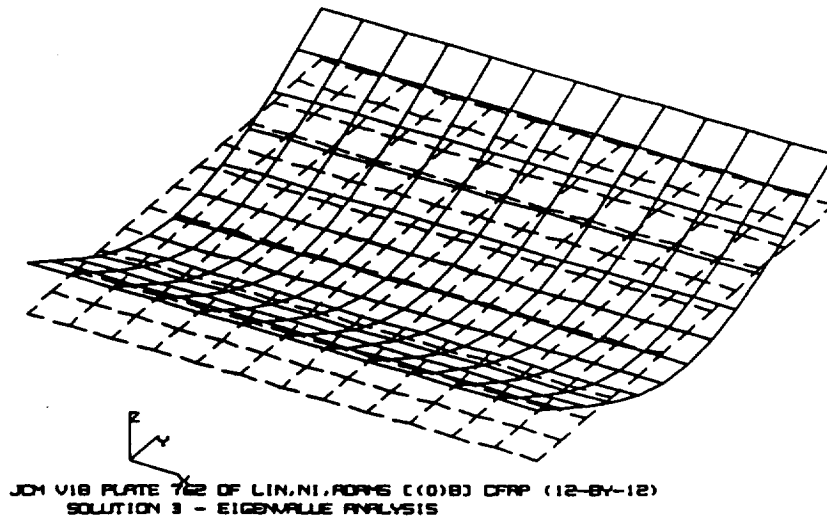
Fig 8b.   Plate 762, Mode 2

Figure 8.   NASTRAN-computed eigenmodes for plate 762

97

JCM VIB PLATE 762 OF LIN,NI,ADAMS [(0)8] CFRP (12-BY-12)
SOLUTION 3 - EIGENVALUE ANALYSIS

Fig. 8c.   Plate 762, Mode 3

JCM VIB PLATE 762 OF LIN,NI,ADAMS [(0)8] CFRP (12-BY-12)
SOLUTION 3 - EIGENVALUE ANALYSIS
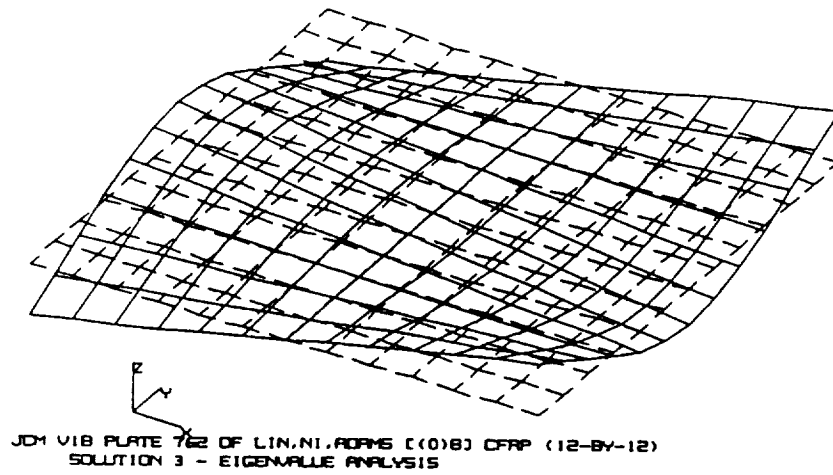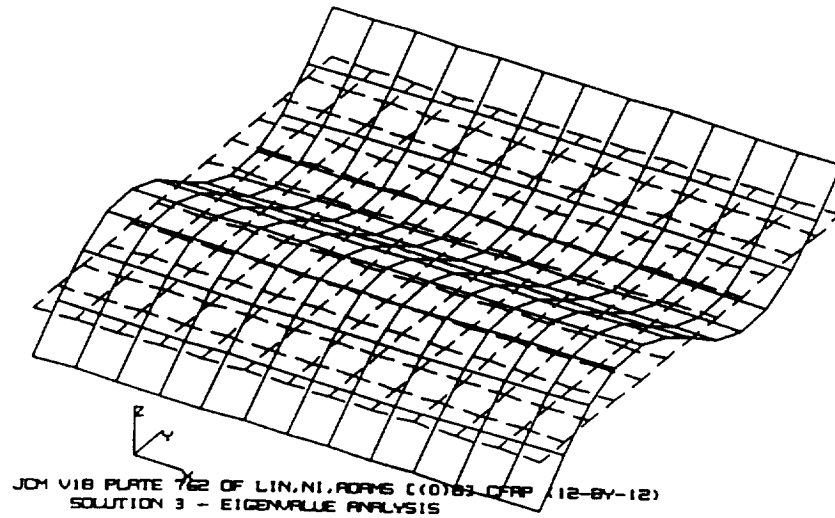
Fig. 8d.   Plate 762, Mode 4

Figure 8.   (Continued)

98

JCM V18 PLATE 762 OF LIN,NI,ADAMS [(0)8] GFRP (12-BY-12)
SOLUTION 3 - EIGENVALUE ANALYSIS

Fig. 8e.   Plate 762, Mode 5

JCM V18 PLATE 762 OF LIN,NI,ADAMS [(0)8] CFRP (12-BY-12)
SOLUTION 3 - EIGENVALUE ANALYSIS

Fig. 8f.   Plate 762, Mode 6

Figure 8.   (Continued)

99

A CASE OF POOR SUBSTRUCTURE DIAGNOSTICS

Thomas G. Butler

BUTLER ANALYSES

Substructuring is a powerful tool. As with any powerful tool the options for managing a job are legion. On the other hand, the NASTRAN Manuals in the Substructuring area are all geared toward instant success, but the solution paths are fraught with many traps for human error. Thus, the probability of suffering a fatal abort is high. In such circumstances, the necessity for diagnostics that are user friendly is paramount. This paper is written in the spirit of improving the diagnostics as well as the documentation in one area where the author felt he was backed into a blind corner as a result of his having committed a data oversight. This topic will be aired by referring to an analysis of a particular structure.
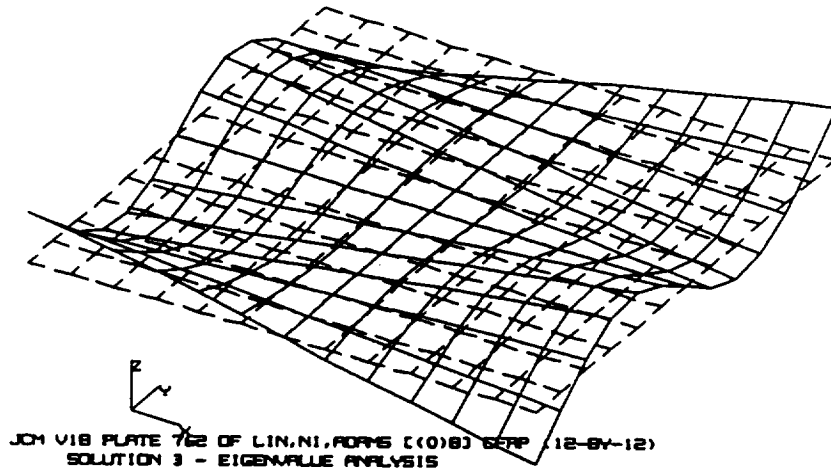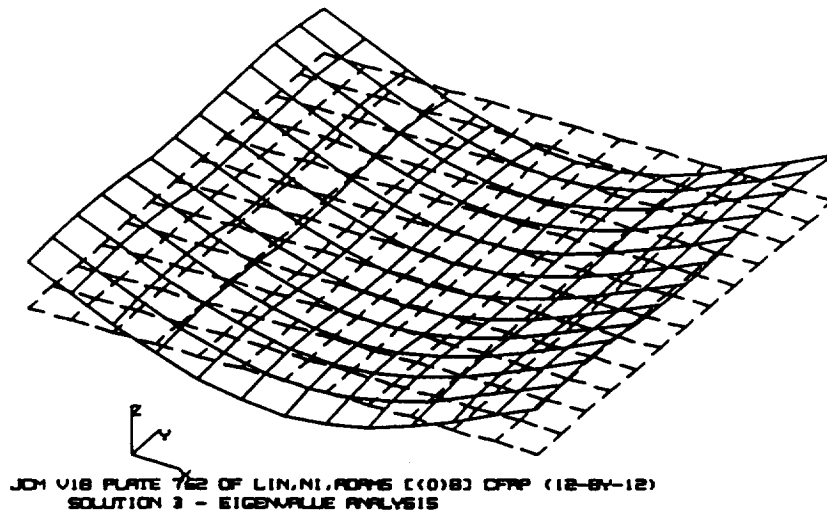
The structure, under discussion, used a number of local coordinate systems that simplified the preparation of input data. The principal features of this problem are introduced by reference to a series of figures.

Figure 1 illustrates a **PILOT** model of the basic component substructure of a full scale structure. This pilot model was used to explore the error that developed in the true structure. In preparation for the investigation into the difficulty that was encountered during a "COMBINE" operation, the pilot basic was cloned 4 times into CLONA, CLONB, CLONC

and CLOND.

Figure 2 tabulates the bulk data for the 5 coordinate systems that were used in the basic component. Coordinate system "5" is cylindrical and was used for its core. Coordinate systems "50, 60, 70 & 80" are rectangular and were used for the four arms with their local X axes pointing outward at zero degrees, 90, 180 and 270 respectively. Each clone retained its own copy of the set of five local coordinate systems. Thus, the Substructure Operating File (SOF) at this point had a complement of 5 x 5 = 25 coordinate systems to catalog. The multiplicity of coordinate systems was at the root of the fatal error which erupted.

Figure 3 illustrates two separate "COMBINE" operations amongst the substructures. In the first "COMBINE", point 51 of P/S CLONC joins with point 71 of P/S CLOND. In the second "COMBINE", point 61 of P/S[1] BASE joins with point 81 of P/S CLONA, while point 61 of P/S CLONA joins with point 81 of P/S CLONB.

During the subsequent linking of substructures, the points that were combined each had their own local coordinate systems. Well this doesn't seem to be a problem, because NASTRAN has a wonderful module called CSTM (Coordinate System Transformation Matrix) which keeps track of all transformations amongst a host of coordinate systems. So the user is disarmed into thinking that

---

1. The abbreviation P/S, meaning pseudo-structure, is used as a generic term for any number of different kinds of substructures: basic, or clones, or condensations, or combined.

NASTRAN can handle anything dealing with coordinates. This was especially true in this case, because, just prior to the abort being described here, a mistake in translating one of the cloned structures was corrected in response to a diagnostic message that declared that points, which were targeted to be joined, were not within tolerance. The error was that one of the translations, defined on a "TRANS" card was off by an eighth of an inch. After the correction a message was issued declaring that all points in the "COMBINE" operation were within tolerance. So the reaction to a subsequent message to the effect that the local coordinate systems were incompatible seemed ridiculous, because NASTRAN had no difficulty in locating the points in space and in pronouncing that they were within tolerance with the coordinate systems that were corrected.

As it turned out there are a number of different coordinate systmes that have to be dealt with here, and the "TRANS" set that was just corrected - though at first suspected - was not at the nub of the problem. The problem arises not in the alignment, which the TRANS coordinates deal with, but in the subsequent mating, which depends of the local DISPLACEMENT coordinates of points that are being brought together.

As a matter of general substructuring principle, when a group of substructures is assembled, any place where parts are linked can involve contributions from 2 or more individuals. At any such place the set of points are merged into a resultant single point. What is not told in the manuals is that the resultant point needs to refer to just one coordinate system. If all of the merging points refer to a common coordinate system, there is no problem. But, when each point has its own local displacement coordinate system, NASTRAN aborts and issues a message #6528

saying that incompatible local coordinate systems have been found. But if the user thinks that the problem has just been corrected, the characterization of the coordinates in message #6528 as being "incompatible" doesn't make sense and he becomes convinced that there must be a bug in NASTRAN and the user is to be absolved of blame. His certitude of blamelessness is further reenforced by the details that are supplied with the diagnostic message. The text of the complete message, shown in Figure 4, refers to local coordinate systems 1 and 10. But if you look at Figure 2, you can verify that no coordinate system was numbered 1 or 10. This seems to further corroborate that NASTRAN got some tables mixed up and is in need of having a bug straightened out.

Gordon Chan of the UNISYS Support Group came to my rescue and published the transformation matrices for the coordinate systems that were involved. The reason that NASTRAN aborted was not because of an error in the code. It deliberately compared the local coordinates at the combining point and found that one pair of signs was aligned while the signs of two other axes were of opposite in sign. The message referring to coordinate systems resulted from a partially completed execution of the COMBINE command. It had reassinged coordinate system ID's in terms of its own internal bookkeeping system, but it phrased the diagnostic in terms of its own scheme of ID's. Unformtunately, that part of its completed operation was never output, because of the abortion, so the diagnostic which was trying to be helpful was confusing the situation even further. However, NASTRAN appeared to be operating properly.

Double checking of coordinate systems 50 through 80 found them to be error free. As a further check, the manual method was

compared to the automatic method of combining. The same diagnostic regarding incompatible local coordinates showed up in this automatic trial as well, but this time referred to pairs of coordinates with other sets of strange identifications; i.e. 2 & 9 and 7 & 14. That diagnostic is shown in Figure 5. Finally a vague, misty fragment seemed to kindle in the back of my brain that had something to do with the data card called "GTRAN". I pored over the Substructure Section of Chapter 1 of the User's Manual to uncover a hint on the use of GTRAN. No help. Nor was the Theoretical Manual any assistance. Figure 1 shows that in the example of the manual COMBINE, points 51 and 71 refer to coordinate systems 50 & 70 respectively. NASTRAN finds that these two systems do not align with each other and so both cannot be allowed to represent that point after a merge. The situation must be reconciled and NASTRAN needs guidance from the user. The avenue by which the user exerts his preference is through the use of GTRAN. The bulk data explanation of GTRAN left many unanswered questions. The only thing left to do was to resort to the old "black box" method of finding out how it behaved. GTRAN was tried out under its options. One option is to refer all connecting points to the overall basic system, and the other is to refer them to the system defined by the TRANS entry. Both worked! Figure 6 shows an excerpt of the output from a successful manual run using GTRAN. It repeats the message about points within tolerance, then gives the tabulation of the resulting points after the COMBINE operation, showing those degrees of freedom that were merged into a single point. This connectivity summary does not, however, refer to any coordinate system. Coordinate ID information is published subsequently in the BGSS. In this case the BGSS shows that it was arbitrated by referring both points to the "0" system (the overall basic).

Figure 7 is an excerpt of a summary of connectivities for the automatic COMBINE case after a proper use of GTRAN. It shows a similar set of connections as in the manual case but amongst BASE, CLONA, and CLONB.

There were many unhappy features relating to documentation in this encounter: (1) the diagnostic itself, (2) the explanation of the diagnostic in Chapter 6, (3) the guide to modeling in Chapter 1, (4) the explanatory notes in the bulk data, and (5) the Theoretical Manual. It is incumbent upon the manuals to acquaint the user with what _its_ needs are so that he can supply necessary data. But in this instance the documentation gave NO hint of how NASTRAN operated internally, so the user was set adrift by a diagnostic that impugns his data as INCOMPATIBLE. For all he knew NASTRAN had some sort of internal default to meet the arbitration needs. Without the help of documentation, the user must look into the code to find out what NASTRAN is doing in subroutine "COMB1". He does not know from the above documentary sources whether NASTRAN takes a default when not supplied with specific direction or aborts. The situation is this. NASTRAN first determines that the points that it is directed to link are collocated. This can be done by temporarily transforming all locations to the overall basic system. But now when it wants to trim all connecting points to a single point, it must assign some coordinate system to that resulting point. But which one? Dave Herting and the savants that helped him with the architecture of SUBSTRUCTURING were aware of the problem and provided for it with the GTRAN card. But as is often the case with programming, the documentation did not coach the user into anticipating the need to guide NASTRAN in the assignment of a coordinate system to a common point.

Rather than overcome the obstacle with the provision of a GTRAN card and then to continue with the analysis of the structure only, I chose to share this experience at the Colloquium and to volunteer a supplement to the documentation so that any subsequent user can be well guided when he encounters message #6528. Figure 8 shows the recommended diagnostic message. Figure 9 shows the recommended supplement to the "COMBINE" section of Chapter 1 on modeling with substructures, and in Chapter 6 on explanation of diagnostics. No suggestions are offered for the Theoretical Manual, because it is currently awaiting a major revision.

I extend my deep appreciation to Gordon Chan for his help in unearthing this problem and for his modification of the diagnostic message in the code. The new release will have the revised diagnostic message. In addition Gordon Chan added a printout of the transformation matrices of the coordinate systems that are indicted.

My hope is that this small effort will save future users much time and frustration when faced with an unsuccessful COMBINE operation in their substructuring work.
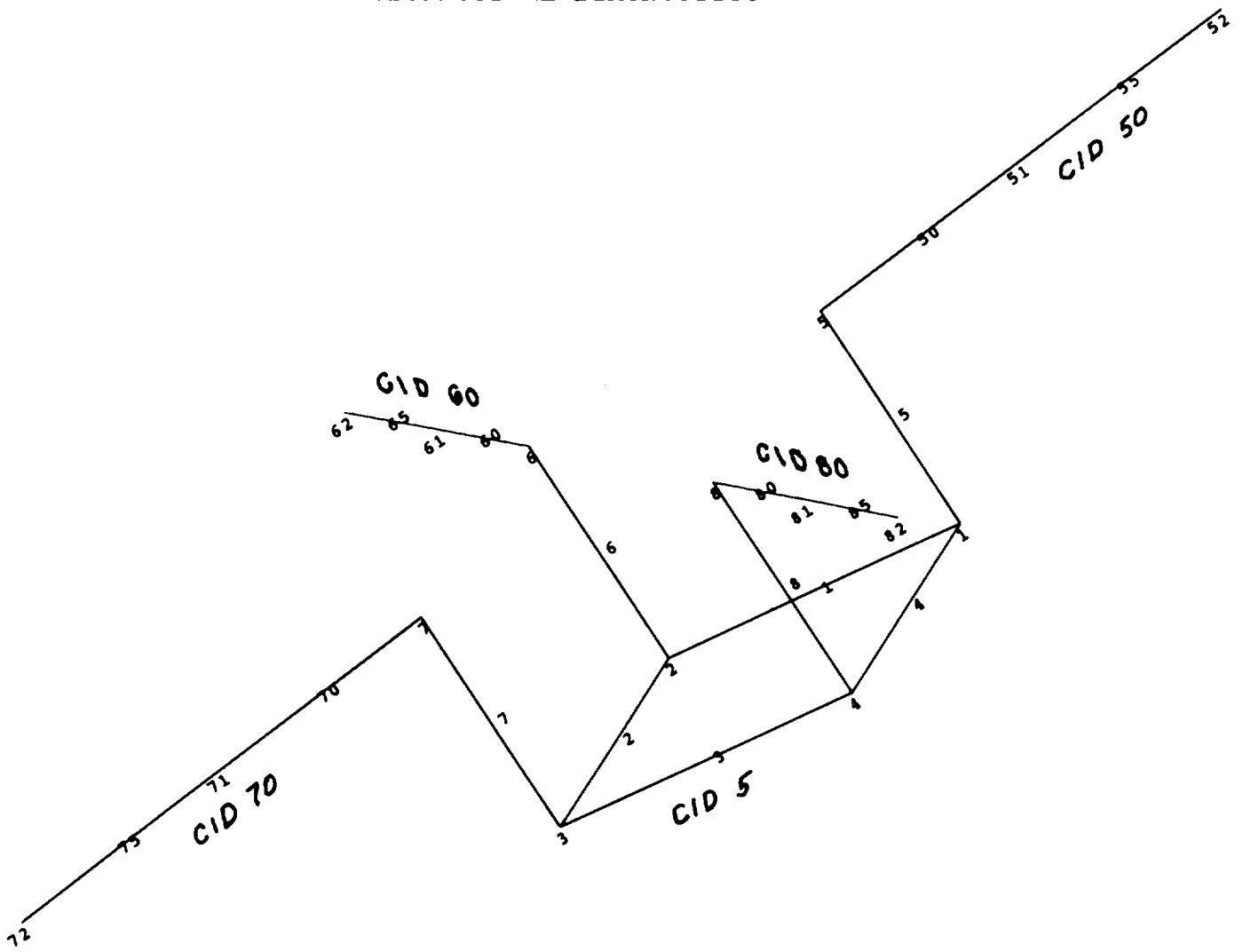
Figure 1. Plot of Basic Component BASE of Pilot Model.

CORD2C	5	0	0.0	0.0	0.0	0.0	0.0	10.0	+CYLN
+CYLN	10.0	0.0	10.0						
CORD2R	50	0	10.0	0.0	10.0	10.0	-10.0	10.0	+RAY0
+RAY0	20.0	-10.0	10.0						
CORD2R	60	0	0.0	10.0	10.0	10.0	10.0	10.0	+RAY90
+RAY90	10.0	20.0	10.0						
CORD2R	70	0	-10.0	0.0	10.0	-10.0	10.0	10.0	+RAY18
+RAY180	-20.0	10.0	10.0						
CORD2R	80	0	0.0	-10.0	10.0	-10.0	-10.0	10.0	+RAY27
+RAY270	-10.0	-20.0	10.0						

Figure 2. Coordinate Systems in Component BASE
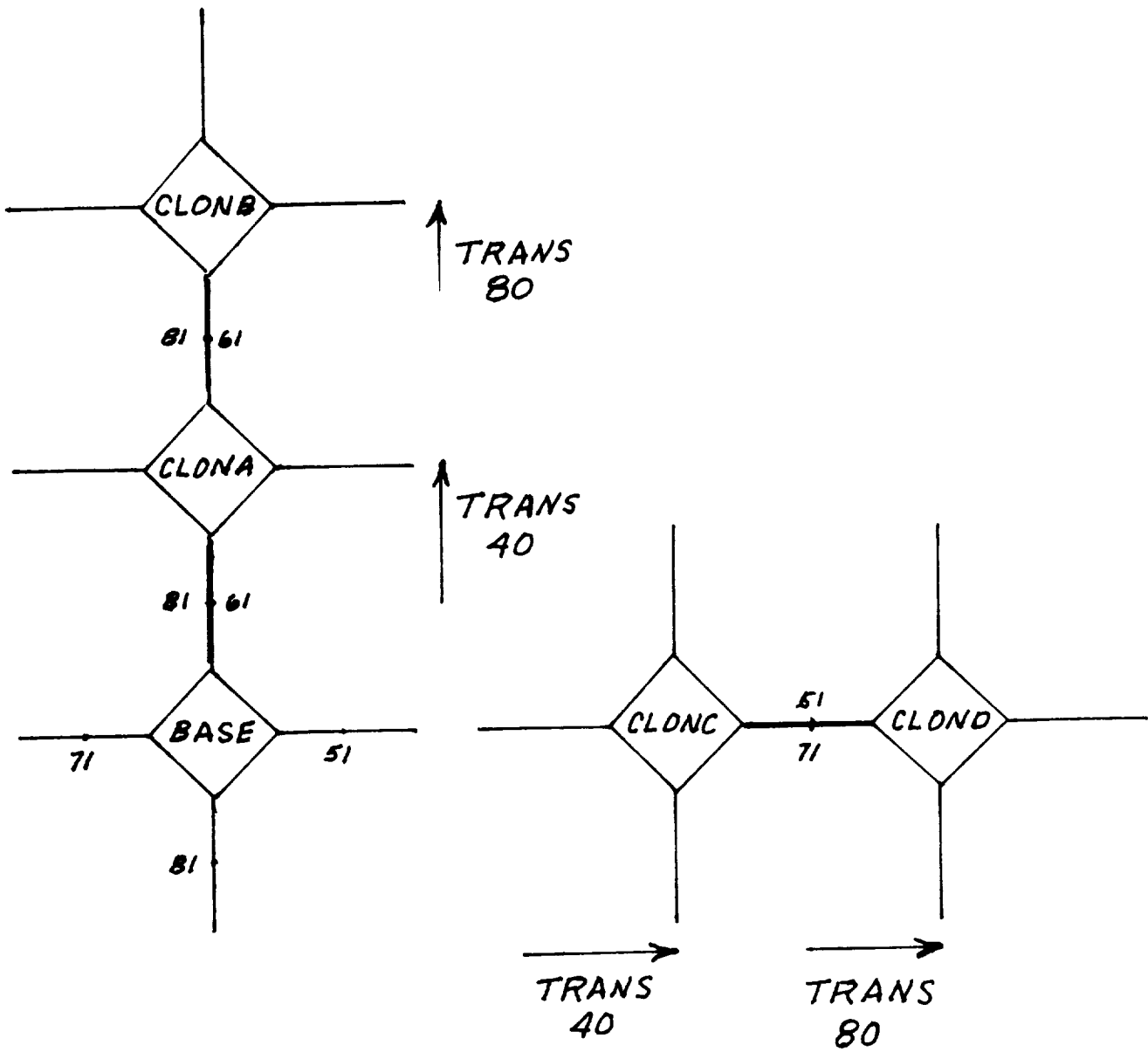
Figure 3.   Connection Diagram of Two COMBINE Operations

USER INFORMATION MESSAGE 6516,
ALL MANUAL CONNECTIONS SPECIFIED ARE
ALLOWABLE WITH RESPECT TO TOLER.

USER FATAL MESSAGE 6528,
INCOMPATABLE LOCAL COORDINATE SYSTEMS
HAVE BEEN FOUND. CONNECTION OF POINTS
IS IMPOSSIBLE, SUMMARY FOLLOWS.

****

THE FOLLOWING MISMATCHED LOCAL COORDINATE
SYSTEMS (CSTM) HAVE BEEN FOUND FOR

LOCAL COORDINATE SYSTEM ID NO.   1
PSEUDOSTRUCTURE ID NO.   1
INTERNAL POINT NO.   2

****

              LOCAL COORDINATE SYSTEM ID NO.   10
              PSEUDOSTRUCTURE ID NO.   2
              INTERNAL POINT NO.   14

 USER FATAL MESSAGE 6537, MODULE COMB1
TERMINATING DUE TO ABOVE ERRORS.

Figure 4.   Diagnostic From Abort of Manual COMBINE

SUMMARY OF AUTOMATICALLY GENERATED CONNECTIONS

| CONNECTED DOF | CONNECTION CODE | PSEUDOSTRUCTURE | | NAMES |
		BASE	CLONA	CLONB
123456	12	7	15	0
123456	12	5	13	0
123456	12	3	11	0
123456	23	0	7	15
123456	23	0	5	13
123456	23	0	3	11

USER FATAL MESSAGE 6528,
INCOMPATABLE LOCAL COORDINATE SYSTEMS
HAVE BEEN FOUND. CONNECTION OF POINTS
IS IMPOSSIBLE, SUMMARY FOLLOWS.

****

THE FOLLOWING MISMATCHED LOCAL COORDINATE
SYSTEMS (CSTM) HAVE BEEN FOUND FOR

LOCAL COORDINATE SYSTEM ID NO.   2
PSEUDOSTRUCTURE ID NO.   1
INTERNAL POINT NO.   5

****

        LOCAL COORDINATE SYSTEM ID NO.   9
        PSEUDOSTRUCTURE ID NO.   2
        INTERNAL POINT NO.   13

****

THE FOLLOWING MISMATCHED LOCAL COORDINATE
SYSTEMS (CSTM) HAVE BEEN FOUND FOR

LOCAL COORDINATE SYSTEM ID NO.   7
PSEUDOSTRUCTURE ID NO.   2
INTERNAL POINT NO.   5

****

        LOCAL COORDINATE SYSTEM ID NO.   14
        PSEUDOSTRUCTURE ID NO.   3
        INTERNAL POINT NO.   13

USER FATAL MESSAGE 6537, MODULE COMB1
TERMINATING DUE TO ABOVE ERRORS.

Figure 5. Diagnostic From Abort of Automatic COMBINE

USER INFORMATION MESSAGE 6516,
ALL MANUAL CONNECTIONS SPECIFIED ARE
ALLOWABLE WITH RESPECT TO TOLER.

SUMMARY OF PSEUDOSTRUCTURE CONNECTIVITIES

INTERNAL POINT NO	INTERNAL DOF NO	DEGREES OF FREEDOM	PSEUDOSTRUCTURE NAMES CLONC	CLOND
-				
	-			
		-		
			-	
16	89	123456	CLONC 72	
17	95	13	CLONC 51	CLOND 71
18	97	123456		CLOND 51
-				
	-			
		-		
			-	

Figure 6

Summary of Connectivities After GTRAN Use in Manual COMBINE

SUMMARY OF AUTOMATICALLY GENERATED CONNECTIONS

CONNECTED DOF	CONNECTION CODE	PSEUDOSTRUCTURE NAMES		
		BASE	CLONA	CLONB
123456	12	7	15	0
123456	12	5	13	0
123456	12	3	11	0
123456	23	0	7	15
123456	23	0	5	13
123456	23	0	3	11

SUMMARY OF PSEUDOSTRUCTURE CONNECTIVITIES

INTERNAL POINT NO	INTERNAL DOF NO	DEGREES OF FREEDOM	* PSEUDOSTRUCTURE NAMES		
			BASE	CLONA	CLONB
-	-	-	-	-	
16	89	123456	BASE 72		
17	95	13	BASE 61	CLONA 81	
18	97	123456		CLONA 52	
-	-	-	-		
33	183	123456		CLONA 2	
34	189	13		CLONA 61	CLONB 81
35	191	123456			CLONB 52
-	-	-			

Figure 7

Summary of Connectivities After GTRAN Use in Automatic COMBINE

USER FATAL MESSAGE 6528

INCOMPATABLE LOCAL COORDINATE SYSTEMS HAVE BEEN FOUND. COMPLETTION OF
CONNECTION IS IMPOSSIBLE. SUGGEST USE OF "GTRAN". SUMMARY IN TERMS OF
JUST-FORMED INTERNAL FREEDOMS AND INTERNAL COORDINATE SYSTEM ID'S PER THE
EQSS & BGSS FOLLOW: ------------

Figure 8. Revised Fatal Diagnostic Message 6528

USER'S MANUAL CHAPTER 1.

ADD THE FOLLOWING TEXT TO SUPPLEMENT THE TOPIC OF THE "COMBINE" OPERATION ON
SUBSTRUCTURING IN THE NASTRAN USER'S MANUAL, PAGE 1.10-39 (14 LINES UP FROM
THE BOTTOM OF THE PAGE.

WHEN POINTS ARE ALIGNED FOR COMBINING AFTER A TRANSLATION AND/OR ROTATION OF
COMPONENTS, THEY BECOME A SINGLE POINT UPON LINKING. IF THE POINTS ABOUT TO
BE CONNECTED REFER TO DIFFERENT LOCAL COORDINATE SYSTEMS, THE SUBSTRUCTURE
ROUTINE "COMB1" DOES NOT IMPOSE A DEFAULT CORRDINATE SYSTEM FOR THE POINT.
SUCH A SITUATION MUST BE ANTICIPATED BY THE ANALYST TO AVOID A FATAL ABORTION.
THE ANALYST CAN ASSIGN A DISPLACEMENT COORDIANTE SYSTEM TO THE RESULTING POINT
THROUGH THE USE OF THE GTRAN CARD. IT OFFERS 3 OPTIONS: (1) TRANSFORM TO THE
OVERALL BASIC SYSTEM, (2) NO TRANSFORMATION, AND (3) TRANSFORM TO THE COORDI-
NATE SYSTEM WHICH WAS DEFINED ON THE SELECTED "TRANS" CARD.

USER'S MANUAL CHAPTER 6.

ADD THE FOLLOWING TEXT AFTER THE FIRST SENTENCE OF DIAGNOSTIC MESSAGE 6528.

EACH POINT IS CARRYING ITS OWN LOCAL COORDINATE SYSTEM INTO THE "COMBINE'D"
POINT AND THEY HAVE BEEN FOUND TO BE DIFFERENTLY ALIGNED; I.E.
INCOMPATABLE. THE USER IS REQUIRED TO ARBITRATE BETWEEN THE COMPETING
LOCAL COORDINATE SYSTEMS. HE IS ADVISED TO CONSIDER USING ONE/OR SEVERAL
"GTRAN" CARDS. (SEE PAGE 1.10-39 OF THE USER'S MANUAL.) HE IS FURTHER
ADVISED TO "DESTROY" THE PSEUDO-STRUCTURE DEFINED IN THE COMBINE OPERATION
IN ORDER TO REMOVE ANY PARTIALLY COMPLETED "COMBINE" DATA FROM THE SOF
(SUBSTRUCTURE OPERATING FILE), BEFORE RERUNNING THE "COMBINE" OPERATION.

Figure 9.   Supplements to Documents in USER'S Manual

ALTERNATIVE METHODS TO MODEL FRICTIONAL CONTACT SURFACES USING NASTRAN

Joseph Hoang

GE Goverment Services, Houston, Texas

SUMMARY

Elongated (slotted) holes have been used extensively for the integration of equipment into Spacelab racks. In the past, this type of interface has been modelled assuming that (i) there is no slippage between contact surfaces, or (ii) there is no load transfer in the direction of the slot. Since the contact surfaces are bolted together, the contact friction provides a load path determined by the normal applied force (bolt preload) and the coefficient of friction. This paper examines three alternate methods that utilize spring elements, externally applied couples, and stress dependent elements to model the contacted surfaces. Results of these methods are compared with results obtained from methods that use GAP elements and rigid elements.

INTRODUCTION

Elongated holes have been used in the design of Spacelab Experiment Equipment mounting provisions. This type of joint is employed where large tolerances are allowed in one direction of the hole for the ease of integration. A simple way to model these interfaces is to use RIGID elements with the assumption that two connecting grid points are not moving against each other when loads are applied. Another common method is to use RIGID elements with the degrees of freedom associated with the longitudinal direction of the elongated hole released. When using this method, it is assumed that the joint did not carry load in its slotted direction.

Due to the assumption involved, neither method yields realistic results. GAP elements have been used to achieve better results. However, when large numbers of GAP elements are used in a complex model, an unreasonably large amount of computer processing time is required to solve the system and, hence, is not economical or practical.

In this paper, three alternative methods are investigated. The first method employs a spring element with a spring rate equal to the maximum load at the connection divided by the gap length. By using a spring element at the connection, the nonlinear frictional

force developed at the gap is replaced by a spring force that increases proportionally with gap distance. The second method used an externally applied couple to represent the frictional forces at the two contacted surfaces. This method creates a local realization of frictional forces when two grid points, representing two contacted surfaces, move against each other. In the third method, two contacted surfaces are connected by elements with stress-dependent material properties. The piecewise linear static analysis rigid format is ultilized to solve element forces at these elements.

A simple stowage container and four supporting columns were developed to represent a typical installation in a Spacelab rack. The container was integrated on supporting columns using the above methods. The models were run on a SUN workstation using CSA/NASTRAN. The results obtained from each method were then compared.

THEORY AND BACKGROUND

Figure 1a shows a typical elongated hole and Figure 1b shows force vs. relative displacement of an elongated hole. The force vs. displacement curves of other elements are shown in Figures 2 through 7.

From inspection, the stress dependent material element is the more appropriate element to simulate elongated hole behavior because the GAP element, spring element and coupled element would generate some error. A rigid element with all three translational degrees of freedom coupled (R123) should be used only when the frictional force is greater than the force at the connection. A rigid element with degrees of freedom associated with the longitudinal direction of the hole released (R23) should be used when, the frictional force and the displacement in elongated direction are small.

117
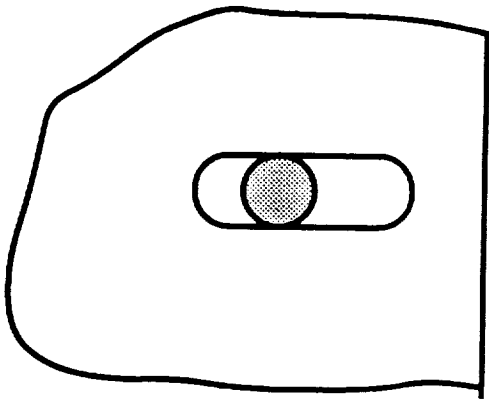
Fig. 1a   Typical elongated hole

Fig. 1b   Force vs. displacement of elongated hole
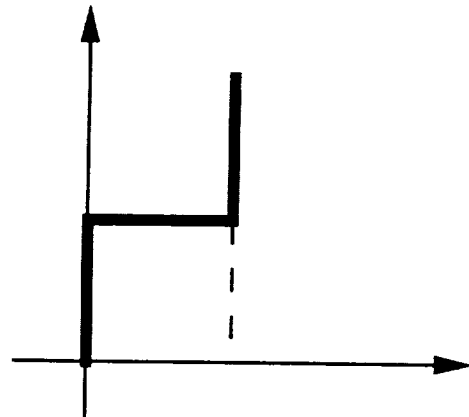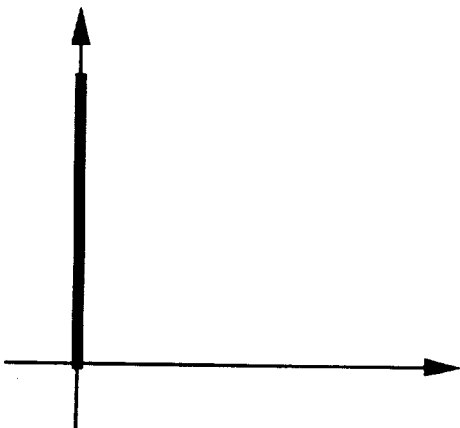

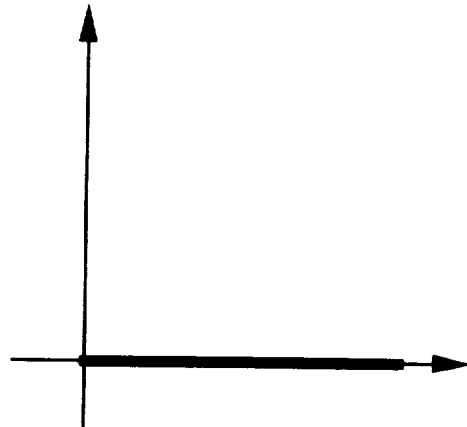Fig. 2   Force vs. displacement of R123 element

Fig. 3   Force vs. displacement of R23 element
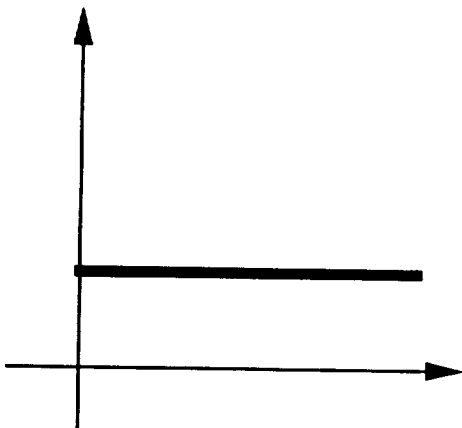

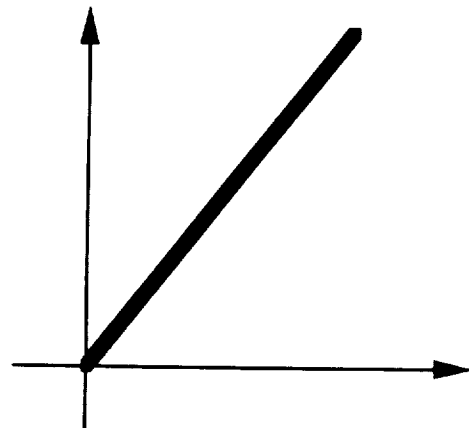Fig. 4   Force vs. displacement of "couple" element

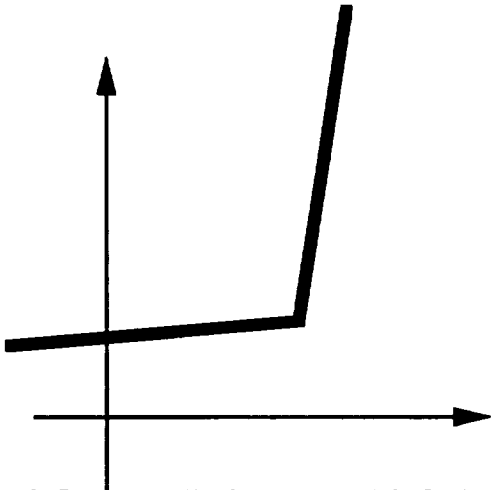Fig. 5   Force vs. displacement of spring element
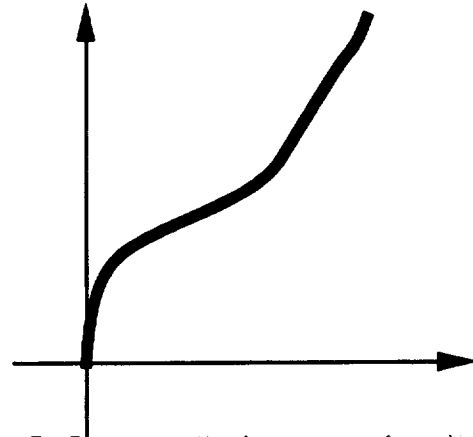
Fig. 6 Force vs. displacement of GAP element
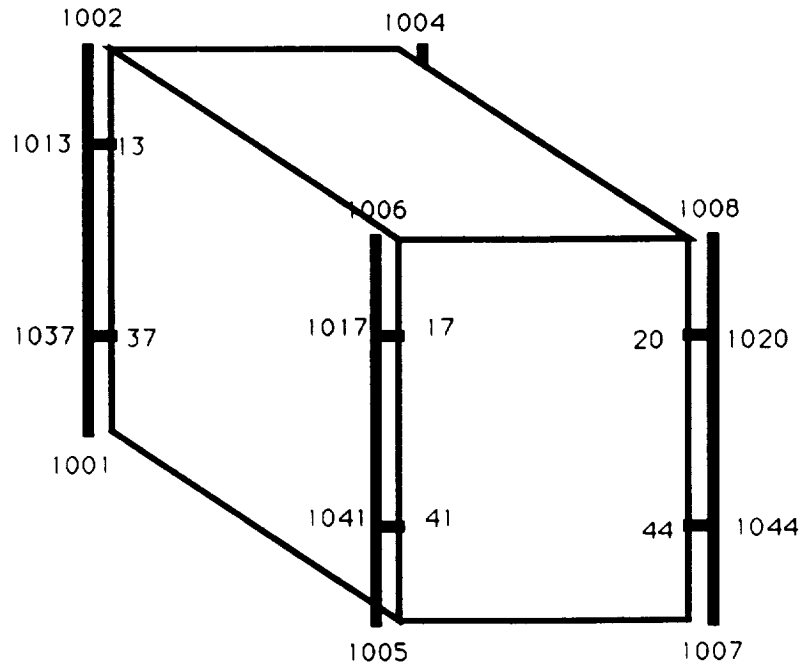

Fig. 7 Force vs. displacement of nonlinear element

Fig. 8   Plot of test subject: a simple box and four supported columns

ANALYSIS AND RESULTS

A simple box is constructed using QUAD2 elements. It is supported by four columns which were modelled using BAR elements. A plot of the structure is shown in Figure 8. In the rear, the box is mounted on two rear columns at grid points 13, 24, 37, and 48 using rigid elements with all three translational degrees of freedom coupled. In front, the box is mounted to the front left column at grid points 17 and 41 and to the front right column at grid points 20, and 44, using a different integrating method. Gravitational loads varying from 0.2g to 4.0g are applied to the model in the X-direction, which is parallel to the slotted direction.

The material and properties of QUAD2 and BAR elements are chosen such that the box is heavier and more flexible than the columns. Since the columns are much stiffer than the box, displacement of the grid point on the column is small as compared to displacement of the grid point on the box. Displacement of the rear panel is closed to the displacement of rear columns because the rear panel interface points are mounted to the rear columns by rigid elements with all three translational degrees of freedom coupled. However, at the front panel, the relative displacement of front panel and front columns are greatly dependent on the type of connecting elements used. It should also be noted that the single point constraint forces developed at the front columns are also dependent on the amount of load that has been transfered to the columns through the front connecting elements.

Properties of each type of connecting element are chosen in such a way that its deformation can follow the elongated hole displacement curve as close as possible. The gap length and frictional force of the contacting surface were chosen arbitrarily at 0.5 inches and 15.0 lbs respectively.

Displacement of the left front interfaces (grid points 17 and 41 were identical and were tabulated in Table 1). The single point constraint force of the left front column (grid points 1005 and 1006) are tabulated in Table 2. Table 3 shows the displacement of the right front interfaces (grid points 20, and 44) while Table 4 shows a single point constraint force of the right front column (grid points 1007 and 1008).

120

TABLE 1   DISPLACEMENT VECTOR OF GRID POINT 17 AND 41
LEFT FRONT COLUME

LOAD G	R123 in	R23 in	COUPLE in	SPRING in	NONLINEAR in	GAP in
0.2	4.609476E-05	1.919124E-01	-1.049302E+00	7.230263E-02	2.630225E-04	2.693819E-01
0.4	9.218953E-05	3.838249E-01	-8.573890E-01	1.446053E-01	7.430014E-04	5.000591E-01
0.6	1.382843E-04	5.757374E-01	-6.654766E-01	2.169079E-01	1.222980E-03	5.002077E-01
0.8	1.843791E-04	7.676498E-01	-4.735641E-01	2.892105E-01	1.702959E-03	5.003563E-01
1.0	2.304738E-04	9.595622E-01	-2.816517E-01	3.615132E-01	2.182937E-03	5.005049E-01
1.2	2.765686E-04	1.151475E+00	-8.973924E-02	4.338158E-01	2.662916E-03	5.006534E-01
1.4	3.226633E-04	1.343387E+00	1.021732E-01	5.061184E-01	1.419462E-01	5.008020E-01
1.6	3.687581E-04	1.535300E+00	2.940856E-01	5.784211E-01	4.199264E-01	5.009505E-01
1.8	4.148529E-04	1.727212E+00	4.859981E-01	6.507237E-01	5.594884E-01	5.010991E-01
2.0	4.609476E-04	1.919124E+00	6.779105E-01	7.230263E-01	5.599684E-01	5.012476E-01
2.2	5.070424E-04	2.111037E+00	8.698230E-01	7.953290E-01	5.604484E-01	5.013962E-01
2.4	5.531372E-04	2.302949E+00	1.061735E+00	8.676316E-01	5.609283E-01	5.015448E-01
2.6	5.992319E-04	2.494862E+00	1.253648E+00	9.399343E-01	5.614084E-01	5.016934E-01
2.8	6.453267E-04	2.686774E+00	1.445560E+00	1.012237E+00	5.618884E-01	5.018419E-01
3.0	6.914214E-04	2.878687E+00	1.637473E+00	1.084540E+00	5.623684E-01	5.019905E-01
3.2	7.375162E-04	3.070599E+00	1.829385E+00	1.156842E+00	5.628484E-01	5.021390E-01
3.4	7.836110E-04	3.262512E+00	2.021298E+00	1.229145E+00	5.633284E-01	5.022876E-01
3.6	8.297057E-04	3.454424E+00	2.213210E+00	1.301447E+00	5.638084E-01	5.024362E-01
3.8	8.758005E-04	3.646336E+00	2.405123E+00	1.373750E+00	5.642884E-01	5.025848E-01
4.0	9.218953E-04	3.838249E+00	2.597035E+00	1.446053E+00	5.647684E-01	5.027333E-01

TABLE 2   FORCES OF SINGLE-POINT CONSTRAINT GRID POINT 1005 AND 1006
LEFT FRONT COLUME

LOAD G	R123 Lbs	R23 Lbs	COUPLE Lbs	SPRING Lbs	NONLINEAR Lbs	GAP Lbs
0.2	-2.480673E+00	-1.619789E-01	-1.516198E+01	-1.607457E+00	-2.415121E+00	-4.313539E-01
0.4	-4.961346E+00	-3.239577E-01	-1.532396E+01	-3.214913E+00	-4.775031E+00	-1.135344E+00
0.6	-7.442019E+00	-4.859366E-01	-1.548594E+01	-4.822370E+00	-7.134942E+00	-3.463185E+00
0.8	-9.922691E+00	-6.479155E-01	-1.564791E+01	-6.429826E+00	-9.494853E+00	-5.791025E+00
1.0	-1.240336E+01	-8.098943E-01	-1.580989E+01	-8.037283E+00	-1.185476E+01	-8.118866E+00
1.2	-1.488404E+01	-9.718732E-01	-1.597187E+01	-9.644740E+00	-1.421467E+01	-1.044671E+01
1.4	-1.736471E+01	-1.133852E+00	-1.613385E+01	-1.125220E+01	-1.553790E+01	-1.277455E+01
1.6	-1.984538E+01	-1.295831E+00	-1.629583E+01	-1.285965E+01	-1.592276E+01	-1.510239E+01
1.8	-2.232606E+01	-1.457810E+00	-1.645781E+01	-1.446711E+01	-1.729169E+01	-1.743023E+01
2.0	-2.480673E+01	-1.619789E+00	-1.661979E+01	-1.607457E+01	-1.965161E+01	-1.975807E+01
2.2	-2.728740E+01	-1.781768E+00	-1.678177E+01	-1.768202E+01	-2.201151E+01	-2.208591E+01
2.4	-2.976807E+01	-1.943746E+00	-1.694375E+01	-1.928948E+01	-2.437144E+01	-2.441375E+01
2.6	-3.224874E+01	-2.105725E+00	-1.710573E+01	-2.089693E+01	-2.673135E+01	-2.674159E+01
2.8	-3.472942E+01	-2.267704E+00	-1.726771E+01	-2.250439E+01	-2.909127E+01	-2.906943E+01
3.0	-3.721009E+01	-2.429683E+00	-1.742968E+01	-2.411185E+01	-3.145117E+01	-3.139727E+01
3.2	-3.969077E+01	-2.591662E+00	-1.759166E+01	-2.571931E+01	-3.381098E+01	-3.372511E+01
3.4	-4.217144E+01	-2.753641E+00	-1.775364E+01	-2.732676E+01	-3.617098E+01	-3.605296E+01
3.6	-4.465211E+01	-2.915620E+00	-1.791562E+01	-2.893422E+01	-3.853089E+01	-3.838079E+01
3.8	-4.713278E+01	-3.077598E+00	-1.807760E+01	-3.054168E+01	-4.089083E+01	-4.070864E+01
4.0	-4.961346E+01	-3.239577E+00	-1.823958E+01	-3.214913E+01	-4.325074E+01	-4.303648E+01

TABLE 3   DISPLACEMENT VECTOR OF GRID POINT 20 AND 44
RIGHT FRONT COLUMN

LOAD G	R123 in	R23 in	COUPLE in	SPRING in	NONLINEAR in	GAP in
0.2	4.609476E-05	1.919124E-01	-1.049302E+00	7.230263E-02	2.569049E-04	2.693819E-01
0.4	9.218953E-05	3.838249E-01	-8.573890E-01	1.446053E-01	7.286069E-04	5.000591E-01
0.6	1.382843E-04	5.757374E-01	-6.654766E-01	2.169079E-01	1.200309E-03	5.002077E-01
0.8	1.843791E-04	7.676498E-01	-4.735641E-01	2.892105E-01	1.672011E-03	5.003563E-01
1.0	2.304738E-04	9.595622E-01	-2.816517E-01	3.615132E-01	2.143713E-03	5.005049E-01
1.2	2.765686E-04	1.151475E+00	-8.973924E-02	4.338158E-01	2.615415E-03	5.006534E-01
1.4	3.226633E-04	1.343387E+00	1.021732E-01	5.061184E-01	1.416968E-01	5.008020E-01
1.6	3.687581E-04	1.535300E+00	2.940856E-01	5.784211E-01	4.196053E-01	5.009505E-01
1.8	4.148529E-04	1.727212E+00	4.859981E-01	6.507237E-01	5.591255E-01	5.010991E-01
2.0	4.609476E-04	1.919124E+00	6.779105E-01	7.230263E-01	5.595973E-01	5.012476E-01
2.2	5.070424E-04	2.111037E+00	8.698230E-01	7.953290E-01	5.606690E-01	5.013962E-01
2.4	5.531372E-04	2.302949E+00	1.061735E+00	8.676316E-01	5.605407E-01	5.015448E-01
2.6	5.992319E-04	2.494862E+00	1.253648E+00	9.399343E-01	5.610124E-01	5.016934E-01
2.8	6.453267E-04	2.686774E+00	1.445560E+00	1.012237E+00	5.614842E-01	5.018419E-01
3.0	6.914214E-04	2.878687E+00	1.637473E+00	1.084540E+00	5.619559E-01	5.019905E-01
3.2	7.375162E-04	3.070599E+00	1.829385E+00	1.156842E+00	5.624276E-01	5.021390E-01
3.4	7.836110E-04	3.262512E+00	2.021298E+00	1.229145E+00	5.628994E-01	5.022876E-01
3.6	8.297057E-04	3.454424E+00	2.213210E+00	1.301447E+00	5.633711E-01	5.024362E-01
3.8	8.758005E-04	3.646336E+00	2.405123E+00	1.373750E+00	5.638429E-01	5.025848E-01
4.0	9.218953E-04	3.838249E+00	2.597035E+00	1.446053E+00	5.643146E-01	5.027333E-01

TABLE 4   FORCES OF SINGLE-POINT CONSTRAINT GRID POINT 1007 AND 1008
RIGHT FRONT COLUMN

LOAD G	R123 Lbs	R23 Lbs	COUPLE Lbs	SPRING Lbs	NONLINEAR Lbs	GAP Lbs
0.2	-2.480673E+00	-1.619789E-01	-1.516198E+01	-1.607457E+00	-2.391965E+00	-4.313539E-01
0.4	-4.961346E+00	-3.239577E-01	-1.532396E+01	-3.214913E+00	-4.713940E+00	-1.135344E+00
0.6	-7.442019E+00	-4.859366E-01	-1.548594E+01	-4.822370E+00	-7.035915E+00	-3.463185E+00
0.8	-9.922691E+00	-6.479155E-01	-1.564791E+01	-6.429826E+00	-9.357891E+00	-5.791025E+00
1.0	-1.240336E+01	-8.098943E-01	-1.580989E+01	-8.037283E+00	-1.167987E+01	-8.118866E+00
1.2	-1.488404E+01	-9.718732E-01	-1.597187E+01	-9.644740E+00	-1.400184E+01	-1.044671E+01
1.4	-1.736471E+01	-1.133852E+00	-1.613385E+01	-1.125220E+01	-1.540400E+01	-1.277455E+01
1.6	-1.984538E+01	-1.295831E+00	-1.629583E+01	-1.285965E+01	-1.578881E+01	-1.510239E+01
1.8	-2.232606E+01	-1.457810E+00	-1.645781E+01	-1.446711E+01	-1.713961E+01	-1.743023E+01
2.0	-2.480673E+01	-1.619789E+00	-1.661979E+01	-1.607457E+01	-1.946158E+01	-1.975807E+01
2.2	-2.728740E+01	-1.781768E+00	-1.678177E+01	-1.768202E+01	-2.178356E+01	-2.208591E+01
2.4	-2.976807E+01	-1.943746E+00	-1.694375E+01	-1.928948E+01	-2.410551E+01	-2.441375E+01
2.6	-3.224874E+01	-2.105725E+00	-1.710573E+01	-2.089693E+01	-2.642749E+01	-2.674159E+01
2.8	-3.472942E+01	-2.267704E+00	-1.726771E+01	-2.250439E+01	-2.874946E+01	-2.906943E+01
3.0	-3.721009E+01	-2.429683E+00	-1.742968E+01	-2.411185E+01	-3.107145E+01	-3.139727E+01
3.2	-3.969077E+01	-2.591662E+00	-1.759166E+01	-2.571931E+01	-3.339342E+01	-3.372511E+01
3.4	-4.217144E+01	-2.753641E+00	-1.775364E+01	-2.732676E+01	-3.571540E+01	-3.605296E+01
3.6	-4.465211E+01	-2.915620E+00	-1.791562E+01	-2.893422E+01	-3.803738E+01	-3.838079E+01
3.8	-4.713278E+01	-3.077598E+00	-1.807760E+01	-3.054168E+01	-4.035932E+01	-4.070864E+01
4.0	-4.961346E+01	-3.239577E+00	-1.823958E+01	-3.214913E+01	-4.268130E+01	-4.303648E+01

DISCUSION

Examination of the displacement of the left and right front panels of the box and the load distribution over four supporting columns indicates that types R123 and R23 are the two extreme cases. For rigid R123 types, the load was distributed evenly over four columns; meanwhile, for rigid R23 types, the load was carried by the rear columns only, and the box acts as a cantilever beam. The exact load distribution pattern is somewhere between the boundary established by these two types of connections. With finer load increments, the displacement curve of a stress dependent material element can be made to match the displacement curve of an elongated hole and, therefore, used as a reference to evaluate performance of other types of connections.

In general, static analysis with GAP elements and piecewise linear analysis employ an iterative scheme for solution. They are costly to run especially when models become complex. For the problem at hand, the GAP element did not yield a corrected solution when under tension load, meanwhile, stress dependent material elements did not perform well when under compression. Therefore, these two types of elements were not suitable for a model with multiple loading cases where the directions of the load at the interfaces are often unknown.

A *couple* type connection shows the same characteristics as the R23 type, with the displacement shifted due to externally applied couple. It is also difficult to use when the direction of the loads at the connection is unknown. However, the solution can be obtained with less computing time.

The solution for rigid elements and spring elements always contains some degree of error, but can be obtained with less computing time, and can be used in problems involving multiple loading conditions. The spring rate can be adjusted to control the relative displacement of the two connecting grid points.

RECOMMENDATION

It is recommended that for problems with multiple loading conditions, models should be run first using R123 type connections. Then, for interfaces that develop forces larger than the frictional forces of the elongated hole, the type R123 connection should be replaced with appropriate spring elements. This methodology yields reasonable results with minimum computer run time.

Hierarchical Tapered Bar Elements

Undergoing Axial Deformation

N. Ganesan and S. K. Thampi

GE Government Services, Houston, Texas

ABSTRACT: A method is described to model the dynamics of tapered axial bars of various cross sections based on the well-known Craig/Bampton component mode synthesis technique. This element is formed in terms of the static constraint modes and interface restrained normal modes. This is in contrast with the finite elements as implemented in NASTRAN where the interface restrained normal modes are neglected. These normal modes are in terms of Bessel functions. Restoration of a few of these modes leads to higher accuracy with fewer generalized coordinates. The proposed models are hierarchical so that all lower order element matrices are embedded in higher order element matrices. The advantages of this formulation compared to standard NASTRAN truss element formulation are demonstrated through simple numerical examples.

1. Introduction: Tapered bars and beams have high strength to weight ratios as well as architectural advantages. They are frequently employed to model structures in diverse applications, such as ship masts, turbine blades, chimney structures or complex frame constructions. NASA (Langley) has tested a truss structure which is made from tapered members to be used in space applications [1]. The technical literature on tapered beams is indeed vast with a long history [2-10]. Tapered beam finite elements are either simple elements (e.g., Lindberg[2], Rouch/Kao[3]) having two degrees of freedom at each end or higher order elements (e.g., Thomas/Dokumaci[4], To[5]) having more than four degrees of freedom. Ovunck[6], Avakian/Beskos[7], Gupta[8], Banerjee/Williams[9] and Spyrakos/Chen[10] have used frequency dependent finite elments in their analysis of tapered bars. Banerjee/Williams[9] have developed exact dynamic stiffness matrices for Bernoulli-Euler beams. However the approach in References [6-10] involves the unknown frequencies of the overall structure. The general framework developed by Engels[11] and applied in References [12-14] allows for the derivation of hierarchical finite elements for any type of structural element. This approach does not require the prior knowledge of system frequencies, thus overcoming the need for an iterative procedure to compute the structural response. In the present paper, a dynamic finite element model for a certain class of tapered bars with loads acting only in the axial direction is developed. The element matrices are presented in parametric form and can be easily extended to formulate the finite elments for a wide variety of tapered bars covering most practical cases. The convergence properties of this dynamic finite element, when compared to the regular finite element, are examined using numerical examples.

2. Assumed Modes Method: The Lagrangian elastic displacement vector $e(x, y, z, t)$ for a generic element can be written as the sum of two separate displacement vectors e_I

and $\bar{e}$.

$$e = e_I + \bar{e} \tag{1}$$

where e_I is a quasi-static displacement vector due to the interface displacements q_I and is expressed as a linear combination of static constraint modes ϕ_I,

$$e_I = \phi_I \, q_I \tag{2}$$

The second part $\bar{e}$ represents the remainder of the total displacement vector e. It is that part of e which is measured relative to e_I by an absolute observer. Clearly, $\bar{e}$ vanishes at the q_I coordinates and therefore can be expressed as a linear combination of assumed modes $\bar{\phi}$ which are restrained at those q_I coordinates

$$\bar{e} = \bar{\phi} \, \bar{q} \tag{3}$$

The vector $\bar{q}$ represents a set of generalized coordinates to be determined as part of the solution. One example of $\bar{\phi}$ modes are the normal modes of the element E restrained at the q_I coordinates. It should be stressed that although restrained normal modes have often unique advantages, they are only one of many possible sets. In fact, $\bar{\phi}$ modes need only be restricted to admissible functions that vanish at the q_I coordinates. Substituting Eqs. (2) and (3) into Eq. (1) yields

$$e = [\phi_I \; \bar{\phi}] \left\{ \begin{array}{c} q_I \\ \bar{q} \end{array} \right\} \stackrel{\text{def}}{=} \phi \, q \tag{4}$$

so that e is written in terms of a linear combination of two sets of assumed modes: (1) static constraint modes and (2) interface restrained assumed modes. It should be noted that the representation of e in Eq. (4) is complete in the sense that any degree of accuracy is theoretically possible as long as enough $\bar{\phi}$ modes are added.

In the standard consistent mass matrix approach, the elastic displacement vector e over the element is represented as a linear combination of interpolation or shape functions. In fact, these shape functions are identical to the static constraint modes ϕ_I and therefore e is approximated by e_I as in Eq. (1). The standard finite element approach therefore totally neglects the displacement $\bar{e}$ in Eq. (1). Ignoring $\bar{e}$ leads directly to a deterioration of the modal content of a typical finite element model. One way to ensure better convergence to a desired model fidelity is suggested by Eq. (4) and leads to dynamic finite element models. Instead of totally neglecting the $\bar{e}$ displacement, one could retain a limited number of $\bar{q}$ coordinates, thereby improving the mass and force distribution models. Of course, adding $\bar{q}$ coordinates also increases the order of the overall model. However, this approach has three important advantages: (1) The model converges much faster, i.e., far fewer degrees of freedom are necessary to attain comparable accuracy; (2) in principle, no further subdivision of basic elements is necessary, thereby simplifying the finite element grid and (3) the model is hierarchical and therefore has all the advantages associated with this property. In addition, these finite element models are directly based on the assumed modes method which provides a sound theoretical basis.

In Reference [11] it is shown that for a linear elastic material, the element kinetic and potential energies T and V can be written as

$$T = \frac{1}{2}\dot{q}^T M \dot{q}, \quad M = \int_E \phi^T \phi \, dm \tag{5}$$

$$V = \frac{1}{2}q^T K q, \quad K = \int_E (B\phi)^T C (B\phi) \, dV \tag{6}$$

in which the matrix C is the material stiffness matrix and B contains the appropriate partial derivatives in x, y and z. Futhermore, the matrices M and K represent the mass and stiffness matrices of a generic finite element E. In partitioned form,

$$M = \begin{bmatrix} M_{II} & M_{IN} \\ M_{IN}^T & M_{NN} \end{bmatrix}, \quad K = \begin{bmatrix} K_{II} & 0 \\ 0 & K_{NN} \end{bmatrix} \tag{7}$$

where

$$M_{II} = \int_E \phi_I^T \phi_I \, dm, \quad M_{IN} = \int_E \phi_I^T \overline{\phi} \, dm, \quad M_{NN} = \int_E \overline{\phi}^T \overline{\phi} \, dm \tag{8}$$

and

$$K_{II} = \int_E (B\phi_I)^T C(B\phi_I)dV, \quad K_{NN} = \int_E (B\overline{\phi})^T C(B\overline{\phi})dV \tag{9}$$

Note that the K_{IN} partition is always zero, which means that no stiffness coupling exists between q_I and $\overline{q}$.

At this point, a few remarks are in order. First, the matrices M_{II} and K_{II} represent the standard finite element consistent mass and stiffness matrices for the element E. The consistent mass matrix approach represents in fact a static condensation or Guyan reduction whereby all noninterface degrees of freedom are eliminated. Secondly, if the interface restrained normal modes are used for the columns of $\overline{\phi}$, then the present approach is identical to the Craig/Bampton component mode synthesis procedure as applied to a finite element. It should be emphasized that the element E is generic. This means that the proposed approach is valid, at least in theory, for any type of element. In the present paper, this general procedure will be applied to the special case of the tapered bars.

3. Tapered Bars: The hierarchical stiffness and mass matrices of the tapered bar are obtained by solving the governing equations of motion for displacement. Figure (1) represents linear tapered bar ab with a straight centroidal axis and the directions of the principal axes being the same for all crossections. The cross sectional area $A(x)$ is given by

$$A(x) = A_a \left(1 + c\frac{x}{L}\right)^n \tag{10}$$

where $c = d_b/d_a - 1$ and A_i, d_i $(i = a, b)$ denote the cross sectional area and the depth respectively. $c > -1$ otherwise the beam tapers to zero between its ends and L is the length of the bar.

126

Although the formulation is valid for any $n > 0$, many practical cases of tapered bars arise when n is one or two, see Figure (2). If the geometrical properties of the element at both ends are given, the shape function for n can be derived as

$$n = \frac{log(A_b/A_a)}{log(d_b/d_a)} \qquad (11)$$

For bars of closed box or I-section of constant width and varying depth, n is not an integer and will vary slightly from Eq. (10) at all x other than the two ends. But the deviations are usually within one percent of the exact values.
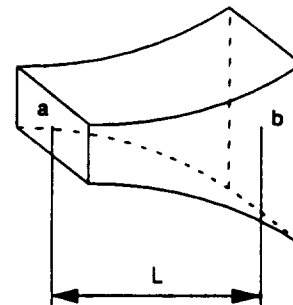
Figure 1.

Tapered Element

4. Static Constraint Modes:
Consider the axial bar element as illustrated in Figure (1). The bar is assumed to undergo vibration along its own axis and as a rigid body can only move along that same axis. The interface displacements are defined as $q_1(t) = u(0, t)$ and $q_2(t) = u(L, t)$, i.e., $q_I = [\ q_1\ q_2\ ]^T$ and the displacement vector e is considered to have only one component, i.e., u. Eq. (4) is therefore written as

$$u = \lfloor\ \phi_1\ \phi_2\ \rfloor q_I + \overline{\phi}\ \overline{q} \qquad (12)$$

Figure 2. Sample Cross Sections

The static constraint modes, ϕ_i can be computed from the differential equation for the axial deformation u at x from end a of the tapered bar,

$$\frac{d}{dx}\left\{EA(x)\frac{du}{dx}\right\} = 0 \tag{13}$$

where E is Young's modulus. Integration of Eq. (13) gives,

$$EA(x)\frac{du}{dx} = C_1 \tag{14}$$

Substituting for $A(x)$ from Eq. (10) and setting $\xi = 1 + c\frac{x}{L}$ gives

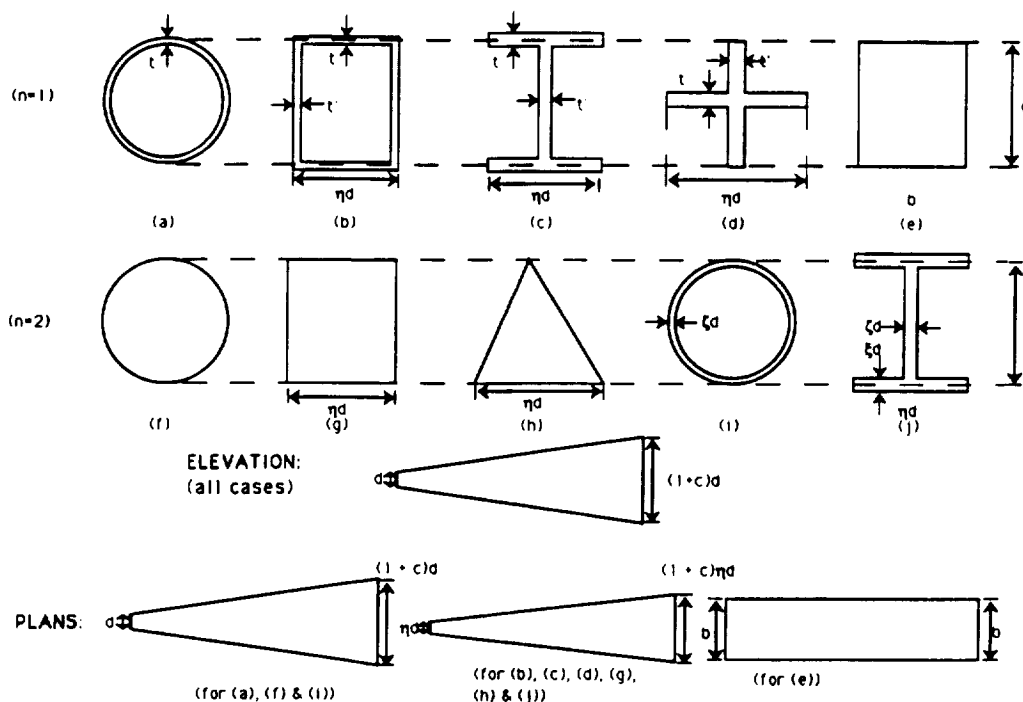$$\frac{du}{d\xi} = \frac{C_1 L}{EA_a c}\frac{1}{\xi^n} \tag{15}$$

Integrating Eq. (15) again,

$$u = \frac{C_1 L}{EA_a c}f(\xi) + C_2 \tag{16}$$

where

$$f(\xi) = -\frac{1}{(n-1)\xi^{n-1}} \text{ for } n \neq 1 \tag{17}$$

$$= \ln \xi \text{ for } n = 1$$

The appropriate boundary conditions for the computation of static constraint modes are given by

$$q_1 = 1, \ q_2 = 0$$
$$q_1 = 0, \ q_2 = 1 \tag{18}$$

The resulting static constraint modes are

$$\phi_1 = \frac{f(\xi) - f(1+c)}{f(1) - f(1+c)}, \quad \phi_2 = \frac{f(1) - f(\xi)}{f(1) - f(1+c)} \tag{19}$$

Note that these constraint modes are in fact the shape functions used in the stiffness matrix of the tapered bar.

At this point, enough information exists to compute M_{II} and K_{II} from Eqs. (8–9). Indeed, for the tapered bar, the kinetic and potential energies T and V are given as

$$T = \frac{1}{2}\int_0^L \rho A(x)\left(\frac{\partial u}{\partial t}\right)^2 dx, \ V = \frac{1}{2}\int_0^L EA(x)\left(\frac{\partial u}{\partial x}\right)^2 dx \tag{20}$$

Substituting Eq. (12) into Eq. (20) gives

$$M_{II} = \int_0^L \rho A(x)\phi_I^T \phi_I dx, \ K_{II} = \int_0^L EA(x)\frac{d\phi_I}{dx}^T\frac{d\phi_I}{dx}dx \tag{21}$$

128

When $n = 1$, the explicit expressions for K_{II} and M_{II} are defined as

$$K_{II} = \frac{EA_a}{L} \frac{c}{\ln(1+c)} \begin{bmatrix} 1 & -1 \\ -1 & 1 \end{bmatrix}, \quad M_{II} = \begin{bmatrix} m_{11} & m_{12} \\ m_{21} & m_{22} \end{bmatrix} \qquad (22)$$

where

$$m_{11} = \frac{\rho A_a L}{4c\ln^2(1+c)} \left[-2\ln^2(1+c) - 2\ln(1+c) + c^2 + 2c \right]$$

$$m_{12} = m_{21} = \frac{\rho A_a L}{4c\ln^2(1+c)} \left[(c^2 + 2c + 2)\ln(1+c) - c^2 - 2c \right] \qquad (23)$$

$$m_{22} = \frac{\rho A_a L}{4c\ln^2(1+c)} \left[2(1+c)^2(\ln^2(1+c) - \ln(1+c)) + c^2 + 2c \right]$$

The counterpart expression for K_{II} when $n \neq 1$ is given as

$$K_{II} = \frac{EA_a c(n-1)(1+c)^{n-1}}{(1+c)^{n-1} - 1} \begin{bmatrix} 1 & -1 \\ -1 & 1 \end{bmatrix} \quad (n \neq 1) \qquad (24)$$

The stifness matrix partitions K_{II} and M_{II} for $n = 2$ are evaluated as

$$K_{II} = \frac{EA_a(1+c)}{L} \begin{bmatrix} 1 & -1 \\ -1 & 1 \end{bmatrix}, \quad M_{II} = \frac{\rho A_a L}{6} \begin{bmatrix} 2 & 1+c \\ 1+c & 2(1+c)^2 \end{bmatrix} \qquad (25)$$

Because of the similarity of the governing equations between axial bars and torsional shafts, Eq. (25) can be used as the stiffness and consistent mass matrices for tapered shafts by replacing the variables A_a, E with J_a, G respectively, where J_a is the polar second moment of area and G is the shear modulus of elasticity. If it is decided that no extra $\bar{q}$ coordinates are to be retained in Eq. (4), then the procedure can be terminated at this stage.

5. Interface Restrained Normal Modes: An entire class of hierarchical models can now be created solely on the basis of choosing the interface restrained assumed modes. In this paper, the set of interface restrained normal modes is used. The normal modes and their corresponding frequencies are obtained from solving the eigenvalue problem associated with the partial differential equation,

$$\frac{\partial}{\partial x} \left\{ EA(x)\frac{\partial u}{\partial x} \right\} = \rho A(x)\frac{\partial^2 u}{\partial t^2} \qquad (26)$$

subjected to the clamped–clamped boundary conditions.

Substituting for A(x) from Eq. (10) and letting $\xi = 1 + cx/L$ gives,

$$\frac{\partial^2 u}{\partial \xi^2} + \frac{n}{\xi}\frac{\partial u}{\partial \xi} = \frac{\rho L^2}{Ec^2}\frac{\partial^2 u}{\partial t^2} \qquad (27)$$

129

For harmonic vibration,

$$u(\xi, t) = U(\xi) \sin \omega t \qquad (28)$$

where t denotes time and ω is the circular natural frequency. Eq. (27) is modified using Eq. (28) as

$$\frac{d^2 U}{d\xi^2} + \frac{n}{\xi}\frac{dU}{d\xi} + \omega^2 \frac{\rho L^2}{Ec^2} U = 0 \qquad (29)$$

The solution of Eq. (29) when $c > 0$ is

$$U(\xi) = \xi^{\frac{1-n}{2}} \left\{ A J_{\frac{1-n}{2}}(\alpha\xi) + B Y_{\frac{1-n}{2}}(\alpha\xi) \right\} \qquad (30)$$

where J and Y are Bessel functions of the first and second kind and $\alpha = \frac{\omega L}{c}\sqrt{\frac{\rho}{E}}$.

For the case of $n = 2$, imposing the clamped–clamped boundary conditions in Eq. (30) yields the characterstic equation for the tapered bar,

$$\sin \alpha c = 0 \qquad (31)$$

The solution of Eq. (31) is

$$\omega = \frac{i\pi}{L}\sqrt{\frac{E}{\rho}}, \quad i = 1, 2, \ldots, \infty \qquad (32)$$

It is noteworthy that the natural frequencies of the tapered bar with clamped ends for the case of $n = 2$ are independent of c and are in fact the same as that of uniform rods. From Eq. (30), the interface restrained normal modes for $n = 2$ becomes

$$\overline{\phi}_i = C_i \frac{\sin(\alpha\xi - \alpha)}{\xi} \qquad (33)$$

where the mass normalization constant C_i must satisfy

$$\int_1^{1+c} \rho A(\xi)\overline{\phi}_i^2(\xi) d\xi = 1 \qquad (34)$$

Substituting Eq. (33) into Eq. (34), C_i is determined as

$$C_i = \sqrt{\frac{2}{\rho A_a L}} \qquad (35)$$

From Eq. (8), the mass matrix partitions are evaluated as

$$M_{NN} = \int_0^L \rho A(x)\overline{\phi}^T\overline{\phi}\,dx = I, \quad M_{IN} = [m_{ji}], \quad m_{ji} = \int_0^L \rho A(x)\phi_j\overline{\phi}_i\,dx \qquad (36)$$

$$i = 1, 2, \ldots, \infty, \quad j = 1, 2$$

130

with

$$m_{1i} = \frac{\sqrt{2\rho A_a L}}{i\pi}, \quad m_{2i} = \frac{\sqrt{2\rho A_a L}}{i\pi}(1+c)(-1)^{i+1} \tag{37}$$

When c is set to zero, Eqs. (25) and (36) reduce to the case of uniform bars. Application of Eq. (33) into Eq. (20) gives the stiffness matrix partitions,

$$K_{IN} = 0, \quad K_{NN} = \text{Diag.} \left[\omega_1^2 \; \omega_2^2 \ldots \right] \tag{38}$$

and ω_i is given by Eq. (32). It can be seen that the tapered bar element matrices consist of very simple terms.

6. Demonstration Examples:

6.1 Tapered Cantilever: This first example is concerned with the cantilevered bar clamped at the right end, see Figure (3). The pertinent structural parameters are $E = 30 \times 10^6$ psi, $\rho g = 0.2839$ lb/in^3, $A_a = 1$ in^2, $A_b = 4$ in^2 and $L = 72$ in.
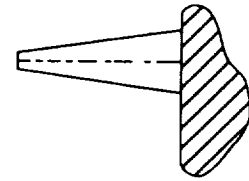
The characteristic equation of this cantilever is given by

$$\alpha \cos \alpha c + \sin \alpha c = 0 \tag{39}$$

Figure 3. Cantilever

Tables (1) and (2) show the number of converged frequencies to within a given percentage relative error when compared to the theoretical frequencies from Eq. (39) for different model orders n.

Note that the bar is subdivided into the requisite number of elements to arrive at the model order n in the standard finite element method as implemented in CSA–NASTRAN whereas in the hierarchical finite element model, the number of bar elements is always one and the requisite interface restrained normal modes are added to arrive at n.

Table 1. Standard Finite Element Method

e	n				
	8	16	24	32	40
< 1 %	1	3	4	5	6
< 5 %	3	6	8	11	14
< 10 %	4	8	12	16	20

131

Table 2. Hierarchical Finite Element Method

e	n				
	8	16	24	32	40
< 1 %	6	14	23	31	39
< 5 %	7	15	23	31	39
< 10 %	7	15	23	31	39

6.2 Planar Truss: Next, consider the planar single-bay truss as illustrated in Figure (4). The parameters are the same as in Section (6.1). The horizontal bar has a uniform cross sectional area of 4 in^2. For planar truss elements, the transverse inertia must be taken into account. This time, however, no 'exact solution' for the frequencies of the structure exists. A reference solution was obtained in two different ways: (1) by constructing a highly refined standard finite element model (2) by retaining a large number of normal modes in the hierarchical model. Both models were refined to the point where no significant change in the frequencies occured and both the models produced the same results.
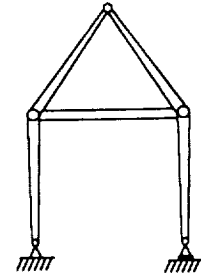
Figure 4. Planar Truss

Table (3) lists the frequencies from the hierarchical finite element model when two normal modes per bar are added (i.e., $n = 16$) as compared to the reference solution. In order to achieve comparable results from standard finite element method, each bar has to be subdivided into five beam elements (i.e., $n = 66$) and consistent mass matrix has to be generated within NASTRAN.

Table 3. Frequency Comparisons For Planar Truss

Mode Number	Reference Frequency (Hz)	Computed Frequency (Hz)	Error %
2	2.606E2	2.606E2	-1.123E-2
3	2.999E2	2.999E2	-1.703E-2
5	6.958E2	6.961E2	-4.763E-2
7	1.467E3	1.468E3	-1.837E-2
9	1.757E3	1.762E3	-2.970E-1
11	2.141E3	2.172E3	-1.432
13	2.889E3	2.898E3	-3.317E-1
14	3.049E3	3.081E3	-1.045
16	3.382E3	3.505E3	-3.622

7. Conclusions For the case of tapered bars, it has been demonstated that the modal synthesis approach, where substructures are assembled to form the overall structure, can be used at the element level itself. This approach has superior convergence characteristics and the advantages of hierarchical formulation.

8. References:

1. W. L. Heard Jr., H. G. Bush, R. E. Wallsom and J. K. Jensen. A mobile workstation concept for mechanically aided astronaut assembly of large trusses. *NASA Technical Paper 2108*, 1-35 (1983).

2. G. M. Lindberg. Vibration of nonuniform beams. *Aero. Quart.* **14**, 387 (1963).

3. K. E. Rouch and J. S. Kao. A tapered beam element for rotor dynamics analysis *J. Sou. Vib.* **66**, 119-140 (1979).

4. J. Thomas and E. Dokumaci. Improved finite elements for vibration analysis of tapered beams. *Aero. Quart.* **24**, 39-46 (1973).

5. T. W. S. To. Higher order tapered beam finite elements for vibration analysis. *J. Sou. Vib.* **63**, 33-50 (1979).

6. B. Ovunck. Dynamic analysis of frameworks by frequency dependent stiffness matrix approach. *Int. Assoc. Bridge Struct. Engg. Publ.* **32**, 137-154 (1972).

7. A. Avakian and D. E. Beskos. Use of dynamic stiffness influence coeffiecients in vibrations of nonuniform beams. *J. Sou. Vib.* **47**, 292-295 (1976).

8. A. K. Gupta. Frequency dependent matrices for tapered beams. *J. Struct. Div.*, *ASCE* **112** 1-17 (1986).

9. J. R. Banerjee and F. W. Williams. Exact Bernoulli-Euler dynamic stiffness matrix for a range of tapered beams. Int. J. Num. Meth. Engg. **21**, 2289-2302 (1985).

10. C. C. Spyrakos and C. I. Chen. Power series expansions of dynamic stiffness matrices for tapered bars and shafts. *Inter. J. Num. Meth. Engg.* **30**, 259-270 (1990).

11. R. C. Engels. Reduced order structural modeling techniques for high energy laser systems. *Final report for AFWL/ARBM* Kirkland, NM (1986).

12. M. Link, J. Moreno-Barragan and M. Weiland. Derivation of finite element models using modal synthesis techniques. *Proc. Euro. Forum Aeroelas. Str. Dyn., DGLR* Bonn (1989).

13. N. Ganesan and R. C. Engels. Hierarchical Bernoulli-Euler beam finite elements. *Comp. Struct.* (to appear) (1992).

14. N. Ganesan and R. C. Engels. Timoshenko beam finite elements using assumed modes method. *J. Sou. Vib.* (to appear) (1992).

TRANSIENT THERMAL STRESS RECOVERY FOR STRUCTURAL MODELS

William Walls
McDonnell Douglas Space Systems Co.
Huntsville Alabama

ABSTRACT

A method for computing transient thermal stress vectors from temperature vectors is described. The three step procedure involves the use of NASTRAN to generate an influence coefficient matrix which relates temperatures to stresses in the structural model. The transient thermal stresses are then recovered and sorted for maximum and minimum values. Verification data for the procedure is also provided.

1.0 INTRODUCTION

There are many occasions when the stresses produced by transient thermal events must be considered. The ascent, on-orbit, and descent phases of a Spacelab mission produce large temperature gradients on the Cargo Element. A method for recovering the thermal stresses produced by these events was developed by the Structural Analysis Group at McDonnell Douglas Space Systems Company-Huntsville (MDSSC-HSV), and has been used for more than six years in Spacelab Evaluation.

Because this method was somewhat unhandy to use, only a limited number of temperature distributions could be run. These were generally chosen on the basis of temperature or temperature difference extremes. Unfortunately, there is no proven relationship between "worst stresses" and "worst temperatures" or "worst temperature differences" for the complex models with which Spacelab has to deal. It was therefore decided to develop a process that would transform transient temperature vectors (which are separately calculated) directly into stress vectors that could then be sorted for maximum and minimum (Max/Min) values.

Section 2 presents the theory used in the procedure, Section 3 describes the procedure, Section 4 presents verification results, and Section 5 contains the conclusions.

2.0 THEORY

The method described assumes that the thermal strains, and hence stresses are linearly proportional to the temperatures. The method, therefore, is not applicable to models having temperature or stress dependent material properties.

An influence coefficient matrix, [TRAS], to transform the temperatures at a models n grids into m stresses can be developed as follows. A temperature of one unit above the reference is applied to a grid in the model while the remaining n-1 grids are held at the reference temperature. The resulting m stresses are then recovered. This is repeated for all n grids in the model. The resulting n sets of stresses are then assembled as columns to form an m by n influence coefficient matrix, [TRAS], that can be used to transform temperature vectors into stress vectors. The transformation is as follows:

$$[STMHST] = [TRAS][TEMPS] \qquad (1)$$

Where;

[STMHST] = Stresses in the finite element model (time history).

[TRAS] = Linear transformation (influence coefficient) from temperatures to stresses.

[TEMPS] = Temperatures at the grids (time history).

Equation (1) is used to recover transient stress vectors from transient temperature vectors.

3.0 PROCEDURE

The procedure used to recover maximum and minimum thermal stresses is divided into three steps. The first step is to generate the influence coefficient matrix [TRAS]. The transient stresses are recovered using equation (1) in the second step. The transient thermal stresses are then sorted for Max/Min data in the third step. Each of these three steps will be described below.

135

3.1   Step 1 - Generation of The Influence
                       Coefficient Matrix [TRAS]

NASTRAN is used to generate [TRAS] as described in Section 2.
NASTRAN Subcase commands are used to accomplish this step with
each subcase corresponding to a grid in the model. It should be
noted that NASTRAN can handle a maximum of sixty-six temperature
load cases. A model having more than sixty-six grids will,
therefore, require multiple runs and subsequent merging of the
output data. An example of a NASTRAN control deck to generate
[TRAS] for the verification model described in Section 4 is
shown in Figure 1. The DUMMOD5 module is used to convert the
OES1 table into a matrix data block which is then written to a
file using the OUTPUT5 module. The extraneous rows (fiber
distances, safety margins, etc.) of [TRAS] are then removed
using a specially developed FORTRAN code.

3.2   Step 2 - Recover Transient Thermal Stress
                         Vectors From Temperature Vectors

The transient temperature vectors must now be obtained. At
MDSSC-Huntsville, the thermal analyses are performed using
SINDA. A FORTRAN code has been written to access the SINDA
output file and recover the desired temperatures along with the
corresponding time vectors. The temperature and time data is
written in OUTPUT5 format. Care should be taken to ensure that
the row order of the temperature vectors is compatible with the
column order of [TRAS].

Equation (1) is then used to recover the transient thermal
stress vectors. This is easily accomplished in a simple DMAP
run using the MPYAD module. The resulting thermal stress
vectors and time vector are written to a file using the OUTPUT5
module.

3.3   Step 3 - Sort Thermal Stress Vectors For
                         Maximum and Minimum Data.

The transient thermal stress vectors are now sorted for Max/Min
data. This step is performed using a specialized FORTRAN code.
This code can search multiple time histories allowing composite
Max/Min tables to be obtained. An example of output from this
program for the Spacelab Multipurpose Experiment Support
Structure (MPESS) is shown in Table 1. The data in Table 1 was
obtained from actual temperature vectors for a Spacelab mission
and encompasses ascent, orbit, and descent.

4.0   VERIFICATION

In order to verify that the procedure is working correctly, a
test case was performed. A simple rectangular plate model was
constructed using QUAD4 and BAR elements. A plot of the plate
model is presented in Figure 2 and the Bulk Data is shown in
Figure 3. The model has thirty-three grids and is homogeneous.
A temperature gradient (see Figure 4) was applied to the model
and the resulting stresses in four elements were recovered using
NASTRAN directly. The results are presented in Figure 5. The
transient thermal stress recovery procedure was then used to
calculate stresses due to the same temperature gradient and the
results are shown in Table 2.

It can be seen from Figure 5 and Table 2 that the results are
the same. This indicates that using [TRAS] to perform the
thermal stress recovery produces the same results as using
NASTRAN directly.

5.0   CONCLUSION

A procedure has been developed to recover thermal stresses in a
NASTRAN model directly from temperatures output by a thermal
model. Because the procedure uses a linear transformation
matrix rather than a computer program, entire thermal stress
time histories may be efficiently obtained and scanned for
Max/Min thermal stress data. Tabular output of the Max/Min data
is then produced. A test case has been executed and the results
indicate that the procedure functions correctly.

137

```
NASTRAN TITLEOPT=0
$
$ RUN TO GENERATE INFLUENCE COEFF. MATRIX FOR THERMAL STRESS RECOVERY.
$
$
$
$
ID  CHECKOUT PLATE
APP DISP
SOL 1,7
TIME 999
DIAG 13,14,21,22,26,42
$
$    WRITE OUT ELEMENT STRESS/FORCE MATRICES
$      WHERE;
$         OES1=STRESSES
$         OEF1=FORCES
$         I=# OF ELEMENTS FOR WHICH STRESSES/FORCES ARE BEING RECOVERED
$
ALTER 106
DUMMOD5  OES1,,,,/ELSEU,,,,/C,N,44/////C,N,1/C,N,1 $
OUTPUT5  ELSEU,,,,//0/15//0 $
OUTPUT5  ,,,,//-9/15//0 $
ENDALTER
CEND
$
TITLE =  ANALYSIS OF PLATE
SUBTITLE = RUN TO GENERATE INFLUENCE COEFFICIENT MATRIX
LABEL = PLATE
MAXLINES = 99999999
  SPC=100
$
SUBCASE 1
  LABEL = APPLY A 1 DEGREE ABOVE REF. TEMP. TO GRID 1
  TEMP(LOAD) = 1
  ELSTRESS=ALL
$
SUBCASE 2
  LABEL = APPLY A 1 DEGREE ABOVE REF. TEMP. TO GRID 2
  TEMP(LOAD) = 2
  ELSTRESS=ALL
$
SUBCASE 3
  LABEL = APPLY A 1 DEGREE ABOVE REF. TEMP. TO GRID 3
  TEMP(LOAD) = 3
  ELSTRESS=ALL
$
SUBCASE 4
  LABEL = APPLY A 1 DEGREE ABOVE REF. TEMP. TO GRID 4
  TEMP(LOAD) = 4
  ELSTRESS=ALL
$
SUBCASE 5
  LABEL = APPLY A 1 DEGREE ABOVE REF. TEMP. TO GRID 5
```

Figure 1.   NASTRAN Control Deck to Generate [TRAS] for the
            Verification Plate Model

```
   TEMP(LOAD) = 5
   ELSTRESS=ALL
$
SUBCASE 6
   LABEL = APPLY A 1 DEGREE ABOVE REF. TEMP. TO GRID 6
   TEMP(LOAD) = 6
   ELSTRESS=ALL
$
SUBCASE 7
   LABEL = APPLY A 1 DEGREE ABOVE REF. TEMP. TO GRID 7
   TEMP(LOAD) = 7
   ELSTRESS=ALL
$
SUBCASE 8
   LABEL = APPLY A 1 DEGREE ABOVE REF. TEMP. TO GRID 8
   TEMP(LOAD) = 8
   ELSTRESS=ALL
$
SUBCASE 9
   LABEL = APPLY A 1 DEGREE ABOVE REF. TEMP. TO GRID 9
   TEMP(LOAD) = 9
   ELSTRESS=ALL
$
SUBCASE 10
   LABEL = APPLY A 1 DEGREE ABOVE REF. TEMP. TO GRID 10
   TEMP(LOAD) = 10
   ELSTRESS=ALL
$
SUBCASE 11
   LABEL = APPLY A 1 DEGREE ABOVE REF. TEMP. TO GRID 11
   TEMP(LOAD) = 11
   ELSTRESS=ALL
$
SUBCASE 12
   LABEL = APPLY A 1 DEGREE ABOVE REF. TEMP. TO GRID 12
   TEMP(LOAD) = 12
   ELSTRESS=ALL
$
SUBCASE 13
   LABEL = APPLY A 1 DEGREE ABOVE REF. TEMP. TO GRID 13
   TEMP(LOAD) = 13
   ELSTRESS=ALL
$
SUBCASE 14
   LABEL = APPLY A 1 DEGREE ABOVE REF. TEMP. TO GRID 14
   TEMP(LOAD) = 14
   ELSTRESS=ALL
$
SUBCASE 15
   LABEL = APPLY A 1 DEGREE ABOVE REF. TEMP. TO GRID 15
   TEMP(LOAD) = 15
   ELSTRESS=ALL
$
SUBCASE 16
   LABEL = APPLY A 1 DEGREE ABOVE REF. TEMP. TO GRID 16
```

Figure 1.   NASTRAN Control Deck to Generate [TRAS] for the
             Verification Plate Model (Continued)

```
    TEMP(LOAD) = 16
    ELSTRESS=ALL
  $
SUBCASE 17
  LABEL = APPLY A 1 DEGREE ABOVE REF. TEMP. TO GRID 17
  TEMP(LOAD) = 17
  ELSTRESS=ALL
  $
SUBCASE 18
  LABEL = APPLY A 1 DEGREE ABOVE REF. TEMP. TO GRID 18
  TEMP(LOAD) = 18
  ELSTRESS=ALL
  $
SUBCASE 19
  LABEL = APPLY A 1 DEGREE ABOVE REF. TEMP. TO GRID 19
  TEMP(LOAD) = 19
  ELSTRESS=ALL
  $
SUBCASE 20
  LABEL = APPLY A 1 DEGREE ABOVE REF. TEMP. TO GRID 20
  TEMP(LOAD) = 20
  ELSTRESS=ALL
  $
SUBCASE 21
  LABEL = APPLY A 1 DEGREE ABOVE REF. TEMP. TO GRID 21
  TEMP(LOAD) = 21
  ELSTRESS=ALL
  $
SUBCASE 22
  LABEL = APPLY A 1 DEGREE ABOVE REF. TEMP. TO GRID 22
  TEMP(LOAD) = 22
  ELSTRESS=ALL
  $
SUBCASE 23
  LABEL = APPLY A 1 DEGREE ABOVE REF. TEMP. TO GRID 23
  TEMP(LOAD) = 23
  ELSTRESS=ALL
  $
SUBCASE 24
  LABEL = APPLY A 1 DEGREE ABOVE REF. TEMP. TO GRID 24
  TEMP(LOAD) = 24
  ELSTRESS=ALL
  $
SUBCASE 25
  LABEL = APPLY A 1 DEGREE ABOVE REF. TEMP. TO GRID 25
  TEMP(LOAD) = 25
  ELSTRESS=ALL
  $
SUBCASE 26
  LABEL = APPLY A 1 DEGREE ABOVE REF. TEMP. TO GRID 26
  TEMP(LOAD) = 26
  ELSTRESS=ALL
  $
SUBCASE 27
  LABEL = APPLY A 1 DEGREE ABOVE REF. TEMP. TO GRID 27
```

**Figure 1. NASTRAN Control Deck to Generate [TRAS] for the
Verification Plate Model (Continued)**

```
      TEMP(LOAD) = 27
      ELSTRESS=ALL
   $
   SUBCASE 28
      LABEL = APPLY A 1 DEGREE ABOVE REF. TEMP. TO GRID 28
      TEMP(LOAD) = 28
      ELSTRESS=ALL
   $
   SUBCASE 29
      LABEL = APPLY A 1 DEGREE ABOVE REF. TEMP. TO GRID 29
      TEMP(LOAD) = 29
      ELSTRESS=ALL
   $
   SUBCASE 30
      LABEL = APPLY A 1 DEGREE ABOVE REF. TEMP. TO GRID 30
      TEMP(LOAD) = 30
      ELSTRESS=ALL
   $
   SUBCASE 31
      LABEL = APPLY A 1 DEGREE ABOVE REF. TEMP. TO GRID 31
      TEMP(LOAD) = 31
      ELSTRESS=ALL
   $
   SUBCASE 32
      LABEL = APPLY A 1 DEGREE ABOVE REF. TEMP. TO GRID 32
      TEMP(LOAD) = 32
      ELSTRESS=ALL
   $
   SUBCASE 33
      LABEL = APPLY A 1 DEGREE ABOVE REF. TEMP. TO GRID 33
      TEMP(LOAD) = 33
      ELSTRESS=ALL
   $
   BEGIN BULK
   $
   SPC1     100        123456  1
   $
   TEMP     1          1       71.0
   TEMPD    1          70.0
   TEMP     2          2       71.0
   TEMPD    2          70.0
   TEMP     3          3       71.0
   TEMPD    3          70.0
   TEMP     4          4       71.0
   TEMPD    4          70.0
   TEMP     5          5       71.0
   TEMPD    5          70.0
   TEMP     6          6       71.0
   TEMPD    6          70.0
   TEMP     7          7       71.0
   TEMPD    7          70.0
   TEMP     8          8       71.0
   TEMPD    8          70.0
   TEMP     9          9       71.0
   TEMPD    9          70.0
```

Figure 1.   NASTRAN Control Deck to Generate [TRAS] for the
             Verification Plate Model (Continued)

```
TEMP     10      10      71.0
TEMPD    10      70.0
TEMP     11      11      71.0
TEMPD    11      70.0
TEMP     12      12      71.0
TEMPD    12      70.0
TEMP     13      13      71.0
TEMPD    13      70.0
TEMP     14      14      71.0
TEMPD    14      70.0
TEMP     15      15      71.0
TEMPD    15      70.0
TEMP     16      16      71.0
TEMPD    16      70.0
TEMP     17      17      71.0
TEMPD    17      70.0
TEMP     18      18      71.0
TEMPD    18      70.0
TEMP     19      19      71.0
TEMPD    19      70.0
TEMP     20      20      71.0
TEMPD    20      70.0
TEMP     21      21      71.0
TEMPD    21      70.0
TEMP     22      22      71.0
TEMPD    22      70.0
TEMP     23      23      71.0
TEMPD    23      70.0
TEMP     24      24      71.0
TEMPD    24      70.0
TEMP     25      25      71.0
TEMPD    25      70.0
TEMP     26      26      71.0
TEMPD    26      70.0
TEMP     27      27      71.0
TEMPD    27      70.0
TEMP     28      28      71.0
TEMPD    28      70.0
TEMP     29      29      71.0
TEMPD    29      70.0
TEMP     30      30      71.0
TEMPD    30      70.0
TEMP     31      31      71.0
TEMPD    31      70.0
TEMP     32      32      71.0
TEMPD    32      70.0
TEMP     33      33      71.0
TEMPD    33      70.0
$
```

Figure 1.   NASTRAN Control Deck to Generate [TRAS] for the
            Verification Plate Model (Concluded)
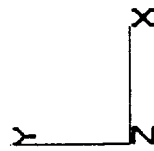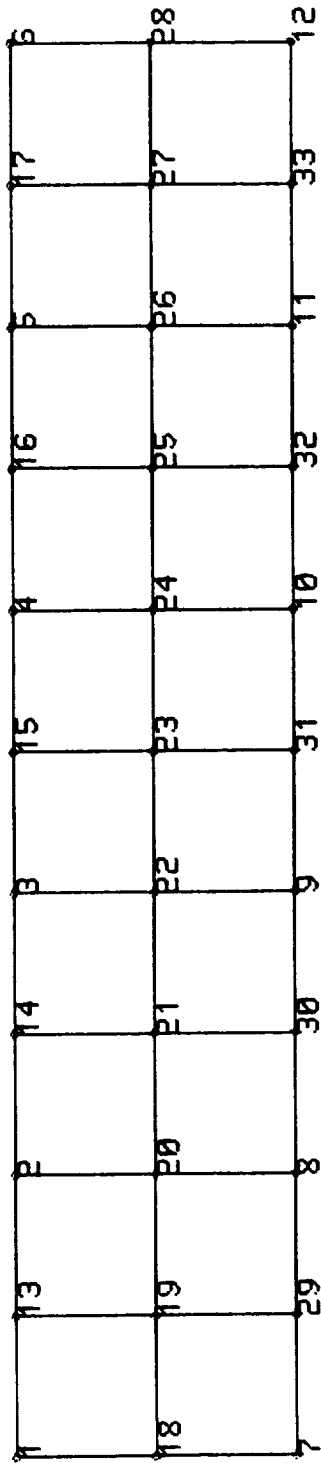
Figure 2. Plate Model Plot

```
$
SPC1      100       123456   1
$
TEMP      55        1        100.0
TEMP      55        2        300.0
TEMP      55        3        600.0
TEMP      55        4        600.0
TEMP      55        5        300.0
TEMP      55        6        100.0
TEMP      55        7        600.0
TEMP      55        8        300.0
TEMP      55        9        100.0
TEMP      55        10       100.0
TEMP      55        11       300.0
TEMP      55        12       600.0
TEMP      55        13       200.0
TEMP      55        14       450.0
TEMP      55        15       600.0
TEMP      55        16       450.0
TEMP      55        17       200.0
TEMP      55        18       350.0
TEMP      55        19       325.0
TEMP      55        20       300.0
TEMP      55        21       325.0
TEMP      55        22       350.0
TEMP      55        23       350.0
TEMP      55        24       350.0
TEMP      55        25       325.0
TEMP      55        26       300.0
TEMP      55        27       325.0
TEMP      55        28       350.0
TEMP      55        29       450.0
TEMP      55        30       200.0
TEMP      55        31       100.0
TEMP      55        32       200.0
TEMP      55        33       450.0
TEMPD     55        70.0
TEMPD     60        70.0
$
$
$                   ********** PLATE **********
$
GRID      1                  0.0      0.0      0.0
GRID      2                  50.0     0.0      0.0
GRID      3                  100.0    0.0      0.0
GRID      4                  150.0    0.0      0.0
GRID      5                  200.0    0.0      0.0
GRID      6                  250.0    0.0      0.0
GRID      7                  0.0      -50.     0.0
GRID      8                  50.0     -50.     0.0
GRID      9                  100.0    -50.     0.0
GRID      10                 150.0    -50.     0.0
GRID      11                 200.0    -50.     0.0
GRID      12                 250.0    -50.     0.0
```

Figure 3. Plate Model Bulk Data

144

GRID	13		25.0	0.0	0.0		
GRID	14		75.0	0.0	0.0		
GRID	15		125.0	0.0	0.0		
GRID	16		175.0	0.0	0.0		
GRID	17		225.0	0.0	0.0		
GRID	18		0.0	-25.0	0.0		
GRID	19		25.0	-25.0	0.0	6	
GRID	20		50.0	-25.0	0.0	6	
GRID	21		75.0	-25.0	0.0	6	
GRID	22		100.0	-25.0	0.0	6	
GRID	23		125.0	-25.0	0.0	6	
GRID	24		150.0	-25.0	0.0	6	
GRID	25		175.0	-25.0	0.0	6	
GRID	26		200.0	-25.0	0.0	6	
GRID	27		225.0	-25.0	0.0	6	
GRID	28		250.0	-25.0	0.0		
GRID	29		25.0	-50.0	0.0		
GRID	30		75.0	-50.0	0.0		
GRID	31		125.0	-50.0	0.0		
GRID	32		175.0	-50.0	0.0		
GRID	33		225.0	-50.0	0.0		
CBAR	1	1	1	13	0.0	0.0	1.0	1
CBAR	2	1	13	2	0.0	0.0	1.0	1
CBAR	3	1	2	14	0.0	0.0	1.0	1
CBAR	4	1	14	3	0.0	0.0	1.0	1
CBAR	5	1	3	15	0.0	0.0	1.0	1
CBAR	6	1	15	4	0.0	0.0	1.0	1
CBAR	7	1	4	16	0.0	0.0	1.0	1
CBAR	8	1	16	5	0.0	0.0	1.0	1
CBAR	9	1	5	17	0.0	0.0	1.0	1
CBAR	10	1	17	6	0.0	0.0	1.0	1
CBAR	11	1	6	28	0.0	0.0	1.0	1
CBAR	12	1	28	12	0.0	0.0	1.0	1
CBAR	13	1	12	33	0.0	0.0	1.0	1
CBAR	14	1	33	11	0.0	0.0	1.0	1
CBAR	15	1	11	32	0.0	0.0	1.0	1
CBAR	16	1	32	10	0.0	0.0	1.0	1
CBAR	17	1	10	31	0.0	0.0	1.0	1
CBAR	18	1	31	9	0.0	0.0	1.0	1
CBAR	19	1	9	30	0.0	0.0	1.0	1
CBAR	20	1	30	8	0.0	0.0	1.0	1
CBAR	21	1	8	29	0.0	0.0	1.0	1
CBAR	22	1	29	7	0.0	0.0	1.0	1
CBAR	23	1	7	18	0.0	0.0	1.0	1
CBAR	24	1	18	1	0.0	0.0	1.0	1
$							
CQUAD4	1	1000	18	19	13	1	
CQUAD4	2	1000	19	20	2	13	
CQUAD4	3	1000	20	21	14	2	
CQUAD4	4	1000	21	22	3	14	
CQUAD4	5	1000	22	23	15	3	
CQUAD4	6	1000	23	24	4	15	
CQUAD4	7	1000	24	25	16	4	
CQUAD4	8	1000	25	26	5	16	
CQUAD4	9	1000	26	27	17	5	

Figure 3. Plate Model Bulk Data (Continued)

```
CQUAD4   10      1000    27      28      6       17
CQUAD4   11      1000    7       29      19      18
CQUAD4   12      1000    29      8       20      19
CQUAD4   13      1000    8       30      21      20
CQUAD4   14      1000    30      9       22      21
CQUAD4   15      1000    9       31      23      22
CQUAD4   16      1000    31      10      24      23
CQUAD4   17      1000    10      32      25      24
CQUAD4   18      1000    32      11      26      25
CQUAD4   19      1000    11      33      27      26
CQUAD4   20      1000    33      12      28      27
$
PSHELL   1000    4000    .7      4000            4000
$
PBAR     1       4000    1.9375  4.85    4.85    7.27
$
MAT1     4000    1.0+7           .33     .000371 13.3-6  70.0
$
ENDDATA
```

Figure 3. Plate Model Bulk Data (Concluded)
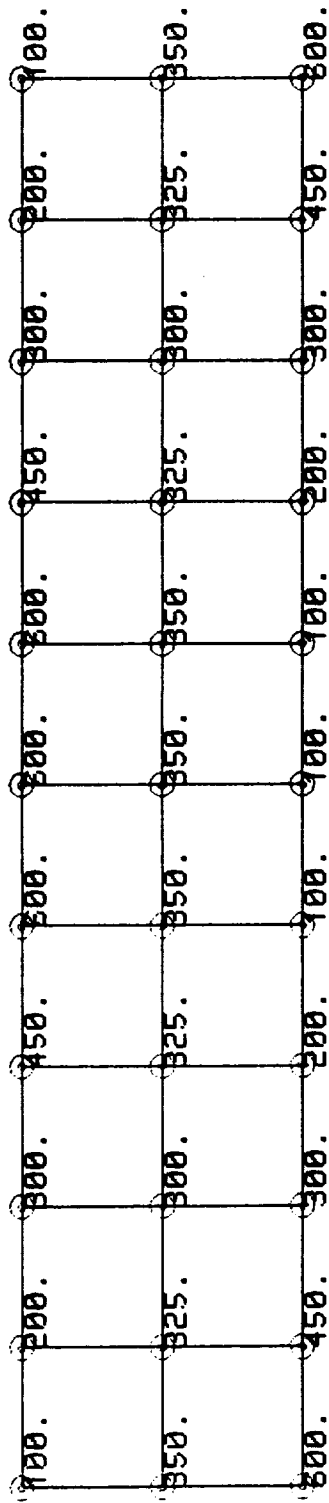
Figure 4. Temperatures Applied to the Plate Model

S T R E S S E S   I N   B A R   E L E M E N T S   (C B A R)

ELEMENT ID.	SA1 SB1	SA2 SB2	SA3 SB3	SA4 SB4	AXIAL STRESS	SA-MAX SB-MAX	SA-MIN SB-MIN	M.S.-T M.S.-C
1	0.0 0.0	0.0 0.0	0.0 0.0	0.0 0.0	4.815285E+03	4.815285E+03 4.815285E+03	4.815285E+03 4.815285E+03	
2	0.0 0.0	0.0 0.0	0.0 0.0	0.0 0.0	1.158353E+03	1.158353E+03 1.158353E+03	1.158353E+03 1.158353E+03	

S T R E S S E S   I N   G E N E R A L   Q U A D R I L A T E R A L   E L E M E N T S   (C Q U A D 4)

ELEMENT ID.	FIBRE DISTANCE	STRESSES IN STRESS COORD. SYSTEM (IN STRESS COORDINATE SYSTEM) NORMAL-X	NORMAL-Y	SHEAR-XY	PRINCIPAL STRESSES (ZERO SHEAR) ANGLE	MAJOR	MINOR	MAX SHEAR
1	-3.500000E-01 3.500000E-01	2.709319E+03 2.709319E+03	4.505912E+02 4.505912E+02	-6.043338E+01 -6.043338E+01	-1.5315 -1.5315	2.709935E+03 2.709935E+03	4.489755E+02 4.489755E+02	1.130980E+03 1.130980E+03
2	-3.500000E-01 3.500000E-01	8.944683E+02 8.944683E+02	2.615569E+02 2.615569E+02	-1.671155E+02 -1.671155E+02	-13.9189 -13.9189	9.358398E+02 9.358398E+02	2.201414E+02 2.201414E+02	3.578712E+02 3.578712E+02

Figure 5.   Thermal Stresses from a Direct NASTRAN Solution of the Plate Model

NASTRAN BAR 106
(SINDA NODE 6000)
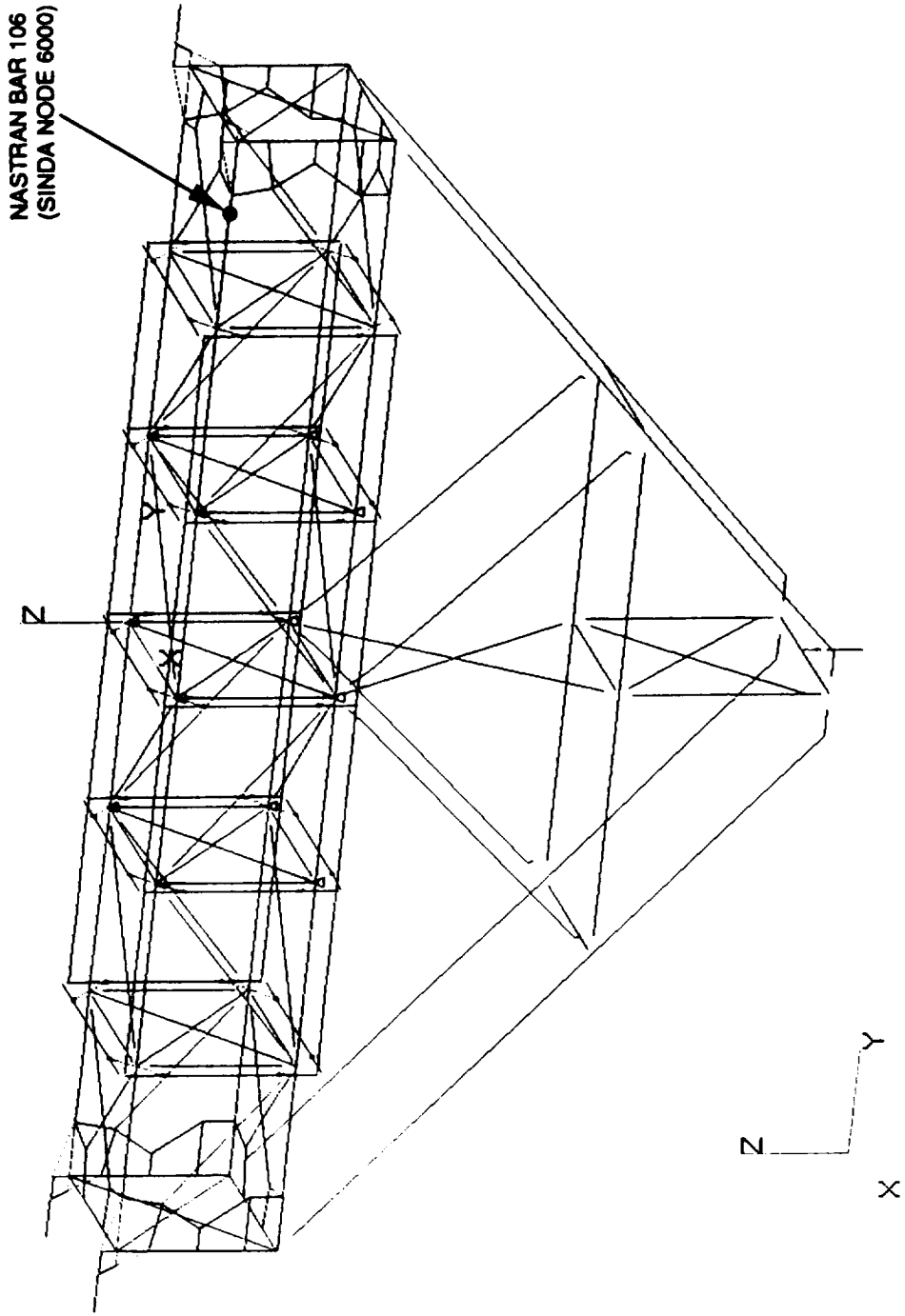
Figure 6.   MPESS Finite Element Model

MPESS THERMAL STRESS
ON ORBIT
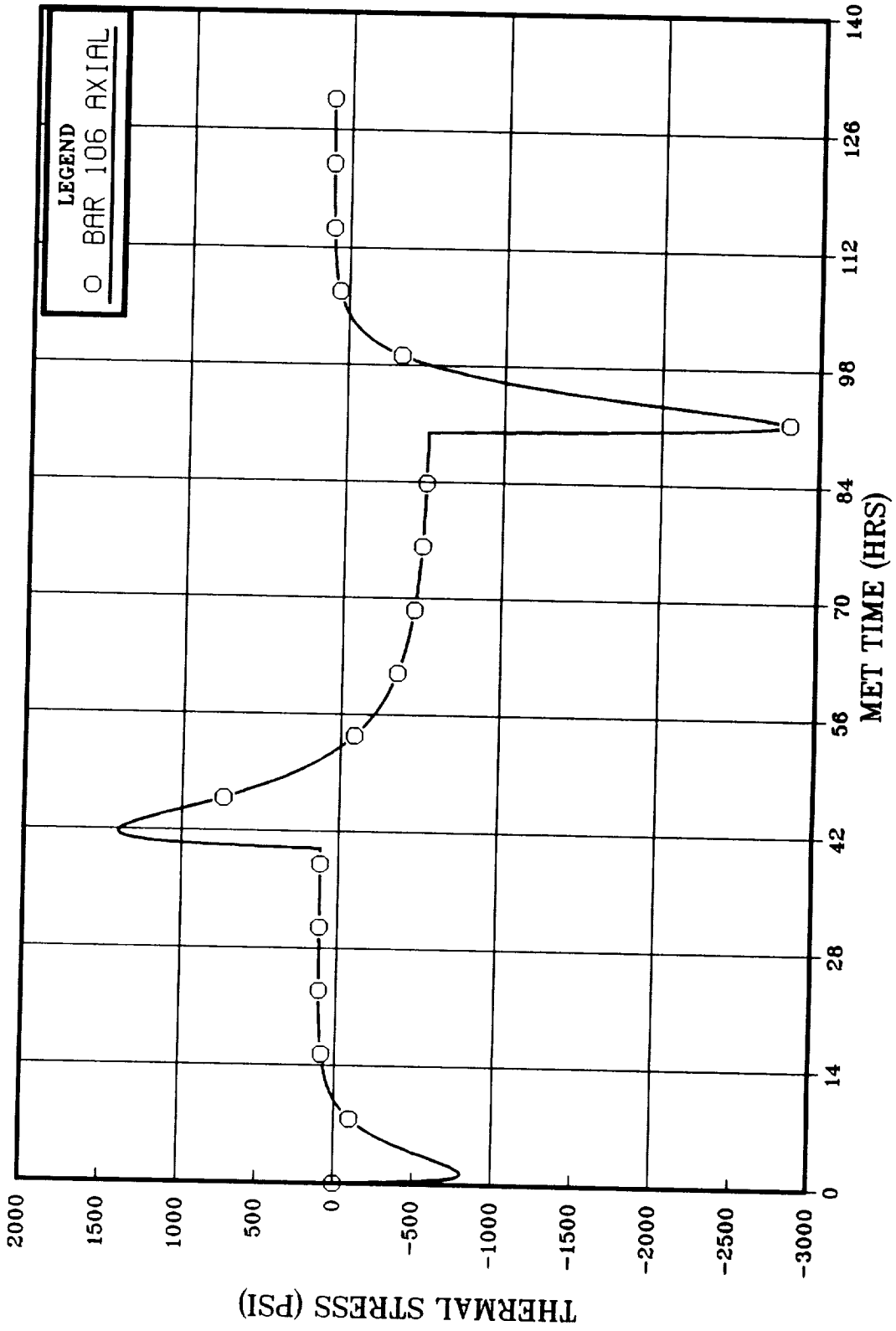
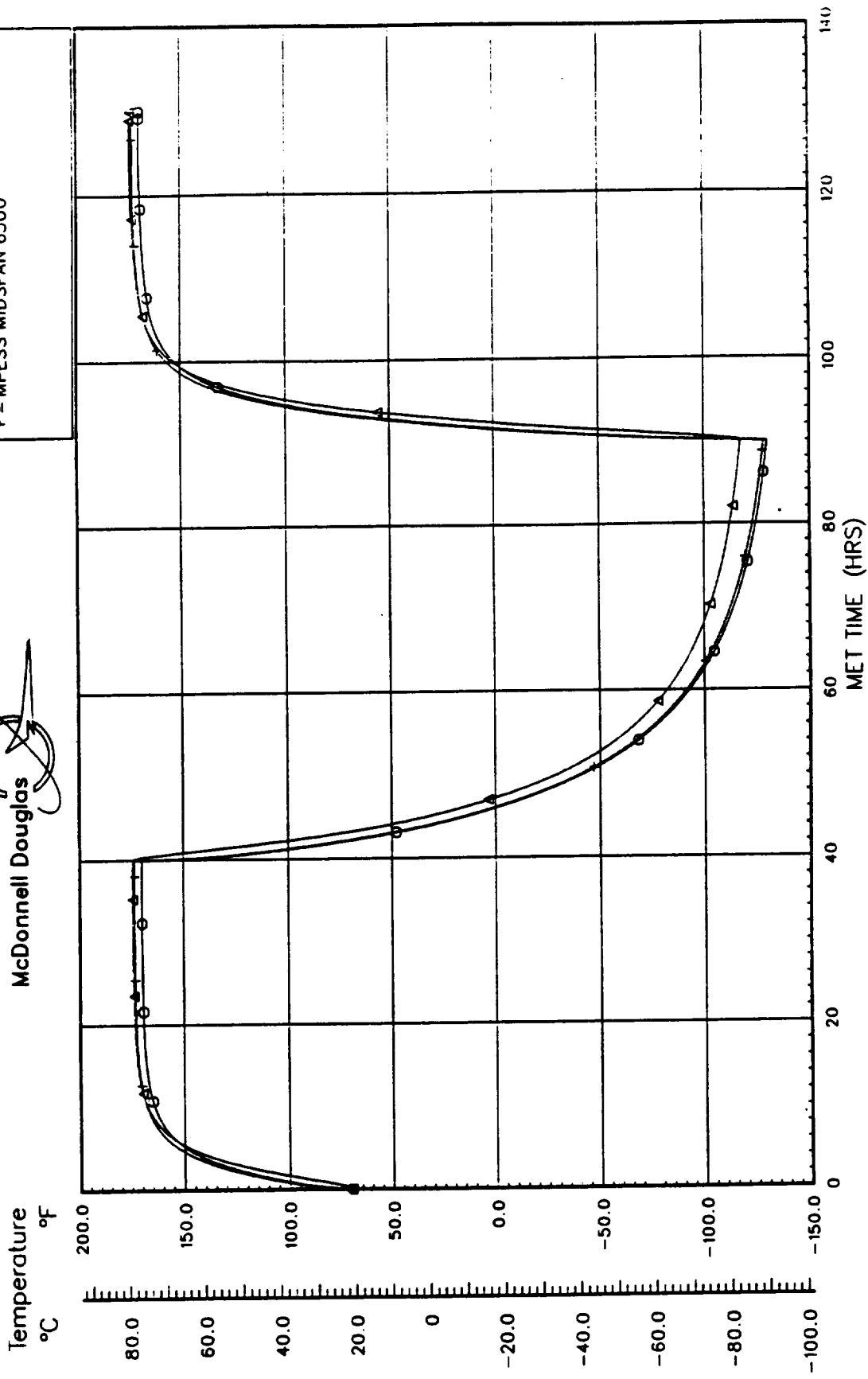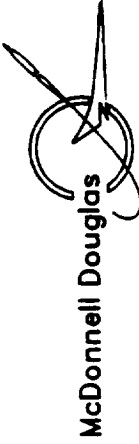Figure 7. MPESS BAR 106 (SINDA Node 6000) Axial Stress Time
History

Figure 8. MPESS BAR 106 (SINDA Node 6000) Temperature Time History

TABLE 1. SPACELAB MULTI - PURPOSE EXPERIMENT SUPPORT STRUCTURE THERMAL STRESS MAX/MIN SUMMARY

ROW	DESCRIPTION	STRESS TYPE	EID	MAX	TIME	CASE	MIN	TIME	CASE
1	CBAR	SA1	106	799.737	92.500	ORBIT	-1574.153	89.950	ORBIT
2		SA2	106	616.297	41.000	ORBIT	-1087.696	91.000	ORBIT
3		SA3	106	1574.153	89.950	ORBIT	-799.737	92.500	ORBIT
4		SA4	106	1087.696	91.000	ORBIT	-616.297	41.000	ORBIT
5		AXIAL	106	1403.170	41.700	ORBIT	-2810.078	41.000	ORBIT
6		SB1	106	536.807	92.000	ORBIT	-815.012	89.950	ORBIT
7		SB2	106	417.387	41.000	ORBIT	-752.511	90.800	ORBIT
8		SB3	106	815.012	89.950	ORBIT	-536.807	92.000	ORBIT
9		SB4	106	752.511	90.800	ORBIT	-417.387	41.000	ORBIT
10	CBAR	SA1	107	280.820	93.700	ORBIT	-134.335	42.800	ORBIT
11		SA2	107	398.181	93.700	ORBIT	-271.673	43.700	ORBIT
12		SA3	107	134.335	42.800	ORBIT	-280.820	93.700	ORBIT
13		SA4	107	271.673	43.700	ORBIT	-398.181	93.700	ORBIT
14		AXIAL	107	1862.010	89.950	ORBIT	-1464.976	94.200	ORBIT
15		SB1	107	412.152	92.900	ORBIT	-379.209	89.950	ORBIT
16		SB2	107	598.601	91.100	ORBIT	-362.067	41.300	ORBIT
17		SB3	107	379.209	89.950	ORBIT	-412.152	92.900	ORBIT
18		SB4	107	362.067	41.300	ORBIT	-598.601	91.100	ORBIT
19	CBAR	SA1	108	1722.223	89.950	ORBIT	-900.599	91.100	ORBIT
20		SA2	108	370.978	41.100	ORBIT	-395.292	0.020	DESCENTH
21		SA3	108	900.599	0.020	ORBIT	-1722.223	81.500	ORBIT
22		SA4	108	395.292	91.500	DESCENTH	-370.978	89.950	ORBIT
23		AXIAL	108	1574.609	91.200	ORBIT	-1176.477	41.100	ORBIT
24		SB1	108	501.320	40.500	ORBIT	-1290.434	90.400	ORBIT
25		SB2	108	250.335	0.570	DESCENTC	-398.063	39.900	ORBIT
26		SB3	108	1290.434	90.400	ORBIT	-501.320	40.500	ORBIT
27		SB4	108	398.063	39.900	ORBIT	-250.335	0.570	DESCENTC

TABLE 2. THERMAL STRESSES IN THE PLATE MODEL FROM THE TRANSIENT THERMAL STRESS RECOVERY PROCEDURE

ROW	ELEMENT TYPE	STRESS COMPONENT	EID	MAX	TIME	CASE	MIN	TIME	CASE
1	CBAR	SA1	1	0.000	0.000	N/A	0.000	0.000	N/A
2		SA2	1	0.000	0.000	N/A	0.000	0.000	N/A
3		SA3	1	0.000	0.000	N/A	0.000	0.000	N/A
4		SA4	1	0.000	0.000	N/A	0.000	0.000	N/A
5		AXIAL	1	4815.285	1.000	CASE1	4815.285	1.000	CASE1
6		SB1	1	0.000	0.000	N/A	0.000	0.000	N/A
7		SB2	1	0.000	0.000	N/A	0.000	0.000	N/A
8		SB3	1	0.000	0.000	N/A	0.000	0.000	N/A
9		SB4	1	0.000	0.000	N/A	0.000	0.000	N/A
10	CBAR	SA1	2	0.000	0.000	N/A	0.000	0.000	N/A
11		SA2	2	0.000	0.000	N/A	0.000	0.000	N/A
12		SA3	2	0.000	0.000	N/A	0.000	0.000	N/A
13		SA4	2	0.000	0.000	N/A	0.000	0.000	N/A
14		AXIAL	2	1158.353	1.000	CASE1	1158.353	1.000	CASE1
15		SB1	2	0.000	0.000	N/A	0.000	0.000	N/A
16		SB2	2	0.000	0.000	N/A	0.000	0.000	N/A
17		SB3	2	0.000	0.000	N/A	0.000	0.000	N/A
18		SB4	2	0.000	0.000	N/A	0.000	0.000	N/A
19	COQUAD4	NORMAL-X AT Z1	1	2709.319	1.000	CASE1	2709.319	1.000	CASE1
20		NORMAL-Y AT Z1	1	450.591	1.000	CASE1	450.591	1.000	CASE1
21		SHEAR-XY AT Z1	1	-60.433	1.000	CASE1	-60.433	1.000	CASE1
22		NORMAL-X AT Z2	1	2709.319	1.000	CASE1	2709.319	1.000	CASE1
23		NORMAL-Y AT Z2	1	450.591	1.000	CASE1	450.591	1.000	CASE1
24		SHEAR-XY AT Z2	1	-60.433	1.000	CASE1	-60.433	1.000	CASE1
25	COQUAD4	NORMAL-X AT Z1	2	894.468	1.000	CASE1	894.468	1.000	CASE1
26		NORMAL-Y AT Z1	2	261.557	1.000	CASE1	261.557	1.000	CASE1
27		SHEAR-XY AT Z1	2	-167.116	1.000	CASE1	-167.116	1.000	CASE1
28		NORMAL-X AT Z2	2	894.468	1.000	CASE1	894.468	1.000	CASE1
29		NORMAL-Y AT Z2	2	261.557	1.000	CASE1	261.557	1.000	CASE1
30		SHEAR-XY AT Z2	2	-167.116	1.000	CASE1	-167.116	1.000	CASE1

MDSSC-HSV

Transient Loads Analysis
For Space Flight Applications

S. K. Thampi, N. S. Vidyasagar and N. Ganesan

GE Government Services, Houston, Texas

ABSTRACT: A significant part of the flight readiness verification process involves transient analysis of the coupled Shuttle-payload system to determine the low frequency transient loads. This paper describes a methodology for transient loads analysis and its implementation for the Spacelab Life Sciences Mission. The analysis is carried out using two major software tools - NASTRAN and an external FORTRAN code called EZTRAN *. This approach is adopted to overcome some of the limitations of NASTRAN's standard transient analysis capabilities. The method uses Data Recovery Matrices (DRM) to improve computational efficiency. The mode acceleration method is fully implemented in the DRM formulation to recover accurate displacements, stresses and forces. The advantages of the method are demonstrated through a numerical example.

1. Introduction: In the past decade, NASA has conducted numerous Spacelab Missions for the advancement of space exploration and research. The Spacelab is a reusable laboratory that is carried in the cargo bay of the Space Shuttle Orbiter. Experiments in several different disciplines such as astronomy, life sciences and material science are accommodated in this modular laboratory for various Shuttle missions. The module also contains utilities, computers and work benches to support the experiments. The experiment hardware is mounted in instrument racks located on either side of the module, in overhead lockers, and in the center aisle, as shown in Figure 1.

During liftoff and landing flight events, the Shuttle and its payload show significant low-frequency transient accelerations due to thrust from the main engines and solid rocket boosters, wind gust, vortex shedding, and launch pad forces during liftoff, and crosswinds and nose-gear slapdown during landing. The levels of acceleration on a specific payload component depend on the response of the Spacelab inside the Orbiter cargo bay and the response of the component inside the Spacelab. Because these responses depend on the dynamic characteristics and interactions of the Orbiter-Spacelab-payload system, a transient analysis of the coupled system is required to determine the quasi-static loads as part of the flight readiness verification process.

Analysis of the coupled system can be carried out using the standard transient analysis capabilities of NASTRAN. However, these procedures have some limitations in terms of computational efficiency and accuracy, especially when dealing with large substructured models [Rf. 1,2]. An alternate procedure which relies on the extensive use of data recovery matrices is presented to overcome some of these limitations. The methodology has been successfully implemented for the analysis of the Spacelab Life Sciences (SLS-2) Mission [Rf.

---

* EZTRAN is developed by Structural Dynamics Research Corporation, San Diego, California

3] which involved large models (in excess of 190000 degrees of freedom) and long simulations (in excess of 4500 time steps). The advantages of the method are demonstrated through a simple example problem in this paper.

2. Overview of Methods: There are two methods for performing dynamic transient analysis in NASTRAN. The Direct Transient Response, available in Rigid Format 9, solves a system described in terms of its physical mass, stiffness and damping matrices.

$$[m]\{\ddot{u}\} + [c]\{\dot{u}\} + [k]\{u\} = \{f\} \tag{1}$$

These equations are numerically integrated to determine the response at the physical degrees of freedom (DOF) as functions of time. The Modal Transient Response method, available in Rigid Format 12, is similar to the direct method, with the exception that it uses the classical modal transformation

$$\{u\} = [\phi]\{Q\} \tag{2}$$

to diagonalize the physical mass, stiffness and damping matrices. The overall response is calculated by including only a small number of the structural modes, making the numerical integration of the generalized equations of motion much faster.

$$[M]\{\ddot{Q}\} + [C]\{\dot{Q}\} + [K]\{Q\} = \{F\} \tag{3}$$

where

$$[M] = [\phi]^T [m][\phi], \ [C] = [\phi]^T [c][\phi], \ [K] = [\phi]^T [k][\phi], \ \{F\} = [\phi]^T \{f\}$$

Physical responses can be recovered from a modal transient analysis through the mode displacement method (Eqn. 2) or the mode acceleration method (Eqn. 4). The former method is more efficient and quite accurate for calculating accelerations if sufficient modes are retained to envelope the frequency content of the forcing functions. However, the latter method is preferred when accurate displacements, element forces and stresses are required from a modal transient analysis. The mode acceleration technique minimizes the loss of accuracy due to modal truncation by including the static response of the truncated high-frequency modes in the solution.

$$\{u\} = [k]^{-1}\left[\{f\} - [m]\{\ddot{u}\} - [c]\{\dot{u}\}\right] \tag{4}$$

The implementation of the mode acceleration procedure in NASTRAN has some disadvantages. In order to include the effects of inertia and damping forces in the load vector in Eqn. 4, the accelerations and velocities at all DOF in the solution set (L-set) must be computed. A static solution must then be performed with the modified load vector at each time step. This requires significant computer processing time if the L-set is large and/or the number of integration steps is large. In addition, there are accuracy problems when

dealing with multi-stage substructured models. For such cases, the mode-acceleration correction is applied only to the residual structure and not to upstream substructures. This leads to modal truncation errors because the component modes are used to represent the static response of the interior degrees of freedom [Rf. 1].

Because of these disadvantages, standard transient analysis procedures in NASTRAN are not suitable for solving large problems involving multi-stage substructured models. Alternate methods are required to overcome these limitations, and yet retain the benefits of the mode acceleration method. Such a procedure, used for transient loads analysis of the SLS-2 Mission configuration, is described in the following section.

3. Alternate Method: The alternate method is based on a slightly different form of the mode acceleration data recovery equation. Assuming that damping is negligible, Eqn. 4 can be expressed in the following convenient form.

$$\{u\} = [\psi]\{p\} - [\phi][\Lambda^{-1}]\{\ddot{Q}\} \tag{5}$$

The first term represents the static portion of the transient response. It is obtained as the product of ψ, the static response caused by a set of *unit loads, I*, and a time varying load scale factor, $p(t)$. Note that the *unit loads* multiplied by the scale factor are equivalent to the applied loads, i.e.,

$$\{f(t)\} = [I]\{p(t)\} \tag{6}$$

The second term in Eqn. 5 represents the dynamic portion of the response. It usually includes only the elastic mode contributions as the rigid body modes (if any) do not contribute to stresses and forces. However, the contribution from rigid body modes to the total displacement, $[\phi_{rb}]\{Q_{rb}\}$, can be included in Eqn. 5 if desired. The computational advantages of the alternate method stem from the size of the $[\psi]$ and $[\phi]$ matrices which are determined by the number of response recovery points, the number of load application points and the number of retained elastic modes. These are usually much smaller than the full model size.

The alternate method is implemented using two major software tools - NASTRAN and an external FORTRAN program called EZTRAN. NASTRAN is used to develop, process and assemble the finite element model of the coupled system, calculate system modes, determine unit load static responses, and create data recovery matrices. EZTRAN calculates the modal initial conditions, solves the generalized equations of motion, and recovers physical results. The following steps describe how the two work in conjunction to perform the various analysis tasks.

3.1 Model Generation and Assembly: Finite element models of the Orbiter, Spacelab and experiment payloads are developed by different organizations and are usually test-verified models. They are assembled into a solution system using the automated multi-stage substructuring features of NASTRAN. Prior to assembly, the quality of each component model is verified by performing a series of analytical checks including rigid body modes check, stiffness matrix equilibrium check, rigid body mass check and an enforced displacement check. At each stage of assembly, the effective DOF in the model is

156

reduced either through a Guyan reduction (REDUCE) or a modal reduction (MREDUCE). A fixed-interface Craig-Bampton modal reduction is the preferred method as it will not compromise the fidelity of test-verified finite element models.

3.2 Loads Definition: The input forcing functions for coupled loads analysis are obtained from previous flight accelerometer data. These are maintained by NASA and provided to payload organizations during design evaluation to refine design loads. The data is provided in terms of discrete force-time coordinate pairs, with the point of application of each force being identified by a node number and component name. They include multiple load cases for liftoff and landing flight events. Load scale factors are generated for each load case by normalizing the system forcing functions with unit loads, as indicated in Eqn. 6. The *unit loads* are defined as the maximum force occuring at each loaded DOF, across all load cases.

3.3 Normal Modes Analysis: A normal modes analysis of the fully assembled system is performed using NASTRAN Rigid Format 3. The rigid body modes and the elastic modes of the system, in a specified frequency range, are recovered and stored in the substructure operating file (SOF) database. The frequency range for modal truncation is decided based on the frequency content of the excitation.

3.4 Unit Load Static Analysis: An inertia relief static analysis is performed on the fully assembled system for unit loads derived from the liftoff and landing forcing functions. An unit load vector is generated for each loaded DOF, and they are sequenced in the same order as the forcing functions to form a unit load matrix. The static analysis is performed using Rigid Format 2 because it is capable of analyzing structures with rigid body modes. SUPORT cards must be included if rigid body modes are present, and the choice of support points has significant effect on the computation of displacement results. A good choice is indicated by low strain energy at the support points. An unreduced model is used for static analysis in order that the full mass matrix be available for calculating internal inertia loads of upstream substructures. The static displacements from the inertia relief solution are recovered and stored in the SOF database.

3.5 Data Recovery Matrices Generation: The alternate procedure requires the generation of acceleration and displacement data recovery matrices. These are formed for each basic substructure by performing two data recovery (Phase 3) restart runs with special DMAP alters. The acceleration DRM is made up of rigid body modes and retained elastic mode vectors. These are extracted from the normal modes database for DOF specified through XYPLOT/XYPEAK requests in the SOL 3 data recovery run.

$$\text{Acceleration DRM} = [\phi_{rb} \quad \phi_{el}] \tag{7}$$

Displacements and displacement dependent responses such as element forces, stresses and substructure interface loads are recovered using the mode acceleration method. The displacement DRM has two partitions. The first consists of the unit load static deflection vectors which are extracted from the static analysis database. The second, which provides

157

the dynamic contribution, is obtained from the normal modes database. A rigid format alter in the SOL 2 data recovery run assembles the full displacement DRM for responses specified through XYPLOT/XYPEAK requests.

$$\text{Displacement DRM} = \begin{bmatrix} \psi & \phi_{el}\Lambda_{el}^{-1} \end{bmatrix} \tag{8}$$

The size of the DRMs is controlled by many factors. The number of rows in the acceleration and displacement DRMs will correspond to the number of response requests in the data recovery runs. Since the number of output requests is usually much smaller than the model size, data recovery operations using DRM procedures are much faster than standard methods. The number of columns in the acceleration DRM will correspond to the number of retained system modes. The number of columns of the displacement DRM will be equal to the sum of the retained elastic modes and the number of load application points.

3.6 EZTRAN Execution: The solution of the generalized equations of motion and the recovery of physical responses are accomplished by EZTRAN using the NASTRAN generated data. The information provided to EZTRAN is shown in Figure 2. The generalized mass and stiffness matrices and the generalized unit forces, $F_u = \phi^T I$, are supplied by NASTRAN through a model file. The scaled forcing functions are supplied through a forcing function file. Specific instructions for an EZTRAN run including load cases to be analyzed, time step information, number of modes to be included, modal damping parameters, and type of initial conditions are entered by the user in an input file. The NASTRAN generated DRMs are supplied through a matrix file. A dictionary file provides identification for the response items in the DRMs.

The modal equations of motion are uncoupled by virtue of linearity and proportional damping assumptions.

$$[M]\left\{\ddot{Q}\right\} + [C]\left\{\dot{Q}\right\} + [K]\left\{Q\right\} = \{F_u\}\{p(t)\} \tag{9}$$

They are solved using a simple recursive algorithm [Rf. 4]. The solution is exact within the limits that the applied forces are assumed to vary linearly between integration steps. The method is unconditionally stable, regardless of integration step size. However, the step size must be sufficiently small so that linear interpolation accurately follows the applied force time histories. Initial conditions are either zero (undeformed structure) or can be automatically computed by EZTRAN, assuming that the system is in steady-state equilibrium with initial non-zero forces. For example, the Orbiter and payloads are initially deflected by gravity, wind loads, and restraining forces at the launch pad attach bolts, and are in steady state equilibrium. The deflections of elastic modes and acceleration of rigid body modes are computed from the initial modal forces by EZTRAN for such cases.

The solution of modal differential equations yields the modal acceleration, $\ddot{Q}$. Physical responses are recovered using these solutions and the DRMs.

$$\left\{\begin{array}{c} \text{Physical} \\ \text{Accelerations} \end{array}\right\} = \begin{bmatrix} \text{Acceleration} \\ \text{DRM} \end{bmatrix} \left\{\ddot{Q}(t)\right\} \tag{10}$$

158

$$
\left\{ \begin{array}{c} \text{Physical Displacements and} \\ \text{Displacement dependent} \\ \text{Responses} \end{array} \right\} = \left[\begin{array}{c} \text{Displacement} \\ \text{DRM} \end{array} \right] \left\{ \begin{array}{c} p(t) \\ \ddot{Q}(t) \end{array} \right\} \tag{11}
$$

3.7 Post Processing: The results from EZTRAN include minimum/maximum summaries and time histories for the response items selected in the data recovery runs. The responses can be scaled by static and dynamic uncertainity factors to account for possible variations in the dynamic models or forcing functions. The results are written to formatted files that can be read by other postprocessing programs to provide extrema reports, response history plots, shock response spectra, relative displacements, and other output.

4. Example Problem: To illustrate the accuracy and efficiency of the alternate method, an example problem was analyzed. The problem consists of simple models of the Orbiter, Spacelab, Floor, Rack and a Box which were assembled into a solution system as shown in Figure 3. Modal reductions were performed at each stage of substructure assembly. The model was analyzed for a dynamic transient load case which had 45 load application points on the Orbiter substructure.

The analysis was performed using three different approaches. The first analysis used the direct transient solution feature of NASTRAN to solve a full, unreduced model of the system (3971 DOF). Although this approach is not practical for most real world problems, it provides an accurate baseline solution without any modal truncation errors. The second analysis used the modal reduced system model (205 DOF) with modes up to 35 Hz being retained in the final solution system. The transient analysis was performed in the modal domain, and the physical responses were recovered using NASTRAN's mode acceleration method. Finally, the transient analysis was performed on the same modal reduced system model using the alternate mode acceleration method. All three cases were undamped with zero initial conditions. The simulations were carried out for 0.5 seconds with an integration time step of 0.001 seconds.

A comparison of the cost and accuracy of the three methods clearly demonstrates the merits of the alternate method. The axial forces in a CBAR element of the BOX substructure are shown in Figure 4. The alternate method produces results which are much closer to the baseline solution than the NASTRAN mode acceleration solution. Similar results were obtained for other displacement dependent responses. In addition to being accurate, the alternate method was also more efficient than the other methods, as shown in Figure 5. The computational advantages of the alternate method become more pronounced as the length of simulation increases.

5. Conclusions: An accurate and efficient method for performing coupled transient loads analysis was presented and compared with the standard transient analysis capabilities of NASTRAN. The procedure uses data recovery matrices to reduce matrix size and computation times. The mode acceleration method is incorporated in the DRM formulations to recover accurate displacements and displacement-dependent quantities like element stresses, element forces and interface loads. The method is ideally suited for large, multi-level

substructured models.

6. References:

1. Chris C. Flanigan. Accurate and effiecient mode acceleration data recovery for superelement models. 1988 MSC/NASTRAN World Users Conference.

2. Chris C. Flanigan. Effiecient and accurate procedures for calcuting displacement data recovery matrices. 1989 MSC/NASTRAN World Users Conference.

3. Spacelab Life Sciences 2 (SLS-2) Design Coupled Loads Analysis Report. *JSC-25200* 1991
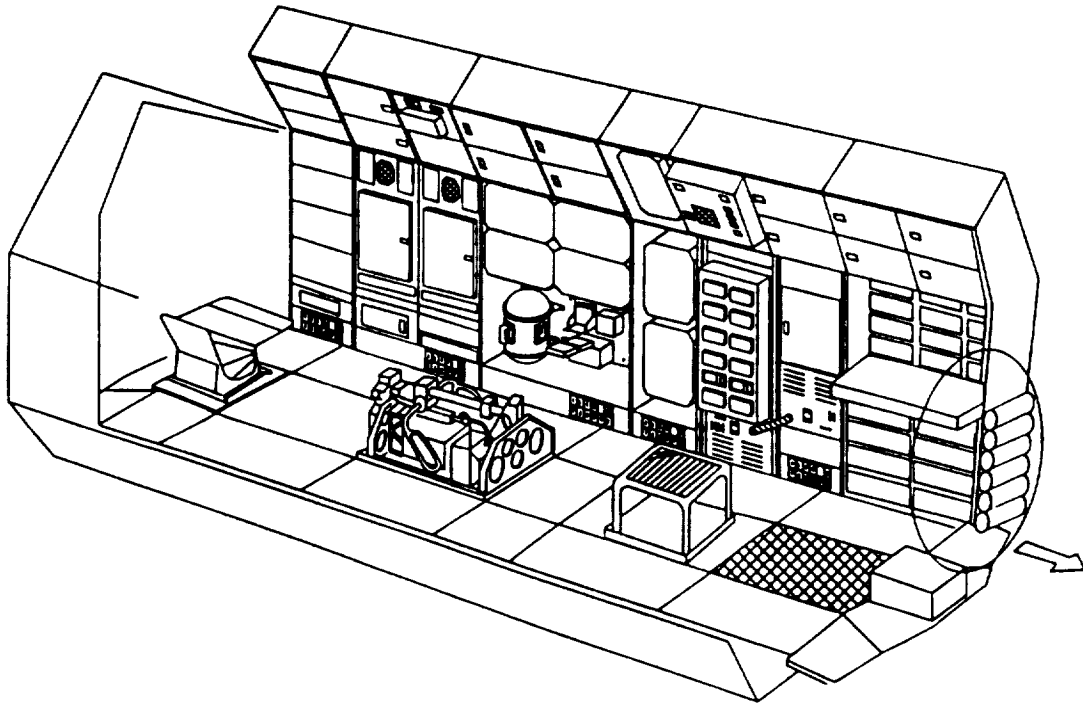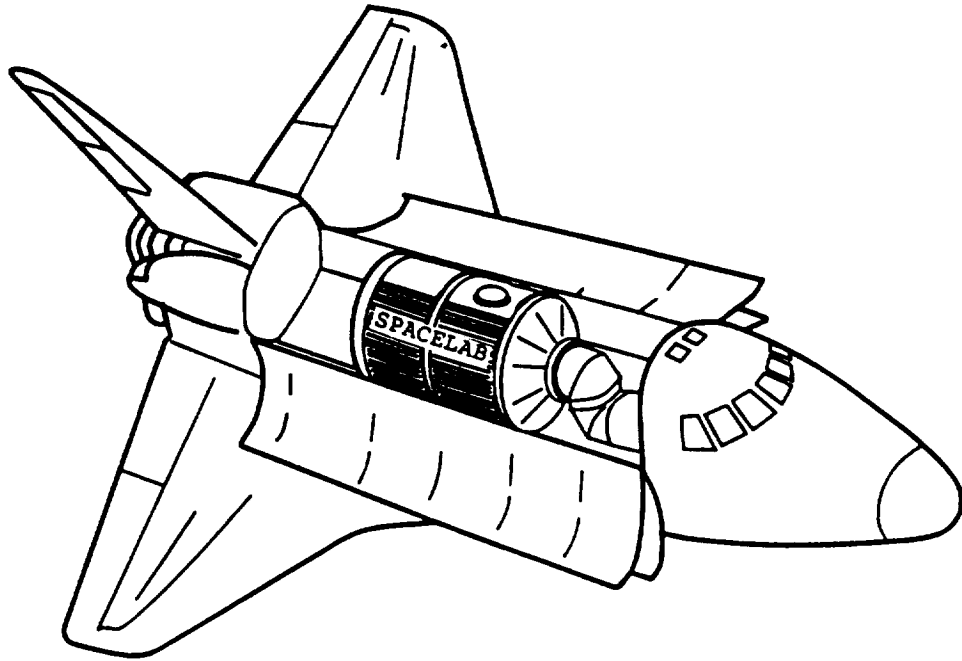
4. EZTRAN User's Manual. Structural Dynamics Research Corporation. 1991.

FIG. 1.   TYPICAL SPACELAB CONFIGURATION
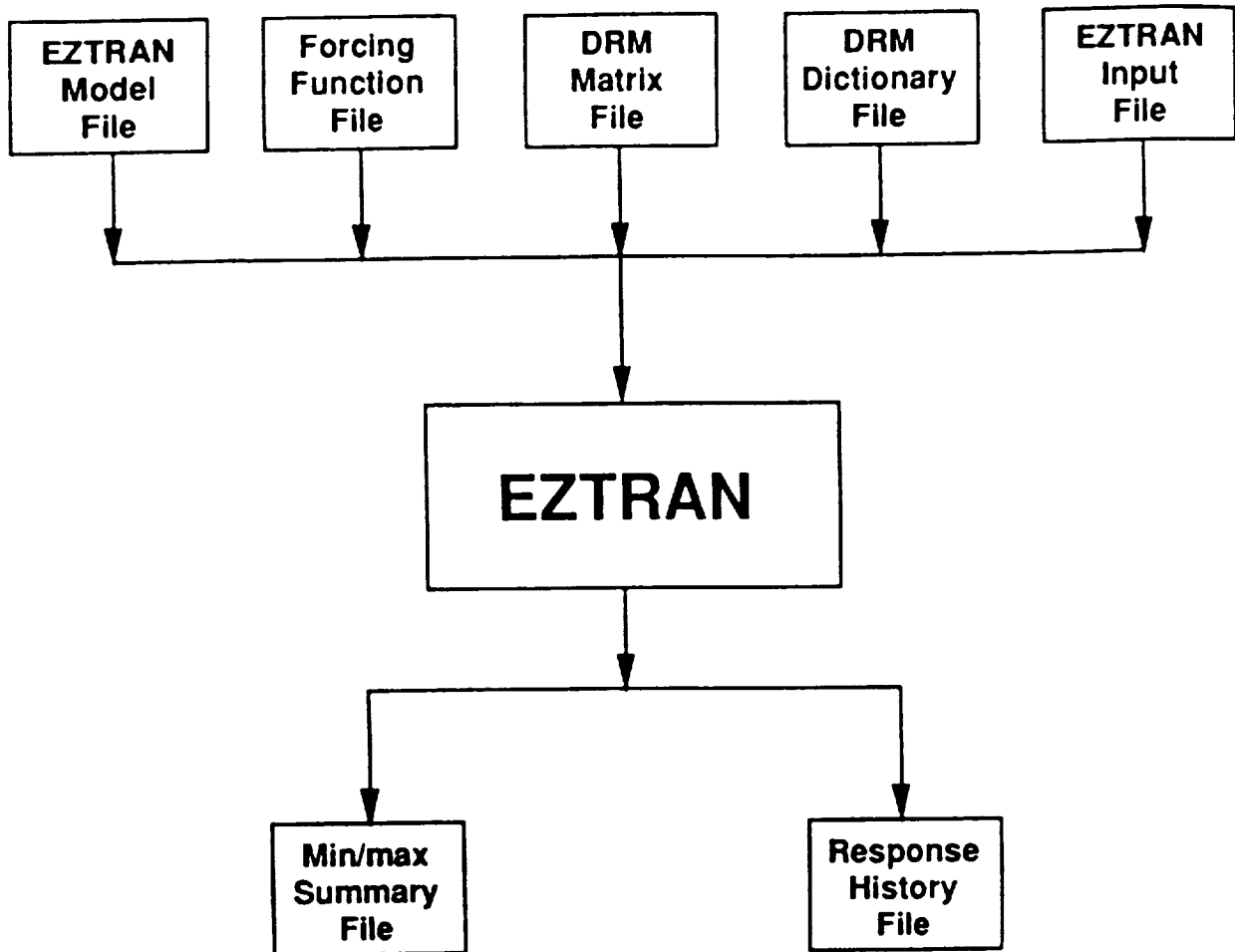
FIG. 2. EZTRAN INPUT AND OUTPUT FILES

162
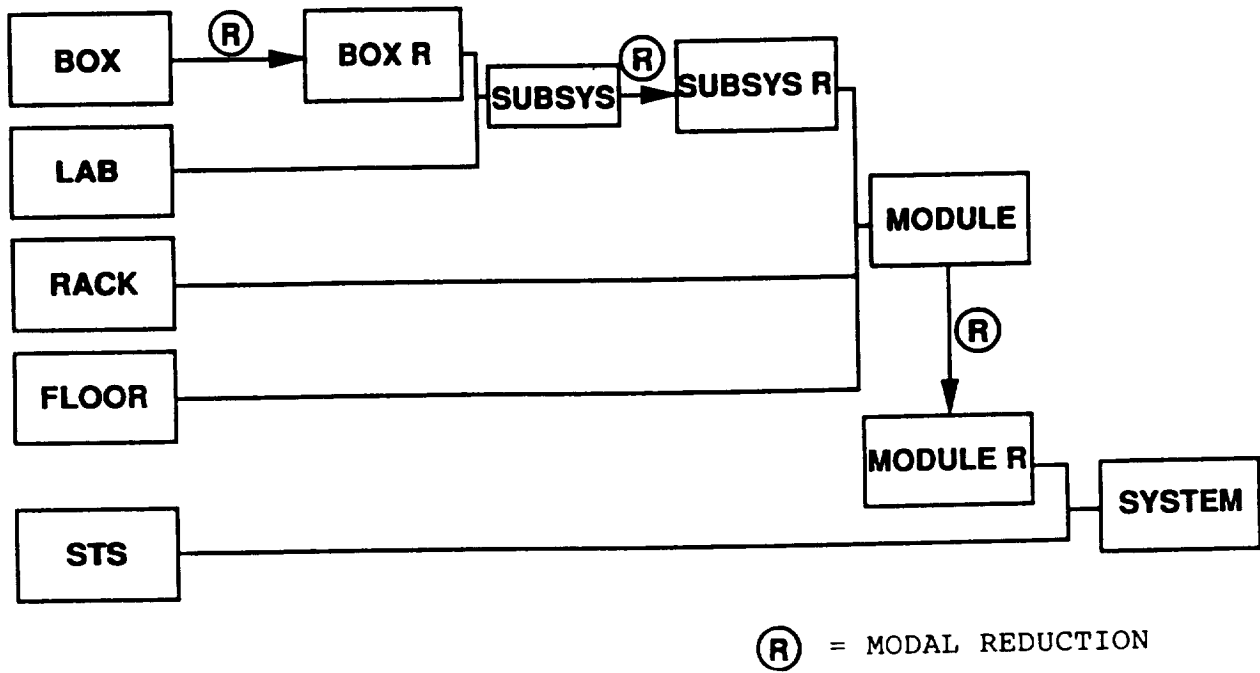
FIG. 3. THE SOLUTION SYSTEM ASSEMBLY SCHEME
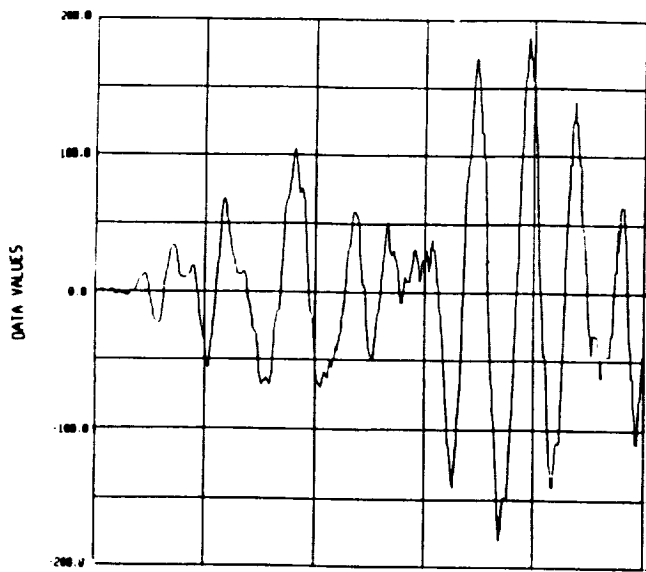
a) DIRECT METHOD
   FULL UNREDUCED MODEL
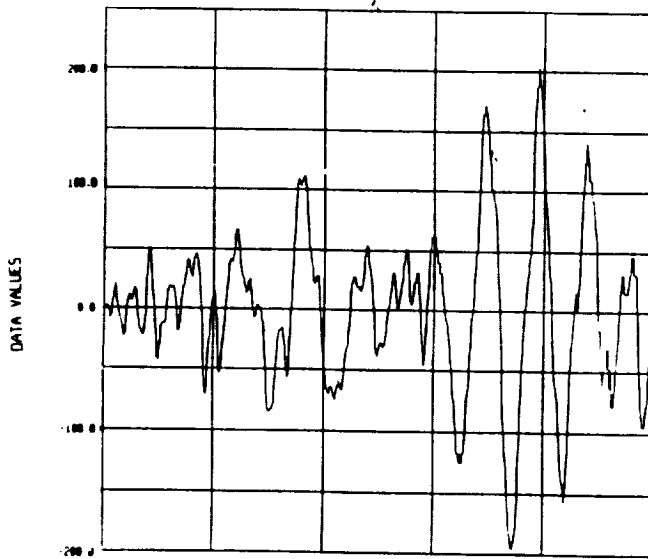
b) NASTRAN MODE
   ACCELERATION METHOD
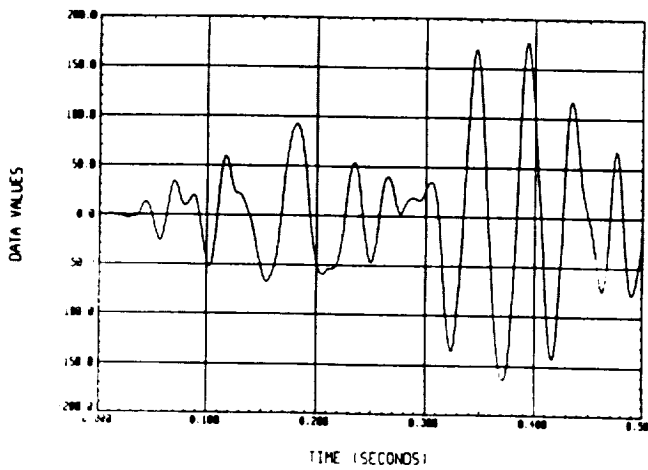
c) ALTERNATE MODE
   ACCELERATION METHOD

FIG. 4. AXIAL FORCE IN CBAR 2031, BOX SUBSTRUCTURE

164
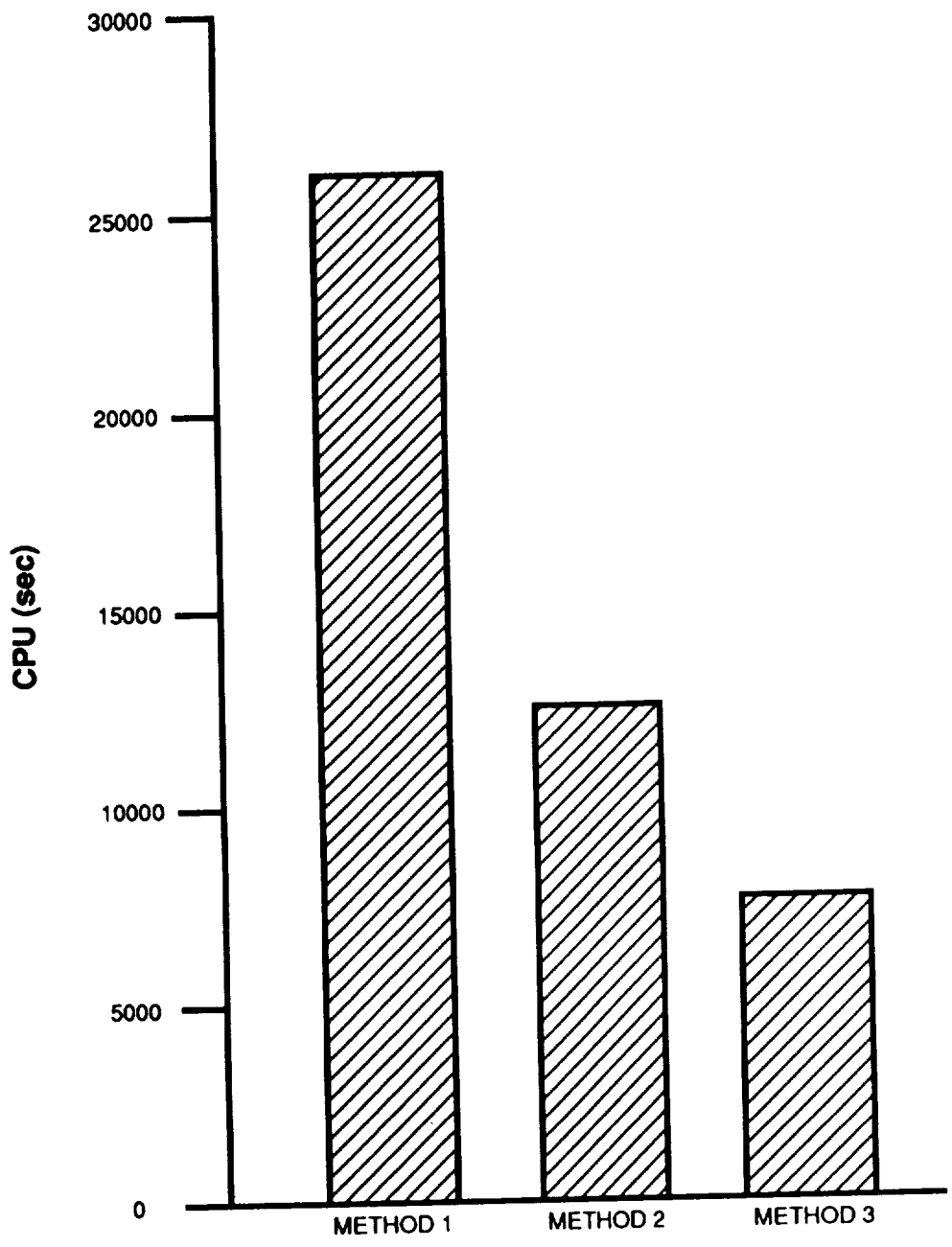
METHOD 1 - NASTRAN Direct Solution of Full Unreduced Model

METHOD 2 - NASTRAN Mode Acceleration Method

METHOD 3 - Alternate Method

FIG. 5. RELATIVE EFFICIENCY OF TRANSIENT ANALYSIS METHODS

165

ACOUSTIC INTENSITY CALCULATIONS FOR
AXISYMMETRICALLY MODELED FLUID REGIONS

by

Stephen A. Hambric and Gordon C. Everstine
Computational Mechanics Division (128)
David Taylor Research Center
Bethesda, MD 20084-5000

ABSTRACT

An algorithm for calculating acoustic intensities from a time–harmonic pressure field in an axisymmetric fluid region is presented. Acoustic pressures are computed in a mesh of NASTRAN triangular finite elements of revolution (TRIAAX) using an analogy between the scalar wave equation and elasticity equations. Acoustic intensities are then calculated from pressures and pressure derivatives taken over the mesh of TRIAAX elements. Intensities are displayed as vectors indicating the directions and magnitudes of energy flow at all mesh points in the acoustic field. A prolate spheroidal shell is modeled with axisymmetric shell elements (CONEAX) and submerged in a fluid region of TRIAAX elements. The model is analyzed to illustrate the acoustic intensity method and the usefulness of energy flow paths in the understanding of the response of fluid–structure interaction problems. The structural–acoustic analogy used is summarized for completeness. This study uncovered a NASTRAN limitation involving numerical precision issues in the CONEAX stiffness calculation causing large errors in the system matrices for nearly cylindrical cones.

INTRODUCTION

An acoustic intensity formulation for general, axisymmetric, fluid domains modeled with TRIAAX elements is presented. Numerical acoustic field solutions to fluid–structure interaction problems currently yield acoustic pressure fields, which may be used to locate high acoustic pressure concentrations. The motivation for calculating and displaying acoustic intensities is to help visualize the energy flow paths which cause high pressure regions. The energy flow fields can then help to identify dominant power paths which flow between structure and fluid, and therefore the important radiating parts of a structure.

The general problem of computing the interaction of an elastic structure with an acoustic fluid can be solved by combining a finite element model of the structure with a fluid loading computed using boundary element [1-11], finite element [12-23], combined finite element/analytical [24-26], T-matrix [27-29], and approximate fluid loading [30-32] techniques. In the fluid finite element approach, the exterior fluid domain is modeled with finite elements truncated at a finite distance from the structure and terminated with an approximate radiation boundary condition to absorb outgoing waves. The principal computational trade-off between this approach and the boundary element approach is that the finite element approach yields large, banded matrices, whereas the boundary element approach yields smaller, densely-populated matrices. This trade-off sometimes favors the finite element approach for long, slender structures like ships which are "naturally banded." In addition, only the fluid finite element approach has directly available an explicit fluid mesh which can be used for graphical display of the wave motion through the fluid. Since a significant part of our interest involves the display of wave propagation through both structure and fluid, we therefore formulate this problem using the fluid finite element approach. The principal drawbacks to fluid finite element modeling are the need for an approximate radiation boundary condition at the outer fluid boundary, the requirements on mesh size and extent (sometimes leading to frequency-dependent fluid meshes [20]), and the difficulty of generating the fluid mesh.

Direct frequency response NASTRAN [33] solutions for axisymmetric regions are described in general, and for domains that are defined using both structural and fluid subregions. Structural regions are modeled using standard structural finite elements (CONEAX, TRIAAX, TRAPAX); fluid regions are modeled with triangular elements of revolution (TRIAAX) using an analogy relating the Helmholtz equation to the elasticity equations used for the structural elements. The analogy is described in detail by Everstine [34] and is summarized for completeness here. The modeling of fluid–structure interaction between fluid and structure domains is also defined, as well as the application of acoustic boundary conditions to fluid models.

The acoustic intensity formulation includes the definition of the intensity quantity, the algorithm used to calculate fluid particle velocities using the pressure distribution in a general triangularized domain, and the calculation of the acoustic intensity vector quantity from pressures and velocities. The formulation has been implemented in the program AcINT (Acoustic INTensity), which functions as a post-processor to NASTRAN. An example, a submerged prolate-spheroidal shell with two sets of boundary conditions, is analyzed for a ring load. The resulting acoustic intensity fields are displayed for a given excitation frequency to illustrate the energy flow paths which result. The acoustic intensity vector plots show the utility of the method in identifying dominant power paths in fluid–structure interaction problems.

STRUCTURAL–ACOUSTIC ANALOGY

From an engineering point of view, it is convenient to be able to make use of existing general purpose finite element codes for analyzing structural-acoustic problems. Finite element codes are widely available, versatile, reliable, well supported, and an abundance of pre- and postprocessors may be used with them. Thus we summarize in this section an analogy [34] between the equations of elasticity and the wave equation of acoustics. This analogy allows the coupled structural acoustic problem to be solved with standard finite element codes like NASTRAN.

The pressure p in an acoustic field satisfies the wave equation

$$\nabla^2 p = \frac{\ddot{p}}{c^2},\tag{1}$$

where ∇^2 is the Laplacian operator, p is the dynamic fluid pressure, c is the wave speed, and dots denote partial differentiation with respect to time.

On the other hand, the x-component of the Navier equations of elasticity, which are the equations solved by structural analysis computer programs, is

$$\frac{\lambda + 2G}{G} u_{,xx} + u_{,yy} + u_{,zz} + \frac{\lambda + G}{G}(v_{,xy} + w_{,xz}) + \frac{1}{G}f_x = \frac{\varrho}{G}\ddot{u},\tag{2}$$

where u, v, and w are the Cartesian components of displacement, λ is a Lamé elastic constant, G is the shear modulus, f_x is the x-component of body force per unit volume (e.g., gravity), ϱ is the mass density, and commas denote partial differentiation.

A comparison of Eqs. 1 and 2 indicates that elastic finite elements can be used to model scalar pressure fields if we let u, the x-component of displacement, represent p, set v = w = 0 everywhere, $f_x = 0$, and $\lambda = -G$. For three-dimensional analysis, the engineering constants consistent with this last requirement are

$$E_e = 10^{20}G_e, \qquad \varrho_e = \frac{G_e}{c^2},\tag{3}$$

where the element shear modulus G_e can be selected arbitrarily. The subscript "e" has been added to these constants to emphasize that they are merely numbers assigned to the elements.

A variety of boundary conditions may also be imposed. At a pressure-release boundary, p = 0 is enforced explicitly like other displacement boundary conditions. For gradient conditions, the pressure gradient $\partial p/\partial n$ is enforced at a boundary point by applying a "force" to the unconstrained DOF at that point equal to $G_e A \partial p/\partial n$, where A is the area assigned to the point and n is the outward normal from the fluid region. For example, the plane wave absorbing boundary condition

$$\frac{\partial p}{\partial n} = -\frac{\dot{p}}{c}\tag{4}$$

167

is enforced by applying to each point on the outer fluid boundary a "force" given by $-(G_e A/c)\dot{p}$. Since this "force" is proportional to the first time derivative of the fundamental solution variable p, this boundary condition is imposed in the analogy by attaching to the fluid DOF a "dashpot" of constant $G_e A/c$. The Neumann condition $\partial p/\partial n = 0$ is the natural boundary condition under this analogy. The next higher order local radiation boundary condition, the curved wave absorbing boundary condition [23,36]

$$\frac{\partial p}{\partial n} = -\frac{\dot{p}}{c} - \frac{p}{r},$$ (5)

where r is the radius of the boundary, is enforced under the analogy by attaching in parallel both a "dashpot" and a "spring" between each boundary point and ground.

At a fluid-structure interface (an accelerating boundary), momentum and continuity considerations require that

$$\frac{\partial p}{\partial n} = -\varrho \ddot{u}_n,$$ (6)

where n is the normal at the interface, ϱ is the mass density of the fluid, and $\ddot{u}_n$ is the normal component of fluid particle acceleration. Under the analogy, this condition is enforced by applying to the fluid DOF at a fluid-structure interface a "force" given by $-(G_e \varrho A)\ddot{u}_n$.

To summarize, the wave equation, Eq. 1, can be solved with elastic finite elements if the three-dimensional region is modeled with 3-D solid finite elements having material properties given by Eq. 3, and only one of the three Cartesian components of displacement is retained to represent the scalar variable p. In Cartesian coordinates, any of the three components can be used. The solution of axisymmetric problems in cylindrical coordinates follows the same approach except that the z-component of displacement is the only one which can be used to represent p.

FINITE ELEMENT FORMULATION OF FLUID-STRUCTURE INTERACTION

There are two fundamental fluid-structure interaction problems of interest in structural acoustics: acoustic radiation, in which a submerged elastic body is subjected to a mechanical excitation applied to the structure, and scattering, in which the structure is subjected to an external incident pressure loading. For general time-dependent problems, the excitation is an arbitrary function of time, whereas in the time-harmonic case of interest here, the excitation has a single circular frequency ω.

Although our specific interest here is the time-harmonic case, we summarize the theory [22,35] for the more general case, which includes an incident loading as well. The radiation problem will be covered as a special case. For scattering, we assume, without loss of generality, that the incident wave propagates in the negative z direction. The speed of such propagation is c, the speed of sound in the fluid.

Within the fluid region, the total pressure p satisfies the wave equation, Eq. 1. Since the incident free-field pressure p_i is known, it is convenient to decompose the total pressure p into the sum of incident and scattered pressures

$$p = p_i + p_s,$$ (7)

each of which satisfies the wave equation.

We now formulate the problem for finite element solution. Consider an arbitrary, submerged, three-dimensional elastic structure subjected to either internal time-dependent loads or an external time-dependent incident pressure. If the structure is modeled with finite elements, the resulting matrix equation of motion for the structural degrees of freedom (DOF) is

$$M\ddot{u} + B\dot{u} + Ku = F - GAp,$$ (8)

where M, B, and K are the structural mass, viscous damping, and stiffness matrices (dimension s x s), respectively, u is the displacement vector for all structural DOF (wet and dry) in terms of the coordinate systems selected by the user (s x r), F is the vector of applied mechanical forces applied to the structure (s x r), G is the rectangular transformation matrix of direction cosines to transform a vector of outward normal forces at the wet points to a

168

vector of forces at all points in the coordinate systems selected by the user (s x f), A is the diagonal area matrix for the wet surface (f x f), p is the vector of total fluid pressures (incident + scattered) applied at the wet grid points (f x r), and dots denote differentiation with respect to time. The pressure p is assumed positive in compression. In the above dimensions, s denotes the total number of independent structural DOF (wet and dry), f denotes the number of fluid DOF (the number of wet points), and r denotes the number of load cases. If first order finite elements are used for the surface discretization, surface areas, normals, and the transformation matrix G can be obtained from the calculation of the load vector resulting from an outwardly directed static unit pressure load on the structure's wet surface. The matrix product GA can then be interpreted as the matrix which converts a vector of negative fluid pressures to structural loads in the global coordinate system. The last two equations can be combined to yield

$$Mü + Bü + Ku + GAp_s = F - GAp_i. \tag{9}$$

A finite element model of the fluid region (with scattered pressure p_s as the unknown) results in a matrix equation of the form

$$Qp̈_s + Cṗ_s + Hp_s = F^{(p)}, \tag{10}$$

where p_s is the vector of scattered fluid pressures at the grid points of the fluid region, Q and H are the fluid "inertia" and "stiffness" matrices (analogous to M and K for structures), C is the "damping" matrix arising from the radiation boundary condition (Eq. 4), and $F^{(p)}$ is the "loading" applied to fluid DOF due to the fluid-structure interface condition, Eq. 6. Using the analogy described in the preceding section, elastic finite elements can be used to model both structural and fluid regions. Material constants assigned to the elastic elements used to model the fluid are specified according to Eq. 3. In three dimensions, elastic solid elements are used (e.g., isoparametric bricks (IHEXi) for general 3-D analysis or solids of revolution (TRIAAX, TRAPAX) for axisymmetric analysis).

At the fluid-structure interface, Eqs. 6 and 7 can be combined to yield

$$\frac{\partial p_s}{\partial n} = \varrho(ü_{ni} - ü_n), \tag{11}$$

where n is the outward unit normal, and $ü_{ni}$ and $ü_n$ are, respectively, the incident and total outward normal components of fluid particle acceleration at the interface. Thus, from the analogy, we impose the fluid-structure interface condition by applying a "load" to each interface fluid point given by

$$F^{(p)} = -\varrho G_e A(ü_{ni} - ü_n), \tag{12}$$

where the first minus sign is introduced since, in the coupled problem, we choose n as the outward normal from the structure into the fluid, making n an inward normal for the fluid region. The normal displacements u_n are related to the total displacements u by the same rectangular transformation matrix G used above:

$$u_n = G^T u, \tag{13}$$

where the superscript T denotes the matrix transpose. Eqs. 10, 12, and 13 can be combined to yield

$$Qp̈_s + Cṗ_s + Hp_s - \varrho G_e(GA)^T ü = -\varrho G_e Aü_{ni}. \tag{14}$$

Since the fluid-structure coupling terms in Eqs. 9 and 14 are nonsymmetric, we symmetrize the problem [21] by using a new fluid unknown q such that

$$q = \int_0^t p_s dt, \qquad q̇ = p_s. \tag{15}$$

If Eq. 14 is integrated in time, and the fluid element "shear modulus" G_e is chosen as

$$G_e = \frac{-1}{\varrho}, \tag{16}$$

the overall matrix system describing the coupled problem can be written as

$$\begin{bmatrix} M & 0 \\ 0 & Q \end{bmatrix} \begin{Bmatrix} u \\ q \end{Bmatrix} + \begin{bmatrix} B & (GA) \\ (GA)^T & C \end{bmatrix} \begin{Bmatrix} u \\ q \end{Bmatrix} + \begin{bmatrix} K & 0 \\ 0 & H \end{bmatrix} \begin{Bmatrix} u \\ q \end{Bmatrix} = \begin{Bmatrix} F - (GA)p_i \\ Av_{ni} \end{Bmatrix}, \tag{17}$$

where v_{ni} ($= u_{ni}$) is the outward normal component of incident fluid particle velocity.

The new variable q is, except for a multiplicative constant, the velocity potential ϕ, since

$$p = -\varrho\phi. \tag{18}$$

Eq. 17 could also be recast in terms of ϕ rather than q as the fundamental fluid unknown, but no particular advantage would result. In fact, the use of q rather than ϕ has the practical advantage that the fluid pressure can be recovered directly from the finite element program as the time derivative (velocity) of the unknown q.

To summarize, both structural and fluid regions are modeled with finite elements. For the fluid region, the material constants assigned to the finite elements are

$$E_e = \frac{-10^{20}}{\varrho}, \quad G_e = \frac{-1}{\varrho}, \quad v_e = \text{unspecified}, \quad \varrho_e = \frac{-1}{\varrho c^2}, \tag{19}$$

where E_e, G_e, v_e, and ϱ_e are the Young's modulus, shear modulus, Poisson's ratio, and mass density, respectively, assigned to the fluid finite elements. The properties ϱ and c above are the actual density and sound speed for the fluid medium. The radiation boundary condition used is the plane wave approximation, Eq. 4, which appears to be adequate if the outer fluid boundary is sufficiently far from the structure [20]. With this boundary condition, matrix C in Eq. 17 arises from dashpots applied at the outer fluid boundary with damping constant $-A/(\varrho c)$ at each grid point to which the area A has been assigned. At the fluid-structure interface, matrix GA is entered using the areas (or areal direction cosines) assigned to each wet degree of freedom. (Recall that GA can be interpreted as the matrix which converts a vector of negative fluid pressures to structural loads in the global coordinate system.)

For radiation problems, the right-hand side of Eq. 17 can be simplified further since the incident pressure p_i is zero, and we obtain

$$\begin{bmatrix} M & 0 \\ 0 & Q \end{bmatrix} \begin{Bmatrix} u \\ q \end{Bmatrix} + \begin{bmatrix} B & (GA) \\ (GA)^T & C \end{bmatrix} \begin{Bmatrix} u \\ q \end{Bmatrix} + \begin{bmatrix} K & 0 \\ 0 & H \end{bmatrix} \begin{Bmatrix} u \\ q \end{Bmatrix} = \begin{Bmatrix} F \\ 0 \end{Bmatrix}. \tag{20}$$

We note that the structural and fluid unknowns are not sequenced as perhaps implied by the partitioned form of Eq. 20. The coupling matrix GA is quite sparse and has nonzeros only for matrix rows associated with the structural DOF at the fluid-structure interface and columns associated with the coincident fluid points. Thus, the grid points should be sequenced for minimum matrix bandwidth or profile as if the structural and fluid meshes comprised a single large mesh. As a result, the structural and fluid grid points will, in general, be interspersed in their numbering, and the system matrices will be sparse and banded.

ACOUSTIC INTENSITY CALCULATIONS

The procedure for solving for the acoustic intensity field in an axisymmetric fluid finite element model using NASTRAN [33] and the acoustic intensity post-processor AcINT is:

* run NASTRAN on a dynamically loaded finite element model of structural elements and fluid elements using direct frequency response analysis, and generate resultant nodal pressures for the fluid region(s);

* run AcINT using the output from NASTRAN to calculate nodal fluid velocities and acoustic intensities.

The nodal pressures, actually the cosine coefficients of nodal pressures, are computed by NASTRAN in response to the AXISYMMETRIC = COSINE command in the case control part of the input data. Since only cosine coefficients are requested, the 2, 4, and 6 DOF are removed by NASTRAN for harmonic zero. The 1 and 5 DOF must be constrained by the user, leaving the 3 DOF to represent the scalar fluid velocity potential.

170

The velocity potential integrated over time is the fluid pressure. Therefore, in the analogy, nodal pressures are obtained by the case control command VELOCITY = ALL (or SETID). The resultant fluid nodal pressures are used as illustrated below to compute acoustic velocities and intensities.

Acoustic Intensity

Intensity is defined as the time averaged product of a pressure with the in-phase component of particle velocity. For time-harmonic analysis, where complex numbers are used, this calculation may be visualized as taking the dot product of the pressure and velocity phasors. Multiplying one complex number by the in-phase part of another complex number is the same operation as multiplying the first number by the complex conjugate of the other number and taking the real part of the result:

$$\vec{I} = \Re [p\vec{v}^*], \tag{21}$$

where p is pressure, and $\vec{v}^*$ is the complex conjugate of velocity. (Often, a factor of 1/2 appears in intensity equations. However there is no factor 1/2 in the equations if the assumption is made that pressures and velocities are "effective" rms values rather than amplitudes. With this assumption, consistency is maintained, and there is no mixing of effective and peak quantities in this formulation.)

Acoustic Velocities

The derivation of acoustic velocities for axisymmetric problems is performed for the cosine coefficients of the Fourier summation about the axis of rotational symmetry (z), where the r, z, and rotation about θ DOF are active. Only the r and z variations of the scalar pressure field are used to calculate the acoustic velocity vector field. The particle velocity in a fluid domain is defined as:

$$\vec{v} = \frac{i}{\omega\varrho}\nabla p = \frac{i}{\omega\varrho}(\frac{\partial p}{\partial r}\hat{i} + \frac{\partial p}{\partial z}\hat{k}) , \tag{22}$$

where ϱ is the fluid density, ω is the circular frequency, i is the square root of -1, $\frac{\partial p}{\partial r}$ and $\frac{\partial p}{\partial z}$ are the pressure derivatives in the r and z directions, and $\hat{i}$ and $\hat{k}$ are unit vectors in the r and z directions, respectively. A first order finite difference approximation of the pressure derivatives at the nodes in an individual TRIAAX element can be made as shown in Figure 1. The pressure differences between nodes are divided by the distances between nodes to approximate the first derivative of pressure in the direction of the two nodes. The approximate pressure
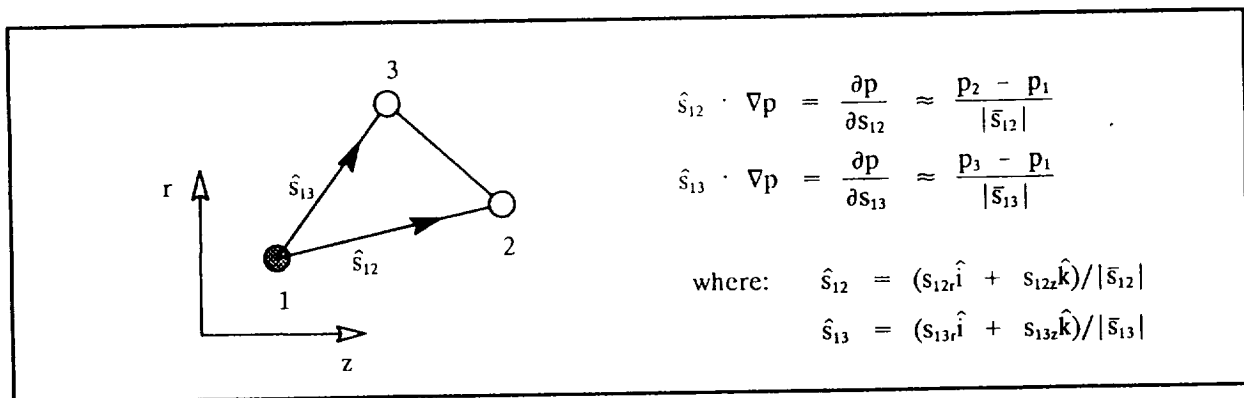

Figure 1. Pressure Gradient Approximation.

gradient equations are written for all nodes connected to the node for which the velocity vector is to be calculated. In the case above, all elements connected to node 1 must be found, and equations are written for each node connected to node 1. No duplicate equations are written when two elements share a common edge. An overdetermined system of equations for the pressure derivatives in the r and z directions is the result, with one

171

equation for each node connected to the primary node. The system of equations is

$$
\begin{bmatrix}
s_{1r} & s_{1z} \\
s_{2r} & s_{2z} \\
\cdot & \cdot \\
\cdot & \cdot \\
\cdot & \cdot \\
s_{Nr} & s_{Nz}
\end{bmatrix}
\begin{Bmatrix}
\dfrac{\partial p}{\partial r} \\
\dfrac{\partial p}{\partial z}
\end{Bmatrix}
=
\begin{Bmatrix}
\dfrac{\partial p}{\partial s_1} \\
\dfrac{\partial p}{\partial s_2} \\
\cdot \\
\cdot \\
\cdot \\
\dfrac{\partial p}{\partial s_N}
\end{Bmatrix}
\tag{23}
$$

where s_{ir} and s_{iz} are the r and z components of the unit vector from the primary node to the connecting node i, and N is the number of connecting nodes.

The derivatives are determined approximately using a least squares approach. The particle velocity vector is then solved for using Equation 22, and the acoustic intensity vector is given by Equation 21. The axisymmetric acoustic intensity field for a complete domain is found by repeating this procedure for each node in the domain. In this way, a complete energy flow solution can be derived from nodal pressures and element connectivities.

EXAMPLES

The axisymmetric model of a submerged, half prolate spheroidal shell is shown in Figure 2. The structure has a semi axes of 10 m and 5 m. The material is steel with a uniform thickness of 25 mm, a Young's modulus (E) of 2.074 E11 N/m^2, a density (ρ) of 7860 kg/m^3, a Poisson's ratio (ν) of 0.3, and a material loss factor of 0.0. The frequency range of interest was 100 to 500 Hz. The problem was analyzed for harmonic zero, commonly referred to as the "breathing mode" of the domain, implying no variation in the solution field about the z axis.
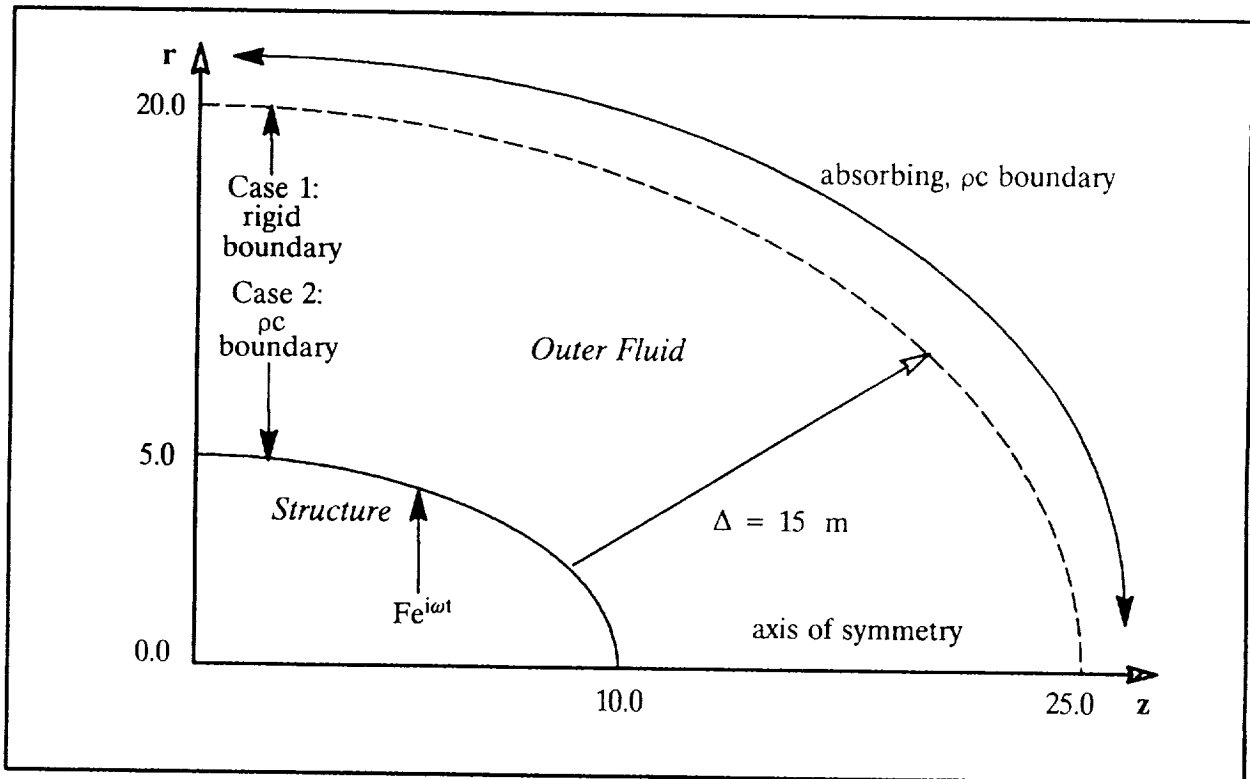

Figure 2. Axisymmetric Model of a Submerged, Half Prolate-spheroid.

172

As shown in the diagram, the structure is submerged in fluid, which was also modeled and interfaced with the structure. The fluid is seawater, with a density (ρ) of 1025 kg/m³ and a speed of sound (c) of 1500 m/s. Two sets of boundary conditions along the left, vertical fluid edge were applied, and are discussed in more detail below.

A finite element (CONEAX) model of the problem is shown in Figure 3. The structure was modeled using axisymmetric conical shell elements. The plate thickness, steel material properties, and the frequency range determine an estimated average flexural wavelength [38] of 0.7 m at 500 Hz, which for a mesh requirement of about eight elements/wavelength translates to a structural mesh density of 0.087 m/element length.

The outer fluid was modeled using TRIAAX elements. The seawater properties and frequency range determine an upper wavelength of 15.0 m and a lower wavelength of 3.0 m. The upper wavelength determines the location of the outer boundary of the fluid mesh, shown as Δ in Figure 2, as one wavelength from the structure, or 15.0 m. The lower wavelength determines the fluid mesh density, which for a minimum of 8 elements/wavelength, specifies a fluid mesh size of 0.375 m/element length. The fluid and structural meshes are distinct at the fluid-structure boundary, but with coincident nodes. These coincident nodes are coupled by area matrices which map fluid pressures to structural forces, as described earlier. Only one fluid DOF was assigned to each mesh point.

The area matrices are input with DMIG cards, which apply area values to the damping, or B2PP matrix. A current limitation of NASTRAN is the program performing nonsymmetric system matrix decompositions when MPC data is used with DMIG input. Despite the DMIG input being declared symmetric, when the MPC equations are used to obtain the BDD matrix, NASTRAN changes the matrix trailer to nonsymmetric. All matrix operations become nonsymmetric as a result, greatly increasing computer time. A sequence of ALTER statements may be used to restore the trailer to its symmetric form. One such sequence (for the 1990 version of NASTRAN, Rigid Format 8) is shown below for BDD.

```
ALTER 119$                              Make BDD trailer symmetric
DIAGONAL BDD/AVEC/*COLUMN*/0.$          Vector of ones
ADD AVEC,/PVEC/(0.0,0.0)$               Vector of zeros (P-Vec)
MERGE BDD,,,,PVEC,/BDDSYM/-1//6$        Dummy merge
EQUIV BDDSYM,BDD$                       BDD now symmetric
```

This alter is inserted before the FRRD module. With the BDD symmetry flag restored, subsequent matrix operations will take advantage of the symmetry of the system, reducing the required computer time. This NASTRAN bug has been fixed by Gordon Chan of Unisys for the 1992 program release.

Since the structural elements are about one-quarter the size of the desired fluid elements, some mesh transitioning in the fluid meshes was required from the mesh density of the structure (0.087 m/element length) to the mesh density of the fluid (0.375 m/element length). The fluid element material properties were assigned according to Eq. 19.

Boundary and Loading Conditions

Two sets of boundary conditions were applied in the problem. In both cases, a ρc impedance, or plane wave absorbing boundary condition was applied to the curved outer fluid boundary; and a point forcing function was applied at z = 6.0 in the positive r direction along the structure, as shown in Figure 2. The structure was constrained in all degrees of freedom at the upper left end. The left vertical fluid boundary was modeled in two ways: (1) as a rigid wall, which reflects incident waves, and (2) as a ρc impedance absorber. DMIG statements inputting $- A/\rho c$ values for all boundary points simulated the ρc plane wave absorber.

Results

The problem may be accurately solved for any set of frequencies from 100 to 500 Hz. Detailed results are presented here for the 100 Hz case for Cases 1 and 2. The numerical output is examined several ways: power input and power radiation calculations, structural displacements, acoustic pressure contour plots, and acoustic intensity vector plots. This set of output provides a nearly complete solution to the structural-acoustic problem.
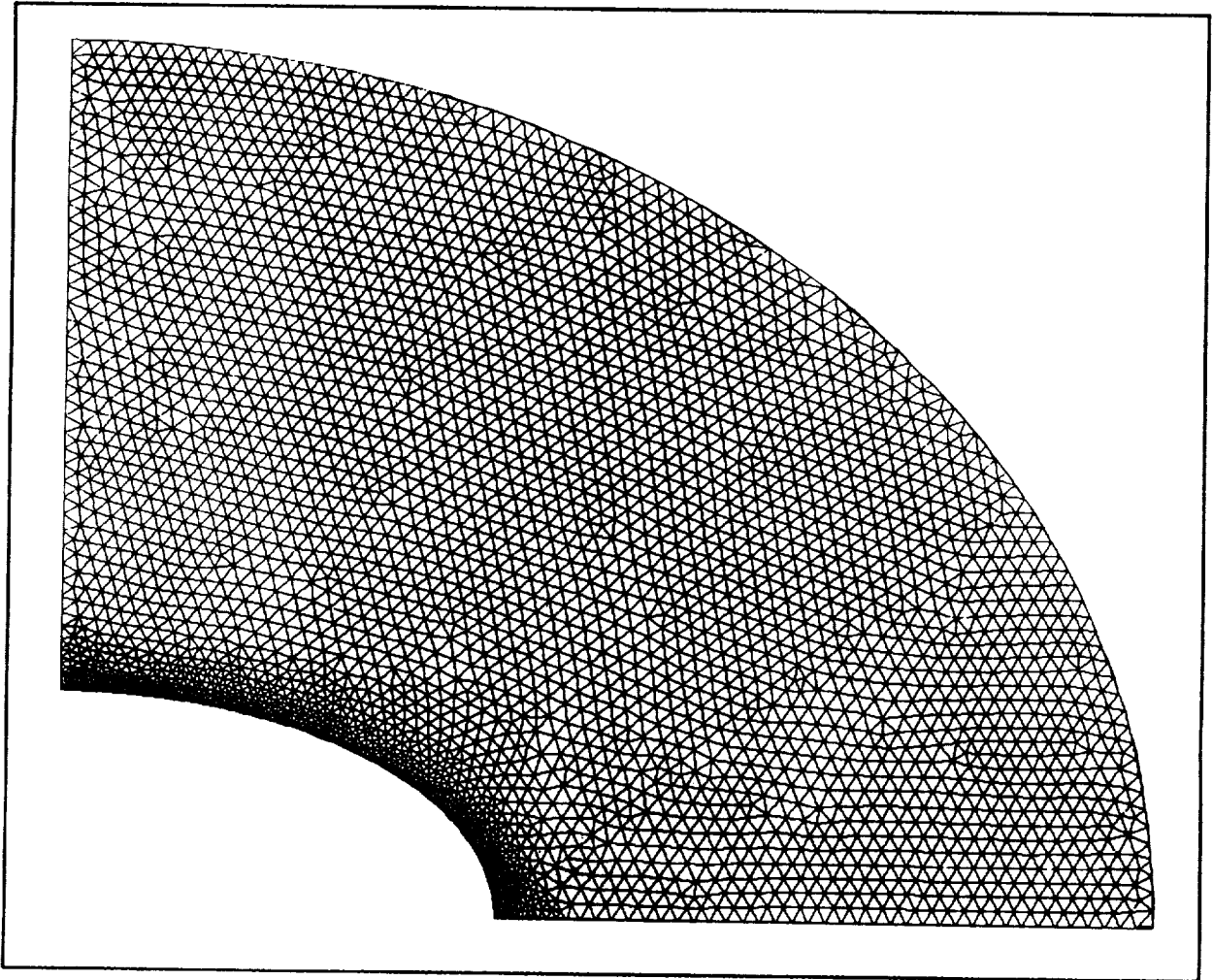
Figure 3. Finite Element Mesh.

Since both materials are lossless, all power entering the structure must eventually be radiated into the fluid. This means the power input by the forcing function must equal the power exiting the system through the plane-wave absorbing outer boundaries. Power input is defined as

$$P_{in} = F_{in} v_{in}^*,$$ (24)

where F_{in} is the radial complex input force (in this case unity), and v_{in}^* is the complex conjugate of the corresponding velocity at the force point. The power radiated through the absorbing boundary may be found by integrating the calculated acoustic intensity field normal to the boundary:

$$P_{rad} = \int_c \vec{I} \cdot \hat{n} \ dA,$$ (25)

where C denotes the boundary contour, $\hat{n}$ is the outward normal vector, and dA is the incremental area. This integration may be converted to a summation over all nodes on the boundary, where

$$P_{rad} = \sum_{i=1}^{n} \vec{I}_i \cdot \hat{n}_i \ A_i.$$ (26)

In this case, $\hat{n}_i$ and A_i are calculated for each node on the boundary, and used with the intensity vector at each node to calculate the power leaving the system. The summation over all boundary nodes gives the total radiated power.

Radiated power is commonly represented by a spherical pressure field with a reference radius of one yard. If the outer boundary is in the far-field, the pressure at one yard is

$$P_{1yard}(dB) = 20\log\sqrt{\frac{\rho c P_{rad}}{2\pi r^2}} + 120, \tag{27}$$

where 120 dB is added to calculate the pressure relative to 1 μPa.

Table1 lists the power quantities defined above, and the relative error calculated by subtracting the radiated power from the input power and normalizing to the input power. The error, about 2% for each case, is probably due to the curved outer boundary. The approximate boundary condition was of a plane-wave absorbing boundary. Since neither the boundary nor the radiated waves is perfectly plane, small reflections at the boundary can occur, causing the power balance to be slightly in error. The radiated power, and therefore the pressure at 1 yard, is higher for Case 2, and the error is either due to the additional left ρc boundary's absorbing more power, or the boundary's causing a small shift in the frequency response of the system. A full frequency sweep would be required to determine the effects of the left absorbing boundary.

Case	Power Input (W)	Power Radiated (W)	%Error	Pressure@1 yard (dB re: 1 μPa)
1	1.499E–8	1.519E–8	–1.33	91.9
2	8.988E–8	8.798E–8	2.11	99.5

Table1. Power Results for 100 Hz.

A plot of the displaced shapes of the structure for both cases is shown in Figure 4. The displacement field of the structure is complex, and a time dependent animation of the structural response is required to visualize fully the movement. The plots shown here are at a single phase angle in the displacement cycle (292.5°), and show that the change in boundary condition does not significantly alter the structural response. A small phase shift has occurred, but the general shape is the same for both cases. The ring loading causes the discontinuity in the waveform at z = 6.0. This point is the source of the waves travelling to the left and right from the load.

Acoustic intensity vector plots are superimposed on acoustic pressure contour plots in Figures 5–8. Figure 5 shows the entire field for Case 1, and Figure 6 is a close-up of the field near the structure. Figure 7 is a plot representing Case 2, and Figure 8 is a closer view. A common pressure scale is used for all plots, with the letters on the contours corresponding to the pressure levels (dB re: 1 μPa). The vector lengths are proportional to the log of the intensity magnitudes. The log of intensity is used in the plots to overcome the 1/r decay in intensity magnitude with distance. Since this is an axisymmetric analysis at circumferential harmonic zero, the acoustic fields are constant for all angles about the z axis, and no net energy may pass through the lower z boundary. All intensity vectors along the lower boundary therefore have zero radial components.

The plots for Case 1 (Figure 5 and Figure 6) show the highest levels of far-field pressures to be in the r and z directions, with values between contours I and J, or 70 to 75 dB. Near-field pressure peaks are indicated near the structure by D contours, or about 100 dB levels. Examining the far-field intensity vectors show a far-field condition (all acoustic energy directed outward) at the outer boundary, with the dominant energy flow paths in the r and z directions. The rigid boundary condition along the left wall is evidenced by the absence of any outward z directed intensity component along it. The near-field intensity vectors shows an energy path that begins at the load point (z = 6.0) and branches to the right and left. At the right, or bottom of the structure, energy flows along the fluid-structure boundary before travelling away toward the far-field at the r = 0 boundary. To the left of the load point, energy re-enters and re-exits the structure twice before radiating outward at the z = 0 boundary. The circulation of power to the left of the load point causes "false sources" to appear where the energy re-exits the structure. Examination of the entire intensity field identifies the load point as the original source of power though.

For Case 2, the use of the ρc boundary (Figure 7 and Figure 8) and at the left edge of the fluid causes the acoustic pressures in the r direction, or upper left of the fluid domain, to decrease significantly from the rigid boundary case, from 75 to 55 dB. The acoustic intensity field shows the reason for the decrease in pressure; the

vectors along the ρc boundary now have a z-directed component, implying power exiting the system through the boundary. The overall radiated power is higher for Case 2, though, due to an increase in the radiated energy along the midsection of the outer boundary. The near-field intensity plot reveals that the circulating power flows between structure and fluid to the left of the load point have disappeared. The energy now flows along the fluid-structure boundary and radiates outward at the top of the structure. To the right of the load however, power now circulates. The dominant path is from the load point to the right; into and out of the structure; then along the structure until r = 0, where some power reenters the structure, and the rest radiates outward along the z axis.

NASTRAN DIFFICULTIES ENCOUNTERED

Two important limitations of NASTRAN became apparant during this study: the BDD damping matrix's being specified as unsymmetric regardless of the symmetric nature of fluid structure interaction and absorbing boundary data input by DMIG cards; and the formulation of stiffness coefficients for CONEAX elements. The BDD matrix trailer may be restored to symmetric using the ALTER statements outlined in the Example section. The difficulties with the CONEAX formulation are not easily fixed however.

Stiffnesses for CONEAX elements are computed analytically by NASTRAN, and involve the inverse of $\Delta r/\Delta l$, where Δr is the difference in radii and Δl is the total distance between the grids defining an element. For perfectly cylindrical shell elements with no variation in radii ($\Delta r/\Delta l = 0$), a different formulation is used to avoid a floating point error caused by a division by zero. However, no provision is made for small relative variation in radii ($\Delta r/\Delta l \approx 0$), and for a small range of elements the analytical computation is corrupted when computer precision limits are reached. Sometimes the error is so drastic that negative values are obtained for self term (diagonal) stiffnesses. The negative stiffnesses are reported to the user when NASTRAN checks the system matrices for singularities. However, sometimes the error may be drastic in the positive sense, i.e., stiffnesses orders of magnitude too large. No error would be reported to the user, and the final solution would be incorrect.

CONEAX stiffness errors were encountered for the example described here at the upper left end of the structure, where the elements become nearly cylindrical. In this case, the stiffnesses of several of the near cylindrical elements were output and analyzed for accuracy. The two end elements were found to have large errors in stiffness. To solve the problem, the radii of the element grid points were set equal, and the end of the structure was approximated as purely cylindrical.

A possible programming solution to the sensitivity of CONEAX stiffnesses to small relative differences in radii is to approximate nearly cylindrical regions as cylindrical. For example, if for a given element $\Delta r/\Delta l$ is below some specified tolerance ϵ, the second grid radius is set equal to the first grid radius. The resulting model would be a stepwise approximation of the nearly cylindrical region. The chief problem is how to choose ϵ. Studies would have to be performed on ranges of nearly cylindrical elements using different levels of computer precision to determine the accuracy limits on the analytical stiffness computation method.

CONCLUSIONS

The combination of structural displacement plots, pressure contours, and acoustic intensity vector fields all serve to reveal the complete state of a structural-acoustic problem. However, one component of the response is missing: the energy flow within the structure. The circulating energy along the structural-acoustic boundary indicated by the intensity plots show power flowing through the structure. A formulation similar to that for acoustic intensity can be performed for the structure; however more than one wave type must be considered. For the axisymmetric shells of revolution (CONEAX) used here, for example, both flexural (composed of both shear and moment waves) and longitudinal waveforms may transport energy through structures. Methods have been developed for general three-dimensional structural models of beams (BAR) and plates (QUAD4) [39], but have not yet been extended to axisymmetric problems. This additional analysis tool will help improve considerably the understanding of structural-acoustic, frequency response problems.
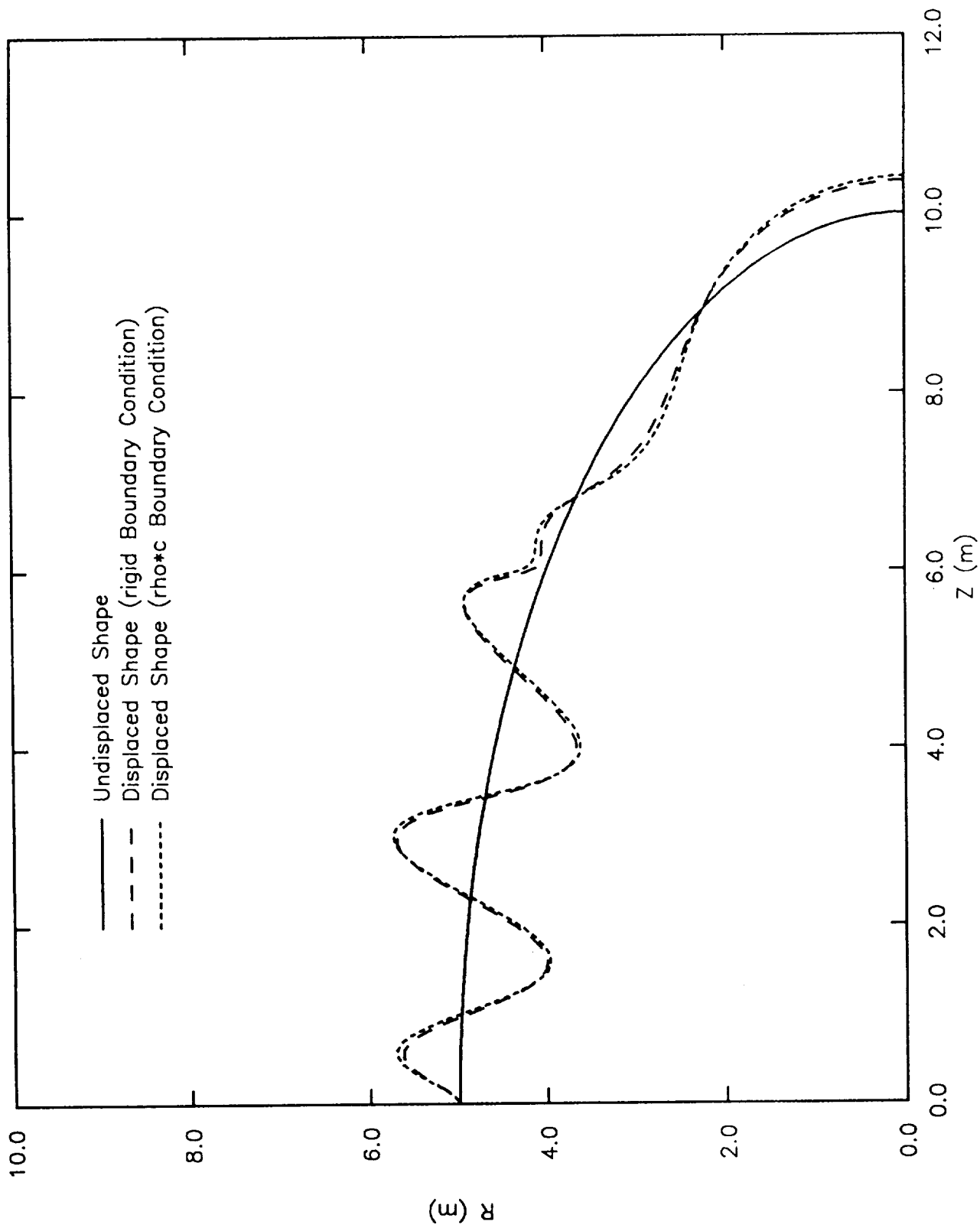
176

Figure 4. Structural Displacements for both Boundary Condition Cases (phase = 292.5°).

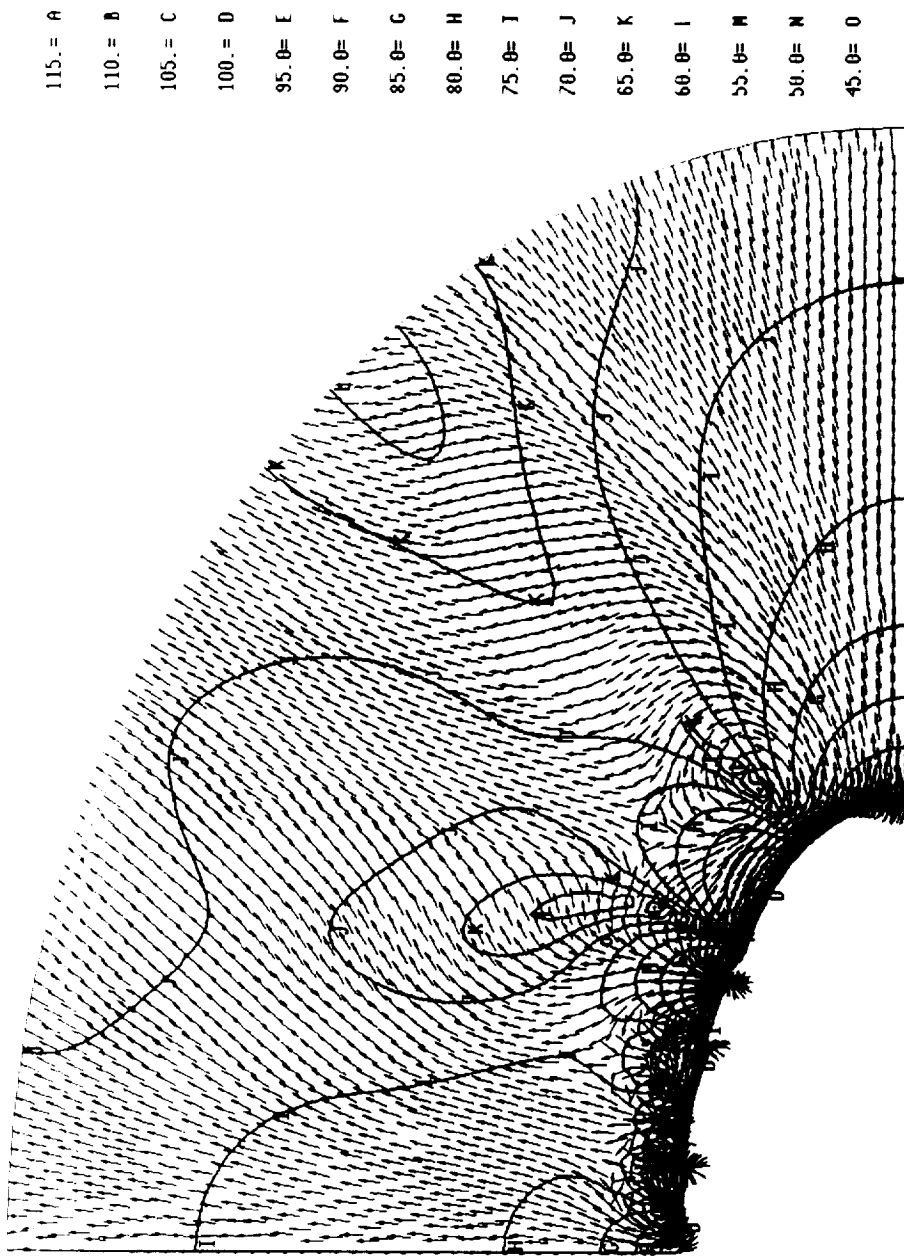|		
115. = A	75.0 = I	
110. = B	70.0 = J	
105. = C	65.0 = K	
100. = D	60.0 = L	
95.0 = E	55.0 = M	
90.0 = F	50.0 = N	
85.0 = G	45.0 = O	
80.0 = H		

Figure 5.   Acoustic Intensities and Pressures for Rigid Vertical Boundary;
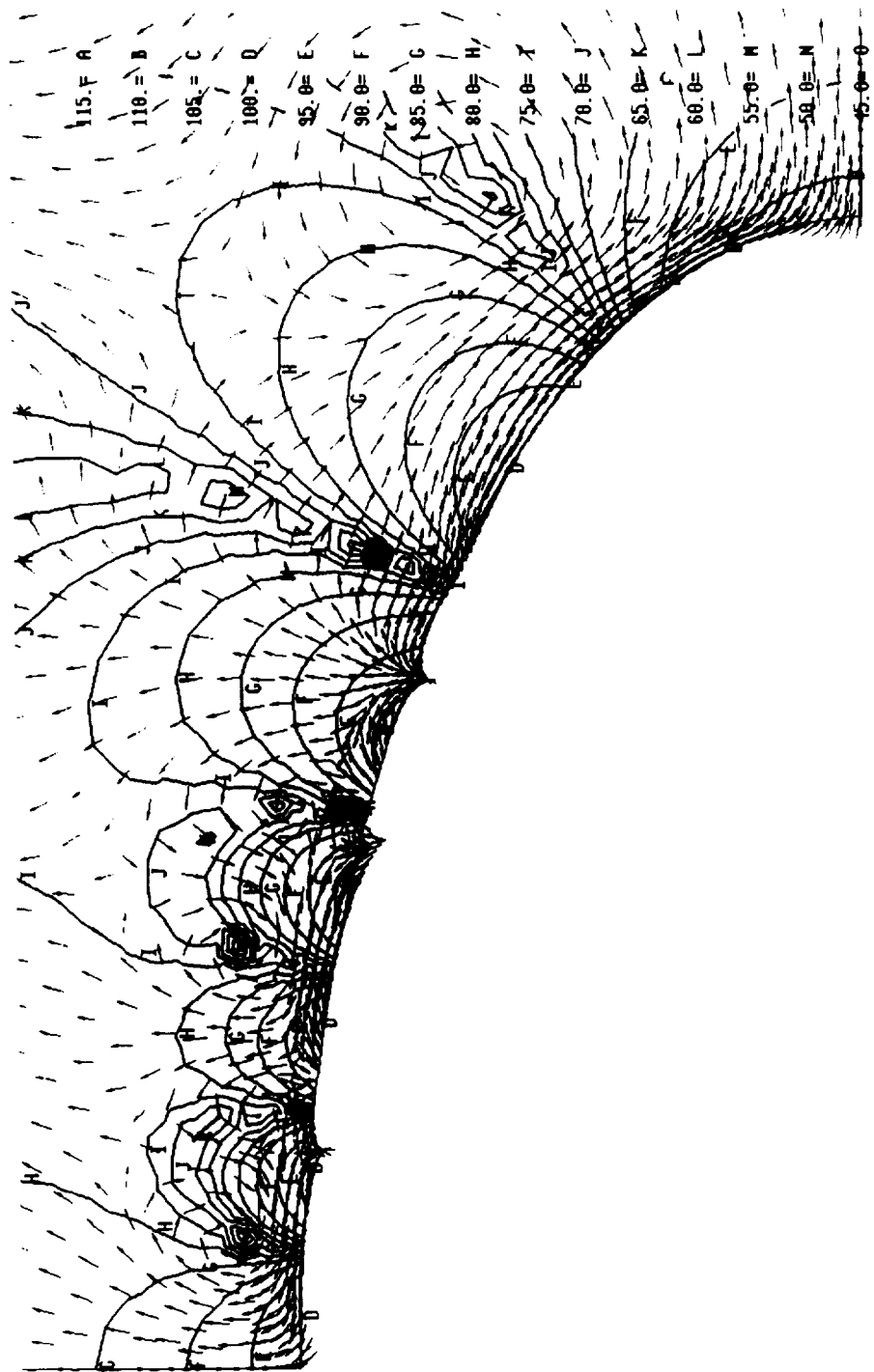Lines Denote Constant Pressure Contours; Vectors Denote Acoustic Intensities.

178

Figure 6. Close-up of Acoustic Intensities and Pressures for Rigid Vertical Boundary; Lines Denote Constant Pressure Contours; Vectors Denote Acoustic Intensities.
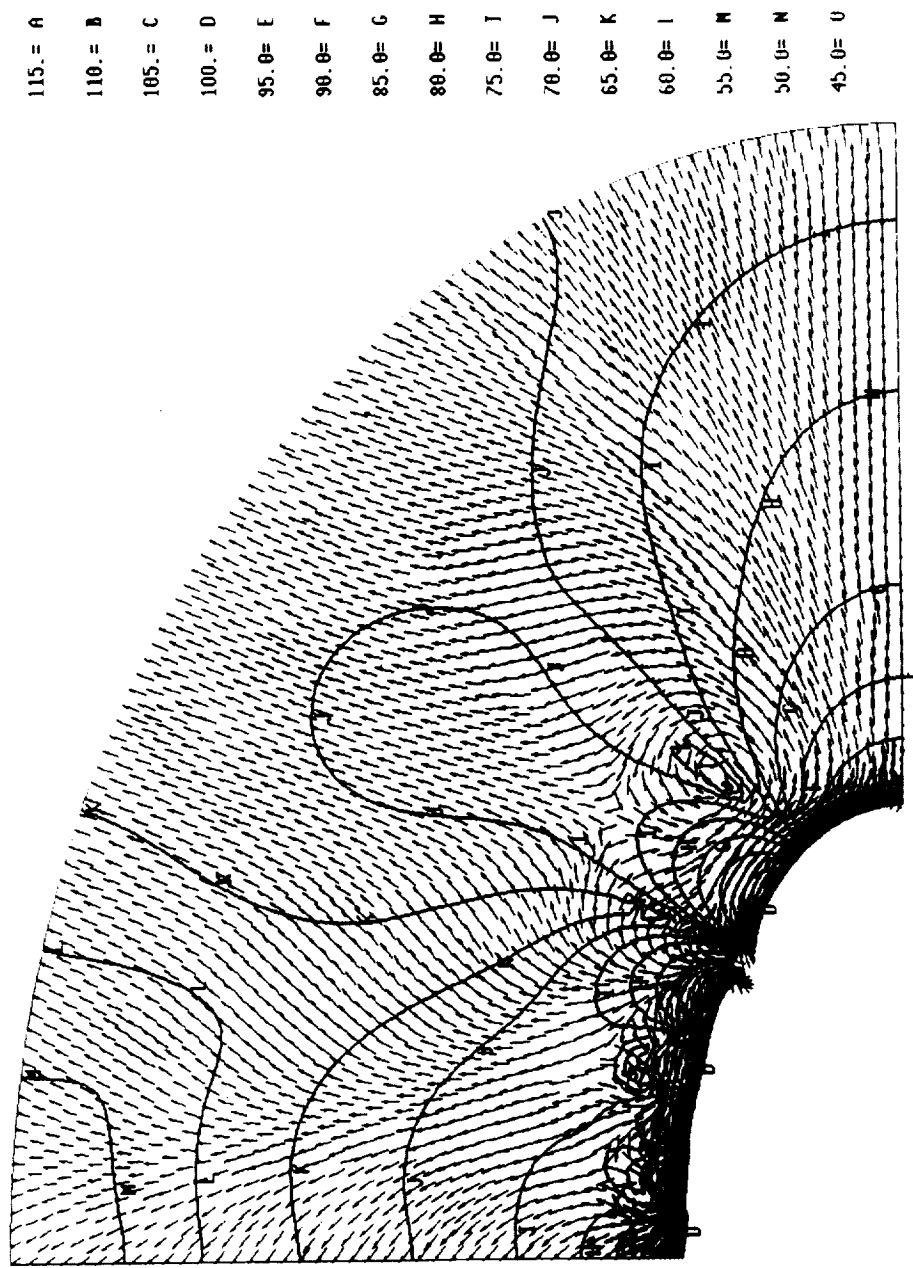
C-3

Figure 7. Acoustic Intensities and Pressures for Absorbing Vertical Boundary; Lines Denote Constant Pressure Contours; Vectors Denote Acoustic Intensities.
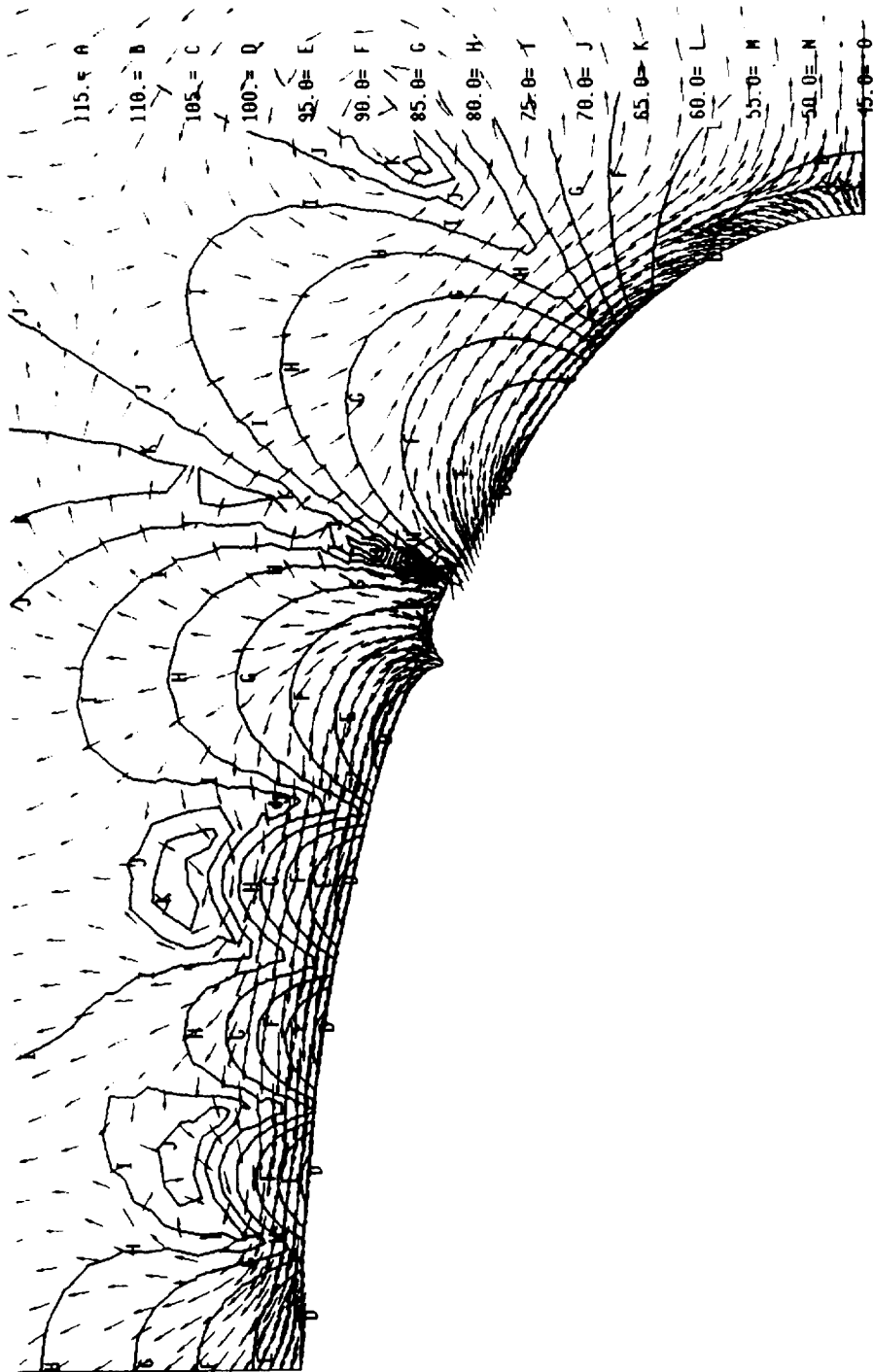
Figure 8. Close-up of Acoustic Intensities and Pressures for Absorbing Vertical Boundary;
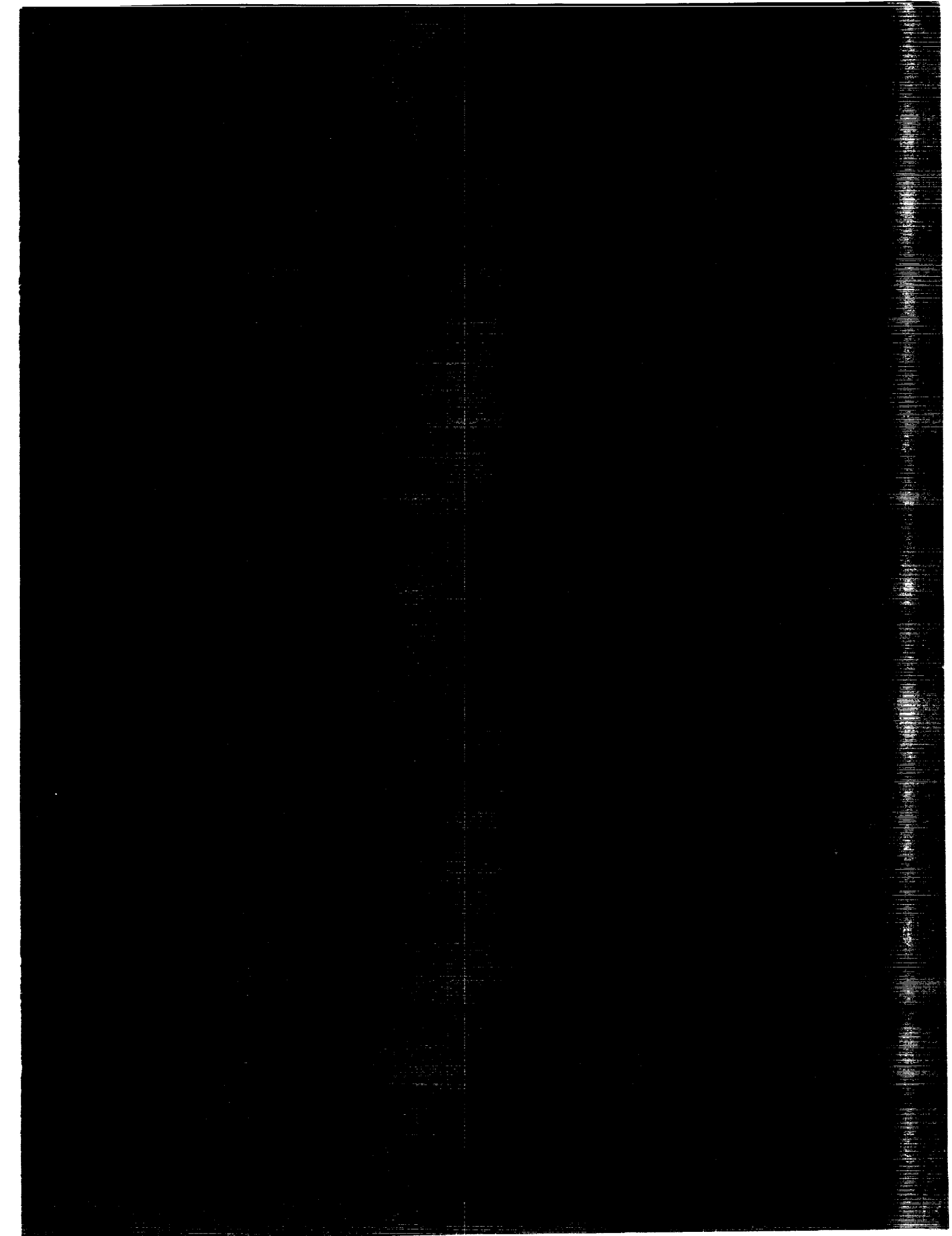Lines Denote Constant Pressure Contours; Vectors Denote Acoustic Intensities.

181

REFERENCES

1. L.H. Chen and D.G. Schweikert, "Sound Radiation from an Arbitrary Body," *J. Acoust. Soc. Amer.*, Vol. 35, No. 10, pp. 1626–1632 (1963).

2. J.J. Engblom and R.B. Nelson, "Consistent Formulation of Sound Radiation from Arbitrary Structure," *J. Appl. Mech.*, Vol. 42, pp. 295–300 (1975).

3. H. Huang, G.C. Everstine, and Y.F. Wang, "Retarded Potential Techniques for the Analysis of Submerged Structures Impinged by Weak Shock Waves," *Computational Methods for Fluid-Structure Interaction Problems*, ed. by T. Belytschko and T.L. Geers, AMD-Vol. 26, The American Society of Mechanical Engineers, New York, pp. 83–93 (1977).

4. D.T. Wilton, "Acoustic Radiation and Scattering from Elastic Structures," *Int. J. Num. Meth. in Engrg.*, Vol. 13, pp. 123–138 (1978).

5. J.S. Patel, "Radiation and Scattering from an Arbitrary Elastic Structure Using Consistent Fluid Structure Formulation," *Comput. Struct.*, Vol. 9, pp. 287–291 (1978).

6. Y.P. Lu, "The Application of Retarded Potential Techniques to Submerged Dynamic Structural Systems," *Innovative Numerical Analysis for the Engineering Sciences*, edited by R. Shaw, W. Pilkey, B. Pilkey, R. Wilson, A. Lakis, A. Chaudouet, and C. Marino, University Press of Virginia, Charlottesville (1980).

7. I.C. Mathews, "Numerical Techniques for Three-Dimensional Steady-State Fluid-Structure Interaction," *J. Acoust. Soc. Amer.*, Vol. 79, pp. 1317–1325 (1986).

8. G.C. Everstine, F.M. Henderson, E.A. Schroeder, and R.R. Lipman, "A General Low Frequency Acoustic Radiation Capability for NASTRAN," *Fourteenth NASTRAN Users' Colloquium*, NASA CP-2419, National Aeronautics and Space Administration, Washington, DC, pp. 293–310 (1986).

9. G.C. Everstine, F.M. Henderson, and L.S. Schuetz, "Coupled NASTRAN/Boundary Element Formulation for Acoustic Scattering," *Fifteenth NASTRAN Users' Colloquium*, NASA CP-2481, National Aeronautics and Space Administration, Washington, DC, pp. 250–265 (1987).

10. A.F. Seybert, T.W. Wu, and X.F. Wu, "Radiation and Scattering of Acoustic Waves from Elastic Solids and Shells Using the Boundary Element Method," *J. Acoust. Soc. Amer.*, Vol. 84, pp. 1906–1912 (1988).

11. G.C. Everstine and F.M. Henderson, "Coupled Finite Element/Boundary Element Approach for Fluid-Structure Interaction," *J. Acoust. Soc. Amer.*, Vol. 87, No. 5, pp. 1938–1947 (1990).

12. O.C. Zienkiewicz and R.E. Newton, "Coupled Vibrations of a Structure Submerged in a Compressible Fluid," *Proc. Internat. Symp. on Finite Element Techniques*, Stuttgart, pp. 359–379 (1969).

13. A. Craggs, "The Transient Response of a Coupled Plate-Acoustic System Using Plate and Acoustic Finite Elements," *J. Sound and Vibration*, Vol. 15, No. 4, pp. 509–528 (1971).

14. A.J. Kalinowski, "Fluid Structure Interaction," *Shock and Vibration Computer Programs: Reviews and Summaries*, SVM-10, ed. by W. Pilkey and B. Pilkey, The Shock and Vibration Information Center, Naval Research Laboratory, Washington, DC, pp. 405–452 (1975).

15. L. Kiefling and G.C. Feng, "Fluid-Structure Finite Element Vibrational Analysis," *AIAA J.*, Vol. 14, No. 2, pp. 199–203 (1976).

16. A.J. Kalinowski, "Transmission of Shock Waves into Submerged Fluid Filled Vessels," *Fluid Structure Interaction Phenomena in Pressure Vessel and Piping Systems*, PVP-PB-026, ed. by M.K. Au-Yang and S.J. Brown, Jr., The American Society of Mechanical Engineers, New York, pp. 83–105 (1977).

17. O.C. Zienkiewicz and P. Bettess, "Fluid-Structure Dynamic Interaction and Wave Forces: An Introduction to Numerical Treatment," *Int. J. Num. Meth. in Engrg.*, Vol. 13, No. 1, pp. 1–6 (1978).

18. M.A. Hamdi and Y. Ousset, "A Displacement Method for the Analysis of Vibrations of Coupled Fluid-Structure Systems," *Int. J. Num. Meth. in Engrg.*, Vol. 13, No. 1, pp. 139–150 (1978).

19. R.E. Newton, "Finite Element Study of Shock Induced Cavitation," Preprint 80-110, American Society of Civil Engineers, New York (1980).

20. A.J. Kalinowski and C.W. Nebelung, "Media-Structure Interaction Computations Employing Frequency-Dependent Mesh Size with the Finite Element Method," *Shock Vib. Bull.*, Vol 51, No. 1, pp. 173–193 (1981).

182

21. G.C. Everstine, "A Symmetric Potential Formulation for Fluid–Structure Interaction," *J. Sound and Vibration*, Vol. 79, pp. 157–160 (1981).

22. G.C. Everstine, "Structural–Acoustic Finite Element Analysis, with Application to Scattering," in *Proc. 6th Invitational Symposium on the Unification of Finite Elements, Finite Differences, and Calculus of Variations*, edited by H. Kardestuncer, Univ. of Connecticut, Storrs, Connecticut, pp. 101–122 (1982).

23. P.M. Pinsky and N.N. Abboud, "Transient Finite Element Analysis of the Exterior Structural Acoustics Problem," *Numerical Techniques in Acoustic Radiation*, edited by R.J. Bernhard and R.F. Keltie, NCA–Vol. 6, American Society of Mechanical Engineers, New York, pp. 35–47 (1989).

24. J.T. Hunt, M.R. Knittel, and D. Barach, "Finite Element Approach to Acoustic Radiation from Elastic Structures," *J. Acoust. Soc. Amer.*, Vol. 55, pp–269–280 (1974).

25. J.T. Hunt, M.R. Knittel, C.S. Nichols, and D. Barach, "Finite–Element Approach to Acoustic Scattering from Elastic Structures," *J. Acoust. Soc. Amer.*, Vol. 57, pp. 287–299 (1975).

26. J.B. Keller and D. Givoli, "Exact Non–reflecting Boundary Conditions," *J. Comput. Phys.*, Vol. 82, pp. 172–192 (1989).

27. A. Bostrom, "Scattering of Stationary Acoustic Waves by an Elastic Obstacle Immersed in Water," *J. Acoust. Soc. Amer.*, Vol. 67, No. 2, pp. 390–398 (1980).

28. M.F. Werby and L.H. Green, "An Extended Unitary Approach for Acoustical Scattering from Elastic Structures," *J. Acoust. Soc. Amer.*, Vol. 74, pp. 625–630 (1983).

29. M.F. Werby and G.J. Tango, "Application of the Extended Boundary Condition Equations to Scattering from Fluid–Loaded Objects," *Eng. Anal.*, Vol. 5, pp. 12–20 (1988).

30. D. Ranlet, F.L. DiMaggio, H.H. Bleich, and M.L. Baron, "Elastic Response of Submerged Shells with Internally Attached Structures to Shock Loading," *Comp. Struct.*, Vol. 7, No. 3, pp. 355–364 (1977).

31. T.L. Geers, "Doubly Asympototic Approximations for Transient Motions of Submerged Structures," *J. Acoust. Soc. Amer.*, Vol. 64, No. 5, pp. 1500–1508 (1978).

32. H.C. Neilson, G.C. Everstine, and Y.F. Wang, "Transient Response of a Submerged Fluid–Coupled Double–Walled Shell Structure to a Pressure Pulse," *J. Acoust. Soc. Amer.*, Vol. 70, No. 6, pp. 1776–1782 (1981).

33. "NASTRAN User's Manual," 1986, NASA SP–222(08), Computer Software Management and Information Center (COSMIC), University of Georgia, Athens, Georgia.

34. G.C. Everstine, "Structural Analogies for Scalar Field Problems," *Int. J. Num. Meth. in Engrg.*, Vol 17, pp. 471–476 (1981).

35. G.C. Everstine, R.S. Cheng, and S.A. Hambric, "Finite Element Solution of Transient Fluid–Structure Interaction Problems," *Nineteenth NASTRAN Users' Colloquium*, NASA CP–3111, National Aeronautics and Space Administration, Washington, DC, pp. 162–173 (April 1991).

36. A. Bayliss and E. Turkel, "Radiation Boundary Conditions for Wave–Like Equations," *Comm. Pure and Appl. Math.*, Vol. XXXIII, No. 6, pp. 707–725 (1980).

37. R.H. Cole, *Underwater Explosions*, Princeton University Press, Princeton, NJ (1948).

38. Cremer, L., Heckl, M., and Ungar, E.E., 1973, *Structure–Borne Sound*, Springer–Verlag, New York.

39. Hambric, S.A., 1990, "Power Flow and Mechanical Intensity Calculations in Structural Finite Element Analysis," *Journal of Vibration and Acoustics*, Vol. 112, No. 4, pp. 542–549.

REPORT DOCUMENTATION PAGE

Public reporting burden for this collection of information is estimated to average 1 hour per response, including the time for reviewing instructions, searching existing data sources, gathering and maintaining the data needed, and completing and reviewing the collection of information. Send comments regarding this burden estimate or any other aspect of this collection of information, including suggestions for reducing this burden, to Washington Headquarters Services, Directorate for Information Operations and Reports, 1215 Jefferson Davis Highway, Suite 1204, Arlington, VA 22202-4302, and to the Office of Management and Budget, Paperwork Reduction Project (0704-0188), Washington, DC 20503

1. AGENCY USE ONLY (Leave blank)	2. REPORT DATE	3. REPORT TYPE AND DATES COVERED
	April 1992	Conference Publication

4. TITLE AND SUBTITLE

Twentieth NASTRAN® Users' Colloquium

5. FUNDING NUMBERS

6. AUTHOR(S)

7. PERFORMING ORGANIZATION NAME(S) AND ADDRESS(ES)

COSMIC, NASA's Computer Software Management and
    Information Center
The University of Georgia
Athens, GA   30602

8. PERFORMING ORGANIZATION REPORT NUMBER

9. SPONSORING/MONITORING AGENCY NAME(S) AND ADDRESS(ES)

National Aeronautics and Space Administration
Washington, DC   20546

10. SPONSORING/MONITORING AGENCY REPORT NUMBER

NASA CP-3145

11. SUPPLEMENTARY NOTES

Also available from COSMIC, Athens, GA   30602

12a. DISTRIBUTION/AVAILABILITY STATEMENT

Unclassified - Unlimited

Subject Category 39

12b. DISTRIBUTION CODE

13. ABSTRACT (Maximum 200 words)

This publication contains the proceedings of the Twentieth NASTRAN®
Users' Colloquium held in Colorado Springs, CO., April 27 through
May 1, 1992. It provides some comprehensive general papers on the
application of finite elements in engineering, comparisons with
other approaches, unique applications, pre- and postprocessing
with other auxiliary programs, and new methods of analysis with
NASTRAN.

14. SUBJECT TERMS	15. NUMBER OF PAGES
NASTRAN, structures, structural analysis, finite element analysis, colloquium	188
	16. PRICE CODE A09

17. SECURITY CLASSIFICATION OF REPORT	18. SECURITY CLASSIFICATION OF THIS PAGE	19. SECURITY CLASSIFICATION OF ABSTRACT	20. LIMITATION OF ABSTRACT
Unclassified	Unclassified	Unclassified	Unlimited

NASA

POSTMASTER